

Nature-based solutions to mitigate salt intrusion

Hendrickx, G.G.

DOI

[10.4233/uuid:12e26179-4ebb-4f05-91bc-590d4c575e98](https://doi.org/10.4233/uuid:12e26179-4ebb-4f05-91bc-590d4c575e98)

Publication date

2024

Document Version

Final published version

Citation (APA)

Hendrickx, G. G. (2024). *Nature-based solutions to mitigate salt intrusion*. [Dissertation (TU Delft), Delft University of Technology]. <https://doi.org/10.4233/uuid:12e26179-4ebb-4f05-91bc-590d4c575e98>

Important note

To cite this publication, please use the final published version (if applicable).
Please check the document version above.

Copyright

Other than for strictly personal use, it is not permitted to download, forward or distribute the text or part of it, without the consent of the author(s) and/or copyright holder(s), unless the work is under an open content license such as Creative Commons.

Takedown policy

Please contact us and provide details if you believe this document breaches copyrights.
We will remove access to the work immediately and investigate your claim.



NATURE-BASED
SOLUTIONS
TO MITIGATE
SALT INTRUSION

GIJS G. HENDRICKX

Nature-based solutions to mitigate salt intrusion

Nature-based solutions to mitigate salt intrusion

Proefschrift

ter verkrijging van de graad van doctor
aan de Technische Universiteit Delft,
op gezag van de Rector Magnificus, prof. dr. ir. T.H.J.J. van der Hagen,
voorzitter van het College voor Promoties,
in het openbaar te verdedigen op
dinsdag 21 januari 2025 om 10:00 uur.

door

Gijs Gabriël HENDRICKX

Ingenieur in de Civiele Techniek,
Technische Universiteit Delft, Nederland,
geboren te Bergen op Zoom, Nederland.

Dit proefschrift is goedgekeurd door de promotoren.

Samenstelling promotiecommissie:

Rector Magnificus	voorzitter
Prof. dr. ir. S.G.J. Aarninkhof	Technische Universiteit Delft, <i>promotor</i>
Dr. ir. S.G. Pearson	Technische Universiteit Delft, <i>copromotor</i>
Dr. ing. J.A.A. Antolínez	Technische Universiteit Delft, <i>copromotor</i>

Onafhankelijke leden:

Prof. dr. C.A. Katsman	Technische Universiteit Delft
Prof. dr. H. Burchard	Universität Rostock, Germany
Prof. dr. G. Coco	University of Auckland, New Zealand
Prof. dr. K.E.R. Soetaert	Universiteit Utrecht
Prof. dr. ir. Z.B. Wang	Technische Universiteit Delft, <i>reserveid</i>



This dissertation is part of the project “Design and operation of nature-based SALTISolutions” (with project number P18-32 Project 7) of the research programme SALTISolutions which is (partly) financed by the Dutch Research Council (NWO).

Keywords: estuaries; salt intrusion; nature-based solutions; *Building with Nature*

Printed by: Ridderprint

Cover by: Gijs Hendrickx

Copyright © 2024 by G.G. Hendrickx

ISBN 978-94-6506-771-1

An electronic copy of this dissertation is available at
<https://repository.tudelft.nl/>.

CONTENTS

Summary	vii
Samenvatting	xi
Preface	xv
1 Introduction	1
I EXPLORATION	
<hr/>	
2 Sensitivity analysis: Method	11
3 Sensitivity analysis: Results	31
II CONCEPTUALISATION	
<hr/>	
4 Nature-based solution: Temporary sill	61
5 Nature-based solution: Intertidal area	77

III EVALUATION

6	Trade-offs: Socio-economy	95
7	Trade-offs: Socio-ecology	117

IV REFLECTION

8	Synthesis	137
9	Concluding remarks	149
	Epilogue	161
	References	167

APPENDICES

A	ANNESI	195
B	Supplementary material: Chapters 2 and 3	197
C	Supplementary material: Chapter 5	207
D	Supplementary material: Chapter 8	211
E	Nature-based solution: Discharge management	215
F	Nature-based solution: Tidal mixing energy	225
	Postface	229
	Acknowledgements	231
	About the author	235
	List of publications	237

SUMMARY

Worldwide, estuaries are centres of life. Their connection with the open seas while providing fertile lands and freshwater has resulted in these regions becoming major hubs of human settlement and activities, which is expected to continue growing in magnitude. However economically useful, the open connection to the seas also poses a challenge: freshwater availability. Via this open connection saline water can enter the estuary and contaminate the freshwater reserves—so-called (estuarine) salt intrusion. This may cause freshwater shortages and damage to all living beings that depend on this invaluable resource.

This research aims to develop mitigation measures to this estuarine salt intrusion following the *Building with Nature*-philosophy. Thus, the goal of this research is to develop *nature-based solutions to mitigate salt intrusion*. This is achieved by (1) exploring the potential of estuary-scale interventions to affect salt intrusion; (2) conceptualising various nature-based solutions that mitigate salt intrusion; (3) evaluating nature-based solutions in a multidisciplinary context; and, to conclude, (4) reflecting on the role of nature-based solutions.

The exploration of potential estuary-scale modifications is a computationally expensive endeavour for which a novel simulation strategy is developed. This strategy is presented in Chapter 2 and proposes the use of machine learning techniques to determine the input space—i.e., which model simulations to execute, and which

to exclude. The aim of the strategy is to put more focus on exploring the output space instead of exploring the input space.

Subsequently, the model simulations are analysed in Chapter 3. Thus, Chapters 2 and 3 present respectively the method and the results of an extensive sensitivity analysis of estuarine salt intrusion to estuary-scale modifications. The end-result of Chapter 3 includes a shortlist of potential nature-based solutions to mitigate salt intrusion, including a ranking based on the sensitivity analysis.

The conceptualisation of nature-based solutions focuses mainly on two potential options: (1) a (temporary) sill, or submerged dam (Ch. 4); and (2) enhancement of intertidal area (Ch. 5). In addition to these novel nature-based solutions, Chapter 6 evaluates a third nature-based solution: shallowing of an estuary. From a physical perspective, this mitigation measure is well-known but mainly poses challenges in the socio-economic domain, which is why it is not extensively covered in the *conceptualisation*-phase of this dissertation but the *evaluation*-phase instead.

Both the sill and the intertidal area show a dependency on estuary class in how effectively the mitigation measures are. For the sill it holds that the weaker the tide, the more effective the sill mitigates landward salt transport—i.e., salt intrusion. When the tide is limited, salt intrusion is largely (if not fully) driven by gravitational circulation, for which the sill functions as a wall beyond which the formed salt wedge can hardly penetrate. However, with tidal energy increasing, the tidal momentum to push the saline water over the sill also increases resulting in more salt intrusion—the sill functions more like a speed-bump than a wall. All in all, a sill is most effective for estuaries with little tidal influence.

Enhancement of intertidal area increases the mixing in the estuary. When the dominant salt transport mechanism is related to the estuarine circulation, this enhanced mixing by increasing the intertidal area reduces the salt intrusion. However, the opposite holds for estuaries in which the salt transport is dominated by the tidal oscillation. This means that in case of salt wedge and partially mixed estuaries, enhancement of the intertidal area reduces salt intrusion; and in case of well-mixed estuaries, the intertidal area increase promotes salt intrusion. Thus, the additional (vertical) mixing caused by the intertidal areas reduces salt intrusion as long as there is something to mix—i.e., as long as there is a (sufficient) vertical salinity gradient.

The evaluation of nature-based solutions is inherently multidisciplinary. In this dissertation, two different perspectives are considered: (1) socio-economy (Ch. 6), and (2) socio-ecology (Ch. 7). In both cases, the Rhine-Meuse Delta is considered as case study.

The socio-economic evaluation addresses the effect of water depth on two major stakeholders in an estuary: a port, and water boards. These stakeholders have opposing interests regarding the water depth: a port benefits from enhanced water depth to facilitate larger vessels, but the resulting contamination of freshwater reserves via salt intrusion is negatively affecting water intakes, and everyone that depends on them. Chapter 6 presents a multidisciplinary evaluation method based on Pareto-fronts, which are to inform decision- and policy-makers. The Pareto-front in Chapter 6 shows that the port performance remains relatively unaffected

for shallowing until two metres with the current bed levels, while the freshwater availability improves. However, beyond this level of shallowing, port performance drops substantially against limited gains in freshwater availability.

The socio-ecological evaluation focuses on the effects of reopening a closed-off estuary on two opposing interests as well: freshwater availability, and estuarine ecosystem functioning. Reopening is beneficial for the ecological diversity in the former estuary, but comes at the costs of returning saline influences into a freshwater lake—i.e., freshwater availability is hampered. The ecological implications are mapped by translating hydrodynamic (model) data to an ecotopes-potential map due to which the ecological impact of interventions can be quantified. As in Chapter 6, Pareto-fronts are used as method to inform decision- and policy-makers. The Pareto-front in Chapter 7 shows an increased ecological diversity in the former estuary without impeding the freshwater availability when partially opening the gates. However, once the salt intrusion reaches the most western water intakes, the freshwater availability drops without major gains in diversity.

This dissertation has shown the complexity of developing future-proof nature-based solutions to mitigate salt intrusion. Building on the lessons learned, the reflection of this dissertation proposes a next step for nature-based solutions: DARE (diverse, adaptive, and robust engineering; Ch. 8). DARE is based on nature's own approach to dealing with uncertainties. The three axes of DARE show how to deal with uncertainties in the three dimensions of engineering: (1) a *diverse* set of solutions to deal with uncertainty in *forcing* conditions; (2) an *adaptive* approach with room to change course in response to the uncertainty that comes with *time*; and (3) *robust*—or even *antifragile*—solutions regarding the uncertainty in *performance*. With DARE, the focus shifts from the input to the output: Which part of the output is desirable, and what are the options to get there?

The nature-based solutions presented in this dissertation form a starting point for further explorations, with work in this dissertation already being used as a stepping stone for other studies. Besides further exploring the opportunities of nature-based solutions to mitigate salt intrusion, next steps also include bringing these findings into practice. This includes reassessing past estuarine modifications from a new perspective, one that is less susceptible to the challenges that the future may have in store.

SAMENVATTING

Wereldwijd zijn estuaria centra van leven. De combinatie van een zee connectie met vruchtbare grond en zoetwaterbeschikbaarheid heeft ervoor gezorgd dat deze gebieden menselijke vestigingen en activiteiten hebben aangetrokken. Een trend die verwacht wordt door te zetten. Ondanks de economische waarde van de open zee connectie, deze connectie creëert ook een uitdaging: zoetwaterbeschikbaarheid. Via deze open connectie kan zoutwater het estuarium binnenstromen en zoetwaterreserves vervuilen—zogenaamde (estuariene) zoutindringing. Dit kan resulteren in zoetwaterterkorten en schade toebrengen aan al het leven dat afhankelijk is van deze onschatbare bron.

Dit onderzoek streeft naar de ontwikkeling van reductiemaatregelen voor estuariene zoutindringing volgens de *Building with Nature*-filosofie (vert.: *Bouwen met de Natuur*). Dus het doel van dit onderzoek is de ontwikkeling van *natuur-gebaseerde oplossingen tegen zoutindringing*. Dit is bewerkstelligd door (1) ontdekken van potentiële estuarium-schaal interventies die de zoutindringing veranderen; (2) conceptualiseren van verschillende natuur-gebaseerde oplossingen tegen zoutindringing; (3) evalueren van natuur-gebaseerde oplossingen in een multidisciplinaire context; en (4) reflecteren op de rol van natuur-gebaseerde oplossingen.

De ontdekking van potentiële estuarium-schaal ingrepen is een computationeel dure aanpak waarvoor een nieuwe simulatiestrategie is ontwikkeld. Deze strategie wordt

in Hoofdstuk 2 behandeld en draagt het gebruik van *machine learning* technieken aan om de invoerruimte te kiezen—m.a.w. welke model simulaties uit te voeren en welke niet. Het doel van deze strategie is om meer focus te leggen op het ontdekken van de uitvoerruimte in plaats van het ontdekken van de invoerruimte.

Vervolgens worden de resultaten in Hoofdstuk 3 geanalyseerd. Dus Hoofdstukken 2 en 3 omvatten respectievelijk de methode en de resultaten van een uitgebreide gevoeligheidsanalyse van zoutindringing op estuarium-schaal aanpassingen. De conclusie van Hoofdstuk 3 bevat een lijst van potentiële natuur-gebaseerde oplossingen tegen zoutindringing, waarbij de oplossingen zijn gerangschikt op basis van de gevoeligheidsanalyse.

De conceptualisatie van natuur-gebaseerde oplossingen focust hoofdzakelijk op twee mogelijke opties: (1) een (tijdelijke) drempel, of onderwater-dam (Hst. 4); en (2) uitbreiding van intergetijd gebied (Hst. 5). Aanvullend op deze nieuwe natuur-gebaseerde oplossingen wordt een derde optie geëvalueerd in Hoofdstuk 6: ondieper maken van een estuarium. Vanuit een fysisch oogpunt is deze oplossing alom bekend, waarbij de uitdagingen vooral in het socio-economische domein liggen. Daarom is deze oplossing niet uitgebreid behandeld in de *conceptualisatie*-fase van dit proefschrift, maar onderdeel van de *evaluatie*-fase.

Zowel de drempel als het intergetijd gebied laten een afhankelijkheid van estuarium-klasse zien op hun effectiviteit. Voor de drempel geldt dat des te zwakker het getij, des te effectiever de drempel het landwaartse zouttransport kan tegenhouden—m.a.w. des te minder de zoutindringing. Met beperkte getijdeslag wordt de zoutindringing (grotendeels) gedreven door gravitatiecirculatie, waardoor de drempel fungeert als muur waar de zouttong nauwelijks langskomt. Echter met grotere getijde-energie komt ook een grotere getijdemoment die het zoute water over de drempel heen kan duwen met meer zoutindringing als gevolg—de drempel wordt dan meer een snelheidsdrempel. Generiek gesproken, een drempel is het meest effectief in estuaria met een klein getij.

Uitbreiding van intergetijd gebied vergroot de menging in het estuarium. Wanneer het dominante zouttransportmechanisme gedreven wordt door estuariene circulatie zorgt deze extra menging voor een afname in zoutindringing. Het tegenovergestelde geldt echter voor estuaria waarin het zouttransport gedomineerd wordt door getijdendispersie. Dit betekent dat in het geval van zouttong- of gedeeltelijk-gemengde-estuaria, de uitbreiding van intergetijd gebied tot een reductie in zoutindringing leidt; en in het geval van goed-gemengde-estuaria, het intergetijd gebied juist zorgt voor extra zoutindringing. Dus de extra (verticale) menging die veroorzaakt wordt door het intergetijd gebied reduceert zoutindringing zolang er iets te mengen valt—m.a.w. zolang er een (degelijke) verticale zoutgradiënt is.

De evaluatie van natuur-gebaseerde oplossingen is inherent multidisciplinair. In dit proefschrift worden er twee perspectieven beschouwd: (1) socio-economie (Hst. 6), en (2) socio-ecologie (Hst. 7). In beide gevallen dient de Rijn-Maas Monding als proeftuin.

De socio-economische evaluatie adresseert het effect van de waterdiepte op twee belangrijke belanghebbenden in een estuarium: een haven en waterschappen. Deze

belanghebbenden hebben tegengestelde voorkeuren qua waterdiepte: een haven is gebaat bij een grotere diepgang waardoor ze grotere schepen kunnen faciliteren, maar dit resulteert in zoutvervuiling van de zoetwaterreserves door middel van toenemende zoutindringing wat de waterschappen schaadt, en iedereen die van hen afhankelijk is. Hoofdstuk 6 presenteert een multidisciplinaire evaluatie methode op basis van Pareto-fronten, welke besluit- en beleidsmakers dienen te informeren. Het Pareto-front in Hoofdstuk 6 laat zien dat het functioneren van de haven relatief onveranderd blijft voor een ondieping tot twee meter ten opzichte van de huidige bodemligging, terwijl de zoetwaterbeschikbaarheid verbetert. Echter zorgt verdere verontdieping voor een substantieële keldering in het presteren van de haven tegen beperkte winsten qua zoetwaterbeschikbaarheid.

De socio-ecologische evaluatie focust op de effecten van het heropenen van een afgesloten estuarium op wederom twee belangrijke belanghebbenden: de waterschappen, en ecologie. Heropening is gunstig voor de ecologische diversiteit in het voormalige estuarium, maar komt met de prijs van het herintroduceren van zoutwater in een zoetwatermeer—m.a.w. de zoetwaterbeschikbaarheid wordt belemmerd. De ecologische implicaties worden in kaart gebracht door een model dat hydrodynamische (model) data vertaalt naar een ecotopen-potentie kaart, waardoor de ecologische impact van interventies gekwantificeerd kan worden. Net als in Hoofdstuk 6 worden Pareto-fronten gebruikt als middel om besluit- en beleidsvorming te informeren. Het Pareto-front in Hoofdstuk 7 laat een toenemende ecologische diversiteit zien in het estuarium zonder belemmering van de zoetwaterbeschikbaarheid voor gedeeltelijke heropening. Echter wordt de zoetwaterbeschikbaarheid flink aangetast zodra de meest-westerse innamepunten beïnvloed worden door zoutindringing, zonder duidelijke toename van de diversiteit.

Dit proefschrift heeft de complexiteit laten zien van het ontwikkelen van toekomstbestendige, natuur-gebaseerde oplossingen voor het reduceren van zoutindringing. Voortbouwend op de geleerde lessen, de reflectie van dit proefschrift draagt een volgende stap omtrent natuur-gebaseerde oplossingen voor: DARE (*diverse, adaptive, and robust engineering*, [vert.: divers, adaptief en robuust ontwerpen]; Hst. 8). DARE is gebaseerd op hoe de natuur omgaat met onzekerheden. De drie assen van DARE representeren hoe om te gaan met onzekerheden in de drie dimensies van het ingenieurschap: (1) een *diverse* collectie van oplossingen vanwege de onzekerheid in *randvoorwaarden*; (2) een *adaptieve* aanpak met ruimte voor koersverandering vanwege de onzekerheid die komt met de *tijd*; en (3) *robuuste*—of zelfs *antifragiele*—oplossingen vanwege de onzekerheid in *prestatie*. Met DARE ligt de focus op de uitvoer in plaats van de invoer: welk gedeelte van de uitvoerruimte—of oplossingsruimte—is wenselijk, en wat zijn de opties om daar te komen.

De natuur-gebaseerde oplossingen gepresenteerd in dit proefschrift vormen een startpunt voor verdere ontdekkingen, waarbij onderdelen van dit proefschrift al gebruikt zijn als basis voor andere studies. Naast het verder ontdekken van mogelijkheden voor natuur-gebaseerde oplossingen tegen zoutindringing, de volgende stappen omvatten ook de vertaling van de bevindingen naar de praktijk. Dit omvat ook de heroverweging van vorige estuariene ingrepen vanuit een nieuw perspectief, één die minder vatbaar is voor wat de toekomst in petto kan hebben.

PREFACE

“The goal of nature-based solutions to mitigate salt intrusion is fascinating, as such a goal cannot be achieved.”

These words were spoken during the first project meeting, on the third day of a four-year project with the goal to do exactly that: develop nature-based solutions to mitigate salt intrusion. The first part is definitely true; the goal to develop nature-based solutions to mitigate salt intrusion is fascinating, you could spend a whole PhD on the topic—as this dissertation is testimony to. The second part is intriguing: why set up a whole PhD project about something that cannot be done, and is this goal indeed unachievable?

Although these words were not intended to discredit the research project presented in this dissertation, they remained intriguing and felt strangely motivating. Why would someone so strongly disbelieve in the potential of nature-based solutions to mitigate salt intrusion; and are their beliefs valid? What is it that makes the marriage of nature-based solutions with estuarine salt intrusion doomed to end up in a divorce; and is this a valid presumption? Has anybody actually tried to put the two in the same room, or did prejudice prevail without even trying? Have they become too narrow-minded regarding the concept of nature-based solutions, or is this concept too narrowly scoped and in need of a thorough reflection?

Whatever the reason may be, the statement was provoking the general understanding of this project’s kick-off meeting. With this statement, they were kicking against the legs of the (virtual) conference table—and the table gave way: The general “understanding” seemed to be a general “belief” in the ability of nature-based solutions to mitigate salt intrusion. Although this belief could be valid, it had not to been tried—yet.

Essentially, the above statement forced everybody to take a step back by putting forward a null-hypothesis:

There are no nature-based solutions to mitigate salt intrusion.

May this dissertation refute this null-hypothesis.

Gijs Hendrickx

*We zijn allemaal maar struikelende diertjes
en de enige taak die wij hebben,
is doen alsof het dansen is.*

Jan Jaap van der Wal

1

INTRODUCTION

Nature-based solutions to mitigate salt intrusion.

It is a concise title, but what does it entail? Where is salt intruding? Why mitigate salt intrusion? What are nature-based solutions and salt intrusion? How can nature-based solutions mitigate salt intrusion?

These are but a few questions that may arise after reading this title. This dissertation aims to address these—and related—questions.

1.1 Motivation

Worldwide, deltas—and the estuaries they contain—are centres of life. Due to the combination of freshwater availability and fertile lands with an open connection to the sea, deltas have become major hubs of human settlement and activity (Fig. 1.1; e.g., Maul & Duedall, 2019)—a trend that is projected to continue (Neumann *et al.*, 2015). Although this connectivity with the sea creates many (economic) possibilities such as ports and is essential for migratory fishes (e.g., Brink *et al.*, 2018; Chen *et al.*, 2023; Rolls, 2011), it also poses the threat of salinisation of freshwater reserves (Costall *et al.*, 2018): There is a direct route for the saline water to intrude landwards, where it can contaminate freshwater reserves. Water

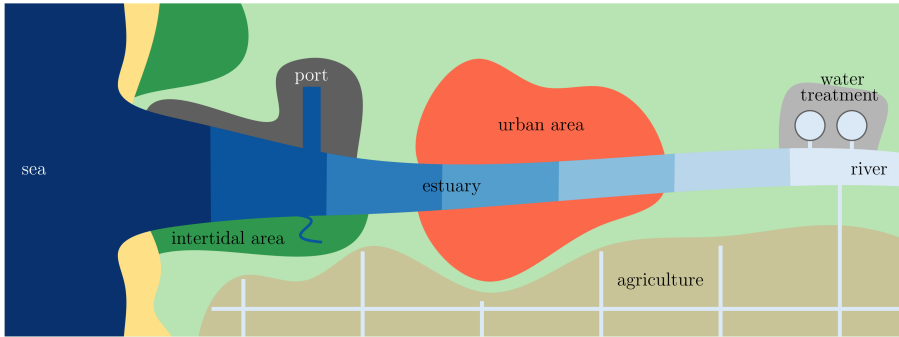


Figure 1.1: Schematic of an estuary including some of its relevant activities/stakeholders. The shades of blue represent salinity levels: darker blue for saline water, and lighter blue for freshwater.

stress—i.e., the unavailability of freshwater—is a global phenomenon (Mekonnen & Hoekstra, 2016), and due to salt intrusion is most profound in coastal areas (Wada *et al.*, 2011), contaminating freshwater reserves via groundwater (e.g., Costall *et al.*, 2018) as well as surface waters (this dissertation).

With the climate changing, the severity and likelihood of water stress is expected to increase (e.g., Distefano & Kelly, 2017; Jones *et al.*, 2024; Veldkamp *et al.*, 2015). Climate change results in (relative) sea level rise (e.g., Katsman *et al.*, 2011; Nicholls & Cazenave, 2010; Slangen *et al.*, 2014) plus increased frequency and duration of droughts (Jones *et al.*, 2024; Lee *et al.*, 2024). Both of these changes enhance estuarine salt intrusion due to increased encroachment of the sea and reduced river discharge (Lee *et al.*, 2024; Yang & Zhang, 2024), and so too, the further reduction of freshwater availability. While the freshwater supply is pressured due to climate change, the expected population growth in coastal regions will increase the demand for it (Small & Nicholls, 2003). Thus as freshwater supply and demand increasingly strain the reserves present, the necessity to secure freshwater availability increases.

To secure freshwater availability, salt intrusion via surface waters can be mitigated by means of hard structures—e.g., dams and locks—, which could mitigate these threats of water stress. However, such hard measures come with many negative side-effects; e.g., estuarine squeeze (similar to coastal squeeze) whereby tidal freshwater environments are threatened (Little *et al.*, 2022); potentially increased flood risk downstream of the structure (Dykstra *et al.*, 2024); and hindrance of vessels and thereby reduced potential for economic development.

On the other hand, nature-based solutions have not yet been widely considered in the context of estuarine salt intrusion mitigation. Nature-based solutions are multidisciplinary, system-based interventions (e.g., de Vriend *et al.*, 2015; van Slobbe *et al.*, 2013), which aim to incorporate and exploit natural dynamics. All in all, the increasing pressures on freshwater availability and the many drawbacks

of hard measures to mitigate salt intrusion have motivated this exploratory study: *How can nature-based solutions mitigate salt intrusion?*

Note that this question encompasses two perspectives: (1) the definition of what constitutes nature-based solutions to mitigate salt intrusion; and (2) the development of nature-based solutions to mitigate salt intrusion. Both these perspectives are considered in this dissertation.

1.2 Context

In exploring nature-based solutions to mitigate salt intrusion, this dissertation brings together two fields of research: (1) *Building with Nature* (in hydraulic engineering), and (2) estuarine salt dynamics. This section aims to give (very) brief overviews of both research fields before defining the knowledge gaps when combining them.

1.2.1 Building with Nature

The term *Building with Nature* reflects a design approach rooted in hydraulic engineering (de Vriend *et al.*, 2015), of which nature-based solutions are the product. In this approach, there is a strong focus on the system as a whole; i.e., the *Building with Nature*-approach extends beyond the physical realm and incorporates socio-economic and ecological perspectives (de Vriend *et al.*, 2015; van Slobbe *et al.*, 2013). Such system understanding enables the development of more robust and/or adaptive measures that move along with changing boundary conditions (Borsje *et al.*, 2011; Temmerman *et al.*, 2013).

The design of nature-based solutions starts with understanding the system (de Vriend *et al.*, 2015; van Koningsveld & Mulder, 2004; van Slobbe *et al.*, 2013); “the system” in this dissertation is “the estuary.” The aim of this system-focused approach is to minimise any potential (negative) side-effects due to the implementation of measures; and, instead, utilise and stimulate ecosystem services as components of the measure (Adger *et al.*, 2005; de Vriend *et al.*, 2015). Therefore, *Building with Nature* is a way of thinking—i.e., a philosophy—instead of a type of engineering solution (de Vriend *et al.*, 2015).

In hydraulic engineering, the term *Building with Nature* is commonly associated with vegetation-based flood defences (e.g., Ourloglou *et al.*, 2020; van Wesenbeeck *et al.*, 2014; Vuik *et al.*, 2016). However, the scope of *Building with Nature* is broader and aims at the development of inclusive measures; new measures for society should be realised with a thorough understanding of the system—natural and societal—as the starting point (de Vriend *et al.*, 2015). Such an holistic view promotes the creation of added value from socio-economic and ecological perspectives (e.g., Adger *et al.*, 2005; Scheres & Schüttrumpf, 2019; van Wesenbeeck *et al.*, 2014).

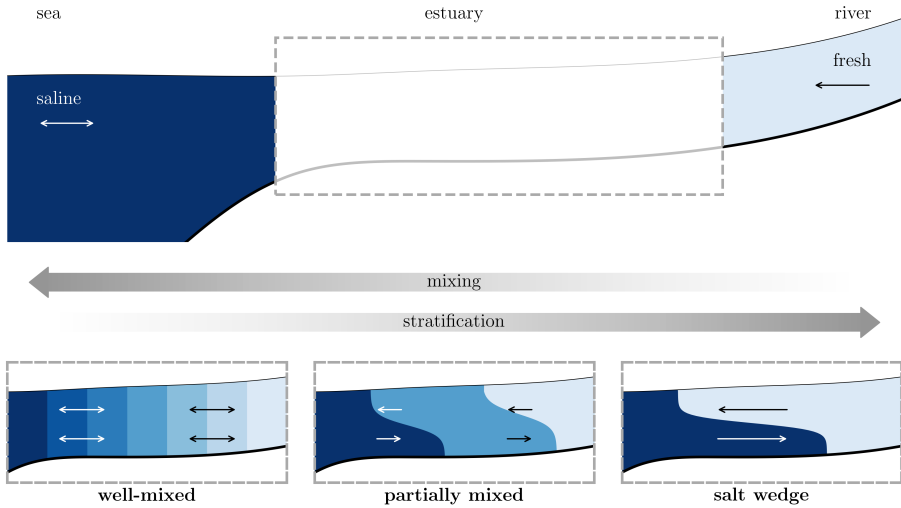


Figure 1.2: Conceptual overview of an estuary. The vertical structure of salinity results from the stratification-mixing balance, where denser, saline water tends to intrude beneath lighter freshwater, which is counteracted by (tidal) mixing.

1.2.2 Estuarine salt dynamics

Before diving into a brief overview of estuarine salt dynamics, it is important to clarify what an “estuary” is: Estuaries are the regions where the river is influenced by the sea. Hydrodynamically, they form the interface between the freshwater river system, and the saline water from the seas and oceans (Fig. 1.2). Their landward extent is commonly defined by the reach of saline influence (e.g., Lerczak *et al.*, 2009; Little *et al.*, 2022; MacCready & Geyer, 2010).

Because saline water is ever so slightly denser than freshwater (2–4%), water flows in estuaries are complex and generally require a three-dimensional perspective. These density differences cause the saline water to move underneath the freshwater, creating a vertical layering in density—so-called “stratification.”

This stratification can be broken down by adding energy to the system, which mixes the stratified components, resulting in a vertically-homogeneous density profile—a well-mixed system. In an estuary, this mixing energy generally originates from the tidal motion (e.g., Geyer & MacCready, 2014; Guha & Lawrence, 2013; Simpson *et al.*, 1990), but (strong) winds and waves also enhance the mixing in an estuary (e.g., Geyer, 1997; Gong *et al.*, 2018; Jongbloed *et al.*, 2022).

As the balance between stratification and mixing greatly influences the estuarine dynamics, estuaries are classified based on these opposing processes. The basic classification system is based on the dominance of one of these two components, resulting in three categories (e.g., Fischer, 1972, Fig. 1.2): (1) salt wedge, (2) partially mixed, and (3) well-mixed. The partially mixed system is an intermediate between the stratification-dominated salt wedge, and the mixing-dominated well-

mixed systems. More recently, Geyer and MacCready (2014) developed a more elaborate classification system containing eight classes. Nevertheless, the balance between stratification and mixing is also at the core of this classification system.

In recent years, a vast body of literature has been developed, aiding our understanding of estuarine salt intrusion (e.g., reviews by Geyer & MacCready, 2014; MacCready & Geyer, 2010). From these many studies, two estuary-scale parameters stand out in their level of influence on the salt intrusion: (1) the water depth (e.g., Chant *et al.*, 2018; Ralston & Geyer, 2019); and (2) the river discharge (e.g., Gong & Shen, 2011; Lerczak *et al.*, 2009). However, estuarine salt intrusion is influenced more generally by the geomorphology of estuaries (Veerapaga *et al.*, 2020), such as the presence of intertidal areas (Lyu & Zhu, 2019; Zhou *et al.*, 2020a). In essence, the estuarine salt intrusion is the result of a battle between the forcing conditions in an arena shaped by the estuarine geomorphology.

The main hydrodynamic forcing conditions include the tide and river discharge (e.g., Geyer & MacCready, 2014; Kuijper & van Rijn, 2011; Lerczak *et al.*, 2009). The flood tide pushes saline water into the estuary during which it introduces energy to mix the water column (e.g., Burchard & Hofmeister, 2008; Ralston *et al.*, 2010b; Simpson *et al.*, 1990). This is counteracted by a seaward push due to the river discharge, which is accompanied by stratifying forces due to the supply of freshwater (e.g., Hetland & Geyer, 2004; MacCready, 1999; MacCready & Geyer, 2010). For a given tidal and fluvial influence, the resulting balance is largely defined by the estuarine geomorphology—i.e., the arena—, where both forcing terms enhance as well as reduce the salt intrusion.

In addition to the tidal and fluvial forcing, there are other external influences at play; examples include storm surges (Geyer, 1997; Kranenburg *et al.*, 2022), sea level rise (Hong & Shen, 2012), artificial barriers (Little *et al.*, 2022), and natural morphological changes (Chen *et al.*, 2019).

As previously mentioned, the estuarine morphology sets the stage in which the forcing conditions reach a balance. The water depth of the system has long been known to be a major factor in determining the salt intrusion (e.g., Hansen & Rattray Jr., 1965, 1966). There is a strong, nonlinear relation between the salt intrusion and the water depth (MacCready & Geyer, 2010; Ralston & Geyer, 2019); thus channel deepening—e.g., to accommodate large(r) vessels—enhances salt intrusion (a common trade-off in estuaries; e.g., Chant *et al.*, 2018; Johnson *et al.*, 1987; Mansur *et al.*, 2023; Ralston & Geyer, 2019; Yuan & Zhu, 2015; Zhang *et al.*, 2011; Zhu *et al.*, 2015).

In addition to the water depth, there are other relevant morphological features substantially impacting the salt intrusion. For example, the estuarine width has a similar effect as the depth on the salt intrusion (Veerapaga *et al.*, 2020; Zhu *et al.*, 2015). The tidal influence on the salt intrusion largely depends on the balance between the width convergence and bottom friction, which define whether the tide is damped or amplified (e.g., Friedrichs & Aubrey, 1988; Savenije & Veling, 2005; van Rijn, 2011). Furthermore, an ebb-dominant system due to, e.g., intertidal

areas reduces the salt intrusion (Cheng *et al.*, 2010, 2013; Pein *et al.*, 2018; Stacey *et al.*, 2008).

Chapter 3 dives deeper into the dominant processes determining the salt intrusion, and which estuary-scale parameters drive these processes. This chapter includes a very brief literature overview (Sec. 3.2) from which hypotheses of potential nature-based solutions are drawn that form the basis for this study.

1.2.3 Knowledge gaps

Sections 1.2.1 and 1.2.2 showcase the tremendous progress achieved in recent years in the fields of, respectively, *Building with Nature* and estuarine salt dynamics. These two disciplines have not yet been connected, which highlights the main knowledge gap addressed in this research: nature-based solutions have not been considered regarding salt intrusion mitigation measures to this day, focusing more on flood safety challenges (e.g., Ourloglou *et al.*, 2020; van Wesenbeeck *et al.*, 2022; Vuik *et al.*, 2016).

This is not to say that there is no—or limited—knowledge on how salt intrusion responds to estuary-scale modifications; Section 1.2.2 provides a brief overview of the extensive research addressing this topic. Despite these efforts, a cross-evaluation of the various measures and an assessment of their efficacy under different boundary conditions is lacking (although a limited analysis has been performed by Veerapaga *et al.*, 2020). Note that the scope of such an “assessment” exceeds the physical perspective; socio-economic as well as ecological perspectives are as relevant (e.g., van Slobbe *et al.*, 2013). Aside from a lack of such multidisciplinary evaluations regarding salt intrusion measures, socio-economic and ecological assessments are generally of a qualitative nature; e.g., the use of hard-to-quantify ecosystem services to address (beneficial) side-effects (e.g., Galván *et al.*, 2021; Landuyt *et al.*, 2013).

Thus, there is both a lack of potential nature-based solutions to mitigate salt intrusion; and a lack of multidisciplinary, quantitative assessment metrics for nature-based solutions.

1.3 Research objective

The objective of the research as presented in this dissertation coincides with its title, namely **developing nature-based solutions to mitigate salt intrusion**. At the core of this objective, there is the implicit hypothesis that such solutions exist. This is, however, by no means trivial. By exploring potential nature-based solutions to mitigate salt intrusion, this implicit hypothesis is tested simultaneously.

The general research objective is divided into four sub-objectives:

- I. Explore the potential impact of estuary-scale modifications on salt intrusion.
- II. Conceptualise various nature-based solutions to mitigate salt intrusion.

III. Evaluate nature-based solutions in a multidisciplinary context.

IV. Reflect on the role of nature-based solutions with future uncertainties.

Every research objective is addressed in the equally-labelled parts of this dissertation (Sec. 1.4).

1.4 Dissertation structure

The structure of this dissertation follows the *Building with Nature*-approach, which can be characterised by four consecutive phases:

- I. **Exploration**—The *exploration*-phase aims at understanding the system, or becoming familiar with the system's processes.
- II. **Conceptualisation**—The *conceptualisation*-phase constitutes the design of potential nature-based solutions, which build upon the knowledge of the system.
- III. **Evaluation**—The *evaluation*-phase resembles the assessment of the drawn nature-based solutions on a multidisciplinary level.
- IV. **Reflection**—The *reflection*-phase critically deliberates the objectives and achievements from which lessons are drawn.

This structure including the chapters of this dissertation are schematised in Figure 1.3.

The exploration of potential nature-based solutions to mitigate salt intrusion consists of an extensive sensitivity analysis using hydrodynamic models. Due to the focus on salt intrusion, three-dimensional models are required, which puts a substantial burden on the computational costs associated with such an analysis. A full, brute-force exploration of salt intrusion responses to the main estuary-scale parameters would therefore become computationally infeasible. In Chapter 2, a novel approach is described to enable explorations with computationally expensive models. Subsequently, Chapter 3 presents the results of the performed sensitivity analysis. The results of the extensive sensitivity analysis accomplish the first objective, and form the basis for the *conceptualisation*-phase.

The conceptualisation of potential nature-based solutions to mitigate salt intrusion includes two studies: (1) placement of a temporary, earthen sill (Ch. 4); and (2) enhancement of intertidal area (Ch. 5). The spatial and temporal scales at which these solutions operate deviate substantially: the sill is a local, short-term measure; enhancing the tidal flats is a large-scale, semi-permanent intervention. Thereby, the wide spectrum of possibilities is loosely defined. Although not all-encompassing, Chapters 4 and 5 address the second objective on nature-based solutions to mitigate salt intrusion.

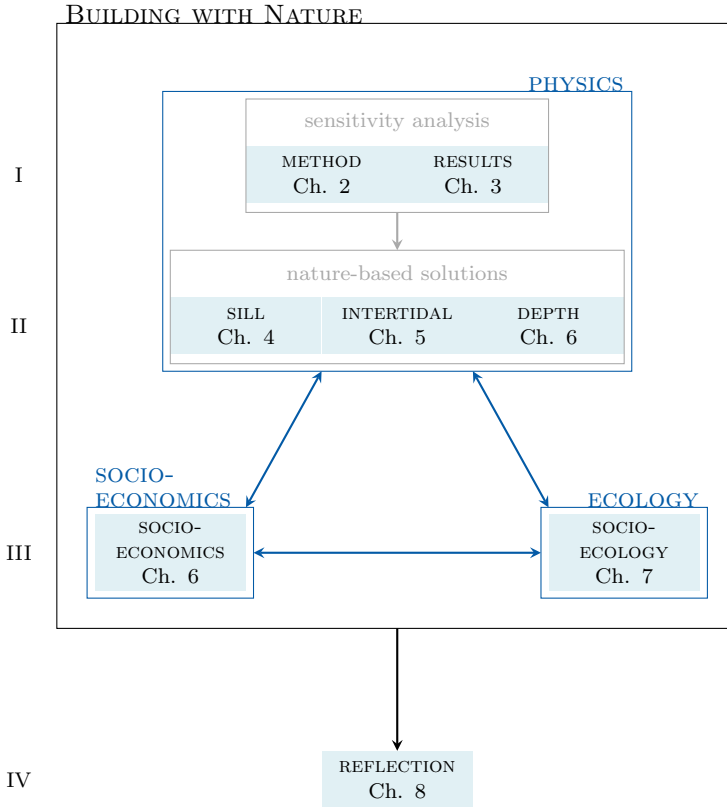


Figure 1.3: Dissertation structure. The three perspectives of the *Building with Nature*-philosophy are reflected in this dissertation’s structure.

The evaluation of potential nature-based solutions to mitigate salt intrusion addresses both a socio-economic (Ch. 6), and a socio-ecological evaluation (Ch. 7). In addition to the physical relevance and complexity of salt intrusion mitigation measures, these chapters highlight and discuss the non-physical perspectives. By providing quantitative methods, Chapters 6 and 7 propose suggestions satisfying the third objective.

At last, the reflection on nature-based solutions to mitigate salt intrusion results in taking a step back: First, by critically reflecting on the future of nature-based solutions (Ch. 8); and subsequently, more specifically focused on nature-based solutions to mitigate salt intrusion (Ch. 9), i.e., this dissertation. This critical reflection—especially Chapter 8—examines the fourth and last objective.

Note that Chapters 2 to 8 are written as stand-alone journal articles. Therefore, some concepts are repeated.

I | EXPLORATION

The aim of the *exploration*-phase is to understand the estuarine system with the focus on how estuarine salt intrusion responds to changes in the estuary's boundary conditions and geomorphology. Thus, the objective is to *explore the potential impact of estuary-scale modifications on salt intrusion*.

This is achieved by an extensive sensitivity analysis of the estuarine salt intrusion to estuary-scale modifications. As such a sensitivity analysis is computationally demanding, Chapter 2 first describes a novel method to explore the output space—i.e., salt intrusion length—with reasonable computational costs. Subsequently, Chapter 3 analyses this output space from a physical perspective. In essence, Chapters 2 and 3 can be considered parts one and two of the same study.



SENSITIVITY ANALYSIS Method

2.1 Introduction

In recent years, the effects of climate change have become more apparent (e.g., Harley *et al.*, 2006; Veldkamp *et al.*, 2015; Vörösmarty *et al.*, 2000; Walther *et al.*, 2002) and with it the need for preparing for the unknown: Natural systems venture out to extremes often absent from the records. Examples of such extremes include the recent droughts in northwestern Europe caused by an extremely low river discharge in the Rhine (Toreti *et al.*, 2022); the increased frequency of mass coral bleaching events recorded over the past decades (Hughes *et al.*, 2018); and the so-called *Black Summer* of 2019/2020 during which an exceptionally large area of Australia's southeast coast was consumed by wildfires (Collins *et al.*, 2021).

This chapter is based on:

Hendrickx, G.G., Antolínez, J.A.A., and Herman, P.M.J. (2023). Predicting the response of complex systems for coastal management. *Coastal Engineering*, **182**:104289.

In addition, sea level rise shifts whole coastlines to new territories and possible modified system responses, as new areas might get inundated.

These changing conditions challenge risk management practices (van Berchum *et al.*, 2019) and require the revision of adaptation and mitigation strategies (Haasnoot *et al.*, 2014). Therefore, explorations to map the impacts of these changing conditions on current land-use as well as determining future-proof socio-ecological systems are necessary. Key in such studies is to achieve a system understanding. While surveying and monitoring often provide insightful knowledge, in this phase, numerical models are a necessity to predict system responses to unseen forcing, socio-economic boundary conditions, and/or human interventions.

This system understanding can be achieved by means of a sensitivity analysis of the system's response to changing conditions; this may include the boundary conditions as well as the geomorphological characteristics. In addition, a proper parameterisation of the physical system and processes in the numerical model is key and non-trivial. Consequently, sensitivity analyses often require experimental designs that rely on a large number of samples. Examples are those following factorial sampling (e.g., Wang *et al.*, 2020) or Monte Carlo sampling (e.g., Saltelli, 2002; Saltelli *et al.*, 1999).

In practice, large experimental designs could be accomplished by running a large number of numerical simulations, often impractical if they were set-up with complex, and thus computationally expensive, hydraulic engineering numerical models, e.g., Delft3D Flexible Mesh (DFM; Kernkamp *et al.*, 2011) or Finite-Volume Community Ocean Model (FVCOM; Chen *et al.*, 2013). Therefore, executing such analyses would result in a computationally infeasible task (Saltelli, 2002).

Traditionally, hydraulic engineers have addressed this problem by (1) developing a series of model reduction techniques; and (2) acceleration of the direct simulations. Regarding model reduction techniques, common practices are:

1. the use of statistical downscaling, for example, to develop parameterisations of physical processes (e.g., Bruun, 1954; Stockdon *et al.*, 2006), or to infer the response of coastal systems to larger scale forcing (e.g., Anderson *et al.*, 2018; Antolínez *et al.*, 2018);
2. the development of behavioural models that combine multiple physics-driven statistics using basic knowledge principles, for example shoreline models (e.g., Antolínez *et al.*, 2019; Ashton *et al.*, 2001; Kragtwijk *et al.*, 2004); and
3. the simplification of numerical models by neglecting certain physical processes in favour of faster running times of which the hydrostatic assumption is the most broadly used in hydrodynamic models (default settings in, e.g., DFM and FVCOM; Chen *et al.*, 2013; Kernkamp *et al.*, 2011).

Regarding the acceleration of the direct simulations, these are often achieved by: (1) developing acceleration techniques (de Vriend *et al.*, 1993; Luijendijk *et al.*, 2019), and (2) using input reduction techniques (Antolínez *et al.*, 2016; Hendrickx *et al.*, 2021; Latteux, 1995; Walstra *et al.*, 2013).

In addition to these reduction techniques, the use of computationally expensive models generally rely on expert judgement to decide the limited number of simulated samples (e.g., Ralston *et al.*, 2010a; Warner *et al.*, 2005); the most efficient reduction technique remains limiting the number of simulations. However, sampling based on expert judgement limits the investigation to the expected: exploring unknown territories is computationally too expensive and therefore discouraged. On the other hand, simplified models limit the output to the assumptions made due to the simplifications (e.g., Kuijper & van Rijn, 2011; MacCready, 1999), which might result in essential processes to be overlooked. Ideally, process-based models can be used for exploratory research of complex systems without skyrocketing computational costs.

Currently, hybrid experimental designs are being adopted to perform larger numbers of simulations (e.g., Bakker *et al.*, 2022; Camus *et al.*, 2011). This so-called Hybrid Downscaling (HD) often contains the following three phases: (1) the sampling of representative input or boundary conditions (Athanasiou *et al.*, 2021; Scott *et al.*, 2020); (2) the simulation of these samples in a numerical model; and (3) the augmentation of the modelled output for the whole input space, which is either achieved statistically (e.g., Rueda *et al.*, 2019; Scott *et al.*, 2020) or using machine learning techniques (e.g., Athanasiou *et al.*, 2022; Itzkin *et al.*, 2022).

Most of the selection schemes deployed in HD select samples in an input space without knowing information about the (often non-linear) response of the system (e.g., Latin hypercube sampling [McKay *et al.*, 1979]; maximum dissimilarity algorithm [Kennard and Stone, 1969]; self-organising maps [Kohonen, 1982]). This turns into an inefficient and costly exploration (e.g., Gramacy & Lee, 2009; Ruessink, 2006). The efficiency of the exploration is expected to improve substantially when the input space considers the available information about the output space when sampling (Gramacy & Lee, 2009). Hence, to influence the selection of samples in the input space by a reduced number of model simulations, a two-step approach is required in which the input space is adaptively updated based on the known part of the output space.

In this chapter, we develop such an adaptive sampling scheme tailored to hydraulic engineering models, such as the aforementioned hydrodynamic models DFM and FV-COM. In this scheme, the sampling in the input space is influenced by the system's response at the previous selected representative samples, requiring to run the model sequentially in parallel batches, promoting a more efficient exploration.

The second phase—the numerical modelling—is executed with a process-based model: DFM (Kernkamp *et al.*, 2011). This ensures that the bias of known fitted parameters is limited when exploring unknown regions in the input space.

The last phase in HD—the augmentation—has received substantial attention over the years. Augmentation methods range from very simplistic procedures such as look-up tables or linear interpolation to more complex regression methods based on statistical and/or probabilistic models. In addition, machine learning is currently gaining popularity and has shown great potential in many fields of research, as in machine learning probability and statistics can coexist. This rise

has led to opt for the inclusion of both generative and discriminative machine learning models (Jebara, 2004), such as a treed Gaussian process, limiting linear model (TGP-LLM; Gramacy & Lee, 2009) and a neural network, respectively.

Hence, the overall aim of this chapter is to provide a methodology for gaining as much information about a complex system for the lowest computational costs. This is applied on a case study implementing the *Building with Nature*-approach. In the application, we address the question how machine learning techniques can assist in applying the *Building with Nature*-approach, i.e., developing nature-based solutions. A sensitivity analysis is at the basis of understanding the system and machine learning tools are implemented to assist in this goal.

To answer the research question, this chapter starts with a description of the proposed methodology (Sec. 2.2) after which it is applied on a case study introduced in Section 2.3: salt intrusion in estuaries. Subsequently, the implications of this newly proposed work-flow are presented and discussed in which the required sample size—or stopping rule—receives additional attention (Secs. 2.4 and 2.5, resp.). At last, the pros and cons of the simulations strategy are summarised in Section 2.6.

2.2 Method

The many available techniques introduced in Section 2.1 have been evaluated and distilled down to a five-step simulation strategy (Fig. 2.1): (1) generate candidate samples, (2) simulate an initial batch, (3) execute an adaptive sampling approach, (4) simulate reverse-predicted extremes, and (5) augment the input space. These five steps are also visualised in Figure 2.1, stating the sample sizes as used in this study. Every step and the sampling techniques used are further elaborated on in Sections 2.2.1 to 2.2.5.

2.2.1 Candidate samples

The first step is to create a dataset with candidate samples. These candidate samples were based on predefined parameter ranges, which reflected physically representative values. When generating the candidate samples, it is important to include a physical check of the samples: although the parameter ranges make physically sense, certain combinations may not. For example, a realistic river discharge of $16,000 \text{ m}^3\text{s}^{-1}$ and a realistic cross-sectional area of $2,500 \text{ m}^2$ result in an unrealistically high river flow velocity of 6.4 ms^{-1} . By applying physical checks—and subsequently using the resulting candidate samples—the physical correctness of the parametric design is enforced.

2.2.2 Initial batch

The second step is to create—and simulate—an initial batch to initiate the subsequent adaptive sampling routine. In this study, the Maximum Dissimilarity Algorithm (MDA; Kennard & Stone, 1969) was used to do so, as it best explores

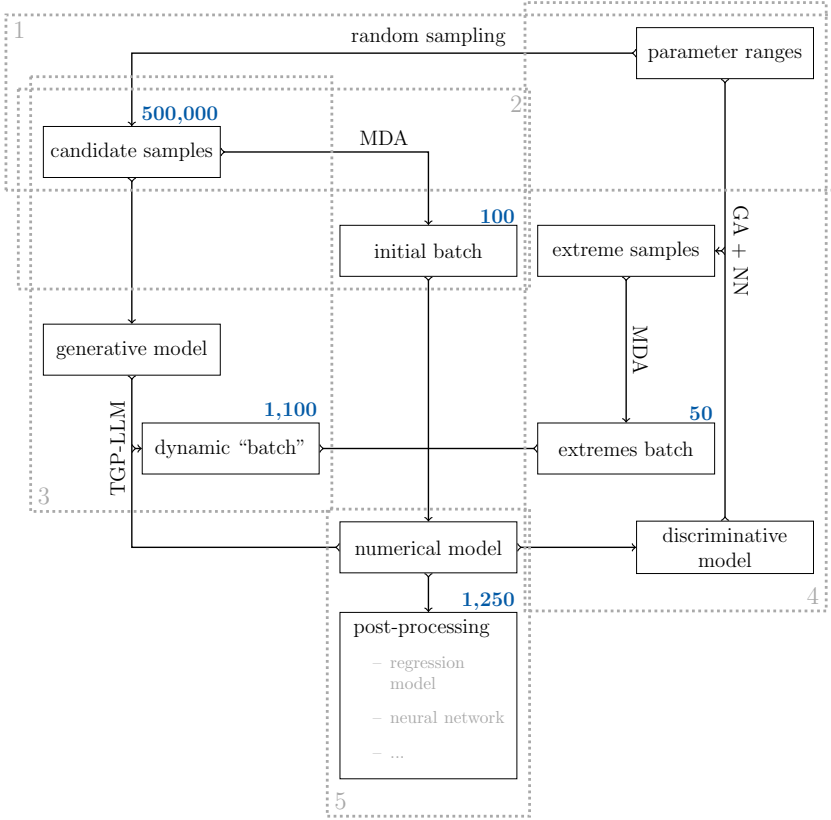


Figure 2.1: Flowchart of the five-step simulation strategy. The numbers reflect the steps of the simulation strategy: (1) generate candidate samples, (2) simulate an initial batch, (3) execute an adaptive sampling approach, (4) simulate reverse-predicted extremes, and (5) post-process the data. The blue-coloured values indicate the sample sizes of the datasets. **MDA**: Maximum Dissimilarity Algorithm; **TGP-LLM**: Treed Gaussian Process, Limiting Linear Model; **GA**: Genetic Algorithm; **NN**: neural network.

the outskirts of the input space by choosing the most dissimilar samples from the candidate samples. At this stage, little is known about the response of the system, thus it is most advantageous to fully focus on exploring the input space. In this study, the initial batch contained 100 samples.

2.2.3 Adaptive sampling

The third step is most dissimilar from commonly employed sampling techniques, as in this step we used a generative model so that the selection of samples in the input space is based on the underlying distribution of the output space. In this study, the adaptive sampling was initiated by fitting a Treed Gaussian Process, Limiting Linear Model (TGP-LLM; Gramacy & Lee, 2009) to the incomplete output space resulting from the initial batch. The TGP-LLM determined the uncertainty in

the output space and suggested which samples were most likely to reduce this uncertainty (Gramacy & Lee, 2009); here, uncertainty is defined by either the greatest standard deviation (active learning-MacKay; MacKay, 1992), or by the maximum expected reduction in the averaged squared error (active learning-Cohn; Cohn, 1996). As simulating regions with high uncertainty provide the highest entropy, these regions are most interesting to investigate further. This study made use of the active learning-MacKay approach: i.e., uncertainty was defined by the largest standard deviation.

The TGP-LLM method (Gramacy & Lee, 2009) was devised to optimally select candidate samples for asynchronous calculations on a supercomputer. The core of this generative method consists of fitting Gaussian process models to the input-output relations obtained from the available runs at a particular moment in the simulation procedure. These models are continuously updated as more results come in. In order to account for heteroscedasticity as well as non-linear behaviour of the output space in different subdomains of the input space, the Gaussian process model is combined with a Bayesian tree regression. This subdivides the input space in several subdomains that show different behaviour. Based on this statistical model, new candidate samples are chosen in order to fulfil different criteria. Most emphasis is placed on areas in the input space where the input-output variance is largest, so as to lead to an optimal reduction of the variance (maximum entropy approach). However, as this selection criterion may lead to exaggerated concentration of samples in a few places only, in addition care is taken to spread the candidate samples sufficiently over the different subdomains of the input space identified by the Bayesian tree regression, as well as to the sufficient spreading of candidate samples within these subdomains, in order to conserve the exploratory nature of the algorithm. For technical details on the method, we refer to Gramacy and Lee (2009).

Only a limited number of samples was selected by the TGP-LLM based on the initial batch. Subsequently, every time a simulation was finished, the TGP-LLM was re-fitted to the updated output space to determine the next input sample(s) with the highest entropy. This continued until a predefined number of samples was simulated. In this study, 1,100 samples were generated and simulated using this adaptive approach.

2.2.4 Reverse-predict extremes

The fourth step is to search for extremes in the output space. This search was facilitated by means of a genetic algorithm (GA) for which the search for the extremes is an optimisation problem.

In order to obtain a fast tool to explore these extremes, a neural network was fitted to the available results from the MDA- and TGP-LLM-based samples. This neural network contained three hidden layers with 50 nodes each.

The implemented GA was designed such that a pool was created instead of the usual singular output. This pool consisted of output values close to the most extreme—or optimal—value. Subsequently, a set of samples was drawn from this

pool by using the MDA on the pool's unique samples. These samples were subsequently simulated to better represent the extremes in the dataset.

2.2.5 Post-processing

The last step of post-processing the data is not as straightforward due to the absence of clear planes through the output space that can be assessed. Moreover, the commonly used methods for sensitivity analyses—such as Sobol' indices (Sobol', 1993, 2001) and ANOVA (Wang *et al.*, 2020)—cannot be used due to the limited sample size.

Therefore, discriminative models have to be used over generative models that require larger datasets (Jebara, 2004). In this study we considered a neural network with the same architecture as described in Section 2.2.4 but which was retrained to the full dataset, i.e., including the GA-based samples. More details on the neural network and its training are given in Appendix A.

2.3 Case study

This case study addresses the first step of developing nature-based solutions to mitigate salt intrusion. Thereby following the *Building with Nature*-approach, which is an approach to solve hydraulic engineering-related problems from a system-level point of view by utilising the system's natural processes (de Vriend *et al.*, 2015). For that reason, the notion of *Building with Nature* has gained momentum in recent years. In the so-called nature-based solutions, the system is viewed from three perspectives: (1) physics, (2) ecology, and (3) socio-economy (van Slobbe *et al.*, 2013). This multiperspective approach results in a very demanding design process.

A challenging phase in the *Building with Nature*-design procedure is to properly understand the underlying physical processes of a natural system, and how the engineering solution will utilise those to achieve certain socio-economic and ecological benefits. This principle is at the basis of the design procedure, and thus an essential feature (e.g., Borsje *et al.*, 2011; de Vriend *et al.*, 2015; van Slobbe *et al.*, 2013).

2.3.1 Physical estuarine system

The methodology described in Section 2.2 is applied to a highly non-linear and non-stationary system to perform a sensitivity analysis: the estuary. Estuaries are complex systems largely due to the interaction of saline seawater and fresh river water. The induced density differences—albeit small—result in complex behaviour of the hydrodynamics, influencing flow structures, sediment dynamics, ecological functioning, and many other aspects (e.g., Geyer & MacCready, 2014; Olabarrieta *et al.*, 2018; Whitfield *et al.*, 2012; Zhou *et al.*, 2020b).

In this case study, the focus point is the salt intrusion length in an estuary and how this is influenced by the forcing and the estuarine geomorphology. The influence of the river discharge and water depth on the salt intrusion are well-known

Table 2.1: Input parameters including their ranges and units (based on Dronkers, 2017; Leuven *et al.*, 2019; Savenije *et al.*, 2008). Figure 2.2 provides visual support of the input parameters. More information about the definitions of the input parameters and the physical restrictions are provided in Appendices B.1 and B.2.

	Parameter	Symbol	Range	Unit
Forcing	Tidal range	a	1.0–5.0	m
	Storm surge level	η_s	0.0–2.0	m
	River discharge	Q	100–16,000	$\text{m}^3 \text{s}^{-1}$
Geomorphology	Channel depth	d_c	5.0–25.0	m
	Channel width	W_c	500–3,000	m
	Channel friction	n_c	0.01–0.05	$\text{m}^{-1/3}\text{s}$
	Flat depth ratio ^a	r_d	–1–1	–
	Flat width	W_f	0–3,000	m
	Flat friction	n_f	0.02–0.05	$\text{m}^{-1/3}\text{s}$
	Convergence	γ	25–1.0	$\times 10^{-5} \text{m}^{-1}$
	Bottom curvature	κ_c	0.0–6.0	$\times 10^{-5} \text{m}^{-1}$
	Meander amplitude	A_m	0–6	km
Meander length	L_m	0–100	km	

^a The flat depth is defined as the product of the flat depth ratio and the tidal range: $d_f = \frac{1}{2} r_d a$. Thereby ensuring that the tidal flats are at all times exposed and flooded during a tidal cycle, i.e., following the definition of a tidal flat.

(e.g., Chatwin, 1976; Hansen & Rattray Jr., 1965; MacCready, 2007; Monismith *et al.*, 2002): negative and positive, respectively. Furthermore, the tide enhances the mixing of the water column and thereby influences the salt intrusion (e.g., MacCready & Geyer, 2010; Simpson *et al.*, 1990). Other geomorphological features have also been investigated separately, such as the bottom curvature (Nunes & Simpson, 1985), tidal flats (Zhang *et al.*, 2012), and meandering (Pein *et al.*, 2018). All in all, many factors influence the salt intrusion length, generally in a non-linear fashion, and Table 2.1 summarises the input space used in this study.

Furthermore, estuaries behave differently based on their class—or type. Such classifications are often linked to the stratification of the system, and how this changes over a tidal cycle, as this largely determines the governing processes in an estuary (e.g., Dijkstra & Schuttelaars, 2021). The mapping of estuaries by Geyer and MacCready (2014) considers two non-dimensional variables in defining such a mapping, which is used in this study as indication of the distribution over the input space.

The two non-dimensional variables are a mixing parameter (M , Eq. 2.1) and the freshwater Froude number (Fr_f , Eq. 2.2), which are indicative for the balancing forces in an estuary: mixing and stratification, respectively (Geyer & MacCready, 2014).

$$M = \sqrt{\frac{c_f u_t^2}{\omega_t N d_c^2}} \quad (2.1)$$

with

$$\begin{aligned} c_f &= \frac{gn_c^2}{d_c^{1/3}} \\ u_t &= \frac{1}{2\sqrt{2}} \sqrt{\frac{g}{d_c}} a \\ N &= \sqrt{\frac{g\beta s_0}{d_c}} \end{aligned}$$

where c_f is the non-dimensional friction coefficient [-]; u_t the tidal flow velocity [ms^{-1}]; ω_t the tidal frequency [s^{-1}]; N the buoyancy frequency [s^{-1}]; d_c the channel depth [m]; and n_c the friction coefficient, defined as Manning's n [$\text{m}^{-1/3}\text{s}$]. In addition, there are three constants included: g is the gravitational acceleration [$g = 9.81 \text{ ms}^{-2}$]; β the haline contraction coefficient [$\beta = 7.6 \times 10^{-4} \text{ psu}^{-1}$]; and s_0 the oceanic salinity [$s_0 = 30 \text{ psu}$].

$$Fr_f = \frac{Q}{W_c d_c c_i} \quad (2.2)$$

with

$$c_i = \sqrt{d_c g \beta s_0}$$

where Q is the river discharge [m^3s^{-1}]; W_c the channel width [m]; and c_i the maximum frontal propagation speed, or internal celerity [ms^{-1}].

Note that not all parameters of the input space are included in this mapping (Tab. 2.1); this mapping does not address the occurrence of tidal flats or meandering of the estuary. Although it is not complete, the M, Fr_f -space by Geyer and MacCready (2014) provides good insights into the distribution of the data over the input space. For visual inspections, scatter plots of the distribution of input, output, and these non-dimensional parameters are included in Figure B.1 (p. 202).

2.3.2 Numerical experimental design

The simulations are performed using the Delft3D Flexible Mesh hydrodynamic modelling software (Kernkamp *et al.*, 2011), where the model configurations are implemented by means of a parametric design. This software is a state-of-the-art process-based model that solves the Reynolds-averaged Navier-Stokes equations assuming hydrostatic pressure and using a k - ε turbulence closure. Due to the focus on the salt dynamics, the simulations are carried out in three dimensions resulting in substantial computational costs.

The parametric design of the estuary follows an idealised geomorphology in which thirteen input parameters are reflected (Fig. 2.2): three forcing conditions and ten geomorphological features (Tab. 2.1). These thirteen parameters are considered governing for the system investigated and are based on literature, as listed in Section 2.3.1 and Table 2.1. When a sparse factorial set of samples would have been used, almost 1.6 million ($N = 3^{13}$) simulations would have been required for the sensitivity analysis. In this study, approximately 1,250 simulations were

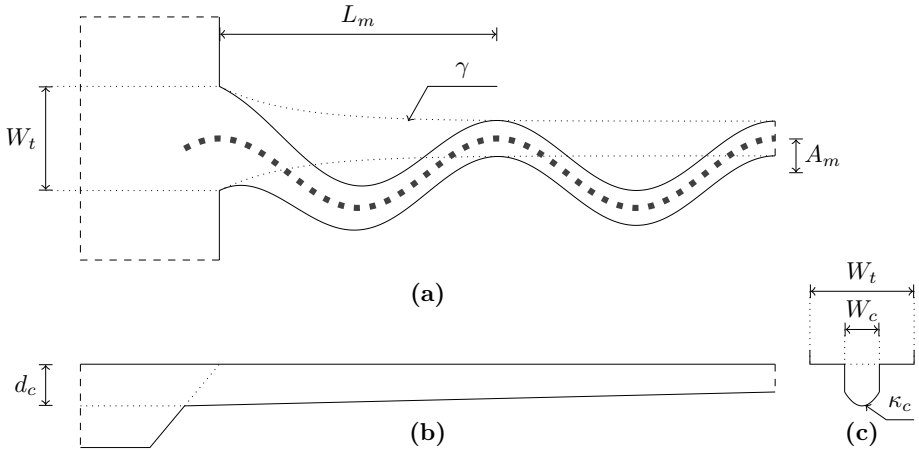


Figure 2.2: Parametric model design zoomed-in near the estuary mouth. (a) Plan view; (b) longitudinal cross-section; and (c) lateral cross-section. The meaning of the symbols are presented in Table 2.1, except for W_t : This is the total width, i.e., $W_t = W_c + W_f$. The grey dots show the location of the “virtual stations” used for the output definitions (Eqs. 2.3a and 2.3b).

performed, where the sample size was in part based on economic considerations but extensively validated afterwards (Sec. 2.5).

Because the case study encompasses a real physical system, there are some restrictions to parameter combinations, which result in dependencies between input parameters. Despite these dependencies, the restrictions are considered relaxed enough to provide enough space for every input parameter to move freely within its range. In essence, the restrictions function as a reduction of the input space required to explore. It does, however, also complicate the analyses by potential false cause-and-effect relations by showing a relation between an input parameter and the output space, while the real driving force is another input parameter. Therefore, one must remain cautious when analysing the data and keep the defined restrictions in mind.

More details on the parametric design and the physical restrictions are presented in Appendices B.1 and B.2, respectively.

The output of the simulations is defined in two dimensions: (1) the salt intrusion length, \mathcal{L} ; and (2) the salt variability, \mathcal{V} . These output variables are extracted from the model output data, which contains a longitudinal cross-section that follows the centre of the channel (dotted line in Fig. 2.2).

The salt intrusion length is defined as the distance from the mouth at which the depth-averaged salinity equals 1 psu, averaged over the tidal cycle. The salt variability is defined as the variation in salinity over a tidal cycle, i.e., the difference between the maximum and minimum salinity during a tidal cycle. This is taken as the average over the estuarine domain, using “virtual stations” every 625 metres (in x -direction). These definitions of the salt intrusion length (\mathcal{L}) and salt variability

(\mathcal{V}) can be expressed as follows:

$$\mathcal{L} \equiv \overline{\delta(\langle s \rangle = 1 \text{ [psu]})} \quad (2.3a)$$

$$\mathcal{V} \equiv \frac{1}{J} \sum_j^J \max_T \{ \langle s \rangle_j \} - \min_T \{ \langle s \rangle_j \} \quad (2.3b)$$

where δ is the distance from the mouth [m]; $\langle s \rangle$ the depth-averaged salinity [psu]; J the number of virtual stations in the model domain; and T the tidal period [s]. The overbar in Equation (2.3a) represents tidal-averaging.

2.4 Results

The implementation of the proposed method is presented in three parts: (1) the distribution of samples for all three sampling methods employed (i.e., MDA, TGP-LLM, and GA; Sec. 2.4.1); (2) the skill of the trained neural network (Sec. 2.4.2); and (3) the progress of sampling in which the sample size of the adaptive sampling step is presented (Sec. 2.4.3), hinting towards potential stopping rules for this step. This order largely follows the work-flow introduced in Section 2.2 followed up by a reflection on the method.

Although the output space is defined by two variables (Eqs. 2.3a and 2.3b), the main focus is on the salt intrusion length (\mathcal{L} , Eq. 2.3a) due to its higher relevance and the correlation between the two output variables.

2.4.1 Sample distribution

All three sampling methods employed functioned as expected, even when considering their sampling selections in a different parameter space: Figure 2.3 shows the candidate samples and the selected samples according to the different methods. Note that the GA did not make use of the candidate samples, as it generates samples as part of its algorithm; the MDA and TGP-LLM do create subsets from the candidate samples.

The MDA-based samples were clearly well-distributed throughout the whole two-dimensional parameter space and decently covered the outlines of the cloud of candidate samples. The undiscovered regions were subsequently well-covered by the samples from the TGP-LLM, which had been able to select samples in the extremes of the parameter space as well; searching algorithms commonly tend to overlook the extremes. At last, the GA-based samples were specifically present in the *strongly stratified* estuary class, which also showed the largest salt intrusion length values (Fig. 2.4). As the GA was designed to search for the maxima in the salt intrusion length, this behaviour is as intended.

Supplementary to Figure 2.3, Figure 2.5 presents the distribution of the samples per input parameter—again, discriminating between the three implemented sampling methods. The three methods clearly show different distributions reflecting their underlying algorithms: (1) the MDA-based samples were clearly located

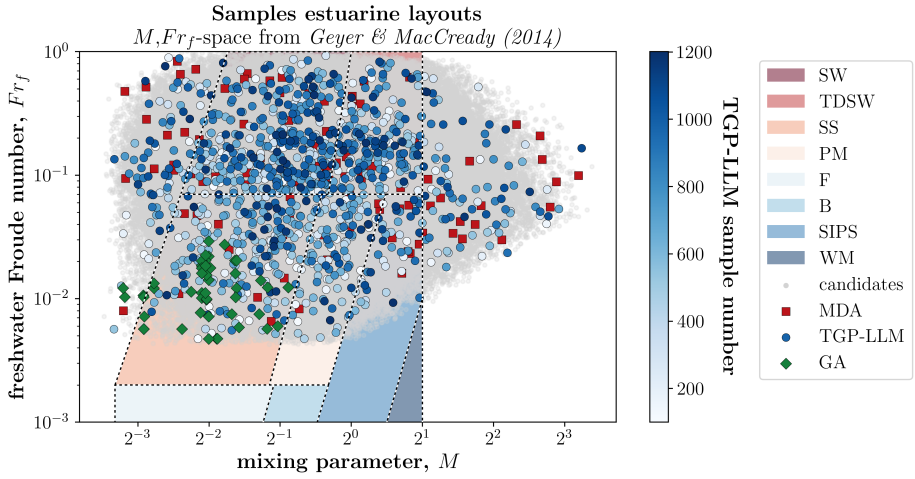


Figure 2.3: Sample distributions with respect to the estuarine classification diagram by Geyer and MacCreedy (2014). SW: salt wedge; TDSW: time-dependent salt wedge; SS: strongly stratified; PM: partially mixed; F: fjord; B: bay; SIPS: strain-induced periodic stratification; WM: well-mixed; MDA: maximum dissimilarity algorithm; TGP-LLM: treed Gaussian process, limiting linear model; GA: genetic algorithm.

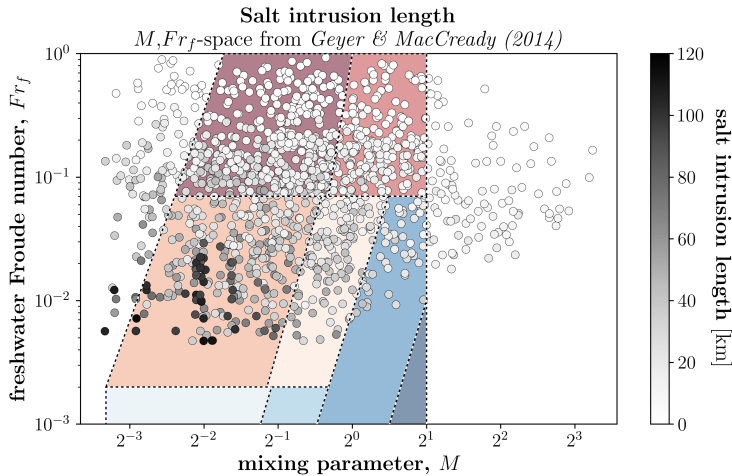


Figure 2.4: Salt intrusion length with respect to the estuarine classification diagram by Geyer and MacCreedy (2014). Shading of estuarine classes as in Figure 2.3.

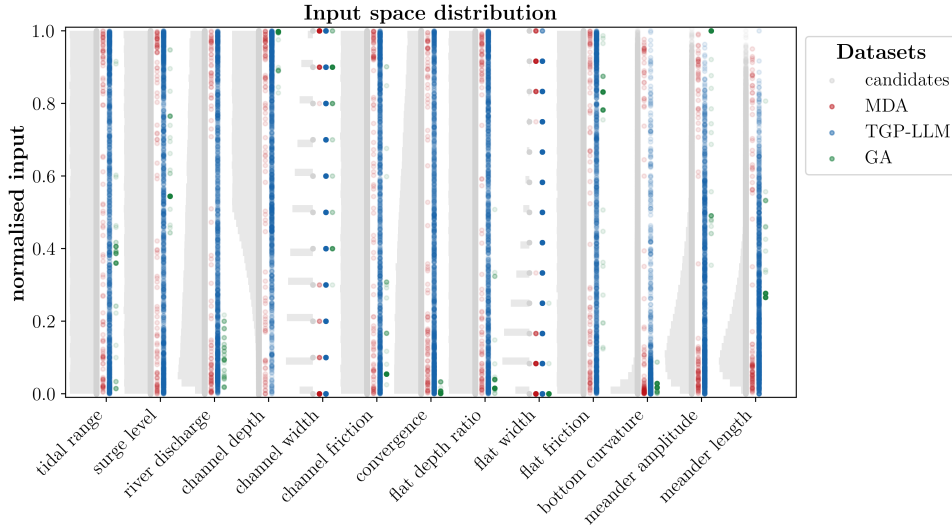


Figure 2.5: Sampling distributions per input parameter and sampling method. The input parameters are normalised with a min-max scaling, where the ranges are as presented in Table 2.1.

at the extremes of the input space; (2) the TGP-LLM covered almost the whole input space with samples; and (3) the GA-based samples are located in the extremes of certain input parameters known to be of relevance for the salt intrusion length, such as the channel depth and the river discharge. As the GA was designed to search for extremes in the output space, this clustering of samples in the extremes of certain input parameters suggests a strong relation between these input parameters and the output. However, it is important to keep possible false cause-and-effect relations in mind when analysing the GA-based samples in Figure 2.5.

2.4.2 Neural network performance

The neural network as introduced in Section 2.2.4 was trained to both output variables. The final neural network—as part of the last step (Sec. 2.2.5)—resulted in a great fit: salt intrusion length has $R_{\mathcal{L}}^2 = 0.9912$; and for salt variability $R_{\mathcal{V}}^2 = 0.9582$ (Fig. 2.6).

The neural network was trained both in steps 4 and 5 of the method (Secs. 2.2.4 and 2.2.5) by splitting the available data in a training dataset (80%) and a testing—or validation—dataset (20%). The neural network only used the training dataset to train during which the testing dataset was never shown. Subsequently, the testing dataset was used to determine the performance of the neural network; this was done to prevent over-fitting of the neural network to the data. More information on the training of the neural network can be found in Appendix A.

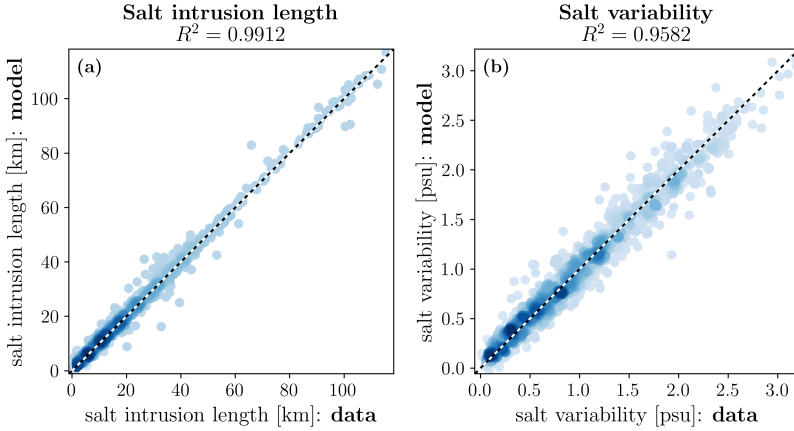


Figure 2.6: Data fit of the neural network to both output variables: (a) salt intrusion length; and (b) salt variability. The shading reflects the density of data points, where density increases with darkness.

2.4.3 Sample size

As the dataset grew, more data became available to train the neural network, hence the neural network improved its capabilities to represent the underlying relations. However, the extent of adaptive sampling to reach a satisfactory dataset remained an open end.

To analyse the progress of system understanding as the dataset grows, neural networks were trained at intervals of 100 samples. Note that the initial batch that contained 100 samples was drawn using only the MDA and was the starting point of the adaptive sampling. The intermediate neural networks were used to predict two types of samples: (1) randomly selected from the first 1,202 samples, i.e., excluding the GA-based samples; and (2) the GA-based samples, reflecting the (expected) extremes in the output space.

As shown in Figure 2.7a, recording the progress of the intermediate neural networks by means of a random selection is not informative: the neural network trained with 100 samples (i.e., MDA only) was already capable of predicting the simulated outputs quite well (black dots in Fig. 2.7a).

However, when looking at extreme values (Fig. 2.7b), a neural network trained on a larger dataset showed substantial better predictive power, where the predictions seem to converge after a dataset of around 800 samples. Although the predictions were not fully in line with the ground truth (black dots in Fig. 2.7b), a larger dataset was better capable of indicating that there are extreme output values, while unable to predict the variance present in the extreme output space. The addition of the GA-based samples to the dataset resulted in a substantial improvement, which is to be expected as these samples are representative for extremes in the output space. This improvement in predictive power of the neural network due

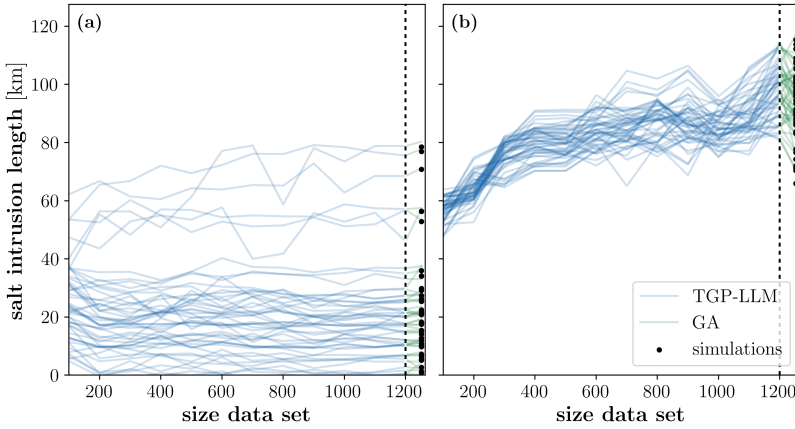


Figure 2.7: Progress of predictive power of neural networks based on size of dataset. (a) Randomly selected samples with average output values; and (b) samples with extreme output values, i.e., sampled with the genetic algorithm.

to the GA-based samples is presented by the green lines in Figure 2.7b—right of the dashed line.

2.5 Discussion

This study aimed at gaining as much information about a complex system against the lowest computational costs. The resulting methodology provides a good understanding of such a complex system, namely salt intrusion in an estuary, while keeping the computational costs manageable.

For the comparison of computational efficiency, the minimum number of samples as stated by Wang *et al.* (2020) is used because the sample size is clearly defined. Sample sizes for, e.g., eFAST (Saltelli, 2002) or Sobol indices (Sobol', 1993) largely depend on the number of samples used for the Monte Carlo simulations, which are part of these methods. This introduces subjectivity to the chosen sample size, which makes them less suitable for such a comparison.

According to Wang *et al.* (2020), the number of samples for the sensitivity analysis with thirteen input parameters equals $N \geq 3^{13} = 1,594,323$, representing a sparse factorial input space. In contrast, the sample size used in this study equals only $N = 1,252$, which is a tremendous reduction in simulations, hence computational costs; more precisely, it is just shy of 0.08% of the samples in the factorial approach. Even though the application of the TGP-LLM creates computational overhead, this does not outweigh the removal of computational costs by reducing the sample size; the most efficient computational costs reduction remains shrinking the sample size. Furthermore, the implementation of the MDA and GA add a negligible computational overhead to the total costs.

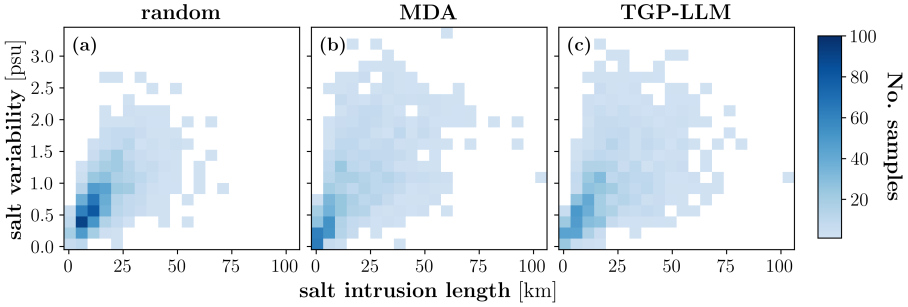


Figure 2.8: The coverage of the two-dimensional output space for three sampling methods: (a) random sampling, (b) MDA, and (c) TGP-LLM. Note that the datasets are of equal size and the samples derived with the GA are not included in (c) but the initial, MDA-based batch is. The output spaces are generated with the neural network for compatibility.

Although the MDA is substantially cheaper than the TGP-LLM and is able to explore the input space well, it has a smaller coverage of the output space (Fig. 2.8b and c). It does, however, cover more of the output space compared to, e.g., random sampling (Fig. 2.8a). Furthermore, the MDA is a non-adaptive selection method—i.e., solely based on the input space—, while the TGP-LLM draws samples based on the output space. This principle has benefits on itself: The aim of the MDA is to explore the input space, while the TGP-LLM aims to “understand” the output space.

Despite almost completely diminishing the sample size compared to the aforementioned methods, the large coverage of the samples allows for a good system understanding (Fig. 2.3). This is further enhanced by using a neural network to augment the output space. This augmentation step is crucial as it greatly enhances the understanding of a complex system without the need for additional expensive numerical model simulations.

The relevance of simulating the extremes in the output space for the performance of the neural network becomes apparent from Figure 2.7. However, it also raises the question whether to wait for so many (expensive) numerical model simulations to apply the genetic algorithm—especially when analysing Figure 2.9. Figure 2.9 shows a similar figure as Figure 2.7 with the major difference being the addition of the GA-based samples to the dataset before training the intermediate neural networks. The result is a tremendous improvement of all intermediate neural networks in their predictive power, also for extremes in the output space.

However, analysing solely Figure 2.9 would result in the misleading conclusion that there was no need for more than 150 simulations, i.e., the MDA- and GA-based samples. In addition to the fact that a data fit improves with more data, training the neural network with a small dataset shows substantial inconsistencies in its predictions, which is clearly shown in Figure 2.10. The shading around the training error represents the spreading of the root-mean-squared-error during training, which is indicative for the inconsistency of the predictions; the predictions become more consistent with increasing size of the datasets used (Fig. 2.10).

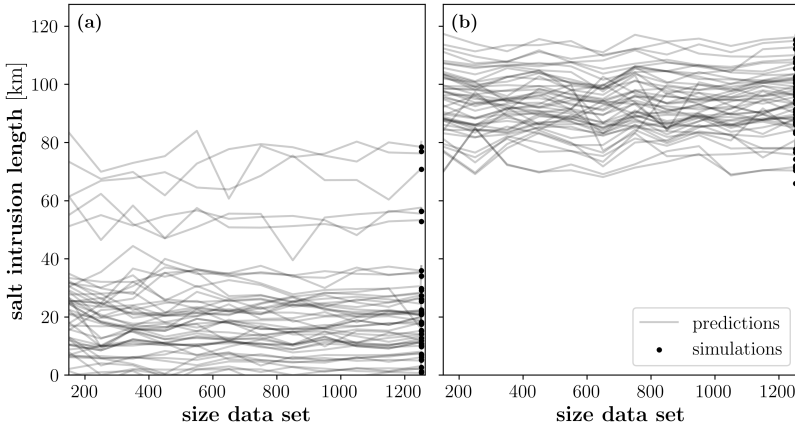


Figure 2.9: Progress of predictive power of neural networks based on size of dataset, where the samples derived with the genetic algorithm are included at every step. (a) Randomly selected samples with average output values; and (b) samples with extreme output values, i.e., sampled with the genetic algorithm.

Furthermore, the GA-based samples that cause such a performance boost in Figure 2.9b are drawn using a neural network trained with 1,202 samples. However, this information is not available during the adaptive sampling and, therefore, cannot be used.

Nevertheless, the genetic algorithm could have been employed at an earlier stage, resulting in a similar predictive power of the final neural network. This conclusion could also be drawn from looking at Figure 2.3, where the last 100–200 samples seem to be concentrated in already densely populated areas in the input space; and from Figure 2.7b, where the predictions of the intermediate neural networks seem to converge after approximately 800 samples.

Furthermore, the neural networks trained with smaller datasets are already able to detect the regions in the input space with extreme values in the output space. This is reflected by Figure 2.11 in which the implementation of the GA with the intermediate trained neural networks all favour samples located at low values of the mixing parameter (M) and freshwater Froude number (Fr_f), which result in the largest salt intrusion length (Fig. 2.4).

However, the GA-pools generated with smaller datasets (1) show a wider spreading, which can be traced back to the inconsistent predictions presented in Figure 2.10; and (2) include samples from regions with lower values of the salt intrusion length, as shown by Figure 2.4. In addition, the estimates of salt intrusion length determined by the intermediately trained neural networks increases with increasing size of the dataset used (Fig. 2.11).

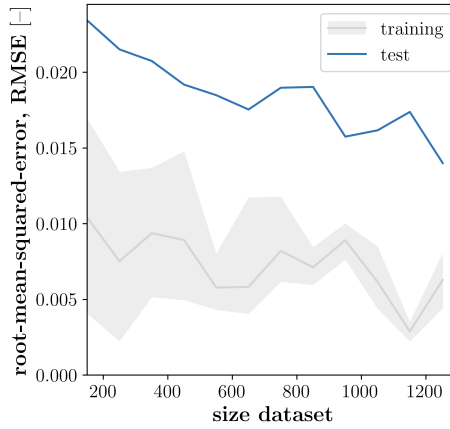


Figure 2.10: Uncertainty in predictions of intermediate neural networks. Training datasets constitute for 80% of the size, and the remaining 20% are used for testing. Gray-shading indicates the spreading in RMSE over the last ten epochs of the training.

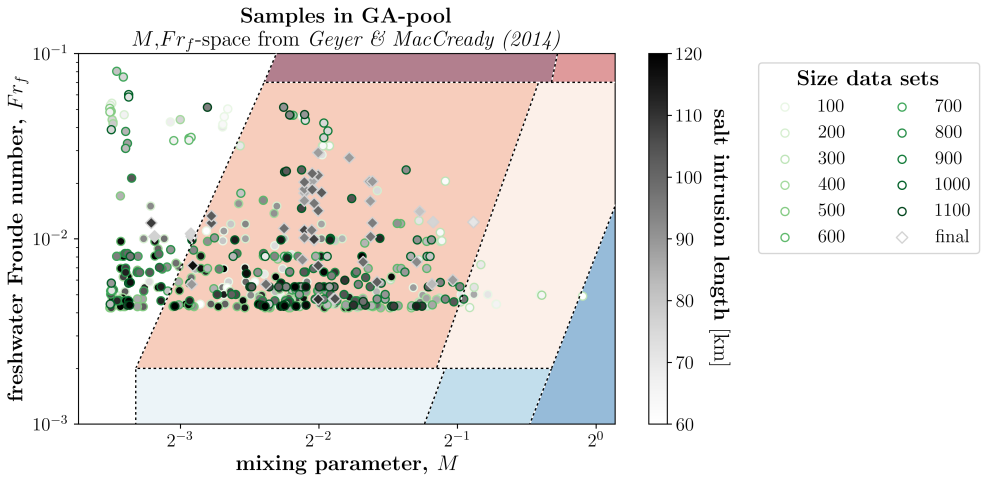


Figure 2.11: Samples in the GA-pool determined with the intermediate trained neural networks overlaid on the estuarine classification diagram by Geyer and MacCready (2014). Shading of estuarine classes as in Figure 2.3. The grey-shading reflects the salt intrusion length, and the edge-colour the size of the datasets

2.6 Conclusion

The proposed simulation strategy mainly focuses on the first and last steps of hybrid downscaling—namely the sampling and the augmentation—, while implementing an expensive, process-based numerical model for the second step: the simulations. The strategy has achieved a major reduction in computational costs by making informed choices in the selection of samples to simulate. Subsequently, the augmentation is facilitated by means of a neural network, which shows to reliably predict the highly non-linear output space (Fig. 2.6).

In the case study addressed in this study, the extremes in the output space have a substantial effect on the level of system understanding achieved (Figs. 2.7 and 2.9). Therefore, the simulation strategy is expected to be improved by employing the genetic algorithm at an earlier stage, or on multiple occasions at certain intervals. However, a sufficiently large dataset is required to reliably train a neural network—or fit another data-driven model—to be used in the objective function of the genetic algorithm, as illustrated by Figure 2.10.

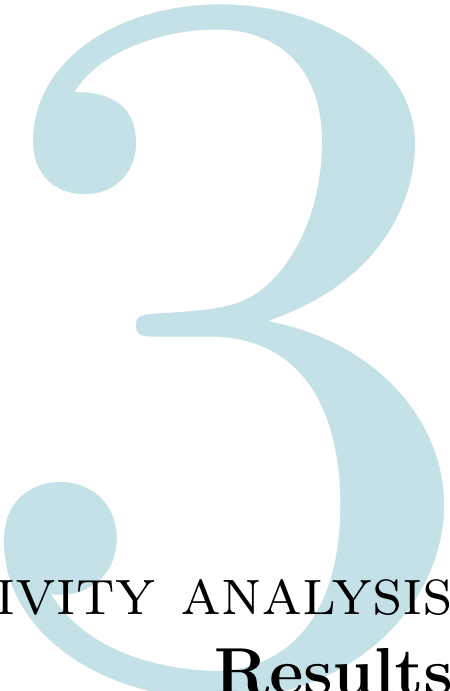
Reflecting on the aim of this study (Sec. 2.1), this chapter has shown the potential of techniques from machine learning for hydraulic engineering practices, with a special focus on enabling the *Building with Nature*-approach. Sensitivity analyses are a useful method to gain insights into the system's behaviour, but generally require large amounts of samples, i.e., simulations. Due to the complexity of models in the field of hydraulic engineering, this often results in computationally infeasible studies: a challenge complicating the evaluation of adaptation and mitigation strategies. This study has shown that hybrid downscaling with techniques from machine learning enables the execution of enlightening sensitivity analyses to come within computational reach. The approach facilitates exploratory studies essential for the development of future-proof socio-ecological systems, especially in light of unknown system states resulting from climate change.

Acknowledgements. We are indebted to Ariana Torres (SURF) for her support in the development of the computational manager for the many simulations executed. This work used the Dutch national e-infrastructure with the support of the SURF Cooperative using grant no. EINF-1548. At last, we would like to thank the two anonymous reviewers for their valuable feedback on the manuscript.

Author contributions. G.H., J.A., P.H. designed the research; G.H. performed the research; G.H., J.A., P.H. analysed the data; G.H., wrote the manuscript; and G.H., J.A., P.H. reviewed the manuscript.

Data availability. The dataset used in this study is publicly available as NEESI: Numerical Experiments of Estuarine Salt Intrusion dataset (Hendrickx, 2023a).

Software availability. The trained and implemented neural network is open-access, named ANNESI (Artificial Neural Network for Estuarine Salt Intrusion; Hendrickx, 2022).

A large, light blue, stylized number '3' is positioned in the background, partially overlapping the title text. The number has a thick, rounded stroke and a decorative swirl at the top.

SENSITIVITY ANALYSIS Results

3.1 Introduction

Around the world, estuarine regions are among the most populated areas with approximately 1.2 billion people living within 100 km from the coastline (Small & Nicholls, 2003). These regions heavily rely on the supply of freshwater from the river systems, which can salinise due to their closeness to the sea (Costall *et al.*, 2018). Currently, water stress—i.e., the unavailability of freshwater—is a global issue (Mekonnen & Hoekstra, 2016), and it is most profound in these coastal regions (Wada *et al.*, 2011). Unsustainable groundwater abstraction is already occurring worldwide (Wada *et al.*, 2010), which is a clear indicator of the current water stress.

This chapter is based on:

Hendrickx, G.G., Kranenburg, W.M., Antolínez, J.A.A., Huismans, Y., Aarninkhof, S.G.J., and Herman, P.M.J. (2023). Sensitivity of salt intrusion to estuary-scale changes: A systematic modelling study towards nature-based mitigation measures *Estuarine, Coastal and Shelf Science*, **295**:108564.

The severity of water stress will likely increase due to climate change (e.g., Distefano & Kelly, 2017; Veldkamp *et al.*, 2015) by means of (relative) sea level rise and increased frequency and duration of droughts. Both will enhance the salt intrusion and so further reduce the availability of freshwater in estuarine regions. In addition, while the supply of freshwater is threatened due to climate change, the demand will grow due to the expected increase in population density in coastal regions (Small & Nicholls, 2003).

Freshwater challenges due to salt intrusion via surface water can be mitigated by means of hard measures, such as dams and locks. However, these measures have many negative side-effects, e.g., blockage of the river flow and disturbance of the environment. This has resulted in the motivation for this study: Are nature-based solutions to mitigate salt intrusion a viable substitute for their hard counterparts?

Nature-based solutions follow the *Building with Nature*-approach (de Vriend *et al.*, 2015) in which there is special attention for the system as a whole. Note that such a system extends beyond the physical domain as it also includes the ecological and socio-economic perspectives (van Slobbe *et al.*, 2013).

Because nature-based solutions attempt to utilise natural processes, they are commonly more resilient to changes in the boundary conditions and can adapt along those changes (Borsje *et al.*, 2011). There are, of course, limitations to the adaptability of a nature-based solution. Nonetheless, this adaptability is of increasing importance due to climate change. Furthermore, including ecological processes that are accommodated by these natural processes also creates additional value from both socio-economic and ecological perspectives (e.g., Scheres & Schüttrumpf, 2019; van Wesenbeeck *et al.*, 2014). Therefore, they accommodate for a sustainable solution on the long term. The application of the *Building with Nature*-approach on the topic of salt intrusion has not yet been studied so far, which is the focus point of this study.

The first step of the *Building with Nature*-approach is to understand the system (de Vriend *et al.*, 2015); in this study, this is the estuarine system. There have been significant developments in attaining knowledge and expertise in understanding salt intrusion in estuaries (see reviews by Geyer & MacCready, 2014; MacCready & Geyer, 2010). For example, many studies have highlighted the importance of the water depth (e.g., Chant *et al.*, 2018; Ralston & Geyer, 2019) and the river discharge (e.g., Gong & Shen, 2011; Lerczak *et al.*, 2009) on the salt intrusion length. In addition to these, many geometric features have been shown to influence the salt intrusion (Veerapaga *et al.*, 2020), such as tidal flats (Lyu & Zhu, 2019; Zhou *et al.*, 2020a). The literature about salt intrusion in estuaries is vast of which a very comprehensive review is presented in Section 3.2.

Due to the complexity associated with salt intrusion processes, state-of-the-art, computationally expensive models are required to assess these processes with sufficient detail. This often yields limitations in terms of number of simulations that can be achieved (e.g., Ralston *et al.*, 2010a; Warner *et al.*, 2005). Alternately, simplified models are used to explore a broader range of input conditions and/or estuary geometries (e.g., Dijkstra & Schuttelaars, 2021; Kuijper & van Rijn, 2011; MacCready, 1999). Although these studies provide valuable insights into the es-

tuarine processes, they may easily overlook important interactions in a system determined by a highly multidimensional parameter space.

The aim of this chapter is to systematically assess the sensitivity of salt intrusion length to changes in system characteristics. Thereby we address the research question how sensitive salt intrusion length is to changes in the forcing conditions and geomorphological features of an estuary. These relations are explored by means of a sensitivity analysis with the aim to enable the evaluation of nature-based solutions to mitigate salt intrusion. Subsequently, this study includes a first overview of the translation from the sensitivity analysis to the validation of hypothesised potential nature-based solutions to mitigate salt intrusion. These potential nature-based solutions are based on literature—reviewed in Section 3.2—and function as design directions.

To answer the research question and evaluate subsequent hypotheses, Section 3.2 presents a literature review from which the hypotheses are drawn. The methodology used to conduct the sensitivity analysis is presented in Section 3.3. The results of the sensitivity analysis are presented in Section 3.4. Section 3.5 further discusses the results and evaluates the posed hypotheses of Section 3.2. Finally, Section 3.6 draws conclusions on the estuarine response to various modifications with a special focus on the hypothesised nature-based solutions.

3.2 Estuarine salt dynamics

Estuarine salt intrusion is the result of a continuously changing competition between inward and outward transport mechanisms. The main driver of the outward transport is the river discharge, which flushes the system and advects salt seaward. Inward transporting mechanisms can be split in tide-averaged shear and tidal flow related mechanisms. Tide-averaged shear is generally referred to as estuarine circulation, which can be decomposed into various driving mechanisms (Burchard & Hetland, 2010), most notably gravitational circulation (e.g., Hansen & Rattray Jr., 1965) and tidal straining (e.g., Jay & Musiak, 1994). An example of the second category is tidal trapping (Fischer *et al.*, 1979), where the timing of the release of salt water that has come in during flood but was temporarily stored—e.g., in side-channels or on tidal flats—causes a net influx of salt (e.g., Garcia *et al.*, 2022; Zhou *et al.*, 2020a).

The strength of the various transport mechanisms is predominantly determined by the hydrodynamic forcing conditions and system geomorphology. In estuaries, the main hydrodynamic forcing consists of the tide and the river discharge (e.g., Geyer & MacCready, 2014). During flood tide, salt water is pushed into the estuary, while introducing energy to mix the water column (e.g., Simpson *et al.*, 1990). In contrast, the river discharge pushes the salt water seaward and provides buoyancy by the supply of freshwater (e.g., Lerczak *et al.*, 2009). Thus, both forcing terms have enhancing and reducing effects on the salt intrusion.

In addition to tidal forcing and river discharge, other key coastal processes modify the salt intrusion length. For example, the occurrence of strong onshore directed winds and the resulting storm surge enhance the salt intrusion in an

estuary (Kranenburg *et al.*, 2022). However, storms have also shown to reduce the estuarine salt intrusion (Geyer, 1997) in which the wind direction plays an important role.

In essence, the estuary's geomorphology largely determines how the estuary responds to these forcing conditions and can even modify the forcing to a certain level. In the end, the balance between the forcing terms determines the salt intrusion length, where the estuarine geomorphological features modify the arena in which this battle is played out. In this study, we focus on the key geomorphological features listed in Table 3.1.

The water depth of the estuary has long been known to be of great influence on the salt intrusion (e.g., Hansen & Rattray Jr., 1965): An increased water depth reduces the vertical mixing as the vertical shear velocity becomes smaller (Chant *et al.*, 2018; MacCready & Geyer, 2010). Furthermore, the fluvial flow velocity reduces as the cross-sectional area increases, which is similarly affected by the width.

In addition to these two basic geometric characteristics, the balance between width convergence and bottom friction determines whether the tidal signal is amplified or damped (e.g., Savenije & Veling, 2005; van Rijn, 2011): Convergence causes tidal amplification, while bottom friction results in tidal damping. As the tide is one of the main forcing conditions, these two geometric features indirectly modify the salt intrusion length by modifying the tidal wave.

Tidal asymmetry plays an important role in the salt intrusion, where an ebb-dominant system reduces the salt intrusion (Cheng *et al.*, 2013; Pein *et al.*, 2018) by stimulating a two-layered flow opposing the gravitational circulation (Cheng *et al.*, 2010; Stacey *et al.*, 2008). Ebb-dominance in an estuary can be enhanced by (1) introducing tidal flats (Friedrichs & Aubrey, 1988); (2) reducing the ratio of the tidal range over the water depth (Friedrichs & Madsen, 1992); and/or (3) increase the river discharge relative to the tidal flux (Nidzieko & Ralston, 2012).

At last, two geometric features enhancing lateral mixing are: (1) lateral depth variation, and (2) meandering (Burchard *et al.*, 2011; Lerczak & Geyer, 2004; Pein *et al.*, 2018). The presence of lateral circulation patterns on their own reduces the salt intrusion by reducing the forward momentum. The lateral circulation pattern originate from laterally directed momentum, which has to draw from the forward momentum due to the conservation of momentum. Despite both a lateral depth variation and meandering promoting the formation of lateral circulation patterns, their net effects on salt intrusion are opposite; lateral depth variation enhances the salt intrusion, while meandering reduces the intrusion.

The lateral depth variation is often represented by a cross-sectional curvature of the bottom profile (e.g., Burchard *et al.*, 2011; Lerczak & Geyer, 2004). The flow velocity in the centre of the channel is larger due to this bottom curvature, which enhances the salt transport in the centre (Burchard *et al.*, 2011; Lerczak & Geyer, 2004). Although the resulting lateral density differences do create lateral circulation patterns (i.e., differential advection; Nunes & Simpson, 1985), this process generally enhances the longitudinal dispersion of salt, i.e., the salt intrusion. The salt moves faster landward during flood where it is pushed to the sides due

to the lateral circulation, but is afterwards not completely flushed out by the ebb flow which is also faster in the centre, while the salt has partly moved to the sides of the channel (Burchard *et al.*, 2011).

Conversely, meandering within the reach of salt intrusion can reduce its landward extent (Pein *et al.*, 2018). The lateral mixing due to the secondary circulation initiated by bends in the estuary reduces the propagation of salt water upstream and so reduces the salt intrusion.

On the basis of the aforementioned processes and studies, we hypothesise six design directions for nature-based solutions to mitigate salt intrusion:

1. reduced cross-section;
2. increased bottom friction;
3. enlarged tidal flats;
4. reduced lateral depth variation;
5. increased meandering;
6. managed river discharge.

The type of estuary is expected to influence the salt intrusion, as different physical processes are dominant per type. In this study, we use the classification by Geyer and MacCready (2014), which divides estuaries into eight classes based on two non-dimensional parameters: (1) the mixing parameter, M (Eq. 3.1); and (2) the freshwater Froude number, Fr_f (Eq. 3.2). Their definitions are presented below (Geyer & MacCready, 2014):

$$M = \sqrt{\frac{c_f u_t^2}{\omega_t N d_c^2}} \quad (3.1)$$

where c_f is the non-dimensional friction coefficient [-]; u_t the tidal flow velocity [ms^{-1}]; ω_t the tidal frequency [s^{-1}]; N the buoyancy frequency [s^{-1}]; and d_c the (channel) depth [m]. These variables are defined as functions of the input space (Tab. 3.1) as follows:

$$\begin{aligned} c_f &= \frac{gn_c^2}{d_c^{1/3}} \\ u_t &= \frac{1}{2\sqrt{2}} \sqrt{\frac{g}{d_c}} a \\ N &= \sqrt{\frac{g\beta s_0}{d_c}} \end{aligned}$$

where g is the gravitational acceleration [$g = 9.81 \text{ ms}^{-2}$]; n_c the Manning's n [$\text{m}^{-1/3}$]; a the tidal range [m]; β the haline contraction coefficient [$\beta = 7.6 \times 10^{-4} \text{ psu}^{-1}$]; and s_0 the oceanic salinity [$s_0 = 30 \text{ psu}$].

$$Fr_f = \frac{Q}{W_c d_c c_i} \quad (3.2)$$

where Q is the river discharge [m^3s^{-1}]; W_c the (channel) width [m]; and c_i the maximum frontal propagation speed, or internal celerity [ms^{-1}]:

$$c_i = \sqrt{d_c g \beta s_0}$$

3

The aforementioned dominant roles of the tide and the river discharge are encapsulated in these non-dimensional parameters, where the mixing parameter (M) reflects the tidal energy, and the freshwater Froude number (Fr_f) the fluvial energy input.

3.3 Method

To perform the sensitivity analysis, we implemented a simulation strategy enabled by machine learning techniques. The use of adaptive sampling allowed the use of computationally expensive models for exploring the salt intrusion length for various estuarine layouts while remaining computationally feasible. This strategy required the description of the input space (Sec. 3.3.1) used by various machine learning techniques to draw the “most valuable samples” following an adaptive sampling approach (Sec. 3.3.2). These selected samples determined the layout of an idealised estuary, which was subsequently simulated using a state-of-the-art hydrodynamic model (Sec. 3.3.3). As the simulated samples do not form clear planes through the explored 13-dimensional space, various techniques have been used to post-process and analyse the output data (Sec. 3.3.4). The implemented simulation strategy is discussed in detail in Hendrickx *et al.* (2023a, Ch. 2) and this section is a brief overview of their work.

3.3.1 Input space

Based on the aforementioned literature on key estuarine characteristics, thirteen input parameters have been selected to include in the sensitivity analysis: three hydrodynamic forcing conditions, and ten geometric features. The definitions of the input parameters are presented in Table 3.1 (modified from Hendrickx *et al.*, 2023a, Tab. 2.1, p. 18) and visualised by the schematic overview of the parametric design in Figure 3.1.

The results from the many estuarine layouts that follow as a combination of the input parameters presented in Table 3.1 (and discussed in Sec. 3.2) allow the investigation of the hypotheses presented in Section 3.2 representing the worldwide variations in estuaries. The parametric design is a simplification of real-life estuaries, which allows the analysis to focus on the relevant estuary-scale parameters and the differences in output they enforce.

Table 3.1: Input parameters including their ranges and units. The values are largely based on datasets included in Dronkers (2017), Leuven *et al.* (2019), and Savenije *et al.* (2008).

	Parameter	Symbol	Range	Unit
Forcing	Tidal range	a	1.0–5.0	m
	Storm surge level	η_s	0.0–2.0	m
	River discharge	Q	100–16,000	$\text{m}^3 \text{s}^{-1}$
Geomorphology	Channel depth	d_c	5.0–25.0	m
	Channel width	W_c	500–3,000	m
	Channel friction	n_c	0.01–0.05	$\text{m}^{-1/3}\text{s}$
	Flat depth ratio ^a	r_d	–1–1	–
	Flat width	W_f	0–3,000	m
	Flat friction	n_f	0.02–0.05	$\text{m}^{-1/3}\text{s}$
	Convergence	γ	25–1.0	$\times 10^{-5} \text{m}^{-1}$
	Bottom curvature	κ_c	0.0–6.0	$\times 10^{-5} \text{m}^{-1}$
	Meander amplitude	A_m	0–6	km
Meander length	L_m	0–100	km	

^a The flat depth is defined as the product of the flat depth ratio and the tidal range: $d_f = \frac{1}{2}r_d a$. Thereby ensuring that the tidal flats are at all times exposed and flooded during a tidal cycle, i.e. following the definition of a tidal flat.

3.3.2 Simulation strategy

For a sensitivity analysis, the number of simulations required for robust results increases rapidly with the number of input parameters; the thirteen input parameters considered in this study would require at least 3^{13} ($\approx 1.6 \times 10^6$) simulations (Wang *et al.*, 2020), which would cover three values per input parameter. As a computationally expensive hydrodynamic model is used for every single simulation (Sec. 3.3.3), this number of simulations becomes computationally infeasible to execute.

Therefore, machine learning techniques have been adopted to optimise the selection procedure of forcing conditions and geomorphological features for simulation (Hendrickx *et al.*, 2023a). The number of simulations is drastically reduced to approximately 1,250 simulations while still being able to gain insights into the response of the system to the parameter variations.

The core of the used simulation strategy follows an adaptive sequential design, where the configuration of the next simulation is based on the output of completed simulations instead of prescribing all model configurations *a priori*. The new set of input parameters are chosen based on the method developed by Gramacy and Lee (2009) in which a treed Gaussian process, limiting linear model determines new samples by maximising the expected entropy. Due to this adaptive sampling technique, the choice to sample an estuary layout is based on the expected added information it will provide; translated to this study, “information” can be expressed as “better understanding the estuarine response.”

This adaptive simulation strategy was initiated by an initial batch of 100 samples for which the maximum dissimilarity algorithm (Kennard & Stone, 1969) was used to explore the outskirts of the input space. As the algorithm’s name

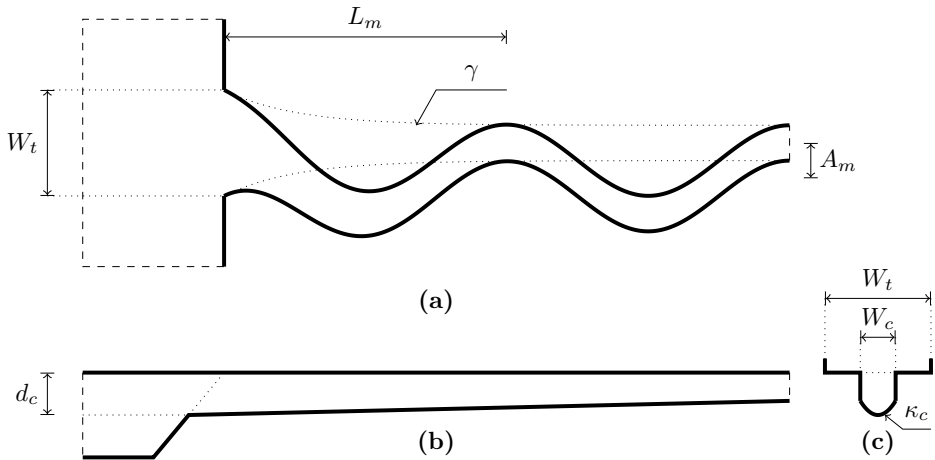


Figure 3.1: Parametric model design. (a) Plan view; (b) longitudinal cross-section; and (c) lateral cross-section. The meaning of the symbols are presented in Table 3.1, except for W_t : This is the total width, i.e., $W_t = W_c + W_f$.

suggests, it selects the most dissimilar samples in a given dataset based on their Euclidean distance (the dataset is normalised such that it forms a unit hypercube, i.e., *min-max* scaling). Subsequently, the adaptive sequential design contributed approximately 1,100 samples to the dataset.

The resulting dataset of approximately 1,200 simulations was used to train a neural network. Together with a genetic algorithm, this neural network was used to predict extremes in the output space, which were subsequently simulated with the hydrodynamic model as well. In this way, 50 additional simulations are executed creating a dataset of approximately 1,250 simulations that has been used for the analysis presented in this chapter.

3.3.3 Hydrodynamic model

The hydrodynamic modelling software used for the simulations is Delft3D Flexible Mesh (Kernkamp *et al.*, 2011), which assumes hydrostatic pressure and solves the Reynolds-averaged Navier-Stokes equations using a $k-\varepsilon$ turbulence closure model. This state-of-the-art hydrodynamic model is used to enable relaxation of most assumptions that restrict the application of many other, simpler models. However, the use of such a process-based model comes at a higher computational cost, which motivated the aforementioned simulation strategy (Sec. 3.3.2; Hendrickx *et al.*, 2023a).

For this exploratory study, an estuary with idealised geomorphology is used as basis for the parametric model design in which all thirteen input parameters are reflected (Tab. 3.1 and Fig. 3.1). The domain of the model consists of two parts: (1) the shelf, and (2) the estuary. The shelf domain is largely constant for all model configurations but the estuary domain changes substantially based on the

provided geomorphological features; e.g., the width of the estuary changes between different simulations.

The definitions of the boundary conditions are kept relatively simple: The tide at sea is fully represented with a tidal period of twelve hours—similar to an S_2 -tide—and there is a constant river discharge. A storm surge level is superimposed on the tidal water levels. The storm surge follows a triangular profile over time from 0 m to its maximum (i.e., η_s) after twelve hours, subsequently reducing back to 0 m (following the same approach as Perk *et al.*, 2019). Furthermore, the upstream channel dimensions are a power function of the river discharge (based on Leuven *et al.*, 2018b) to ensure reasonable flow conditions upstream.

The shelf model domain is a square of 30×30 km. Its grid resolution increases from the seaward boundary to the estuary mouth, with cell sizes decreasing from $1,000 \times 1,000$ m to 62.5×62.5 m. The estuarine domain has a length of 200 km and a varying width. The grid resolution decreases further upstream, with cell sizes increasing from 62.5×62.5 m at the estuary mouth to $\leq 250 \times 1,000$ m at the upstream boundary; due to the convergence of the estuary, the grid cells are reduced in width.

The extent of the high resolution in the estuary domain—i.e., the grid resolution of 62.5×62.5 m—is determined based on an estimated salt intrusion length plus half the tidal excursion; both are determined analytically following Savenije (1989, 1993). The transition between different grid resolutions is facilitated by using triangular grid cells.

The models have been discretised vertically by twenty σ -layers. We are aware that Z -layers are preferred, especially for modelling of salt wedges (Stelling & van Kester, 1994). However, σ -layers have been used to accommodate for the large range of water depths considered in this study (Tab. 3.1).

The initial salt concentration in the hydrodynamic model is based on an analytical model (Savenije, 1989, 1993) to reduce the spin-up time. To ensure that the results are not influenced by the initial conditions, the first eight days of the simulation are considered part of the spin-up time. The model data of the ninth simulated day is used for subsequent analyses. One day of data suffices, as the tidal forcing consists of only one tidal component, which occurs exactly twice per day due to its 12-hour period. Therefore, there are no neap-spring cycles or alike in the tidal forcing, which would require a longer simulation period.

The simulations were executed on a supercomputer. A single Delft3D Flexible Mesh simulation was run in parallel on 32 cores and has an execution time between fifteen minutes and five days—largely influenced by the geomorphology of the estuary, and thus the grid size.

3.3.4 Post-processing

The output of the simulations is expressed in terms of the salt intrusion length. This length is defined as the distance from the mouth of the estuary at which the depth- and tide-averaged salinity equals 1 psu. Because the salinity data is retrieved in a discrete manner from the hydrodynamic model's numerical grid, the

salinity is linearly interpolated between data points to determine the salt intrusion length.

As the used simulation strategy results in a reduced dataset (Sec. 3.3.2), standard quantification methods for sensitivity analyses cannot be used (such as Saltelli *et al.*, 2006; Sobol', 2001; Wang *et al.*, 2020). Instead, we apply a regression analysis. A multiple regression model and neural network are fitted with the input and output data to determine the underlying relations between the input parameters and the output variable, i.e., salt intrusion length.

Although the predictive capability of a neural network is generally superior to the multiple regression model for highly dimensional input spaces, the neural network is often perceived as a *black box* as it is hard to retrieve what is exactly going on internally. The multiple regression model, on the other hand, is valuable precisely due to its transparency, where the over-fitted regression coefficients function as a quantification of the sensitivity of the salt intrusion length to the input parameters. Consequently, both regression methods are used in this study: The multiple regression model and its regression coefficients to gain insights into the response of the salt intrusion length to the 13-dimensional input (Sec. 3.3.4.1); and the neural network as predictive tool allowing to explore the hypothesised nature-based solutions to mitigate salt intrusion (Sec. 3.3.4.2).

3.3.4.1 Regression model

The implemented regression model is defined as:

$$\hat{y} = \underbrace{C}_{\text{constant}} + \underbrace{\sum_i^{\mathcal{P}} c_i x_i}_{\text{linear}} + \underbrace{\sum_{i \leq j}^{\mathcal{P}} c_{i,j} x_i x_j}_{\text{nonlinear}} \quad (3.3)$$

where c_i and $c_{i,j}$ are the regression coefficients; x_i (or x_j) is the input parameter i (or j); and \mathcal{P} the number of parameters ($\mathcal{P} = 13$).

The regression model is over-fitted to the data by optimising the values of the regression coefficients to provide the best fit. The over-fitting causes the regression model unsuitable for predictive purposes but by doing so, provides insights into the data it represents.

The regression coefficients provide a quantification of the sensitivity of the output to the input parameters: The larger the absolute value of a regression coefficient, the larger the connectivity between the input parameter(s) and the output data. The level of connectivity is a quantification of the sensitivity of the output to the input parameter(s). The sign of the coefficient's value represents a positive (+) or a negative (−) relation between the input parameter(s) and the output, i.e., the salt intrusion length.

Note that the input data has to be normalised for this approach to work properly, as otherwise the order of magnitude of the input values determine the order of magnitude of the regression coefficients. This normalisation follows the *zero mean, unit variance*-approach.

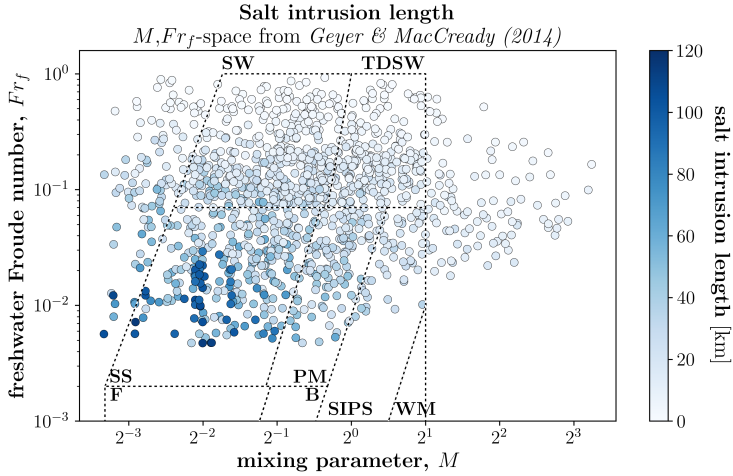


Figure 3.2: Simulated estuary configurations overlaying the classification diagram by Geyer and MacCready (2014). The data is colour-coded with the salt intrusion length. **SW**: salt wedge; **TDSW**: time-dependent salt wedge; **SS**: strongly stratified; **PM**: partially mixed; **F**: fjord; **B**: bay; **SIPS**: strain-induced periodic stratification; **WM**: well-mixed.

3.3.4.2 Neural network

The neural network used contains three hidden layers of 50 nodes each. Overfitting the neural network has been prevented by subdividing the output data in a training and testing (or validation) dataset (80% and 20%, resp.). While training, the neural network only uses the training data, while the testing data was used to validate the predictive power of the neural network. The best fit is reached when the neural network shows the smallest error on the testing data. More details on the neural network and its training are given in Appendix A.

3.4 Results

For the presentation of the results, the over-fitted regression model as well as the neural network are used. Both models show a great fit with the data: The regression model has an $R^2 = 0.9581$, and the neural network linearly correlates even better, with $R^2 = 0.9912$. Here, the R^2 -score is the coefficient of determination for which $R^2 = 1.0$ is the best possible score and negative values are possible, reflecting increasingly worse performing models. These great fits have been achieved while the dataset covers a multitude of estuary classes as defined by Geyer and MacCready (2014), which is illustrated in Figure 3.2.

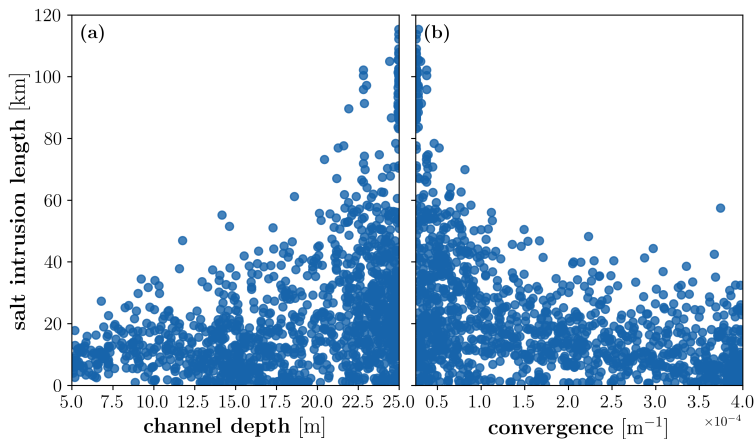


Figure 3.3: Simulated salt intrusion length as function of (a) the channel depth, d_c , and (b) the convergence, γ .

3.4.1 Upper limits of salt intrusion length

The projection of the salt intrusion length on the M, Fr_f -space presented in Figure 3.2 shows a gradient in the salt intrusion length in response to both the mixing parameter (M , Eq. 3.1) and the freshwater Froude number (Fr_f , Eq. 3.2). This indicates that the salt intrusion length is generally the largest for *strongly stratified* estuaries in comparison to the other estuary classes.

As we are comparing non-dimensional numbers with the salt intrusion length—a dimensional variable—it is important to stress that these results hold for the ranges used in this study (Tab. 3.1). Although the explored input space is representative for estuaries worldwide, these results do not exclude the theoretical possibility of large salt intrusion lengths for large values of the freshwater Froude number and/or mixing parameter.

In Figure 3.2, the salt intrusion length reduces for increasing values of the mixing parameter and/or freshwater Froude number. This implies that the five input parameters—out of the thirteen—that are reflected by these non-dimensional numbers largely explain the variability in the salt intrusion length. The mixing parameter increases for (1) increasing tidal range, $M \propto a$; (2) decreasing channel depth, $M \propto d_c^{-17/12}$; and (3) increasing (channel) friction, $M \propto n_c$. The freshwater Froude number increases for (1) increasing river discharge, $Fr_f \propto Q$; (2) decreasing channel depth, $Fr_f \propto d_c^{-3/2}$; and (3) decreasing channel width, $Fr_f \propto W_c^{-1}$.

The variability in salt intrusion length visible in Figure 3.2 suggests that the salt intrusion can be large, unless a limiting factor is imposed. One such limiting factor is the channel depth, as shown in Figure 3.3a: A smaller channel depth enforces a reduction in the salt intrusion length. A larger channel depth does not necessarily result in a larger salt intrusion length, but is an enabler of large salt intrusion lengths.

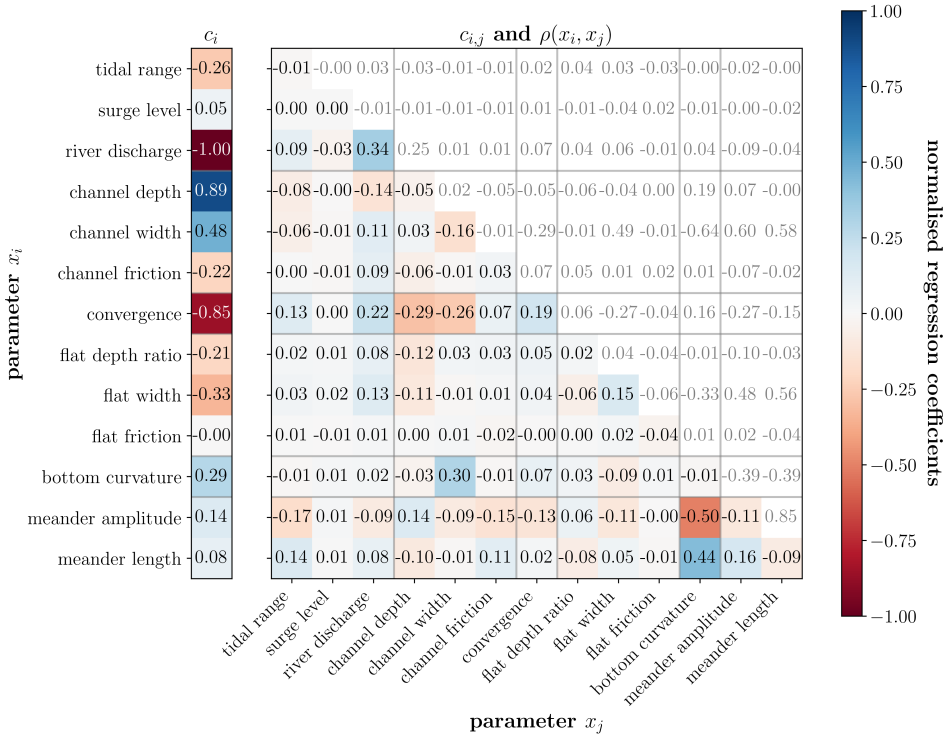


Figure 3.4: System's response represented by the (normalised) regression coefficients of the over-fitted regression model (Eq. 3.3). The colour-coding represents the value of the regression coefficients, where a large absolute value is indicated by a darker colour and reflects a higher dependency of the output on the input parameter(s). Grey values represent the Pearson correlation coefficients, $\rho(x_i, x_j)$.

Similar relations between the salt intrusion length and other input parameters exist (Fig. B.1, p. 202), most notably with the convergence (Fig. 3.3b). Although the M, Fr_f -space shows to explain a large part of the variability in the salt intrusion length (Fig. 3.2), this study shows the additional relevance of other estuary-scale parameters such as the convergence (Fig. 3.3b).

3.4.2 Importance of input parameters

The multiple regression model is able to encapsulate most of the variations in the output as shown by the great fit with the data, while being a linear model (Eq. 3.3).

The regression coefficients show the sensitivity of the output to changes of the input parameter(s) and are presented as a matrix in Figure 3.4. The linear regression coefficients are presented in the most left column (titled c_i), and the quadratic and interaction terms are shown in the thirteen-by-thirteen matrix (ti-

ted $c_{i,j}$), which is symmetrical over its diagonal. The colour-coding represents the value of the regression coefficient, which is of interest for the sensitivity analysis. The grey-values in the matrix represent the Pearson correlation coefficients between parameters x_i and x_j : $\rho(x_i, x_j)$. The Pearson correlation coefficient has a range $\rho(x_i, x_j) \in [-1, +1]$ and a larger absolute value of the coefficient indicates a stronger correlation between the variables, where the sign is indicative for a positive (+) or negative (−) relation.

From this matrix follows that the salt intrusion length is highly dependent on the river discharge, channel depth, and convergence as well as the interaction between the convergence with the river discharge, channel depth, and channel width. In addition, the interactions between the bottom curvature with the meandering specifications happen to be of substantial influence on the salt intrusion length. On the other hand, the friction of the tidal flats does not seem to influence the results. Figure 3.4 also suggests that the surge level is irrelevant for the salt intrusion length, which is in contradiction with literature (Kranenburg *et al.*, 2022). Although the presented salt intrusion length is taken as the tide averaged value, no substantial changes arise when considering the tidal maximum, which questions the implementation of the surge level in our parametric design.

The nonzero correlations in Figure 3.4 follow from the physical input check (App. B.2), and highlight potential false cause-and-effect relations. For example, the strong correlation between the meander amplitude and length ($\rho(A_m, L_m)$) is commonly seen in nature (e.g., Leuven *et al.*, 2018a), and therefore, explicitly included in the physical input check. However, these meandering parameters are also both negatively correlated to the bottom curvature, while such a relation is not included in the physical check, and therefore, must follow via another input parameter—most likely the channel width. These correlations might explain the relatively high value of their first-order interaction regression coefficients seen in Figure 3.4, c_{κ_c, A_m} and c_{κ_c, L_m} , as no clear direct relation between the salt intrusion length and the combination of these parameters can be seen in the raw data.

3.4.3 Salt intrusion gradients

The neural network is used to determine the partial gradients of the salt intrusion length with respect to one of the input parameters. These gradients are estimated using the forward Euler scheme:

$$\frac{\partial L_s}{\partial x_i} \approx \frac{L_s(\mathbf{x} + \mathbf{n}_i) - L_s(\mathbf{x})}{\Delta x_i} \quad (3.4)$$

where L_s is the salt intrusion length estimate [m]; x_i an input parameter; \mathbf{x} the vector of input values; \mathbf{n}_i the null-vector except the i -th element, which equals Δx_i ; and Δx_i a very small step in the range of x_i :

$$\Delta x_i = \frac{\max\{x_i\} - \min\{x_i\}}{1,000}$$

Note that for the determination of the gradients, the salt intrusion is estimated with the neural network both at \mathbf{x} and $\mathbf{x} + \mathbf{n}_i$. This minimises any bias of the neural network to be reflected in the salt intrusion gradients.

Overall, the computed absolute gradients in salt intrusion length are largest for larger values of the salt intrusion length; i.e., modifications of the estuarine system result in the largest changes in the salt intrusion when the salt intrusion length is already large.

However, this relation vanishes when the partial derivatives are normalised with the input parameter and salt intrusion length:

$$p_i = \frac{\partial L_s}{\partial x_i} \frac{x_i}{L_s} \quad (3.5)$$

where $\partial L_s / \partial x_i$ equals the partial derivative as stated in Equation (3.4).

Equation (3.5) reflects how much the salt intrusion length changes relatively compared to a relative change in the input parameter. Note that this relative gradient p_i describes the power relation between the input parameter, x_i , and the salt intrusion length:

$$L_s \propto x_i^{p_i} \quad (3.6)$$

which is a commonly used form to describe the relation between estuarine characteristics and the salt intrusion length both in theoretical and empirical studies; e.g., the relation between the salt intrusion length and the river discharge is often described by such a power relation, where according to literature p_Q is in the range $-1/7$ to -1 (e.g., Monismith *et al.*, 2002; Ralston & Geyer, 2019; Savenije, 1993). Figure 3.5a confirms that p_Q varies around those values, and that the absolute value of p_Q increases with a higher river discharge.

Furthermore, the relative gradient, p_Q , shows a trend in the M, Fr_f -space (Fig. 3.5b) that may be a consequence of the freshwater Froude number definition (Eq. 3.2), which is linearly related to the river discharge.

Figure 3.6 presents relative gradients for the input parameters that are related to the other hypothesised nature-based solutions. (A complete overview of all input parameters is presented in Fig. B.2, pp. 203–206, similarly to Fig. 3.6.) Where p_Q shows a dependence on the estuary class (Fig. 3.5), the relative gradient of the channel depth, p_{d_c} , shows less variability (Fig. 3.6a). The values of p_{d_c} might depart from the general range for very small values of the salt intrusion length ($L_s \rightarrow 0$), as with the outliers in p_Q (Fig. 3.5a); this is likely due to the definition of p_i (Eq. 3.5) in which the derivative is divided by the salt intrusion length (L_s).

Both the relative gradients with respect to the channel depth (p_{d_c}) and channel friction (p_{n_c}) show the direct relevance of these input parameters as well as a gradient in their values in the M, Fr_f -space (Fig. 3.6a and b). The remainder of the input parameters that are associated with the hypothesised nature-based solutions show only a weak direct contribution to the salt intrusion length (Fig. 3.6c to f).

Note that the partial derivatives of the estuarine configurations with a larger salt intrusion must be considered with care—i.e., the data points located in the *strongly stratified*-class (Fig. 3.2). The implementation of the genetic algorithm

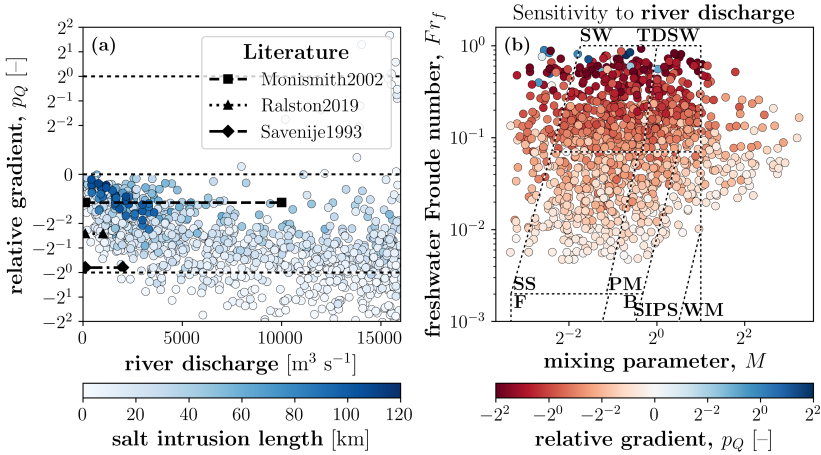


Figure 3.5: The relative gradient in salt intrusion with respect to the river discharge, p_Q : (a) as function of the river discharge; (b) displayed on the M, Fr_f -space by Geyer and MacCready (2014) with the same class-labels as in Figure 3.2. Data from literature displayed in (a): Monismith2002, Monismith *et al.* (2002); Ralston2019, Ralston and Geyer (2019); Savenije1993, Savenije (1993).

to “find” these extremes results in limited variations in certain input parameters, which complicates the determination of a reliable partial derivative to these input parameters for such extremes in the output.

Furthermore, the relative gradient tends to be more sensitive to minor errors in the predictive power of the neural network for small values of the salt intrusion length, as these errors are relatively larger—especially for salt intrusion lengths near zero, where also a sign-change might occur.

3.5 Discussion

Before discussing the presented results, the discussion reflects on the abilities and limits of the simulation strategy and the study in general (Sec. 3.5.1). Subsequently, the results are discussed by interpreting their physical meaning and relevance (Sec. 3.5.2); and translating these findings to the implications for nature-based solutions to mitigate salt intrusion (Sec. 3.5.3).

3.5.1 Simulation strategy

The implemented method allows for exploring a wide range of possible estuary configurations covering many estuary classes (Fig. 3.2). However, the many input parameters complicate analyses due to the interaction effects that may obscure single-parameter trends. Nevertheless, clear correlations are visible between various input parameters and the salt intrusion length, e.g., the channel depth and convergence in Figure 3.3. We have implemented various analysis methods to

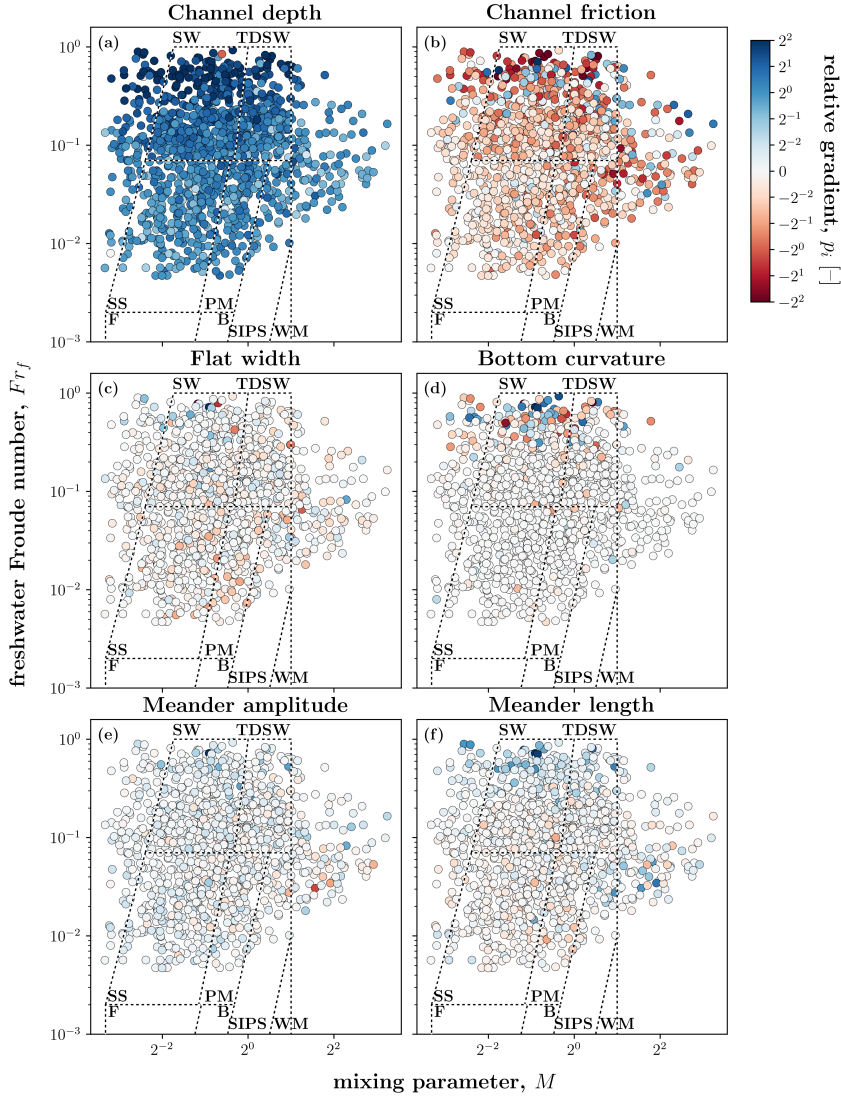


Figure 3.6: Estimates of the relative gradient in salt intrusion with respect to six input parameters (cq. Eq. 3.5), which are related to the hypothesised nature-based solutions displayed on the M, Fr_f -space by Geyer and MacCready (2014) with the same class-labels as in Figure 3.2.

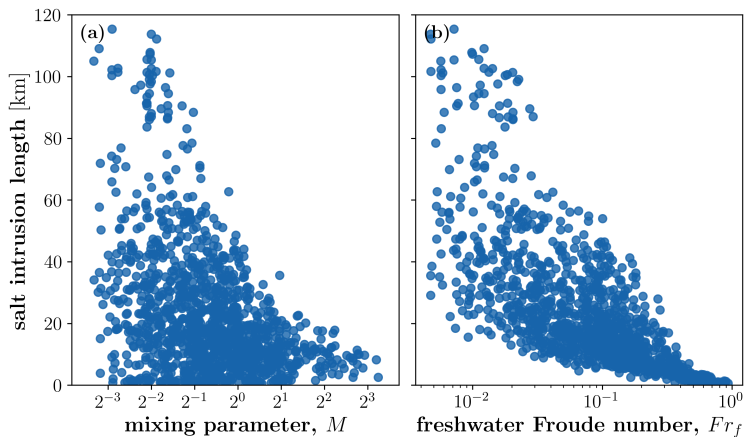


Figure 3.7: Simulated salt intrusion length as function of non-dimensional numbers. (a) the mixing parameter (M , Eq. 3.1), and (b) the freshwater Froude number (Fr_f , Eq. 3.2).

contribute to a general understanding of the system, where especially the neural network provides an easy-accessible tool to determine changes in salt intrusion due to modifications in the estuary.

The choice for an idealised model schematisation implies that the model results could not be calibrated or validated against real data. The absolute values should therefore be considered as estimates. However, given the predictive capacity of the 3D process-based modelling software, we assume that the model correctly represents the governing physics. Resulting values form a physical sound basis for the sensitivity analysis of this study, i.e., changes to various estuary-scale parameters. The calibration parameters were kept constant throughout, which diminishes their influence on the results when analysed in comparison to each other.

Nevertheless, the implementation of a storm surge—represented by a temporary rise in water level (similar to Perk *et al.*, 2019)—seems to be too simplified to capture its effect on the salt intrusion. This approach leaves out the surface shear stress induced by the wind over the whole domain, which would add landward momentum of the saline, offshore waters.

3.5.2 Physical interpretation

The non-dimensional space suggested by Geyer and MacCready (2014) to classify estuaries largely explains the variability in salt intrusion length (Fig. 3.2), where the salt intrusion length is suppressed for larger values of the mixing parameter (M) and/or the freshwater Froude number (Fr_f). This principle is explicated in Figure 3.7, where larger values of both non-dimensional parameters put a limit on the maximum salt intrusion length.

The correlations shown in Figures 3.2 and 3.7 between the non-dimensional

parameters and the salt intrusion length suggest that the input parameters used in the calculation of M and Fr_f (Eqs. 3.1 and 3.2) largely control the variability in the salt intrusion length. This is in part supported by the results presented in Figure 3.4 in which the regression coefficients are displayed. Especially the input parameters that define the freshwater Froude number (Eq. 3.2) light up in Figure 3.4. The effect of the mixing parameter (Fig. 3.7a) is weaker than that of the freshwater Froude number and seems to be dominated by the channel depth, as the tidal range and channel friction are of less relevance according to Figure 3.4. That the channel depth and river discharge are of importance to the salt intrusion is not surprising, as analytical relations have been developed that relate the salt intrusion length to primarily the water depth and river discharge (e.g., Hansen & Rattray Jr., 1965; Monismith *et al.*, 2002; Savenije, 1993). In such relations, the tidal influence on the salt intrusion is often reflected by means of a diffusion coefficient (e.g., Gong & Shen, 2011; Monismith *et al.*, 2002).

3.5.2.1 Tidal damping

Our results show that other input parameters not represented in the M, Fr_f -space are relevant for the determination of the salt intrusion length as well. Figure 3.4 highlights the importance of the convergence of the estuary, which is supported by Figure 3.3b and in line with the findings of Wei *et al.* (2017).

The influence of the convergence on the salt intrusion length is twofold: (1) the convergence, in combination with the bottom friction, strongly influences the propagation of the tidal wave (e.g., Friedrichs & Aubrey, 1994; Hunt, 1964; Prandle & Rahman, 1980) and thereby the tidal mixing capacity in the estuary; and (2) the width—and thereby the cross-sectional area—over the estuary is determined based on the convergence, which causes the local fluvial flow velocity to change.

The joint effect of the convergence and channel friction on the tide is encapsulated by a tidal damping coefficient (van Rijn, 2011):

$$\delta = \frac{1}{2} \left(\frac{f}{c_t} - \gamma \right) \quad (3.7)$$

with

$$f = \frac{8}{3\pi} \frac{gn_c^2 u_t}{d_c^{4/3}}$$

$$c_t = \sqrt{gd_c}$$

where f is a friction parameter [s^{-1}]; c_t the frictionless tidal wave celerity [ms^{-1}]; γ the convergence (Tab. 3.1) [m^{-1}]; u_t the tidal velocity [ms^{-1}], similarly defined as for the mixing parameter (M , Eq. 3.1). Note that the damping coefficient is positive when the tidal range is damped, and negative when the tide is amplified; i.e., the tidal damping coefficient describes the tidal propagation by the following exponential decay function:

$$a(x) = a_0 \exp[-\delta x]$$

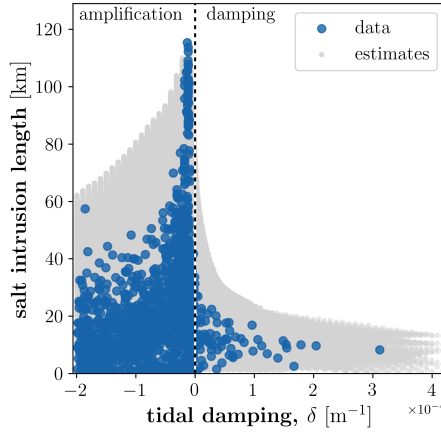


Figure 3.8: Salt intrusion length as function of the tidal damping coefficient (δ , Eq. 3.7). A negative damping coefficient reflects tidal amplification. Blue points represent the results derived from the raw data; and the grey dots the estimates by the neural network.

where a_0 is the tidal range at the mouth of the estuary [m].

Figure 3.8 presents the salt intrusion length as function of the tidal damping coefficient (Eq. 3.7) in two ways: (1) derived from the raw data (blue points); and (2) derived from estimates by the neural network exploring the whole (relevant) input space (grey dots). This addition of estimates by the neural network to the raw data is also used in subsequent figures (Figs. 3.9 to 3.11) to fill the sparsely sampled input space.

Figure 3.8 shows the suppression of the salt intrusion length by the tidal damping coefficient, where the largest salt intrusion occurs around the tipping point between amplification and damping, i.e., $\delta = 0$. This is representative for an “ideal estuary” in which the tidal range and velocity remain spatially constant due to the balancing forces of amplification by convergence and damping by friction (e.g., Dronkers, 2017; Savenije & Veling, 2005).

The reason the salt intrusion peaks when the convergence and friction are in balance follows from the dual effect of the tide on the salt intrusion: On the one hand, the tidal energy mixes the water column reducing the gravitational circulation; on the other hand, the tidal momentum increases the landward reach of the saline water. Thus the maximum salt intrusion can be achieved when there is sufficient tidal momentum pushing the saline water upstream but not enough to reduce the stratification and the gravitational circulation.

However, the effects of a damped or amplified system are not symmetrical as the amplification of the tide results in a larger salt intrusion length compared to a damped system. This suggests that the tide enforces an upper bound on the salt intrusion length, which is in line with the regression coefficients related to the tidal range in Figure 3.4 showing a negative relation between the tidal range and the salt intrusion length.

The non-monotonic response of the salt intrusion length to the damping coefficient as presented in Figure 3.8 is also in line with the partial derivative with respect to the channel friction, which has both a positive and negative sign (Fig. 3.6b), illustrative for the change in salt intrusion length for increasing value of the tidal damping coefficient (Fig. 3.8).

3.5.2.2 Tidal asymmetry

The tide and its influence on the salt intrusion length is also influenced by the tidal asymmetry of the estuary (Cheng *et al.*, 2013; Pein *et al.*, 2018). In Section 3.2, three aspects were introduced that modify the tidal asymmetry of an estuary: (1) tidal flats (Friedrichs & Aubrey, 1988), (2) tidal range to water depth ratio (Friedrichs & Madsen, 1992), and (3) river over tidal flux (Nidzieko & Ralston, 2012). To analyse their effects on the salt intrusion length, three ratios have been defined:

1. The ratio of the bank-full cross-sectional areas of the tidal flats over the channel:

$$\alpha = \frac{\frac{1}{2}a(r_d + 1)W_f}{\left(d_c + \frac{1}{2}a\right)W_c} \quad (3.8)$$

2. The ratio of the tidal range over the water depth—i.e., channel depth:

$$\Gamma = \frac{a}{d_c} \quad (3.9)$$

3. The ratio of the river flux over the tidal flux:

$$\varphi = \frac{Q}{2P/T} \quad (3.10)$$

where P is the tidal prism [m^3], as defined by van Rijn (2011); and T the tidal period [$T = 43,200 \text{ s}$].

Although these three ratios do not solely encompass the effects of ebb-dominance, a larger value represents an increase of ebb-dominance of the system.

The effects of these ratios on the salt intrusion length are presented in Figure 3.9. These results support the statement of a reduction in salt intrusion length for increased ebb-dominance. Again, these three ratios—and thereby the ebb-dominance—impose an upper limit on the salt intrusion length.

The effects of the tidal ratio, Γ , on the salt intrusion length are stronger than the mixing parameter (Fig. 3.7a) even though the mixing parameter (M , Eq. 3.1) embeds the tidal ratio (Γ , Eq. 3.9): $M \propto \Gamma d_c^{-5/12} n_c$. This suggests that the effect of the mixing parameter on the salt intrusion length is dominated by the tidal ratio.

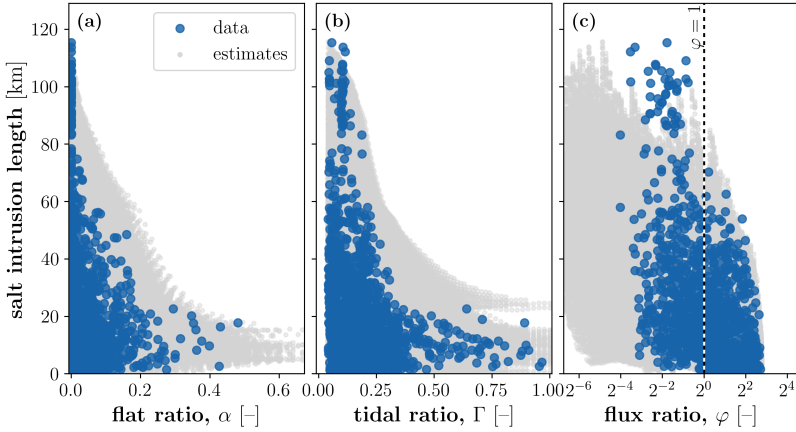


Figure 3.9: Salt intrusion length as function of tidal asymmetry. (a) the flat ratio (α , Eq. 3.8), (b) the tidal ratio (Γ , Eq. 3.9), and (c) the flux ratio (φ , Eq. 3.10). Blue points represents the results derived from the raw data; and the grey dots the estimates by the neural network.

3.5.2.3 Lateral circulation

The meandering of the estuary is described by two input parameters, namely the meander amplitude (A_m) and the meander length (L_m). This complicates the analysis of the effects of meandering on the salt intrusion length. Therefore, the sinuosity of the estuary is considered, which describes the degree of meandering and is composed of both the meander amplitude and length:

$$S = \frac{1}{L_m} \int_0^{L_m} \sqrt{1 + \left(\frac{dy}{dx}\right)^2} dx \quad (3.11)$$

with

$$y(x) = A_m \sin \left[\frac{2\pi}{L_m} x \right]$$

where y is the centre-line of the estuary [m]; and x the longitudinal coordinate [m]. Note that a straight estuary has $S = 1$ and the introduction of meanders results in $S > 1$.

Figure 3.10 shows a minor effect of the sinuosity on the salt intrusion when analysing the simulated samples, which is contradictory to the findings by Pein *et al.* (2018). However, when the estimates of the neural network covering the whole input space are considered, there seems to be no distinct relation between the sinuosity and the salt intrusion length.

The differences found between the study by Pein *et al.* (2018) and the results shown in Figure 3.10 can be explained by the method used to introduce meanders to the estuary: In Pein *et al.* (2018), a straight estuary has three bends in the region of maximum salt intrusion—where it has the most influence on the salt

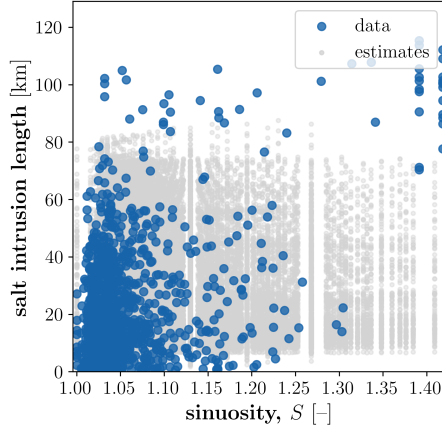


Figure 3.10: Salt intrusion length as function of the sinuosity (S , Eq. 3.11). Blue points represent the results derived from the raw data; and the grey dots the estimates by the neural network.

intrusion; we applied the meanders throughout the estuary. Furthermore, Pein *et al.* (2018) state that the length of the estuary remains the same even with the addition of meanders, while we follow the centre-line of the estuary when defining the salt intrusion length. If meanders in our simulations do not lead to shortening of the salt intrusion length—measured along the thalweg of the estuary—they will still lead to a shortening in Cartesian space, more or less in proportion to the effective length increase they cause.

The effects of bottom curvature on the salt intrusion length are considered as the relative increase in channel depth in the centre of the estuary, defined as a depth ratio:

$$\Delta = \frac{d_c + \Delta d_c}{d_c} \quad (3.12)$$

with

$$\Delta d_c = \frac{1}{12} \kappa_c W_c^2$$

where Δd_c is the additional depth along the estuarine centre line [m]. Note that Δd_c averaged over the lateral axis equals zero and thus that the channel depth (d_c) reflects the laterally averaged channel depth.

This relation is displayed in Figure 3.11 from which no clear relation can be drawn, similar to the effect of meandering (Fig. 3.10). Despite the strong relation between the salt intrusion length and the channel depth, the enhancement of the maximum channel depth caused by the bottom curvature—albeit small—does not follow this pattern. Furthermore, the hypothesised enhanced salt intrusion due to the lateral circulation (Burchard *et al.*, 2011) is also not deducible from Figure 3.11.

The absence of a clear relation between the salt intrusion and both the meandering (Fig. 3.10) and the bottom curvature (Fig. 3.11) raises the question how relevant the lateral circulation patterns are with respect to the other considered

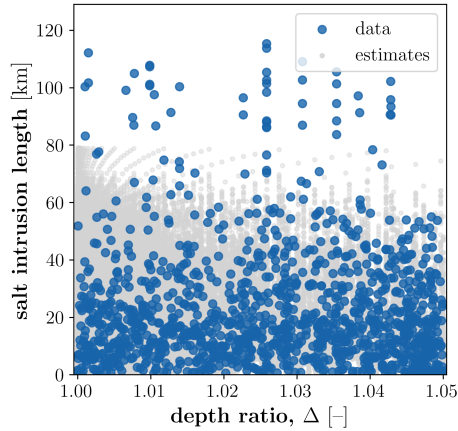


Figure 3.11: Salt intrusion length as function of the depth ratio (Δ , Eq. 3.12). Blue points represent the results derived from the raw data; and the grey dots the estimates by the neural network.

estuary-scale modifications. On the other hand, the interactions between the meandering characteristics and the bottom curvature are highlighted in Figure 3.4, which indicates a substantial sensitivity of the salt intrusion length to these first-order interaction terms. However, this relevance is not apparent from correlation plots showcasing these first-order interactions.

This distorted image might be the cause of how the bottom curvature is scaled, where its distribution hints towards a log-based scaling instead of a linear-scaling. Because the input parameters are normalised with the *zero mean, unit variance*-method (Sec. 3.3.4.1) and the fact that the bottom curvature is very skewed towards lower values, this might cause discrepancies in the sensitivities.

Another potential cause—which would also reflect upon the meandering characteristics—is the strong correlation between these three input parameters and the channel width (Fig. 3.4). This seems more reasonable due to the fact that there is a clear (positive) relation between the salt intrusion and the channel width.

Re-scaling of the input parameters to account for the imposed physical restrictions—leading to uncorrelated parameters—removed some of the interactions in the linear model but did not change the nature of the relations with salt intrusion length (results not shown).

At last, it is important to note that the Coriolis effect has not been included in this study. This could, however, have a substantial influence on the lateral circulation patterns (e.g., Cheng *et al.*, 2017) as well as on the salt intrusion length (e.g., Wei *et al.*, 2017).

3.5.3 Nature-based solutions

In this section, the results and their physical reflections are translated to the hypothesised nature-based solutions (Sec. 3.2).

As expected, the reduction of the cross-section greatly reduces the salt intrusion length—as illustrated by Figures 3.3 and 3.4. Although the channel depth is a more effective measure than the width (Fig. 3.4) and explains a large part of the variation in salt intrusion length, it is a difficult parameter to use as a basis of nature-based solutions. In many estuaries, water depth is maintained at a deeper level than its equilibrium value to accommodate access of large vessels to port areas. Various possibilities might exist to reconcile nature-based solutions to mitigate salt intrusion with harbour access, but the current study does not allow to evaluate these possibilities. One option could be to reduce the depth in a non-uniform way in space—e.g., just behind or around harbour access points. Therefore, focusing on the width instead of the depth in reducing the cross-sectional area could provide a more viable solution to mitigate salt intrusion. In this respect, Figure 3.4 suggests that manipulating the width is less effective than manipulating the depth, but that the interaction between both is minimal and as a consequence, the two measures to change the cross-sectional area can be considered complimentary. However, manipulating the depth is likely more effective because it also influences the stratification and mixing in the estuary.

The friction in the estuary competes with the tidal amplification effect of the convergence (Eq. 3.7). Figure 3.8 highlights the importance of the balance between tidal damping and amplification. The evaluated values of the bottom friction are representative for natural bottom covers. However, the effective bottom friction can be further enhanced by (1) artificially enhancing the bottom friction, e.g., by means of large boulders or even rocks on the bottom; and (2) naturally occurring bed forms, such as ripples and sand waves. The implementation of vegetation at the bottom of the channel might not be suitable in practice, as for vegetation to sustain, light must reach the vegetation, which poses a substantial constraint on the water depth; and submerged vegetation in practice is limited to areas with low current velocity. In addition, ship propellers may pose problems in intensely used estuaries.

Changing the bottom friction as a nature-based solution will require careful consideration of its interaction with the convergence. As shown in Figure 3.8, an increased bottom friction can either reduce or enhance the salt intrusion, depending on whether the tide is amplified or damped. Counterintuitively, smoothening the bed may therefore in some cases also result in less salt intrusion.

The introduction of tidal flats to both sides of the estuarine channel places an upper limit on the salt intrusion length (Fig. 3.9b). On the other hand, Figure 3.6c does not display a uniform picture of the implementation of tidal flats. Analysing both Figures 3.6c and 3.9a, demonstrates the relevance of the water depth on the tidal flats—i.e., the flat depth—for its efficiency to mitigate salt intrusion; this is also illustrated by the comparable values of their regression coefficients in Figure 3.4.

The addition of tidal flats has been shown to have many other benefits to an estuarine system, such as wave and surge reduction and coastline stabilisation (e.g., de Vriend *et al.*, 2015; Temmerman *et al.*, 2013; van Wesenbeeck *et al.*, 2014). Even if the tidal flat friction does not prevent salt intrusion very effectively

(Fig. 3.4), the tidal flats allow for ecological development; e.g., in intensely used and dredged estuaries—such as the Western Scheldt in the Netherlands—tidal flats are the only refuges for benthic life, with deeper channels almost devoid of any organisms (Ysebaert *et al.*, 2003).

From this study, both the lateral depth variation—described by the bottom curvature, κ_c —and the meandering of the estuary have no profound effects on the salt intrusion (Figs. 3.10 and 3.11). This might be due to several reasons: (1) these hypothesised nature-based solutions are minor interventions that do not make a significant contribution; (2) the representative input parameters and their ranges do not capture the full potential of these optional nature-based solutions; and/or (3) the representative input parameters are implemented incorrectly in the parametric design. Although a parametric design as implemented in this study comes with the cost of simplifying complex features to fit an idealised setting, our investigations of the data suggest the first: The results do align with the literature concerning the remainder of the input parameters—with the exception of the surge level, which is considered an ill-implementation in the parametric design.

Nevertheless, it is important to discriminate between estuary-wide uniform changes to an estuary—as investigated in this study—and local adaptations of the estuary. The implementation of nature-based solutions can also be considered more in the domain of local modifications, such as the local introduction of meanders as described by Pein *et al.* (2018). Therefore, we recommend not to discard the hypotheses enhancing the lateral circulation.

At last, the river discharge is a dominant factor for the salt intrusion length (Fig. 3.4). Therefore, it is noteworthy to pose the potential of river discharge management as an optional nature-based solution to mitigate salt intrusion. This can be realised on two different temporal scales: (1) small-scale by releasing the river water in a pulse-like fashion during a drought, exploiting the nonlinear response of the salt intrusion length to temporal changes in river discharge (e.g., Biemond *et al.*, 2022; Gong & Shen, 2011; Hetland & Geyer, 2004; Monismith, 2017); and (2) large-scale by replenishing freshwater reserves during high river discharges to be released during droughts, in essence reducing the variability in river discharge.

3.6 Conclusion

The presented study encompasses an extensive numerical experiment analysing the sensitivity of the salt intrusion length with respect to thirteen estuary-scale parameters. The use of machine learning techniques enabled us to implement a computationally expensive, state-of-the-art hydrodynamic modelling framework for this exploratory study, which would otherwise be computationally infeasible. Three different analysis methods have been implemented to deduce the underlying relations in the 1,252 model simulations: (1) analysis of the raw output data; (2) over-fitting a regression model and analysing its regression coefficients; and (3) implementing a neural network to determine gradients in the salt intrusion length with respect to the input parameters.

Table 3.2: Qualitative scoring of the hypothesised nature-based solutions including the relevant input parameters. The scores range from insignificant (\pm) to high potential ($++$). Input parameters included between brackets show additional relevant parameters for the hypotheses.

Hypothesis	Parameter(s)	Score
reduced cross-section	d_c, W_c	++
increased bottom friction	$n_c (n_f, \gamma)$	+
enlarged tidal flats	$r_d, W_f (a)$	+
reduced lateral depth variation	κ_c	\pm
increased meandering	A_m, L_m	\pm
managed river discharge	Q	++

In general, the non-dimensional space used by Geyer and MacCready (2014) to classify estuaries (M and Fr_f , Eqs. 3.1 and 3.2, resp.) largely determine the response of the estuary (Figs. 3.2 and 3.7), and thereby the five input parameters of which they are composed of are considered essential estuarine characteristics: tidal range, river discharge, (channel) depth, (channel) width, and (channel) friction. In addition, our results show that the convergence of an estuary (Figs. 3.3b and 3.8) and the presence of tidal flats (Fig. 3.9a) should also be considered as essential parameters in determining the extent of the salt intrusion length in estuaries.

The key finding of this study is the capping relation between an input parameter—or combination of input parameters—and the salt intrusion length, which is indicative of a complex relation between the estuarine response and its characteristics. In other words, favourable settings for large salt intrusion for a single parameter (e.g., large channel depth) is not enough to guarantee this will occur; in most cases, smaller intrusion lengths are observed (Fig. 3.3a). It is the complex interplay of different estuarine characteristics that determine whether a maximum intrusion event occurs, and how often. This yields a promising perspective towards the development of (nature-based) solutions to mitigate salt intrusion, as it indicates that large salt intrusion lengths are the exception and the result of a combination of unfavourable estuarine characteristics. Therefore, modifying one of the relevant characteristics will mitigate the salt intrusion in the estuary, which allows for flexibility in the choice and implementation of (nature-based) solutions.

Reflecting back on the hypothesised nature-based solutions, Table 3.2 shows an overview of the effectiveness of mitigating salt intrusion for all hypothesised nature-based solutions. As elaborated on in Section 3.5, four of the six posed hypotheses show potential to mitigate salt intrusion. This leaves two hypotheses unfit for salt intrusion mitigation: (1) the reduced lateral depth variation; and (2) the meandering estuary. Their relevance in mitigating salt intrusion has been shown in this study to be non-existing—or at best minor (Figs. 3.10 and 3.11).

The reduced water depth can be combined with reducing the width, as they both reduce the cross-sectional area through which the river discharge has to flow, enhancing the relative river flow velocity compared to the available river discharge. In this way, the freshwater Froude number (Fr_f , Eq. 3.2) is enlarged, which has a capping effect on the salt intrusion length (Fig. 3.7b). Thereby, modifying the

cross-sectional area mainly acts to enhance the flushing by river flow. A major question for this type of solutions is whether they can be morphologically stable. If a restriction is added to an otherwise broad and deep estuary, the sediment restricting the flow locally will be subject to increased flow velocities and become unstable. In many cases, however, it is possible to stop—or reduce—dredging in order to reduce the depth, and those solutions appear stable from a physical perspective.

The bottom friction in combination with the convergence modify the tidal wave in the estuary. The bottom friction enhances the tidal mixing (M , Eq. 3.1) and the tidal damping (Eq. 3.7); and the convergence amplifies the tidal wave in the estuary (Eq. 3.7) concentrating the tidal energy over a smaller cross-sectional area for enhanced mixing. Here, the bottom friction in the channel is relevant, while the bottom friction on the tidal flats is of no importance in the mitigation of salt intrusion.

The presence of tidal flats is relevant in mitigating salt intrusion (Fig. 3.9a). This is not so much due to the friction they impose, but rather due to their water storage and effect on tidal asymmetry. The irrelevance of the flat friction allows for variety in ecological development on these flats, creating system-specific additional value to the system; an important component of the *Building with Nature*-philosophy (e.g., de Vriend *et al.*, 2015; van Slobbe *et al.*, 2013).

Although boundary conditions are harder to influence compared to the geomorphological features of an estuary, the fluctuations in river discharge due to the seasons can be smoothed to reduce the fluctuations in salt intrusion over the year. This would provide a more constant and reliable salt distribution in an estuary, which makes spatial planning easier.

All in all, there are clear—albeit sometimes quite complex—correlations between (a combination of) estuary-scale parameters and the salt intrusion length in an estuary. These relations all describe a capping behaviour of the salt intrusion length. Thus, unfavourable characteristics do not necessarily result in a large salt intrusion length as long as one dominant characteristic suppresses the salt intrusion. This behaviour is ideal for the development and implementation of (nature-based) solutions to mitigate salt intrusion.

Acknowledgements. We are indebted to Ariana Torres (SURF) for her support in the development of the computational manager for the many simulations executed. This work used the Dutch national e-infrastructure with the support of the SURF Cooperative using grant no. EINF-1548. At last, we would also like to thank the three anonymous reviewers for their valuable feedback on the original manuscript; their suggestions greatly improved the manuscript.

Author contributions. G.H., S.A., P.H. designed the research; G.H., J.A., P.H. developed the methodology; G.H. performed the research; G.H., W.K., Y.H., P.H. analysed the data; G.H. wrote the manuscript; and G.H., W.K., J.A., Y.H., S.A., P.H. reviewed the manuscript.

Data availability. The dataset used in this study is publicly available as NEESI: Numerical Experiments of Estuarine Salt Intrusion dataset (Hendrickx, 2023a).

Software availability. The trained and implemented neural network is open-access and named ANNESI (Artificial Neural Network for Estuarine Salt Intrusion; Hendrickx, 2022).

II | CONCEPTUALISATION

The aim of the *conceptualisation*-phase is to present the design of potential nature-based solutions to mitigate salt intrusion. Therefore, the objective is to *conceptualise various nature-based solutions to mitigate salt intrusion*.

The results of the *exploration*-phase (i.e., Ch. 3) form the basis for the *conceptualisation*-phase. Two potential nature-based solutions to mitigate salt intrusion are presented in more detail: Chapter 4 considers the temporary placement of a sill to mitigate the landward propagation of saline water during a drought; and Chapter 5 analyses the effects of intertidal area on the estuarine salt intrusion for various estuary classes.

4

NATURE-BASED SOLUTION

Temporary sill

4.1 Introduction

Worldwide, deltas are among the most densely populated and heavily utilised regions with 40% of the population living within 100 km from the coastline (Maul & Duedall, 2019). Due to their closeness to the sea, these regions largely rely on freshwater supply from rivers for their drinking water, which are susceptible to salt contamination (Costall *et al.*, 2018).

Especially during a drought, this much-needed freshwater supply is lacking, causing a direct and indirect reduction of the freshwater availability: directly by a reduced inflow of freshwater to the system, and indirectly by an enhanced salt intrusion (e.g., Gong & Shen, 2011; Lerczak *et al.*, 2009) causing the contamination of the available freshwater. A recent example includes the severe and persistent

This chapter is based on:

Hendrickx, G.G., Manuel, L.A., Pearson, S.G., Aarninkhof, S.G.J., and Meselhe, E.A. (2024). An earthen sill as a measure to mitigate salt intrusion in estuaries. *Estuaries and Coasts*, **47**(5):1199–1208.

drought event in the Lower Mississippi River (LMR), causing an unprecedented advancement of the salt wedge, which threatened to contaminate drinking water intakes of the City of New Orleans (LA, USA). Such strains on freshwater—i.e., water stress—are expected to increase in frequency due to the changing climate (Distefano & Kelly, 2017; Veldkamp *et al.*, 2015). Therefore, it is important to develop salt intrusion mitigation measures.

One such mitigation measure to safeguard the freshwater availability is the construction of a temporary earthen sill—i.e., a submerged, broad-crested dam from local sediments—during a (severe) drought event. The US Army Corps of Engineers has been experimenting with this concept in the LMR near New Orleans giving good results under exceptional drought conditions (Fagerburg & Alexander, 1994; Johnson *et al.*, 1987); and were forced to construct the sill again recently, namely October 2022 and August 2023. Here, a sill is constructed with locally retrieved sediments that remain in place during low flow conditions in order to block the saline water from propagating landward until the sill is naturally flushed away during moderate and high flow conditions, restoring the bed to its pre-intervention state (Fagerburg & Alexander, 1994). This sill aims to halt the upstream propagation of the salt wedge driven by estuarine circulation, and thereby attempts to exploit natural processes to achieve its goal. As the estuarine circulation promotes stratification in the estuary—i.e., saline water flowing underneath less-dense freshwater—, a sill aims to halt the upstream-flowing saline water by blocking the lower part of the water column while allowing for continuation of navigation operations and enabling the discharge of freshwater downstream higher in the water column. Therefore, the construction of the temporary sill in the LMR during a drought can be considered a nature-based solution, where its temporary character is an important component: A permanent sill—equivalent to a submerged weir—would obstruct the flow during non-drought conditions, increasing flood risk in its vicinity (e.g., Villemonte, 1947).

Despite the successes of a temporary earthen sill in the LMR, there is—perhaps surprisingly—not much uptake in other estuaries globally. A more general uptake of this strategy is hampered by a lack of knowledge on the processes causing the mitigation of salt intrusion due to sill construction. Thus, the export of this concept to other estuarine systems requires understanding on how such a sill performs under a variety of fluvial and coastal conditions.

The aim of this chapter is to determine under which boundary and geomorphological conditions a sill is a viable (nature-based) solution to mitigate salt intrusion. In this way, we address the research question of how a sill mitigates salt intrusion in an estuary. The findings from this research subsequently result in design guidelines on the implementation of a sill as mitigation measure for salt intrusion.

4.2 Method

The viability of a sill as a (nature-based) solution to mitigate salt intrusion is assessed by means of numerical experiments. Idealised estuarine morphologies are

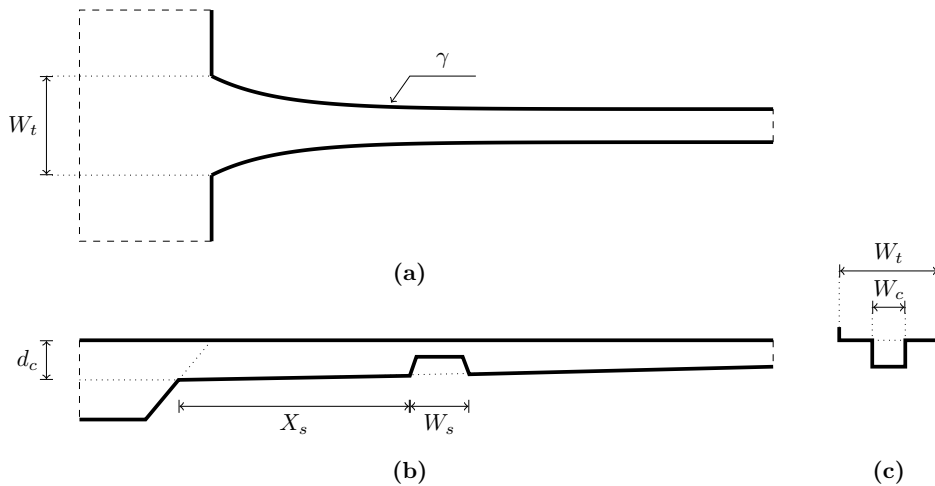


Figure 4.1: Parametric model design. (a) Plan view; (b) longitudinal cross-section; and (c) lateral cross-section. The meaning of the symbols are presented in Table 4.1, except for W_t and X_s : W_t is the total width, $W_t = W_c + W_f$; and X_s the sill location, $X_s = (1 + \lambda_s) L_s^0$.

used to explore various options using a parametric design (Sec. 4.2.1.1) to (1) carefully control the model parametrisation, (2) isolate the various governing processes, and (3) reduce the computational costs. In analysing the estuarine responses to the sill and in determining the processes driving these different responses, a salt flux decomposition is performed (Sec. 4.2.2).

4.2.1 Numerical experiments

The idealised estuaries represent both a generally representative morphology and a morphology representative for the LMR, bridging the step from the idealised estuaries to the LMR. Both estuarine layouts were based on a convergent estuary, where the measures of the “General” estuaries were chosen such that with the same geomorphology we could represent various estuarine classes (Tab. 4.2). The hydrodynamic modelling software used for these numerical experiments is briefly introduced in Section 4.2.1.2.

4.2.1.1 Idealised estuarine geomorphology

For the idealised estuarine geomorphology, a parametric design of an estuary with a sill is used (Fig. 4.1). The boundary conditions are prescribed by a constant river discharge and a single tidal component, i.e., the tidal signal is represented by a monochromatic sine wave with an amplitude and period as described in Table 4.1: a semi-diurnal tide for the “General” estuary, and a diurnal tide for the LMR-representation. Therefore, we assessed quasi-steady states of an estuary.

The water depth on top of the sill is described relative to the channel depth (Tab. 4.1). As this study only considers sills and no gullies, this ratio does not

Table 4.1: Input parameters for the idealised simulations including their values/ranges and corresponding units. The values in the column *General* are used for the model simulations as labelled in Table 4.2.

	Parameter	Symbol	Values		Unit
			General	LMR	
Forcing	Tidal range	a	0.5 – 4.0	0.6	m
	Tidal period	T_t	12	24	h
	River discharge	Q	200 – 1,000	4,950	$\text{m}^3 \text{s}^{-1}$
Geomorphology	Estuary length	L_e	200,000	200,000	m
	Channel depth	d_c	13.0	30.5	m
	Channel width	W_c	500	750	m
	Flat depth	d_f	–	15.0	m
	Flat width	W_f	0	500	m
	Bottom friction	n	0.023	0.010	$\text{s m}^{-1/3}$
	Convergence	γ	40	40	$\times 10^{-6} \text{ m}^{-1}$
Sill	Sill depth ratio ^a	δ_s	0.1 – 1.0	0.5	–
	Sill length	W_s	1,000	200	m
	Sill location ratio ^b	λ_s	-0.25 – 0.25	-0.25 – 0.25	–

^a The sill depth is defined as ratio to the channel depth: $d_s = \delta_s d_c$.

^b The sill location is defined with respect to the salt intrusion length without a sill (L_s^0): $X_s = (1 + \lambda_s) L_s^0$.

exceed one: $\delta_s \leq 1$. The sill height is subsequently defined as:

$$h_s = (1 - \delta_s) d_c.$$

where δ_s is the sill depth ratio [-]; and d_c the channel depth [m].

We consider the location of the sill relative to the salt intrusion length without a sill (L_s^0) by varying the location ratio (λ_s , Tab. 4.1):

$$X_s = (1 + \lambda_s) L_s^0$$

where λ_s is the sill location ratio [-]; and L_s^0 the reference salt intrusion length [m].

The numerical experiments consisted of three sets of analyses: (1) responses for three estuary classes; (2) responses for tidal influence in salt wedge systems; and (3) responses for a representation of the LMR. Table 4.1 shows an overview of all input parameters for these numerical experiments, where the boundary conditions for the first two sets of experiments are presented in Table 4.2, including their estuary classes.

This study implemented a rectangular cross-section despite any potential influences this may have on the subtidal flow (e.g., Schulz *et al.*, 2015; Valle-Levinson, 2008). A rectangular cross-section allowed us to focus on the longitudinal effects of the laterally oriented obstruction, namely the sill. Furthermore, previous research has shown that lateral variations in the cross-sectional profile have a limited impact on the salt intrusion length, which is dominated by other, more relevant estuary-scale variables; thus their effects on the salt intrusion length are on a lesser order of magnitude (Hendrickx *et al.*, 2023c, Ch. 3).

Table 4.2: Boundary conditions per estuary configuration with the estuary class based on the estuarine Richardson number (Ri_E ; Fischer, 1972, Eq. 5.3, p. 79) and Geyer and MacCready (2014, GM14).

Label	a [m]	Q [m^3s^{-1}]	Ri_E	GM14
salt wedge/micro-tidal	0.5	1,000	salt wedge	salt wedge
partially mixed	3.0	500	partially mixed	partially mixed
well-mixed	4.0	200	well-mixed	partially mixed
macro-tidal	4.0	1,000	partially mixed	time-dependent salt wedge

4.2.1.2 Hydrodynamic model

The implemented hydrodynamic modelling software for all numerical experiments is Delft3D Flexible Mesh (Kernkamp *et al.*, 2011). This modelling software implements the hydrostatic pressure assumption and solves for the Reynolds-averaged Navier-Stokes equations. Turbulent structures are resolved using the k - ε turbulence closure model.

Due to the focus on salt intrusion, three-dimensional models were used with a combination of Z - and σ -layers to discretise the vertical axis; Z -layers are known to be best suited for numerically solving salt wedge dynamics (e.g., Stelling & van Kester, 1994), while σ -layers are preferred for representing water levels as they follow the water surface (Deltares, 2022). In addition, σ -layers may cause numerical mixing at steep slopes—such as a sill—due to hydrostatic inconsistency (Haney, 1991). Thus, the vertical discretisation implemented in this study contains Z -layers (static vertical discretisation) for the majority of the water column topped with σ -layers (dynamic vertical discretisation) to accommodate water level changes.

For the description of the model domain, the distinction is made between the shelf and estuarine subdomains. The shelf is a square of 30×30 km with a grid resolution of 62.5×62.5 m near the estuarine mouth, which decreases to the domain's boundaries reaching a resolution of $1,000 \times 1,000$ m. The estuarine domain is 200 km long and its width converges from the mouth (Tab. 4.1) to an upstream minimum based on the river discharge (similar to Hendrickx *et al.*, 2023c); upstream widths vary between approximately 200 and 980 m. The grid resolution at the mouth corresponds with the shelf subdomain—i.e., 62.5×62.5 m—and coarsens towards the upstream boundary, where it is $< 250 \times 1,000$ m; the < 250 m follows from the grid being squeezed by the lateral deformation induced by the convergence. The extent of the high resolution in the estuarine subdomain is set to surpass both the sill's placement (X_s) and salt intrusion length (L_s) to ensure that the area of interest is within the high resolution grid. Nesting between different grid resolutions was accommodated for by triangular grid cells. This parametric design of the estuary and the model's grid are similar to Hendrickx *et al.* (2023c).

The model simulation duration varied per estuary class due to differing spin-up times, which varied from eight days (salt wedge) to 59 days (well-mixed). Subse-

quently, the quasi-steady state analyses were based on the last day of the simulation, i.e., the ninth day (salt wedge) or the 60th day (well-mixed), which included either two tidal cycles (semi-diurnal) or a single tidal cycle (diurnal).

The numerical experiments did not consider any morphological dynamics, i.e., the bed level was stationary. Thus, the flushing of the sill—as mentioned in Section 4.1—was not included.

4.2.2 Salt flux decomposition

To explain the differences in system responses to the introduction of a sill, we performed a salt flux decomposition. Such a decomposition discriminates the various driving mechanisms of the sub-tidal salt flux (e.g., Dronkers & van de Kreeke, 1986; Lerczak *et al.*, 2006; Ralston *et al.*, 2010a). The total salt flux can be written as:

$$F = \overline{\int usdA} \quad (4.1)$$

where u is the flow velocity [ms^{-1}]; s the salinity [psu]; and A the cross-sectional area [m^2]. The over-line indicates tidal averaging, i.e., taking the temporal average over a tidal cycle.

This salt flux can be decomposed in four components (Garcia *et al.*, 2022): the salt flux related to (1) net flow, (2) tidal oscillation, (3) estuarine circulation, and (4) time-dependent shear. The relevant velocity and salinity components are defined by Equations (4.2a) to (4.2e), where ξ represents either the flow velocity, u , or the salinity, s :

$$\xi_* = \xi - \xi_2 - \xi_1 \quad (4.2c)$$

$$\xi_1 = \frac{\overline{\int \xi dA}}{\overline{\int dA}} \quad (4.2a)$$

$$\xi_3 = \frac{\overline{\xi_* dA}}{\overline{dA}} \quad (4.2d)$$

$$\xi_2 = \frac{\overline{\int \xi dA}}{\overline{\int dA}} - \xi_1 \quad (4.2b)$$

$$\xi_4 = \xi_* - \xi_3 \quad (4.2e)$$

such that $u = u_1 + u_2 + u_3 + u_4$. Subsequently, the total salt flux (i.e., Eq. 4.1) can be represented by the sum of these four components:

$$F \approx \underbrace{u_1 s_1 \int dA}_{F_1} + \underbrace{u_2 s_2 \int dA}_{F_2} + \underbrace{\int u_3 s_3 d\bar{A}}_{F_3} + \underbrace{\int u_4 s_4 dA}_{F_4} \quad (4.3)$$

where F_i corresponds with the salt flux component as previously numbered: F_1 relates to the net flow; F_2 to the tidal oscillation; F_3 to the estuarine circulation; and F_4 to the time-dependent shear.

In general, the landward salt fluxes are dominated by the components related to the tidal oscillation (F_2) and the estuarine circulation (F_3), as (1) the net flow (F_1) always results in a seaward directed salt flux, and (2) the time-dependent shear (F_4) is considered a residual term—which is generally an order of magnitude smaller than the other components—and therefore often excluded from the analysis or included in either F_2 or F_3 (e.g., Dronkers & van de Kreeke, 1986; Garcia & Geyer, 2023; Lerczak *et al.*, 2006; Ralston *et al.*, 2010a).

4.3 Results

The results presented in this section are grouped by the three sets of analyses, as introduced in Section 4.2.1.1: (1) estuary classes (Sec. 4.3.1); (2) tidal influence in salt wedge systems (Sec. 4.3.2); and (3) LMR-representation (Sec. 4.3.3).

In all results, the salt intrusion length (L_s) is defined as the tidal- and depth-averaged 1-psu isohaline. Despite our focus on salt wedge estuaries, this value is considered representative; the depth-averaged salt intrusion is highly correlated with both the depth-minimum and -maximum salt intrusion length. To compare the various estuarine responses to the introduction of a sill, we have normalised all salt intrusion lengths with the reference case, i.e., the salt intrusion length in the same estuary without a sill (L_s^0).

By default, the height of the sill is half the water depth, i.e., $\delta_s = 0.5$. This has been found to be the generally most effective sill height in limiting the salt intrusion (Fig. 4.4), and thus highlights the differences between estuarine responses.

4.3.1 Estuary classes

The influence of the placement of a sill changes considerably from a salt wedge system (large effect) to a well-mixed estuary (small effect; Fig. 4.2). In general, the salt intrusion length reduces with seaward placement of the sill. However, the overall influence of the sill on the salt intrusion in the well-mixed estuary is limited. The estuarine response for this estuary class shows fluctuations in its response (Fig. 4.2). These fluctuations are the result of the large tidal oscillation of the salt intrusion length: The variation in salt intrusion length over the tidal cycle (noise, $\pm 30\%$) exceeds the variation in salt intrusion length as function of the sill placement (signal, $\pm 5\%$). This means that the signal is highly distorted, and the noise dominates the output. Due to this insensitivity of the salt intrusion to the sill location, sills are not a relevant mitigation measure in well-mixed estuaries.

In addition, Figure 4.2 shows that the sill can both reduce and enhance the salt intrusion length. This means that when placed incorrectly, a sill might act counterproductively in mitigating salt intrusion. Especially for the partially mixed estuary, a sill has to be placed relatively far seaward to reduce salt intrusion; in case of the salt wedge estuary, the salt intrusion length is almost completely defined by the placement of the sill.

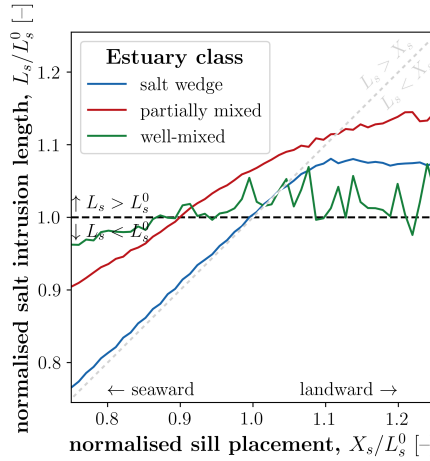


Figure 4.2: Salt intrusion length for three estuary classes (Tab. 4.2) as function of the sill placement ($\delta_s = 0.5$).

Given that the salt intrusion length is most strongly modified by a sill in salt wedge systems (Fig. 4.2), and motivated by real-life implementation in such a system, we focus in the remainder of this study on salt wedge estuaries.

4.3.2 Tidal influence on salt wedge

These results consider the influence of the tidal range on salt wedge estuaries, i.e., the micro- and macro-tidal systems as labelled in Table 4.2. Both variations in the longitudinal sill placement (X_s) and the sill height (h_s) are considered; the sill length (W_s) has been found of less relevance on the salt intrusion, as later discussed in Section 4.4.2.

Figure 4.3 shows that the salt intrusion is reduced if the sill is placed seaward of the reference salt intrusion ($X_s < L_s^0$), but enhanced if the sill is placed landward ($X_s > L_s^0$). This holds for both tidal range values, and indicates a difference between the partially mixed estuary shown in Figure 4.2 and the macro-tidal estuary presented in Figure 4.3.

Aside from this general response between the sill location and the salt intrusion length, the tidal range clearly has an influence on how the salt intrusion is reduced by the sill. While the sill halts the salt intrusion for a small tidal range ($a = 0.5$ m), it is overspilled for a large tidal range ($a = 4.0$ m). Despite the sill overspilling, it reduces the salt intrusion length compared to the reference case—i.e., without sill.

The effectiveness of reducing the salt intrusion by a sill is also influenced by the height of the sill. How the salt intrusion is affected by the sill height is, again, related to the tidal range (Fig. 4.4). For both a small and a large tidal range, the salt intrusion reduces with sill height for $h_s/d_c \leq 0.5$. Once the sill height

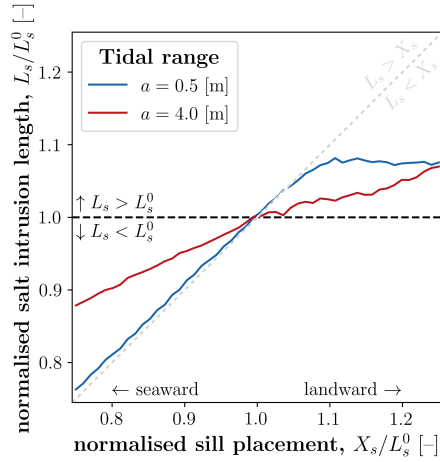


Figure 4.3: Salt intrusion length for various sill placements as well as a small and large tidal range ($\delta_s = 0.5$).

exceeds half the water depth ($h_s/d_c > 0.5$), the responses deviate: For a small tidal range ($a = 0.5$ m), the salt intrusion length remains approximately equal to the sill location; and for a large tidal range ($a = 4.0$ m), the salt intrusion length increases beyond the reference case, i.e., without a sill.

The different responses due to the changes in tidal range can be explained by decomposing the sub-tidal salt fluxes. These salt flux components have been determined for the idealised model simulations without a sill for both tidal range values. The addition of a sill causes some minor irregularities in the salt fluxes around the sill's location (not shown) but does not affect the overall spatial distribution of the salt flux components. These spatial distributions are displayed in Figure 4.5 in which the most relevant salt flux components are highlighted: tidal oscillation and estuarine circulation (F_2 and F_3 in Eq. 4.3, resp.). The longitudinal distance is normalised by the salt intrusion length, as beyond this point all salt fluxes are zero; and the salt fluxes are normalised with their maximum absolute value to better compare between different estuaries—i.e., the salt fluxes are normalised such that $F_i \in [-1, 1]$.

Figure 4.5 shows a clear difference between the dominant salt flux components based on the tidal range whilst both representing salt wedge systems. The landward salt flux is fully driven by the estuarine circulation for a small tidal range with negligible contributions of the other components (Fig. 4.5a). For a large tidal range, the landward salt flux is largely shared between the estuarine circulation and tidal oscillation, and a minor contribution of the time-dependent shear component (Fig. 4.5b).

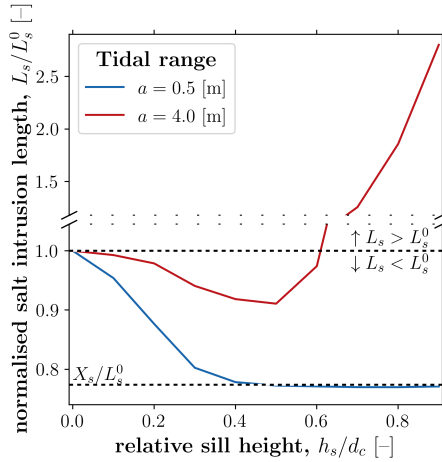


Figure 4.4: Salt intrusion length for various sill heights for both tidal ranges. Note the break in the y -axis.

4.3.3 Lower Mississippi River

As a sill has been successfully implemented in the LMR in the past, an idealised representation of the LMR is included (Tab. 4.1). The LMR is forced by a very small diurnal tide and is river-dominated, resulting in a strong salt wedge. Figure 4.6 presents the response of the idealised LMR with the results as presented in Figure 4.3 as reference. The idealised LMR shows a similar behaviour of the salt intrusion length with respect to the sill placement: The salt intrusion length is reduced when the sill is placed seaward of the reference salt intrusion length ($X_s < L_s^0$), and vice versa. This behaviour is in line with our other results (Fig. 4.3) despite the differences in estuarine geomorphology (Tab. 4.1), such as the introduction of shallow areas.

For $X_s < L_s^0$, the idealised LMR behaves similarly to the micro-tidal system (blue line in Fig. 4.6), which is expected from the similar spatial pattern of salt flux components (Fig. 4.7). However, the enhancement of the salt intrusion length for $X_s > L_s^0$ is not as profound as the micro-tidal system.

4.4 Discussion

We concluded from Figure 4.2 that sills are most viable in (time-dependent) salt wedge systems. Therefore, in Sections 4.4.1 and 4.4.2, we focus on these estuary types, i.e., the micro- and macro-tidal systems (Tab. 4.2). In Section 4.4.3, we address the relevant estuarine characteristics for the suitability of a sill as salt intrusion mitigation measure.

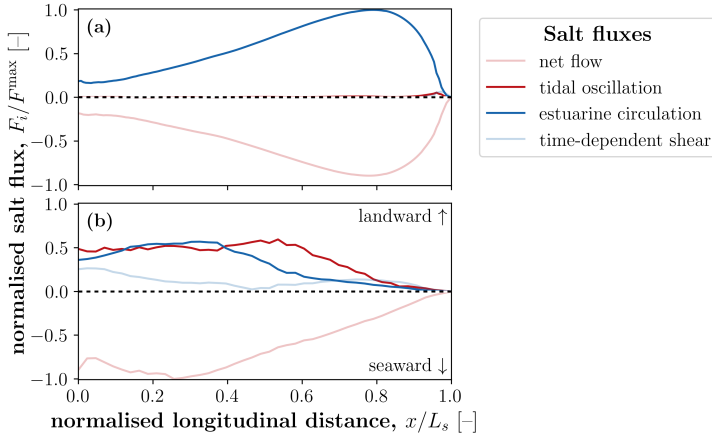


Figure 4.5: Spatial distribution of salt flux components for (a) a small tidal range, $a = 0.5$ m; and (b) a large tidal range, $a = 4.0$ m. These figures show the salt fluxes for the reference cases, i.e., without a sill.

4.4.1 Sill placement

Whether a sill halts the salt intrusion or slows down its landward progression is in part determined by the dominant salt flux components, which are highly susceptible to the tidal range. For a smaller tidal range, the estuarine circulation dominates the landward salt flux (Fig. 4.5a). The estuarine circulation is driven by the density difference between salt and freshwater, and is often referred to as the gravitational circulation (e.g., Hansen & Rattray Jr., 1965) as gravity is the driving force of this circulation. This aligns with the landward progression of the salt wedge being halted by the sill when the estuarine circulation is the driving force: The denser saline water flows underneath the lighter freshwater driven by gravity, but when the denser saline water meets an obstacle, it must overcome this gravitational pull to pass the barrier, i.e., the sill. As the driving force of the landward movement of the salt wedge—i.e., gravity—counteracts the upward movement of the salt wedge, the salt wedge movement (largely) vanishes when it meets the sill.

The landward—and subsequently seaward—momentum input from the tidal oscillations provides the salt wedge enough momentum to push the salt wedge over the sill. As this momentum is not gravity-driven, the driving force of the salt wedge does not disappear when meeting the sill. However, the sill functions as a sink of the tidal momentum causing the salt intrusion to be reduced with respect to an estuary without a sill (Fig. 4.3). When the estuarine circulation is the driving mechanism of the landward salt flux, the salt wedge experiences the sill as a “wall;” while the sill becomes a “speed bump” for a tidally driven salt wedge.

When the sill is placed landward of the reference salt intrusion length—i.e., the salt intrusion length without a sill—, it enhances the salt intrusion (Figs. 4.3 and

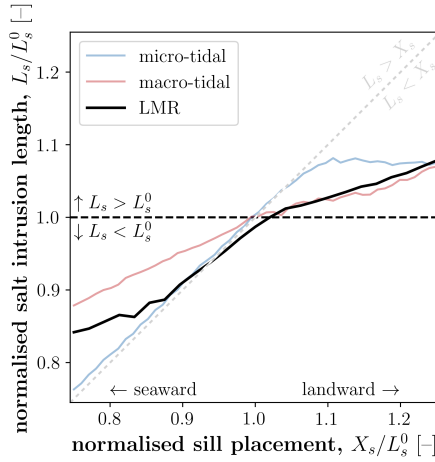


Figure 4.6: Salt intrusion length for various sill placements for the idealised representation of the LMR. The micro- and macro-tidal estuaries from Figure 4.3 are included for comparison.

4.6). This behaviour originates from the sill blocking the seaward flow of freshwater in the lower part of the water column due to which the bottom saline water is experiencing less resistance to flow landward due to the sill implementation. Therefore, the sill's location in the estuary is crucial for its implementation, as a wrongly placed sill can enhance salt intrusion instead of mitigating it. Note that the enhancement of the salt intrusion length is in the order of kilometres due to the local stimulation of the estuarine circulation (Figs. 4.3 and 4.6).

4.4.2 Sill dimensions

Figure 4.4 presents the influence of the sill height on the salt intrusion, which shows that the sill becomes more effective for larger sill heights when $h_s/d_c \leq 0.5$; beyond this point, the sill does not improve ($a = 0.5$ m) or even enhances salt intrusion ($a = 4.0$ m). The increased salt intrusion for higher sills ($h_s/d_c > 0.5$) in case of a large tidal range ($a = 4.0$ m) results from the large difference in flow area over the sill between high and low water, where during low water the sill substantially reduces the flow area and can even become emergent. This results in a push-over of (part of) the salt wedge, which can subsequently not fully return back over the sill trapping the saline water at the landward side of the sill. This is not as relevant in case of a small tidal range ($a = 0.5$ m), because (1) the difference in flow area over the sill between high and low water is smaller; and (2) there is less momentum to push the saline water over the sill. Hence, the higher sills ($h_s/d_c > 0.5$) perform similar to a sill blocking half the water depth ($h_s/d_c = 0.5$). Thus, increasing the sill height is beneficial until approximately halfway the water depth.

As a higher sill requires more sediment, is morphologically less stable, potentially impedes navigation, and increases construction costs, a lower but elongated

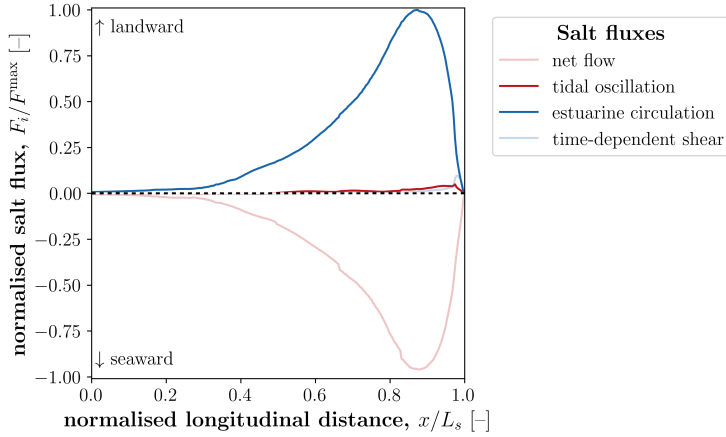


Figure 4.7: Spatial distribution of salt flux components for the idealised representation of the LMR. This figure shows the salt fluxes for the reference case, i.e., without sill.

sill might be preferred. Figure 4.8 shows the effect of the (relative) sill height in case the sill volume (V_s) is maintained by modifying the sill length; a sill length $W_s = 1,000$ m in combination with a sill depth ratio $\delta_s = 0.5$ is used as reference (Tab. 4.1)—labelled V_s^0 in Figure 4.8. Figure 4.8 shows that elongating the sill to compensate for a reduction in the sill height is not very effective, with negligible differences for larger sill heights ($h_s/d_c \geq 0.4$). Thus, the sill height remains the dominant factor in reducing the salt intrusion (Fig. 4.8)—in combination with the sill’s location in the estuary (Fig. 4.3).

4.4.3 Estuary suitability

Despite this study addressing idealised morphologies and a limited subset of estuary conditions, our results indicate that a sill shows the most promising implementation potential for salt wedge estuaries (Fig. 4.2). Here, the classification by Geyer and MacCready (2014) provides a better guide of suitability of a sill than the often used estuarine Richardson number. Sills are effective salt intrusion mitigation measures in both salt wedge and time-dependent salt wedge systems (Fig. 4.3), where the strength of the tidal component is inversely related to the efficacy of the sill. Therefore, we expect a sill as salt intrusion mitigation measure to be of interest in river-dominated estuaries, with decreasing efficacy for increasing tidal energy; e.g., in the Ebro River, the (Lower) Mississippi River, the Amazon River, and the Chang Jiang River (i.e., estuaries classified as [time-dependent] salt wedge in Geyer & MacCready, 2014, their Fig. 6). Note, however, that the implementation of a sill might be constrained by other functions, such as the accessibility of a port and the required sill height (Fig. 4.4).

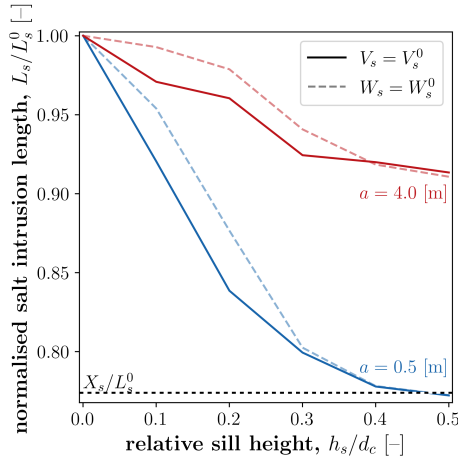


Figure 4.8: Salt intrusion length for various sill heights while maintaining a constant sill volume for both tidal ranges. Dashed lines reflect the sills with a constant sill length (W_s^0) with $V_s \neq V_s^0$, as presented in Figure 4.4.

4.5 Conclusion

A (temporary) sill can be a viable solution in a salt wedge system, both micro- and macro-tidal (i.e., the investigated tidal ranges of 0.5 and 4.0 m, resp.). However, the efficacy of the sill to mitigate salt intrusion is reduced with increasing tidal range, i.e., tidal energy. This behaviour can be explained by analysing the salt flux components (Fig. 4.5): When salt transport is dominated by the estuarine circulation (F_3 in Eq. 4.3), the sill functions as a barrier—or wall—for the landward moving salinity; while salt transport dominated by the tidal oscillation (F_2 in Eq. 4.3) experiences the sill as a speed bump, reducing its landward momentum but not fully halting it. In other words, the stronger the salt wedge in the estuary, the more effective a sill is in mitigating salt intrusion.

A major constraint of the implementation of a sill is the required sill height: The sill must block a substantial part of the water column to be effective, with the sill height half of the water column resulting in the most effective mitigation (Fig. 4.4). This is related to the height of the salt wedge with respect to the sill height. In addition, the longitudinal placement of the sill with respect to the expected salt intrusion length plays a major role in the efficacy of the sill: If the sill is placed seaward of the reference salt intrusion length ($X_s < L_s^0$), the salt intrusion reduces; otherwise ($X_s > L_s^0$), the sill *enhances* the salt intrusion (Figs. 4.3 and 4.6). As salt intrusion length predictions are still susceptible to large uncertainties, the location of the sill should be taken great care of.

Although a sill can be an effective mitigation measure to salt intrusion in various estuarine systems, the constraints on the placement and its height limit its widespread use. As many estuaries around the world provide just sufficient depth

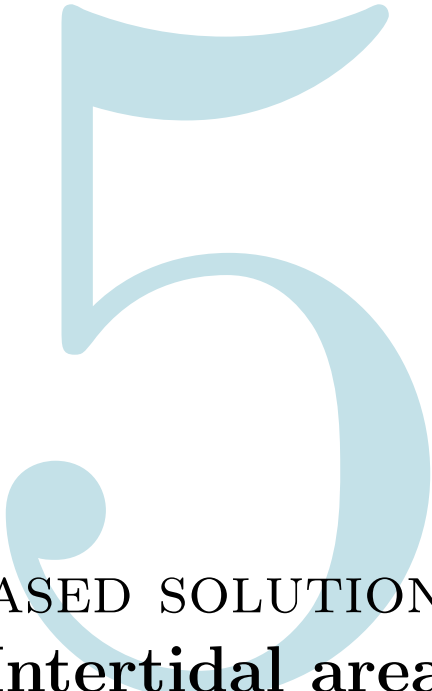
to accommodate vessel passage, the placement of a sill would result in unacceptable hindrance to these ports. Because the LMR is at places deeper than the maintained depth, the sill is a viable salt intrusion mitigation measure without obstructing vessel movements. Thus, despite the efficacy of a well-designed and -placed sill to mitigate salt intrusion, socio-economic constraints limit its general viability as a mitigation measure during droughts.

Acknowledgements. We are indebted to Peter M.J. Herman for his contributions to the research design, which greatly added value to the study and subsequent manuscript. In addition, we would like to thank Herman W.J. Kernkamp for his support with the hydrodynamic modelling software, Delft3D Flexible Mesh. The Tulane co-authors, Laura Manuel and Ehab Meselhe, are grateful for the opportunity to work with the TU Delft team on this research effort. The Tulane co-authors participated in this effort as part of the Mississippi River Delta Initiative – MissDelta supported by the National Academy of Science. This work used the Dutch national e-infrastructure with the support of the SURF Cooperative using grant numbers EINF-4075 and EINF-7152. At last, we would also like to thank the two anonymous reviewers for their valuable feedback on the original manuscript; their suggestions greatly improved the manuscript.

Author contributions. G.H., S.P., S.A., E.M. designed the research; G.H. performed the research; G.H., L.M., S.P., S.A., E.M. analysed the data; G.H., wrote the manuscript; and G.H., L.M., S.P., S.A., E.M. reviewed the manuscript.

Data availability. The dataset used in this study is publicly available (Hendrickx *et al.*, 2024a).

Software availability. Processing code for the salt flux decomposition is open-source (Hendrickx, 2023b).



NATURE-BASED SOLUTION

Intertidal area

5.1 Introduction

Estuaries are human attractors due to their provision of freshwater and fertile soils, which has led them to become heavily modified over time (Pont *et al.*, 2002). The supply of freshwater by the rivers is essential for these regions due to their connectivity with the sea, which promotes salinisation—and thereby contamination—of the freshwater reserves (Costall *et al.*, 2018). This can lead to water stress—i.e., the shortage of freshwater (Wada *et al.*, 2011)—, which is amplified by the high population densities found in coastal regions near estuaries. Water scarcity occurrences and their severity are likely to increase due to (relative) sea level rise, and increased frequency and duration of droughts induced by climate change (Distefano & Kelly, 2017; Veldkamp *et al.*, 2015). In addition to their direct reduction

This chapter is based on:

Hendrickx, G.G., and Pearson, S.G. (2024). On the effects of intertidal area on estuarine salt intrusion. *Journal of Geophysical Research: Oceans*, **29**(9):e2023JC020750.

of the freshwater supply, both sea level rise and increased droughts also promote salt intrusion, which indirectly puts a strain on the freshwater availability.

Meanwhile, estuaries are increasingly constrained due to human interventions, increasing their vulnerability to the changing environment (Pont *et al.*, 2002). These human modifications often include the reduction of intertidal area and the channelisation of the estuary: e.g., the Westerschelde in the Netherlands (Nnafie *et al.*, 2019; van Dijk *et al.*, 2021); the Newark Bay in the United States (Chant *et al.*, 2018); and the Yangtze River in China (Lyu & Zhu, 2019). These developments have increased the vulnerability of these estuarine systems to storm surges (e.g., Temmerman *et al.*, 2013; Zhang *et al.*, 2021) as well as salt intrusion, threatening the freshwater availability (e.g., Hendrickx *et al.*, 2023c; Yang & Wang, 2015). Besides the increased vulnerability, the channelisation and its associated reduction—or even complete removal—of intertidal area greatly damages the estuarine ecosystem (e.g., Seitz *et al.*, 2014; van der Wal *et al.*, 2017; van Wesenbeeck *et al.*, 2014).

Recent studies have shown that intertidal areas influence the salt intrusion in estuaries (e.g., Geyer *et al.*, 2020; Hendrickx *et al.*, 2023c; Lyu & Zhu, 2019; Siemes *et al.*, *in review*; Zhou *et al.*, 2020a), hence the freshwater availability. Tidal flats have been found to reduce salt intrusion (Hendrickx *et al.*, 2023c; Lyu & Zhu, 2019), but their influence has also been shown to be negligible, or even enhance salt intrusion (Siemes *et al.*, *in review*). This discrepancy begs the question of what the influence of intertidal areas is on salt intrusion, and what the underlying mechanisms are.

The aim of this chapter is to investigate the effects of intertidal area on the salt intrusion for different estuary classes. Thereby we address the research question how tidal flats influence estuarine salt intrusion. Instead of exploring all possible estuarine configurations (as in Hendrickx *et al.*, 2023c, Ch. 3), we limit ourselves to the three main estuary classes allowing for a more detailed analysis.

5.2 Method

Central to this study on the effect of intertidal areas on the salt intrusion is a sensitivity analysis exploring different descriptions of tidal flats (Sec. 5.2.1). The effects are determined using a three-dimensional hydrodynamic model: Delft3D Flexible Mesh (Sec. 5.2.2); and we use a salt flux decomposition to distinguish the driving mechanisms of salt transport. This decomposition method is presented in Section 5.2.3.

5.2.1 Sensitivity analysis

To explore the effects of intertidal area on the salt intrusion, we use idealised estuarine morphologies: funnel-shaped estuaries with a centralised channel. The morphology of the idealised estuaries are inspired by the Westerschelde (the Netherlands), Pungue (Mozambique), and Hau (Vietnam). These are defined by estuary-scale parameters in a similar fashion as in Hendrickx *et al.* (2023c). The forcing

Table 5.1: Input parameters including their values or ranges and corresponding units. The idealised geomorphology of the estuaries is inspired by the Westerschelde (the Netherlands), Pungue (Mozambique), and Hau (Vietnam).

Parameter	Symbol	Value	Unit
Tidal range	a	1.0 – 4.0	m
River discharge	Q	200 – 10,000	m^3s^{-1}
Channel depth	d_c	10.0	m
Channel width	W_c	2,500	m
Flat depth ratio	r_d	-1.0 – 1.0	–
Flat width ratio	r_W	1.0 – 2.0	–
Bottom friction	n	0.023	$\text{m}^{-1/3}\text{s}$
Convergence	γ	5.6×10^{-5}	m^{-1}

conditions (tidal range and river discharge) and the parametric design of the tidal flats are varied to investigate their effects on the salt intrusion in an estuary. Table 5.1 gives an overview of the input space explored in this study.

The depth and width of the tidal flats follow from two ratios we have varied (Tab. 5.1): (1) the flat depth ratio, $r_d \in \{0.00, 0.25, \dots, 1.00\}$; and (2) the flat width ratio, $r_W \in \{1.0, 1.2, \dots, 2.0\}$. These are similarly defined as in Hendrickx *et al.* (2023c) resulting in the flat depth (d_f) and width (W_f):

$$d_f = \frac{1}{2}r_d a \quad (5.1)$$

where r_d is the flat depth ratio [-]; and a the tidal range [m];

$$W_f = (r_W - 1) W_c \quad (5.2)$$

where r_W is the flat width ratio [-]; and W_c the channel width [m].

Hendrickx *et al.* (2023c) showed that spatially varying bottom friction—i.e., separate bottom friction values for the channel and the intertidal areas—had little effect on the salt intrusion length. As such, we have applied a uniform bottom friction coefficient (n , Tab. 5.1).

The cross-sectional profile of the estuaries follow a generalised normal distribution. The flat depth ratio (r_d) defines the base of the distribution; and the flat width ratio (r_W) defines the cut-off of the distribution's tail (Fig. 5.1a). Thus, the channel remains constant for all estuarine layouts to which an intertidal area is added based on these two ratios. These ratios are explored using a factorial space, which results in a two-dimensional space (r_d, r_W -space).

The effects of tidal flats on the salt intrusion are considered for three estuary classes: (1) salt wedge, (2) partially mixed, and (3) well-mixed. The classification is based on the estuarine Richardson number (Fischer, 1972):

$$Ri_E = \frac{g\beta s_0 Q}{W_c u_t^3} \quad (5.3)$$

where g is the gravitational acceleration [$g = 9.81 \text{ ms}^{-2}$]; β the haline contraction coefficient [$\beta = 7.6 \times 10^{-4} \text{ psu}^{-1}$]; s_0 the salinity (at the mouth) [$s_0 = 30 \text{ psu}$]; Q

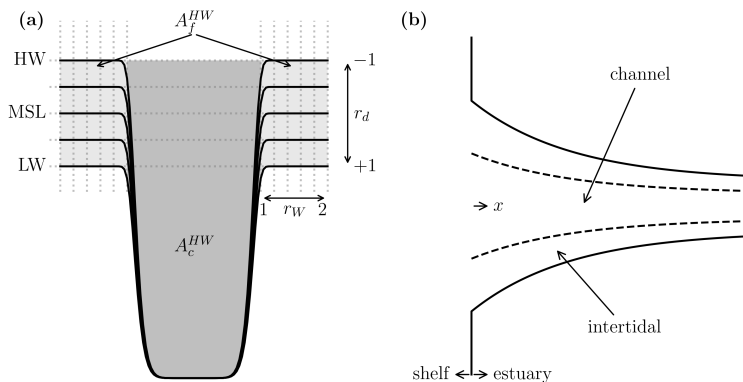


Figure 5.1: Parametric design of estuaries: (a) Cross-section: r_d is the flat depth ratio; r_W the flat width ratio (Tab. 5.1); A_c^{HW} the channel cross-sectional flow area; and A_f^{HW} the flat cross-sectional flow area (Eq. 5.7). (b) Planar view. **LW**: low water; **MSL**: mean sea level; **HW**: high water.

5

the river discharge [m^3s^{-1}]; W_c the channel width ($W_c = W - W_f = W/r_W$) [m]; and u_t the tidal flow velocity [ms^{-1}], which is estimated as:

$$u_t \approx \frac{a}{2\sqrt{2}} \sqrt{\frac{g}{d_c}}$$

where a is the tidal range [m]; and d_c the channel depth [m]. This estimation of the tidal velocity equals the root-mean-squared velocity of a monochromatic wave.

The estuarine Richardson number describes the level of stratification in the estuary resulting in three classes: (1) $Ri_E > 0.8$, salt wedge; (2) $0.08 < Ri_E < 0.8$, partially mixed; and (3) $Ri_E < 0.08$, well-mixed. The chosen forcing conditions—i.e. tidal range, a , and river discharge, Q —per class are given in Table 5.2 including their estuarine Richardson numbers. These forcing conditions result in similar classifications of the estuaries according to the classification by Geyer and MacCready (2014, not shown). Note that the forcing conditions representing the estuarine classes in Table 5.2 investigate only a small part of the input space to enable in-depth analyses of the driving mechanisms. For a fuller coverage of the input space, we refer the reader to Hendrickx *et al.* (2023c).

5.2.2 Hydrodynamic model

The idealised estuaries as described in Section 5.2.1 are simulated using a process-based hydrodynamic modelling software: Delft3D Flexible Mesh (Kernkamp *et al.*, 2011). This software solves the Reynolds-averaged Navier-Stokes equations assuming hydrostatic pressure and implementing the $k-\varepsilon$ turbulence closure model.

The model domain of the parametric design consists of two sub-domains: (1) the shelf, and (2) the estuary. The shelf domain is a square of 30×30 km. The grid resolution varies from $1,000 \times 1,000$ m at the offshore boundaries to 62.5×62.5

Table 5.2: Boundary conditions per estuary class. The estuarine Richardson numbers are based on Equation (5.3).

Class	a [m]	Q [m ³ s ⁻¹]	Ri_E [-]
Salt wedge	1.0	10,000	16.2
Partially mixed	2.0	500	0.101
Well-mixed	4.0	200	0.00507

m near the mouth of the estuary. In between, the grid resolution transitions in steps of a factor of two: 500×500 , 250×250 , and 125×125 m. The different grid resolutions are connected using triangular grid cells.

The estuary domain is a deformed rectangle of 200 km length and varying width, depending on the intertidal area definition (Tab. 5.1). The deformation follows from the convergence, as the estuary's channel width exponentially decreases from 2,500 m (Tab. 5.1) to a minimum channel width of 600 m. The grid resolution in the estuary moves from 62.5×62.5 m at the mouth to $< 250 \times 1,000$ m at the upstream boundary. The high resolution region reached until 150 km landward after which the grid transitions to a coarser resolution in a similar fashion as in the shelf domain. The < 250 m near the upstream boundary follows from the deformation of the rectangular grid induced by the convergence.

Due to the focus on salt dynamics, the estuaries are simulated in three dimensions, where the vertical is discretised with a hybrid Z, σ -layering. Five σ -layers are placed on top of the Z -layers, which are more suitable for computing pycnoclines (Stelling & van Kester, 1994). The interface between the two vertical discretisation methods is at $z_{Z,\sigma} = -4.0$ m resulting in $\Delta\sigma \in [0.4, 1.2]$ m depending on the tidal range and moment in the tidal cycle. Within the estuarine domain, the Z -layers have equal thickness $\Delta Z = 1.0$ m, which grows beyond $z_{cst} = -10.0$ m in the offshore domain—i.e., the shelf domain—with a factor of 1.10.

5.2.3 Salt flux decomposition

The transport of salt is driven by multiple factors with differing relevance depending on the boundary conditions and estuarine morphology. Decomposing the salt fluxes provides insights into these driving forces (e.g., Dronkers & van de Kreeke, 1986; Garcia *et al.*, 2022; Lerczak *et al.*, 2006; Ralston *et al.*, 2010a). The total salt flux is the product of the flow velocity and the salinity, integrated over the cross-sectional area normal to the flow velocity, positive in the landward direction:

$$F = \overline{\int us \, dA} \quad (5.4)$$

where u is the flow velocity [ms⁻¹]; s the salinity [psu]; and A the cross-sectional area [m²]. The over-bar represents temporal averaging over a tidal cycle.

The salt flux decomposition discriminates between four salt flux components: the salt flux related to (1) net flow or river discharge, (2) tidal oscillation, (3) estuarine circulation, and (4) time-dependent shear. These components are build

up by differing the mathematical moment of temporal and/or spatial integration. Equations (5.5a) to (5.5e) list the building blocks, where ξ is either representing the flow velocity, u , or the salinity, s :

$$\xi_1 = \frac{\overline{\int \xi \, dA}}{\int \, dA} \quad (5.5a) \quad \xi_* = \xi - \xi_2 - \xi_1 \quad (5.5c)$$

$$\xi_3 = \frac{\overline{\xi_* \, dA}}{dA} \quad (5.5d)$$

$$\xi_2 = \frac{\int \xi \, dA}{\int \, dA} - \xi_1 \quad (5.5b) \quad \xi_4 = \xi_* - \xi_3 \quad (5.5e)$$

Thus, ξ_1 represents the average over the tide and integration over the cross-section; ξ_2 the integration over the cross-section; ξ_3 the average over the tide; and ξ_4 the remainder. The sum of the flow velocity components, i.e. Equations (5.5a) to (5.5e) with $\xi = u$, equals the flow velocity, u : $\sum_{i=1}^4 u_i = u$. Subsequently, the resulting four salt flux components are defined as:

$$F_1 = u_1 s_1 \int \, dA \quad (5.6a)$$

$$F_2 = u_2 s_2 \int \, dA \quad (5.6b)$$

$$F_3 = \int u_3 s_3 \, d\bar{A} \quad (5.6c)$$

$$F_4 = \int u_4 s_4 \, dA \quad (5.6d)$$

where F_i follows the prior numbering of salt flux components [$\text{psu m}^3\text{s}^{-1}$]: F_1 relates to the net flow; F_2 to the tidal oscillation; F_3 to the estuarine circulation; and F_4 to the time-dependent shear. The sum of these salt flux components represents the total salt flux:

$$F \approx \sum_{i=1}^4 F_i$$

The salt flux related to the net flow (F_1) is offshore-directed (negative), compensating for the other components, which are generally all landward-directed (positive). The flux component related to the time-dependent shear is a residual term (Eq. 5.5e) and generally an order of magnitude smaller than the other fluxes; therefore, it is often excluded from analyses or included in either F_2 or F_3 (e.g., Dronkers & van de Kreeke, 1986; Garcia *et al.*, 2022; Lerczak *et al.*, 2006; Ralston *et al.*, 2010a). In this study, we focus on the salt flux components related to the tidal oscillation (F_2) and the estuarine circulation (F_3) for these reasons.

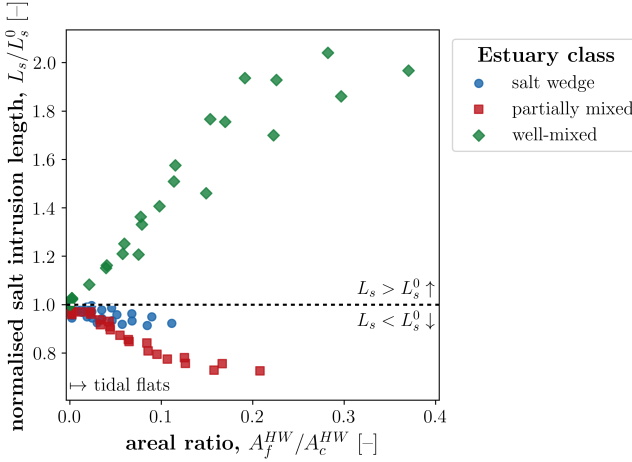


Figure 5.2: Influence of cross-sectional areas at high water on the salt intrusion length (Eq. 5.7 and Fig. 5.1a). $A_f^{HW}/A_c^{HW} = 0$ represents an estuary without intertidal area, which is the reference case from which L_s^0 is derived.

5.3 Results

The salt intrusion length is normalised relative to the reference cases without tidal flats, L_s^0 (i.e., $r_W = 1.0$). The values of these reference salt intrusion lengths are $L_{s,SW}^0 = 11.9$ km (salt wedge), $L_{s,PM}^0 = 43.1$ km (partially mixed), and $L_{s,WM}^0 = 27.9$ km (well-mixed). The effects of the flat depth and width ratios (r_d and r_W) can be encapsulated by a single, combined variable: the wet cross-sectional area of the tidal flats. In Figure 5.2, the cross-sectional area of the channel as well as the tidal flats are considered at high water at the mouth of the estuary. This is reflected by adding the tidal amplitude to the depth profile:

$$A^{HW} = \int_W d(x_0, y) + \frac{1}{2}a \, dy \quad (5.7)$$

where $d(x_0, y)$ is the cross-section profile based on the generalised normal distribution at $x = x_0$, i.e., at the mouth. The cross-sectional area of the channel, A_c^{HW} , considers the width-integration over the channel width (W_c); the remainder reflects the cross-sectional area of the tidal flats, A_f^{HW} (Fig. 5.1a). Further results are presented using the areal ratio, A_f^{HW}/A_c^{HW} (similar to ratios used in Dronkers, 1978; Okubo, 1973).

The cross-sectional flow area of the tidal flats (A_f^{HW}) increases from salt wedge to well-mixed estuaries (Fig. 5.2) due to the larger tidal range imposed to achieve the different estuary classes (Tab. 5.2).

For both the salt wedge and partially mixed estuary classes, an increased areal ratio reduces the salt intrusion length, while the opposite is true for the well-mixed estuary (Fig. 5.2). In case of the well-mixed estuary, increasing the intertidal area

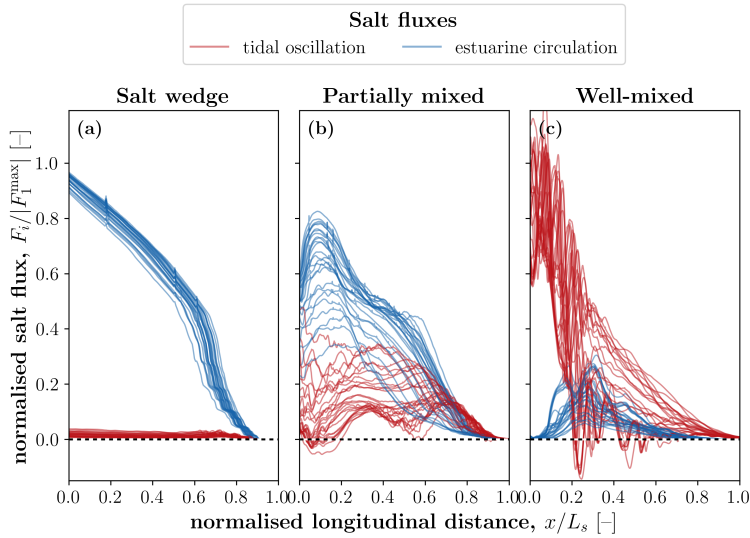


Figure 5.3: Spatial distribution of the major salt flux components (tidal oscillation and estuarine circulation) for all three estuary classes: **(a)** salt wedge, **(b)** partially mixed, and **(c)** well-mixed. The spatial distributions are displayed between the mouth (0.0) and the extent of the estuarine salt intrusion (1.0).

can more than double the salt intrusion length compared to the reference case (i.e., without intertidal area).

The spatial distributions of the salt flux components show a shift from being dominated by the estuarine circulation in a salt wedge estuary (Fig. 5.3a) to tidal oscillation in a well-mixed estuary (Fig. 5.3c). The introduction of intertidal area does little to change the dominant salt flux component in these estuaries that are strongly dominated by either the estuarine circulation or the tidal oscillation related salt fluxes.

However, the partially mixed estuary shows a transition between these salt flux components (Fig. 5.3b), where the intertidal area has a profound influence on the the spatial distribution of the salt flux components (Fig. 5.4): Increasing the intertidal area causes the dominant component of the landward salt flux to shift from estuarine circulation to tidal oscillation. A complete overview of all salt flux components and their dependencies on the areal ratio for all three estuary classes is given in Figure C.1 (p. 209).

5.4 Discussion

Salt intrusion is affected by the expansion of intertidal area in two opposite directions: it increases for well-mixed estuaries; but decreases for salt wedge and partially mixed estuaries (Fig. 5.2). In case of the well-mixed estuaries, the intertidal area facilitates the influx of saline water over the flats (Fig. 5.5c). This influx

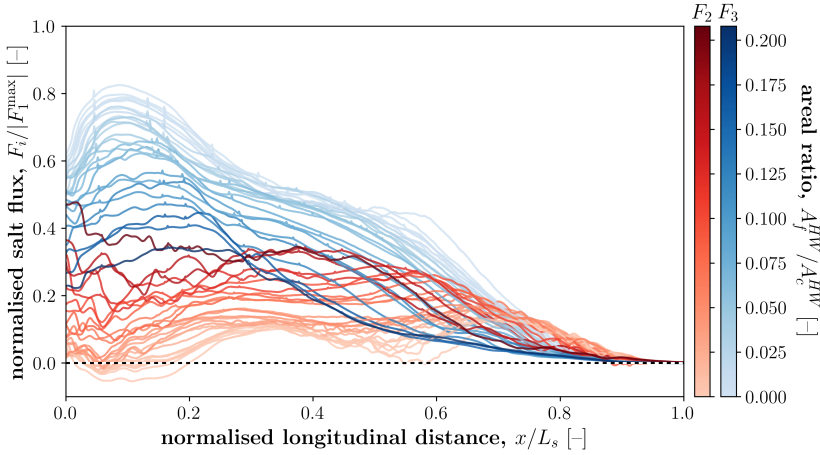


Figure 5.4: Spatial distribution of the major salt flux components in the partially mixed estuary: F_2 , tidal oscillation (Eq. 5.6b); and F_3 , estuarine circulation (Eq. 5.6c). The colour-grading represents the areal ratio for the partially mixed estuary class (using Eq. 5.2). Same data as Figure 5.3b.

is absent for the other estuarine classes, where the salt fluxes are negligible on the intertidal areas (Figs. 5.5a and b; in line with Geyer *et al.*, 2020).

The influx over the intertidal flats in well-mixed estuaries increases with increasing intertidal area: Figure 5.6 distinguishes between the salt fluxes in the channel and on the tidal flats. For both the salt wedge and partially mixed estuaries, the in- and effluxes are balanced both in the channel and on the flats (Figs. 5.6a and b); however, the flats are a strong importer of saline water for well-mixed estuaries, which is compensated for via the channel (Fig. 5.6c).

In well-mixed estuaries, this influx over the intertidal area and efflux in the channel follows a typical barotropic circulation pattern (e.g., Bosboom & Stive, 2021; Kjerfve, 1978; Wang *et al.*, 1999). This planar circulation pattern is also clearly visible in the residual flow patterns (Fig. 5.7c). However, it is missing for the salt wedge and partially mixed estuaries (Figs. 5.7a and b). The negligible role of the intertidal area on the salt fluxes for the salt wedge estuary (Fig. 5.6a) is in line with Geyer *et al.* (2020); and this statement can be extended to partially mixed estuaries as well (Fig. 5.6b).

In addition to the total salt fluxes and flow patterns, the enhancement of intertidal areas also changes the distribution of salt flux components: Figure 5.4 shows an increasing dominance of the tidal oscillation of the landward salt flux with increasing intertidal area, i.e., increasing areal ratio A_f^{HW}/A_c^{HW} . (An overview with all estuary classes is presented in Fig. C.1, p. 209.)

In compound channels like those featured in this study, the abrupt depth change between shallow intertidal areas and the main channel enhances mixing (e.g., De Leo *et al.*, 2022; Stocchino *et al.*, 2011; van Prooijen *et al.*, 2005). This mixing is intensified by the tidal influence (He *et al.*, 2023). This increase in tidal mixing is

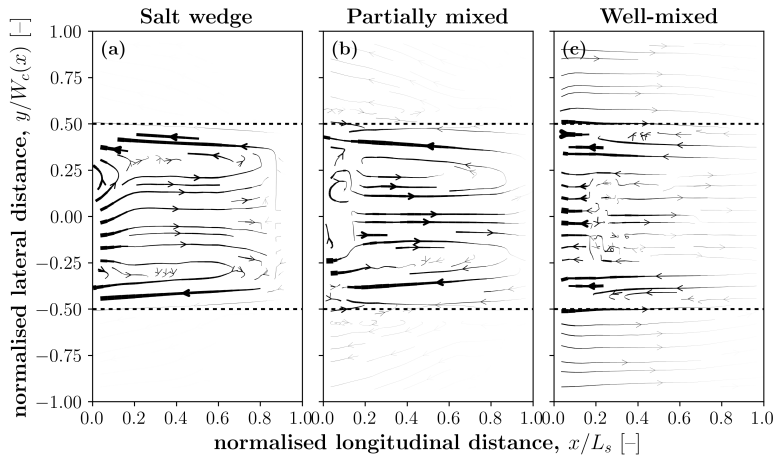


Figure 5.5: Streamlines of tide-averaged, depth-integrated salt fluxes (Eq. 5.4) for the three estuarine classes: (a) salt wedge, (b) partially mixed, and (c) well-mixed. The flux-field represents the estuary with the maximum flat width (i.e., $r_W = 2.0$) and the flat depth at mean-sea-level (i.e., $r_d = 0.0$). The width of the streamlines represent the flux magnitude. Note that the y -axis is such normalised that the convergence of the estuary is compensated for.

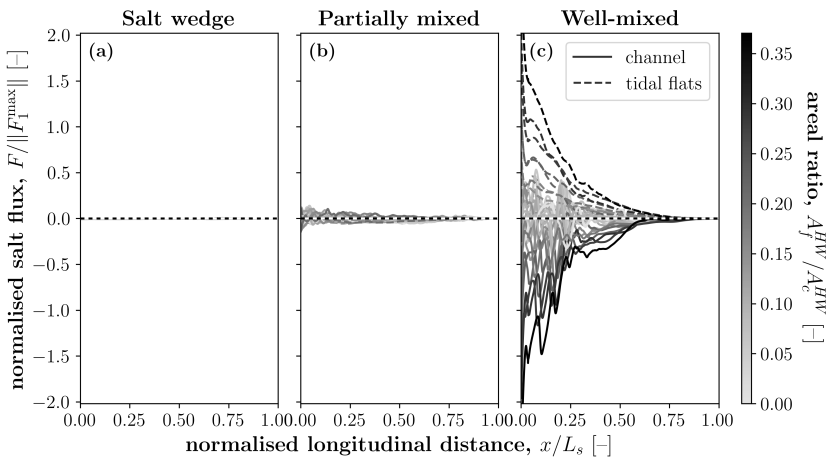


Figure 5.6: Spatial distribution of the total salt flux (Eq. 5.4, F) distinguishing between the channel and the tidal flats for all three estuarine classes: (a) salt wedge, (b) partially mixed, and (c) well-mixed.

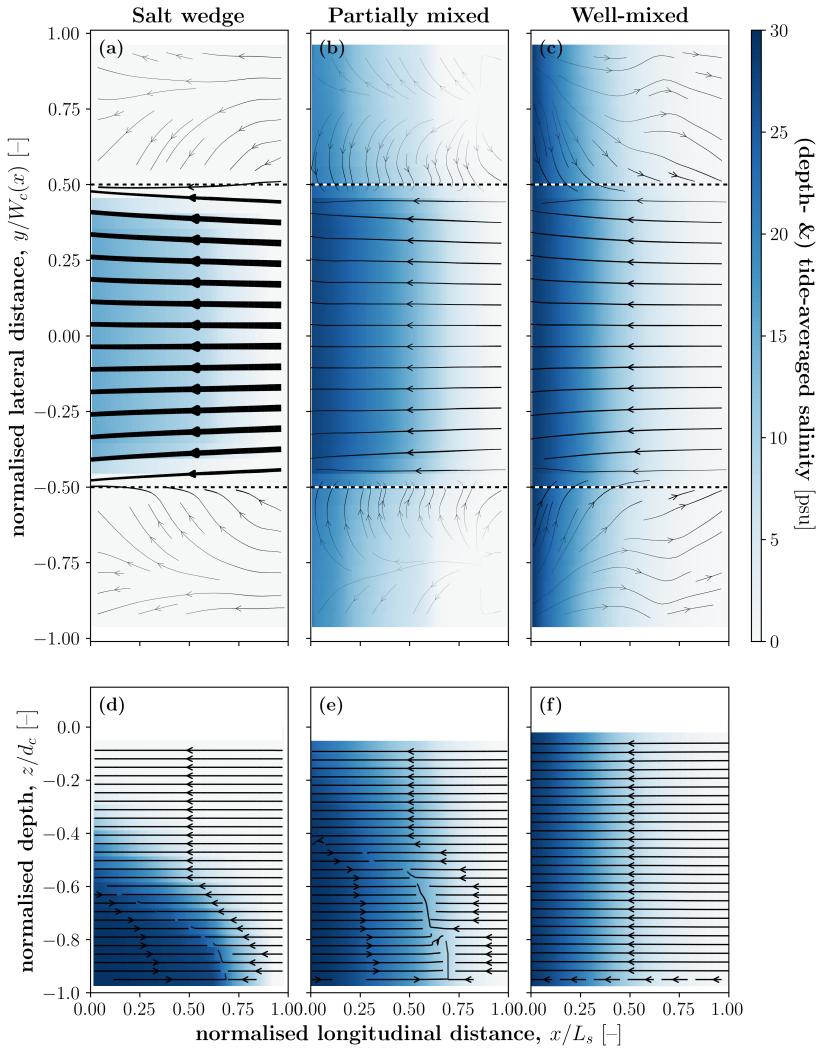


Figure 5.7: Spatial distribution of the flow velocity and salinity, both considered tide- (and depth-averaged), for all three estuary classes: (a,d) salt wedge, (b,e) partially mixed, and (c,f) well-mixed. The flow-fields are represented for the same estuaries as in Figure 5.5. The width of the streamlines represents the flow magnitude (in the top row); the blue-shading the salinity.

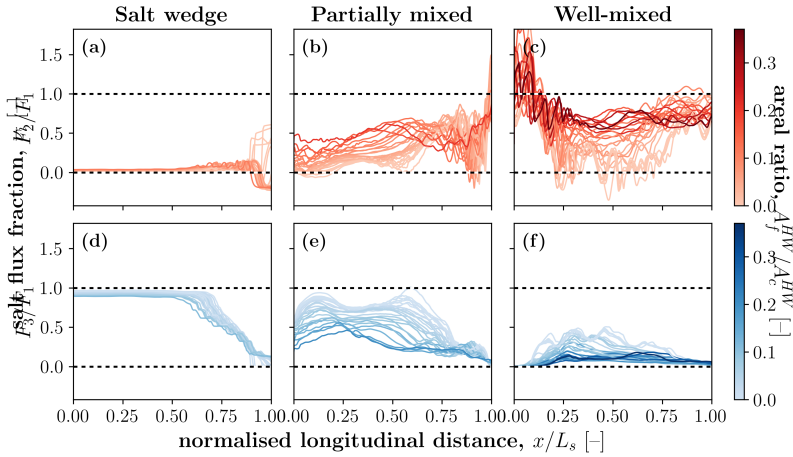


Figure 5.8: Salt flux fractions as function of the areal ratio related to (a–c) the tidal oscillation, ν_2 ; and (d–f) the estuarine circulation, ν_3 , for all three estuary classes: (a,d) salt wedge, (b,e) partially mixed, and (c,f) well-mixed.

5

reflected by an increased contribution of the tidal oscillation to the salt balance. To illustrate the relative contribution of the tidal flux, Hansen and Rattray Jr. (1965, 1966) proposed the use of a salt flux fraction. We have generalised this definition to reflect the importance of any of the salt flux components:

$$\nu_i = -\frac{F_i}{F_1} \quad (5.8)$$

where F_i is salt flux i with $i \in \{2, 3\}$ (i.e., Eqs. 5.6b and 5.6c) [$\text{psu m}^3\text{s}^{-1}$]; and F_1 the salt flux related to the net flow (Eq. 5.6a) [$\text{psu m}^3\text{s}^{-1}$].

As F_1 is the seaward-directed salt flux and the other salt flux components are landward directed, the flux fraction ν_i (Eq. 5.8) quantifies the contribution— or fraction—of the salt flux F_i to the landward flux. Due to the opposing directions— i.e., opposing signs—of the fluxes, Equation (5.8) includes a minus-sign such that $\nu_i \in [0, 1]$.

Estuarine circulation reduces with increasing intertidal area (Fig. 5.4) for all three estuarine classes (Fig. 5.8d–f), whereas the tidal flux gains relevance (Fig. 5.8a–c). When the dominant salt flux component is related to the estuarine circulation, this suppression by the intertidal area reduces the salt intrusion; thus, suppressing the estuarine circulation in salt wedge and partially mixed estuaries decreases the salt intrusion (Fig. 5.2a and b). However, in case the dominant salt flux is related to the tidal oscillation, reducing the estuarine circulation—and hence further enhancing the tidal flux—will promote salt intrusion; this is the case for well-mixed estuaries (Fig. 5.2c). This is consistent with the increased tidal dispersion—and correspondingly salt intrusion—due to tidal trapping identified by Dronkers (1978) and Okubo (1973).

Note, however, that the fractions in Figure 5.8 do not always add up to 1—especially in case of the well-mixed estuary (Fig. 5.8c and f). This discrepancy is related to a larger contribution of the time-dependent shear (F_4) for the partially mixed and well-mixed estuaries (Fig. C.1, p. 209).

The suppression of the estuarine circulation by the introduction of intertidal area as found in this study contradicts the findings by Zhou *et al.* (2020a). In their study, the addition of intertidal area instead stimulated the estuarine circulation. Their modelled increase in estuarine circulation was attributed to tidal straining (Zhou *et al.*, 2020a), using the decomposition method proposed by Burchard *et al.* (2011). Following this reasoning, the estuarine circulation must increase in our study as well, since our width-to-depth ratio favours tidal straining (Schulz *et al.*, 2015). This discrepancy is expected to result from the inclusion of a net flow due to the river discharge in our study, which is neglected in the studies of Schulz *et al.* (2015) and Zhou *et al.* (2020a). Furthermore, the simulations executed in our study consider the whole estuarine domain (Fig. 5.1b), while Zhou *et al.* (2020a) only consider a cross-sectional slice of the estuary. Thus, the baroclinic effects of enlarging the intertidal area are magnified where barotropic effects are dominant; e.g., increasing ebb-dominance of an estuary generally reduces its salt intrusion (e.g., Cheng *et al.*, 2013; Hendrickx *et al.*, 2023c; Pein *et al.*, 2018).

In all of the estuaries we investigated, there is a shift from salt fluxes driven by estuarine circulation to tidal oscillation as the areal ratio increases (Fig. 5.8). However, the effects of areal ratio on salt intrusion differ greatly (Fig. 5.2): from mild reduction of the salt intrusion for salt wedge estuaries, substantial reduction of salt intrusion for partially mixed estuaries, to enhancement of salt intrusion in well-mixed estuaries. This discrepancy relates to the ability of the tidal mixing to overcome the stratification; a balance expressed by the Simpson number (e.g., Burchard *et al.*, 2011; Geyer & MacCready, 2014; Simpson *et al.*, 1990):

$$Si = -\frac{g\beta d_c^2}{c_f u_t^2} \frac{\partial s}{\partial x} \quad (5.9)$$

with

$$c_f = \frac{gn^2}{d_c^{1/3}}$$

where the longitudinal salinity gradient is determined on an estuary-scale, i.e., based on the salt intrusion length; c_f is the nondimensional friction coefficient [-]; and n the Manning's n [$\text{m}^{-1/3}\text{s}$] (Tab. 5.1).

The partially mixed and salt wedge estuaries we investigated have a value $Si > 0.2$, which is marked as the transition value at which tidal mixing cannot overcome stratification throughout the tidal cycle (e.g., Cheng *et al.*, 2013; Geyer & MacCready, 2014; Stacey & Ralston, 2005). The estuarine circulation scales with the Simpson number (Burchard & Hetland, 2010; Geyer & MacCready, 2014), and even more so for large Simpson numbers (i.e., $Si > 0.2$; Geyer & MacCready, 2014; Ralston *et al.*, 2008). Thus, increasing the tidal mixing in such systems reduces the landward salt transport—i.e., reduces the salt intrusion.

Table 5.3: Simpson number per estuary class (Si , Eq. 5.9). Extended input space with respect to Table 5.1 indicated in italics.

Class	a [m]	Q [m ³ s ⁻¹]	Ri_E [-]	Si [-]
Salt wedge	1.0	10,000	16.2	3.53
Partially mixed	<i>1.0</i>	<i>200</i>	<i>0.325</i>	<i>0.489</i>
	2.0	500	0.101	0.244
	<i>4.0</i>	<i>10,000</i>	<i>0.254</i>	<i>0.364</i>
Well-mixed	4.0	200	0.00507	0.0941

To further investigate this phenomenon, we extended the input space with two additional sets of boundary conditions representing estuaries classified as “partially mixed” (Tab. 5.3). Both added estuaries showed a similar response to the salt wedge estuary; i.e., there is a weak reduction in the salt intrusion length for increasing intertidal area (not shown).

These scaling relations with the Simpson number and the findings of this study suggest the following: (1) for $Si > 0.2$ (permanently stratified), the addition of tidal mixing by enlarging the intertidal area reduces the salt intrusion length; (2) for $Si < 0.2$, the addition of tidal mixing enhances tidal dispersion causing the salt intrusion to increase; and (3) the mitigating effect of intertidal areas on salt intrusion increases the closer the Simpson number gets to its critical value, i.e., $Si = 0.2$ —so long as it remains above this value.

5.5 Conclusion

The enhancement or reduction of salt intrusion as a function of intertidal area depends on the estuary class (Fig. 5.2): the enlargement of intertidal area reduces the salt intrusion in salt wedge and partially mixed estuaries; in well-mixed estuaries, the effect is opposite.

The driving mechanisms of salt intrusion—i.e., the salt flux components (Eqs. 5.6a to 5.6d)—are similarly affected by intertidal area, independent of estuary class. The estuarine circulation is damped by increasing intertidal area (Fig. 5.8). As estuarine circulation is the dominant driver of landward salt transport in salt wedge and partially mixed estuaries, suppressing this mechanism results in a reduction of the salt intrusion. However, in well-mixed estuaries, the landward tidal salt flux is dominant, which is enhanced by enlarging the intertidal area. Therefore, the salt intrusion grows with increasing intertidal area in well-mixed estuaries.

Differences between our study and existing literature can be explained by several factors, including (1) the addition of a river discharge that influences both the longitudinal salinity gradient and the barotropic circulation patterns, which can dominate the system; and (2) the model design decisions, which may affect the connectivity between the channel and intertidal area (e.g., the type of vertical discretisation).

Whether the enlargement of intertidal area increases or reduces salt intrusion has been linked to the Simpson-number (Si , Eq. 5.9). For permanently stratified estuaries ($Si > 0.2$), the increase of intertidal area has a negative effect on the salt intrusion. This is because the introduced mixing due to the intertidal flats reduces the dominant salt flux driven by the estuarine circulation. On the other hand, for $Si < 0.2$, larger intertidal areas cause an increase in salt intrusion, as the additional mixing contributes to the tidal dispersion. The closer the Simpson number is to its critical value of $Si = 0.2$ (i.e., the tipping point in the stratification-mixing balance), the stronger the influence of the intertidal area on the salt intrusion.

Acknowledgements. We are indebted to Peter M.J. Herman and Stefan G.J. Aarninkhof for their contributions to the early stages of the research design, which greatly added value to the study and subsequent manuscript. This work used the Dutch national e-infrastructure with the support of the SURF Cooperative using grant no. EINF-4075. At last, we would also like to thank the two anonymous reviewers for their valuable feedback on the original manuscript; their suggestions greatly improved the manuscript.

Author contributions. G.H., S.P. designed the research; G.H. performed the research; G.H., S.P. analysed the data; G.H. wrote the manuscript; and G.H., S.P. reviewed the manuscript.

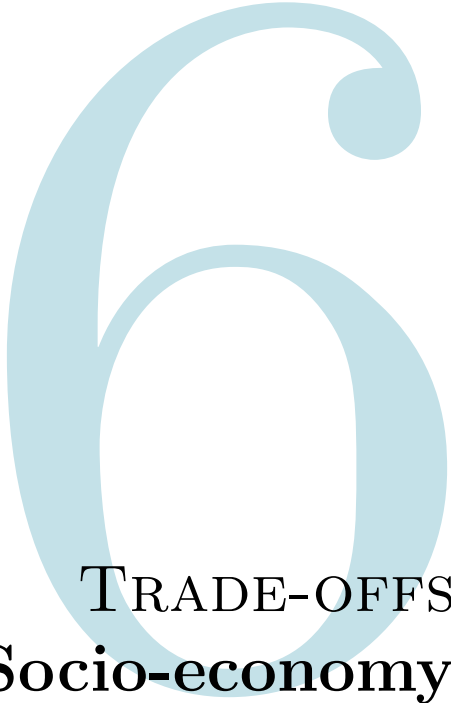
Data availability. The dataset used in this study is publicly available (Hendrickx & Pearson, 2024a).

Software availability. Processing code for the salt flux decomposition is open-source (Hendrickx, 2023b).

III | EVALUATION

The aim of the *evaluation*-phase is to assess nature-based solutions to mitigate salt intrusion on a multidisciplinary level. Thereby, the objective is to *evaluate nature-based solutions in a multidisciplinary context*.

Two novel approaches to evaluate (nature-based) solutions are presented: Chapter 6 addresses the socio-economic trade-off between port logistics and freshwater availability by means of modifying the estuarine water depth; and Chapter 7 focuses on the socio-ecological balance by assessing the implications of reopening a previously-closed estuary.



6

TRADE-OFFS

Socio-economy

6.1 Introduction

Globally, deltas have been attractors of human activity and other forms of life alike. This is because they provide fertile soils and access to freshwater, as well as an open connection to the sea (Maul & Duedall, 2019; Pont *et al.*, 2002). In addition, estuaries are also ecologically valuable systems due to their high biodiversity (Tangelder *et al.*, 2017), and their calm waters function as nurseries (Breine *et al.*, 2011; Tulp *et al.*, 2008).

With their attractiveness, estuaries house many different stakeholders with often conflicting interests: (1) communities require fresh surface waters for drinking water, agriculture, and industry, and low water levels for safety (e.g., Temmer-

This chapter is based on:

Bakker, F.P., **Hendrickx, G.G.**, Keyzer, L.M., Iglesias, S.R., Aarninkhof, S.G.J., and van Koningsveld, M. (*in review*). Trading off dissimilar stakeholder interests: Changing the bed level of the main shipping channel of the Rhine-Meuse Delta while considering freshwater availability. Submitted to *Environmental Challenges*.

man *et al.*, 2013; Wada *et al.*, 2011); (2) ports demand sufficient water depths and low current velocities to facilitate safe operations for deep-draughted vessels (van Koningsveld *et al.*, 2023); and (3) ecological diversity facilitates estuarine resilience (e.g., Folke *et al.*, 2002; Loreau *et al.*, 2003), which arises from a multitude of gradients generally present in natural estuaries (e.g., Mestdagh *et al.*, 2020; Tangelder *et al.*, 2017; Ysebaert *et al.*, 2003).

Over time, humans have interfered in the estuarine system to optimise performances considered important: e.g., (1) channel deepening to improve the accessibility of the port (e.g., Best, 2019; Johnson *et al.*, 1987); (2) closing off of estuaries for water safety (e.g., Figueroa *et al.*, 2022; Orton *et al.*, 2023); and (3) the creation of freshwater buffers for freshwater availability (e.g., Morris, 2013; Tönis *et al.*, 2002). However, such large-scale interventions generally have negative side-effects for other estuarine functions not considered in the assessments (e.g., de Vet *et al.*, 2017; van Wesenbeeck *et al.*, 2014; Yang *et al.*, 2010).

With the ongoing urbanisation of estuaries and worldwide globalisation (Maul & Duedall, 2019), conflicting stakeholder objectives become more stringent. Simultaneously, the changing climate pressures the estuarine functions supporting these objectives; e.g., resulting in reduced freshwater availability (Alcamo *et al.*, 2007; Distefano & Kelly, 2017; Kumar *et al.*, 2013). As a result, decisions and policies must be made regarding more sensitive trade-offs in a crowded, high-stakes environment.

An example of a trade-off of conflicting stakeholder objectives is the increasing interest in deeper waterways to limit vessel waiting times—i.e., improve port efficiency (Almaz & Altiok, 2012)—, while there is increasing demand for freshwater (Distefano & Kelly, 2017; Vörösmarty *et al.*, 2000). Deeper estuaries are, however, known to cause more salt intrusion (e.g., Hansen & Rattray Jr., 1965; Hendrickx *et al.*, 2023c; Veerapaga *et al.*, 2020), pressuring freshwater availability. Worldwide, the economic advantages of port expansions push channels to be deepened to facilitate further port development and growth; e.g., Bahía Blanca, Argentina (Zilio *et al.*, 2013); Hudson River, NY, USA (Ralston & Geyer, 2019); Mekong Delta, Vietnam (Nguyen & Le, 2023); Mississippi River, LA, USA (Johnson *et al.*, 1987); Niger Delta, Nigeria (Dada *et al.*, 2016); Pearl River, China (Yuan & Zhu, 2015); Rhine-Meuse Delta, the Netherlands (Cox *et al.*, 2022); Yangtze River, China (Chen *et al.*, 2019).

During normal conditions, such deepening generally does not strain the freshwater availability. However, it is during droughts that the deepened channels may cause freshwater shortages. Substantial efforts are made to limit the impact of such channel deepening during threatening events: e.g., in the Lower Mississippi River (LA, USA), a temporary earthen sill is placed during droughts to halt the landward propagation of the salt wedge (Fagerburg & Alexander, 1994; Hendrickx *et al.*, 2024b; Johnson *et al.*, 1987). Nevertheless, the freshwater reserves were recently severely stressed (e.g., end of 2023; Miller & Hiatt, 2024); in the Rhine-Meuse Delta (RMD), the Netherlands, a costly and complex freshwater distribution network transports freshwater from upstream to downstream locations to comply

with the freshwater demands during a drought in response to the deepening of the main channel (HydroLogic, 2015, 2018).

Both these examples reflect rare, extreme events for the cases of the Mississippi River (Miller & Hiatt, 2024) and the RMD (Toreti *et al.*, 2022; Wegman *et al.*, *in review*). However rare and extreme, such severe droughts fall within a trend of increasing droughts worldwide (Zhao *et al.*, 2024), and are projected to increase in frequency and duration (Jones *et al.*, 2024; Lee *et al.*, 2024). Therefore, the pressure on estuaries and their livability will increase with climate change as well.

The clear opposing objectives of stakeholders pose a challenge for decision- and policy-makers. Not only are the effects of water depth on the port logistics and accessibility as well as on the up-time of water intakes both highly nonlinear, their performance metrics do not align and are not easily translated to monetary units. As a result, decision- and policy-makers are forced to compare apples with oranges.

Therefore, this chapter presents a general method that enables decision- and policy-makers to assess trade-offs of opposing socio-economic stakeholder objectives. Thereby we address the research question of how to systematically quantify trade-offs of multiple dissimilar, conflicting stakeholder interests in highly-urbanised and intensely-utilised estuaries. The research is limited to the two stakeholder interests of freshwater availability and cargo delays that are affected by the design bed level of the estuary's main channel. We implemented the method to the case study of the severely dry year of 2022 in the RMD of which the main channel has recently been deepened, but where shallowing is considered as an option to improve freshwater availability.

The chapter is structured as follows. Section 6.2 provides a detailed overview of the trade-off in the RMD. Section 6.3 describes the materials and methods used to quantify the effects of a changing bed level on the objectives of the port and freshwater intakes. Section 6.4 presents the obtained trade-off curve of the performance indicators. Sections 6.5 and 6.6 provide a discussion and our conclusions respectively.

6.2 Case study: lower Rhine-Meuse Delta

6.2.1 System description

The RMD is the delta of the confluence of the Rhine (Waal and Lek branches) and Meuse rivers (Fig. 6.1). This delta consists of multiple branches with five emissaries with the Nieuwe Waterweg (NWW) being the principal outlet under average discharge conditions, with an open connection to the North Sea. The main source of freshwater to the RMD is the snowmelt- and rain-fed Rhine river with an average discharge of $2,160 \text{ m}^3\text{s}^{-1}$, compared to the on average $290 \text{ m}^3\text{s}^{-1}$ contributed by the rain-fed Meuse river (Sperna Weiland *et al.*, 2015).

The magnitude and division of the incoming freshwater over the branches are regulated by weirs and discharge sluices. This is based on the measured water level of the Rhine at Lobith, where the river enters the Netherlands. The multi-objective goal of this water management system is to jointly (1) guarantee water safety,

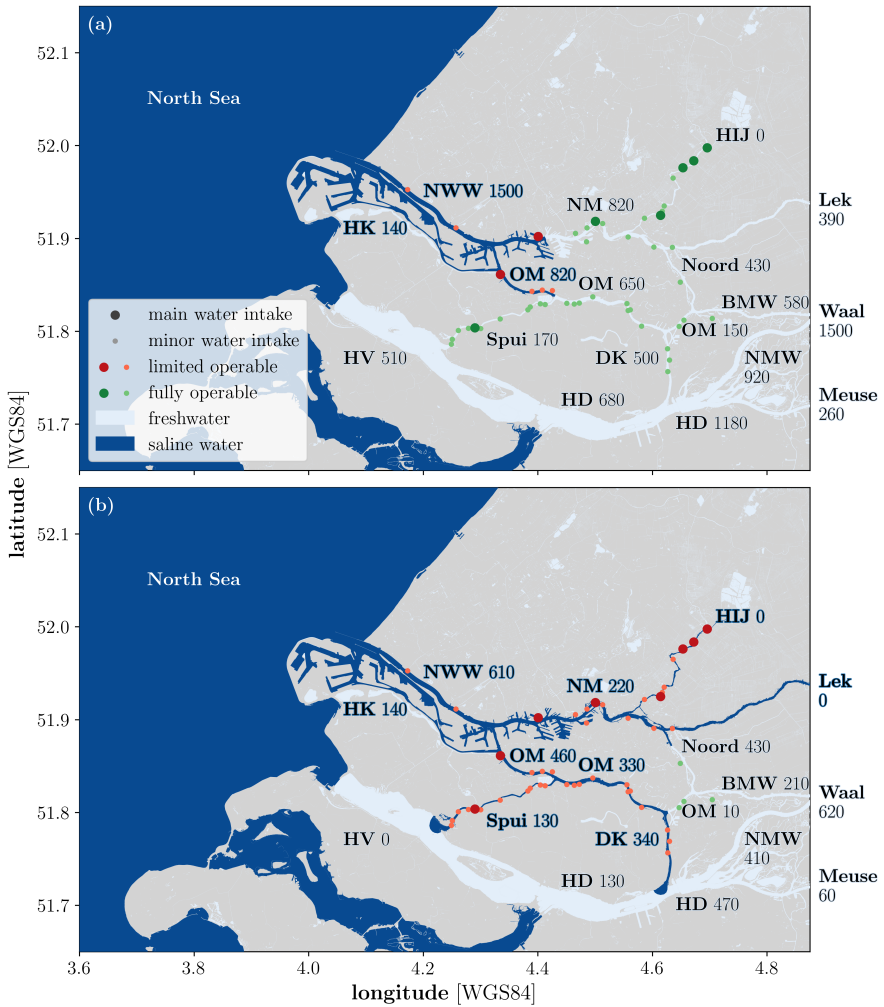


Figure 6.1: Overview of the Rhine-Meuse Delta highlighting the branches it is made off, including their discharge and the brackish water extent (a) during average conditions, and (b) during a drought. The water intake stations that are affected by the brackish water are highlighted. BMW: Beneden Merwede; DK: Dordtsche Kil; HD: Hollands Diep; HIJ: Hollandse IJssel; HK: Hartel Kanaal; HV: Haringvliet; N: Noord; NM: Nieuwe Maas; NMW: Nieuwe Merwede; NWW: Nieuwe Waterweg; OM: Oude Maas. (Discharges and salt intrusion based on de Vries, 2014; HydroLogic, 2019b; van der Wijk, 2016.)

(2) provide and store freshwater, (3) facilitate inland shipping, and (4) protect ecological values (Rijkswaterstaat, 2019).

The NWW is designed to convey $1,500 \text{ m}^3\text{s}^{-1}$ to limit salt intrusion. This design discharge is achieved by regulating the Haringvliet Sluices (Rijkswaterstaat, 2019), which are located at the mouth of the Haringvliet, south of the NWW (HV in Fig. 6.1). Together with a meso-tidal amplitude of about 1.5 m at the mouth of the NWW, this estuary is classified as a salt wedge estuary (de Nijs *et al.*, 2011). Under such average conditions, the salt intrusion reaches 24 km inland, near the Botlek harbour (Fig. 6.1a; de Nijs *et al.*, 2009).

When the discharge in the Rhine at Lobith drops below $1,700 \text{ m}^3\text{s}^{-1}$, the design discharge of the NWW cannot be maintained due to which the saline water intrudes beyond the Botlek far into the Nieuwe Maas (Fig. 6.1b). To convey as much freshwater as possible through the NWW in this situation, the Haringvliet Sluices remain almost entirely closed (Rijkswaterstaat, 2019). The further the discharge at Lobith drops, the more salt water intrudes landward. Besides the damage to inland shipping due to the shallow upstream water depths (Vinke *et al.*, 2022, 2024), freshwater availability along the northern branches of the RMD becomes especially pressured, as the brackish water reaches the mouths of the Hollandsche IJssel and the Lek (Fig. 6.1b)—two branches with many water inlets and hardly any discharge, which is exacerbated during droughts (van den Brink *et al.*, 2019; Wegman *et al.*, *in review*). The upstream end of the Hollandsche IJssel becomes fully brackish within a few days due to continuing water extractions (van Zaanen *et al.*, 2022).

Most recently, such extreme drought events occurred in 2018 and 2022 in the RMD (Toreti *et al.*, 2022; Toreti *et al.*, 2019; Wegman *et al.*, *in review*). During these droughts, the discharge at Lobith remained below $1000 \text{ m}^3\text{s}^{-1}$ —with a minimum of $679 \text{ m}^3\text{s}^{-1}$ in 2022—for roughly four and two consecutive months in 2018 and 2022, respectively, causing significant damage (Rijkswaterstaat, 2023; Vinke *et al.*, 2022; Wegman *et al.*, *in review*).

6.2.2 Port of Rotterdam

Located in the RMD is the Port of Rotterdam, which is the largest port in Europe. It is a major stakeholder in the delta with high national and international interests. The port forms the gateway of many types of cargo and products through intermodal transport to North-Western and Central Europe. In 2022, the Port of Rotterdam transhipped 467.4 million tonnes of cargo (Port of Rotterdam, 2024).

The Port of Rotterdam can roughly be subdivided into a deepwater/offshore part, and a shallower, inland part. The inland harbour basins are connected to the sea through the open connection of the NWW and Scheur, which we jointly refer to as NWW. The bed levels of the port basins and waterways are maintained by dredging according to a maintained bed level (MBL) design (Fig. 6.2). This design facilitates the access of the deepest-draughted vessels in each specific port basin's fleet.

In the port, vessels are prone to tidal restrictions depending on their characteristics: draught, length, type, destination, etc. Vertical tidal restrictions entail regulations for minimum under keel clearance with respect to the MBL. These result in water level thresholds. Moreover, horizontal tidal restrictions prescribe specific current velocities and set limits for exceeding them. These restrictions interact with congestion of port infrastructure—i.e., terminals, turning basins, waterways, and anchorage areas—, leading to delays in cargo transfers (Bakker *et al.*, 2024).

In 2019, the NWW has been deepened from 14.5 to 16.2 m to facilitate sea-going vessels of the New Panamax class with a maximum draught of 15.0 m. In continuation of the NWW, the Nieuwe Maas has a MBL of 14.5 m decreasing to a minimum of 11.5 m that is used by sea-going (cruise) vessels to moor in Rotterdam (near intake station 4 in Fig. 6.2). More details on the Port of Rotterdam and its nautical logistics can be found in Bakker *et al.* (2024).

6.2.3 Freshwater users

The water management in the Netherlands is regulated by water boards of which four are located in the RMD (Fig. 6.2): (A) Hollandse Delta; (B) Delfland; (C) Schieland & Krimpenerwaard; and (D) Rijnland. These four water boards are responsible for approximately four million inhabitants (Unie van Waterschappen, 2022), and require freshwater to fulfil three main requirements (Klijn *et al.*, 2012): (1) minimum (and maximum) water levels, (2) water quality, and (3) water quantity for consumption, such as for drinking water and irrigation.

The water boards have several water intake locations throughout the RMD, which are depicted in Figure 6.2. These predominantly consist of pumping stations that remove excess water from the polders to the river system during wet conditions, and vice versa during dry conditions. In addition, the water boards redistribute water amongst themselves using pumping stations, creating alternative routes for the freshwater. They are currently only used during severe droughts when the brackish water reaches some of the upstream water intake stations (Fig. 6.1b; van der Heijden *et al.*, 2024).

Note that the demand for freshwater increases during droughts, in particular for irrigation. A precipitation deficit of around 0.225 m will result in a shortage of freshwater for the stakeholders. A further deficit will result in insufficient water levels and flushing capacity (Klijn *et al.*, 2012). This occurred in 2018 and 2022, during which the water boards had to make intensive use of the alternative freshwater supply routes (Hesen, 2021; van der Heijden *et al.*, 2024). However, the operation of these systems leads to damage to the canal system due to increased water levels and current velocities (HydroLogic, 2018). Improvements to the systems have been realised to increase its capacity with costs in the millions of euros. This led to fewer problems during the drought of 2022 (van der Heijden *et al.*, 2024).

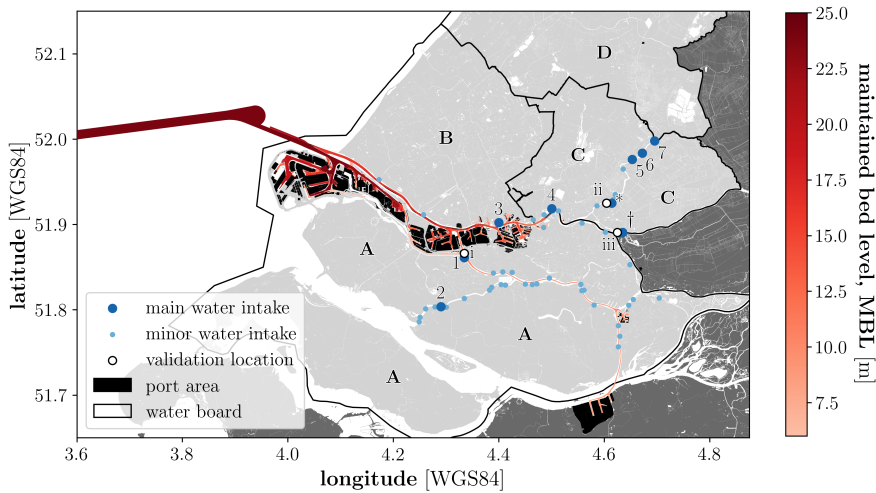


Figure 6.2: Overview of the land-based and water-based functions in the Rhine-Meuse Delta, including the design of maintained bed levels of the Port of Rotterdam and the water intake stations. Labelled water boards: (A) Hollandse Delta; (B) Delfland; (C) Schieland & Krimpernerwaard; and (D) Rijnland. The numbered water intake stations correspond with Table 6.1. The water intake station labelled with a * represents the water intake stations upstream of the Hollandsche IJssel (5, 6, and 7). The lower case, Roman numerals represent locations of data validation presented in Figure 6.4: (i) Spijkenisse-burg, (ii) Krimpen a/d IJssel, and (iii) Kinderdijk.

6.2.4 Future challenges

The freshwater availability in the RMD is expected to become further pressured due to recent climatological and socio-economic developments. These developments include (1) reduced freshwater supply due to more frequent and severe low discharge events in the Rhine (Buitink *et al.*, 2023; Sperna Weiland *et al.*, 2015) and increased water usage upstream (Klijn *et al.*, 2012); (2) increased salt intrusion due to the lower discharges in the NWW and the increased offshore water levels due to sea level rise (van Alphen *et al.*, 2022); and (3) higher freshwater demands due to more frequent and longer droughts and increased flushing discharge requirements to combat the groundwater salt intrusion (Klijn *et al.*, 2012).

Although the current water managerial solutions are claimed to be a robust system (HydroLogic, 2019a), they may become inadequate with these developments. Extracting more freshwater from upstream to facilitate the downstream needs, causes reversed discharges in the Hollandse IJssel and Lek branches, which exposes them to further salinisation; a problem that arose during the droughts of 2018 and 2022 (Fig. 6.1b; HydroLogic, 2019b; Wegman *et al.*, *in review*). As a result, freshwater was redirected from the major rivers to flush these branches, which caused further damage to inland shipping activities (HydroLogic, 2019b; Vinke *et al.*, 2022, 2024). Moreover, the operation of the system leads to damage to the water boards, and further extensive investments that are required to increase

the capacity of the solution may not be cost-effective. Thus, not all stakeholder objectives can be satisfied during a drought in the RMD in its current state.

6.3 Method

To test the effect of bed level change in intensively-utilised estuaries, we must quantify the implications for the affected stakeholders. Therefore, we designed a general method that enables weighing off dissimilar stakeholder interests (Fig. 6.3). Once a problem has been registered—generally raised by one or more stakeholders—, the following four steps set up the multidisciplinary trade-off method:

1. Select a minimal set of design parameters that quantify the main properties of the area of interest or measure.
2. Determine stakeholders that are affected by this set of design parameters and define a single performance indicator per stakeholder that reflects their performance.
3. Define quantification methods that translate the environmental conditions to the performance indicators.
4. Select models—or a pipeline of models—that are able to reflect the environmental conditions based on the set of design parameters.

After the performance indicators are quantified, a trade-off method should be deployed to weigh the two stakeholder interests, for which we selected multi-objective or Pareto optimisation.

In this study, we apply above method to the RMD to the severely dry year of 2022. For this, we selected the MBL as the design parameter, considered as bed level change, Δz . A positive value (i.e., $\Delta z > 0$) reflects an increase in MBL—i.e., increased water depth—and vice versa. To determine the affected environmental conditions, we used a hydrodynamic model of the RMD that could determine the effects of bed level change on the local hydrodynamics (Sec. 6.3.1). Its output data was subsequently used in models that quantify the effects of hydrodynamic changes on cargo delays (Sec. 6.3.2) and freshwater availability (Sec. 6.3.3). At last, we translated these effects into performance indicators, which allowed for the construction of a Pareto-front to provide insights into the relevant trade-off between the stakeholder interests (Sec. 6.3.4).

6.3.1 Hydrodynamic model and scenarios

To quantify the stakeholder interests described in Sections 6.3.2 and 6.3.3, data on water levels, flow velocities, and salinity are required throughout the RMD domain. To simulate the effects of changing the MBL on the hydrodynamics and salt intrusion, we used a coarser version of “Operationeel Stromingsmodel Rotterdam” (OSR). OSR is run operationally to provide information for the pilots in the Port of Rotterdam and is well-calibrated for water levels and current velocities

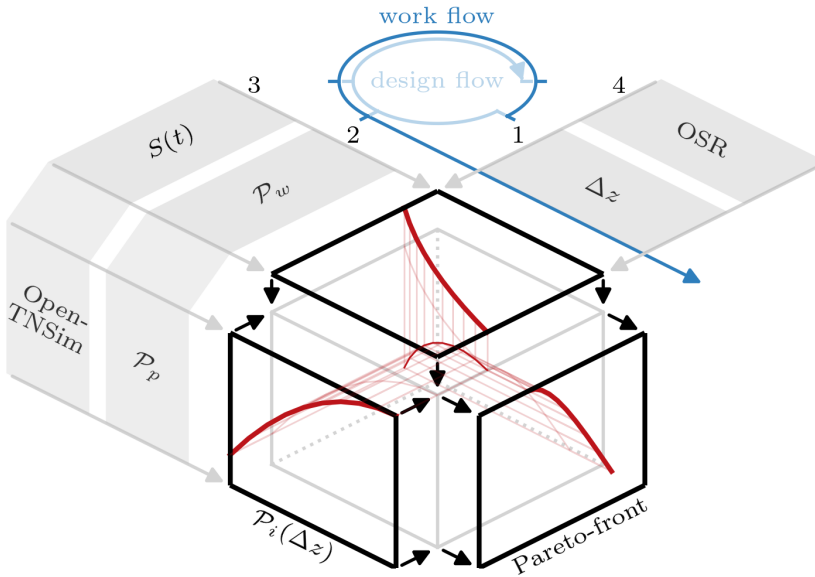


Figure 6.3: The conceptual model of the trade-off method of dissimilar stakeholder objectives. Numbering follows the design flow as presented in the text. Note that the work flow is reverse to the design flow ending with a Pareto-front.

(Kranenburg *et al.*, 2015). The hydrodynamic model is used to hindcast the year 2022, in which a severe drought occurred (Toreti *et al.*, 2022; Wegman *et al.*, *in review*). Such conditions are leading in the design and performance of especially the freshwater availability.

Although not the main objective of the model, salinity predictions are good ($R^2 = 0.9073$; Fig. 6.4a), where the largest errors occur at higher salinity levels (Fig. 6.4b). With the focus on breaching a threshold value ($s_c = 150 \text{ mg Cl}^- \text{ l}^{-1}$), it is most relevant whether the model predicts the exceedence of this threshold correctly, which it does for 91.1% of the time (Fig. 6.4a); when incorrect, it generally underpredicts the salinity—i.e., the model predicts a higher freshwater availability.

The reference model run simulates the MBL of the NWW as the existing situation (16.2 m; $\Delta z = \pm 0.0 \text{ m}$). Based on the distribution of draughts of vessels that navigate the NWW, we drew a total of five shallowed MBL designs ranging from 11.2 m ($\Delta z = -5.0 \text{ m}$) to 15.2 m ($\Delta z = -1.0 \text{ m}$), with steps of 1.0 m. Shallower MBL designs were not assessed, as these were expected to result in an unreasonably poor port performance. Additionally to these runs, a scenario of a deepening of 1.0 m to a MBL of 17.2 m was assessed to show the effect of a further deepening ($\Delta z = +1.0 \text{ m}$).

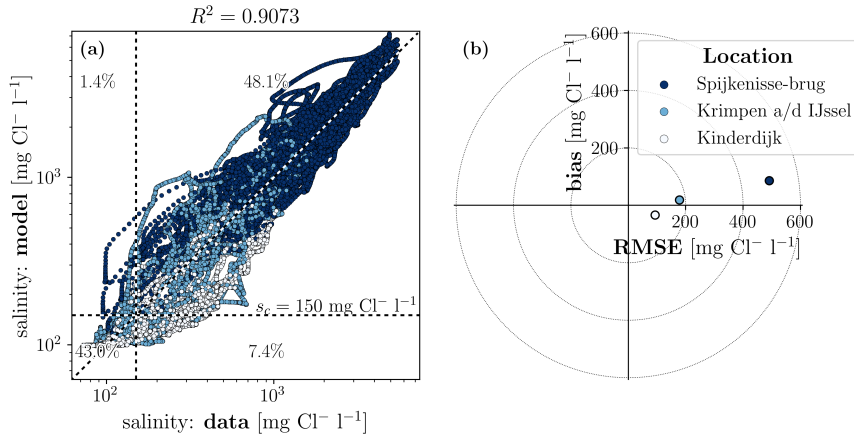


Figure 6.4: Predictive power of hydrodynamic model regarding salinity. (a) Measurements versus predictions with the salinity threshold ($s_c = 150 \text{ mg Cl}^{-1} \text{ l}^{-1}$) marked with a black, dashed line; and (b) target plot displaying the root-mean-squared-error (RMSE) and bias. Locations are shown in Figure 6.2: (i) Spijkensse-brug, (ii) Krimpen a/d IJssel, and (iii) Kinderdijk.

6

6.3.2 Quantifying cargo transfer delays

A port relies principally on its efficiency and throughput. An efficient port means that cascading waiting times in cargo transfers due to downtime and congestion of port infrastructure should be limited. Shallower MBLs can increase these waiting times, since more vessels will be prone to tighter tidal windows, decreasing the port's accessibility. Moreover, shallower bed levels can decrease the throughput to the inland port, as the deepest-draughted vessels of a fleet may be unable to navigate the access channel. If these vessels are redirected to more offshore terminals, this can further decrease the port's efficiency due to congestion of these terminals.

To quantify the effects of bed level change on this parameter, we deployed the nautical traffic model OpenTNSim (Bakker & van Koningsveld, 2023). This discrete-event model estimates the cascading waiting times of vessels due to the interaction between tidal downtime and berth congestion. To apply the model to the RMD, we schematised three main features based on hindcasted Automatic Identification System (AIS) data for the year 2022, hydrodynamic model results, and geospatial data: (1) the Port of Rotterdam's wet infrastructure; (2) vessels of call, including their properties, such as draught, laytimes and speed; and (3) tidal hydrodynamics, namely water levels and current velocities. The tidal restriction regulations are taken from the port authority's policy. For simplicity, the model is solely implemented on a selection of terminals in harbour basins that are connected by the North Sea through the NWW. Hence, indirect effects on other terminals are not taken into account. Based on the AIS data analysis, twelve terminals have been selected over different harbour basins. These terminals are prone to tidal

restrictions that change with bed level change and affect at least twenty vessels of call. More details on the data preparation and processing as well as model set-up can be found in Bakker *et al.* (2024).

As the shallower bed levels are expected to fully restrict the passage of the deepest-draughted vessel through the NWW, the cargo throughput to the inland terminals may drop. We assume that this is not acceptable for the port, and therefore this throughput will be maintained in the model using replacement coasters. This means that arriving vessels with excess draughts are assumed to be redirected to a feeder terminal in the offshore port. There they will be lightened and the excess cargo will be transferred to and transshipped by coasters with a total equivalent transport capacity to the inland terminal. Moreover, departing vessels with the excess draughts are loaded with their excess cargo at the offshore feeder terminal. Again, this cargo is transshipped by coasters from the inland terminal.

6.3.3 Quantifying freshwater availability

The interest of the inhabitants of a delta—or surrounding an estuary—were reflected by freshwater availability. Therefore, the water intake stations in the delta are crucial in providing this commodity to them. Water intakes can only extract water from the river system if salinity levels are below a certain threshold; in the Netherlands, this threshold is $150 \text{ mg Cl}^- \text{ l}^{-1}$ (or 0.27 psu). Furthermore, water intakes can often only extract water using gravity, i.e., the water level in the river system must exceed a critical water level threshold—this is generally around mean water level. Therefore, water extraction—i.e., freshwater supply—only occurs if the following two criteria are met:

$$\eta(t) > \eta_c \quad (6.1a)$$

$$s(t) < s_c \quad (6.1b)$$

where η is the water level in the river system [m]; η_c the water level threshold of the water intake [m]; s the salinity in the river system [psu]; and s_c the salinity threshold of the water intake [psu].

Both the supply and demand of freshwater fluctuate on different time scales: daily, seasonally, etc. Therefore, water intake locations—or collections of water intakes—generally have some form of storage capacity. These storage volumes follow a basic volume balance:

$$\frac{dV}{dt} = E(\eta, s) - D(t) \quad (6.2)$$

where E is the supply of freshwater [m^3s^{-1}], which is a function of the water and salinity levels (Eq. 6.4); and D the demand for freshwater [m^3s^{-1}].

The storage volume is bounded by a minimum volume of zero—i.e., $V = 0$ —and by a maximum capacity:

$$0 \leq V \leq V_c \quad (6.3)$$

where V_c is the storage capacity associated with the (collection of) water intake(s) [m^3] (Tab. 6.1).

The supply of freshwater in Equation (6.2) is a binary relation depending on Equations (6.1a) and (6.1b):

$$E = \begin{cases} E_{\max} & \text{if Eqs. 6.1a and 6.1b} \\ 0 & \text{else} \end{cases} \quad (6.4)$$

where E_{\max} is the maximum extraction rate of the water intake [m^3s^{-1}] (Tab. 6.1).

When both the demand exceeds the supply—or extraction rate—and the storage is empty, water shortages occur. We defined water shortage as the demand that cannot be provided by the combination of water supply and reserves:

$$S = \begin{cases} D - E - \max \left\{ -\frac{dV}{dt}; 0 \right\} & \text{if } V < D - E \\ 0 & \text{else} \end{cases} \quad (6.5)$$

where D is the freshwater demand of the (collection of) water intake(s) [m^3s^{-1}] (Tab. 6.1); E the extraction rate [m^3s^{-1}] (Eq. 6.4); and V the stored freshwater volume of the (collection of) water intake(s) [m^3]. The last term (i.e., the max-function) reflects the use of the remainder of stored freshwater—if any.

To apply the above method to the situation in the RMD, we selected the main water intakes and their collections based on van der Wijk (2020), which are presented in Table 6.1. Since the hydrodynamic model was found to predict poorly in the Hollandsche IJssel, the main water intakes in this branch—marked with asterisks in Table 6.1—were evaluated based on the modelled hydrodynamic data at Krimpenerwaard (Fig. 6.2). Furthermore, Gemaal Winsemius and Inlaat Bernisse used the same hydrodynamic data; and Krimpenerwaard was projected on hydrodynamic data at the mouth of the Lek—i.e., at Kinderdijk (marked with † in Fig. 6.2).

6

6.3.4 Performance indicators

Using the processing methods as described in Sections 6.3.2 and 6.3.3, we have defined performance indicators reflecting port functioning and freshwater availability. For the port, we made use of cargo delays, where a perfect port performance ($\mathcal{P}_p = 1$) would be achieved if no cargo has delays, i.e., vessel waiting times are zero:

$$\mathcal{P}_p = 1 - \frac{\sum_i^N V_{c,i} T_{w,i}}{\sum_i^N V_{c,i} T_{t,i}} \quad (6.6)$$

where N is the number of vessels entering the port during the period of interest [-]; $V_{c,i}$ the cargo volume of the vessel i [m^3]; $T_{w,i}$ the waiting time of the vessel i [s]; and $T_{t,i}$ the transfer time of the cargo of the vessel i [s]. Note that \mathcal{P}_p is bounded by zero and, thus, cannot become negative: $\mathcal{P}_p \in [0, 1]$.

The transfer time of a vessel's cargo is the total time a vessel would take to unload its cargo after arriving at the port or departing at a previous terminal, and to load new cargo and depart the port or arrive at a next terminal. This includes additional waiting time.

Table 6.1: Specifications of the main water intakes in the Rhine-Meuse Delta without emergency water supply (derived from van der Wijk, 2020). Numbering of the water intakes reflects the locations numbered in Figure 6.2. Numbers post-fixed with an asterisk are collectively considered at Krimpen aan de IJssel, marked by an asterisk in Figure 6.2. V_c : storage capacity; D : freshwater demand; E_{\max} : maximum extraction rate.

	Water board	Intake station	V_c [m ³]	D [m ³ s ⁻¹]	E_{\max} [m ³ s ⁻¹]
A.	Hollandse Delta	1 Inlaatsluis Spijkenisse	4,000,000	9.1	23.0
		2 Inlaatsluis Bernisse			23.0
B.	Delfland	(2) Gemaal Winsemius	492,000	2.75	4.0
		3 Schiegemeaal			3.0
C.	Schieland & Krimpenerwaard	4 Mr. U.G. Schilthuis	528,000	2.5	4.5
		5* Snelle Sluis & Gemaal Abraham Kroes			3.3
		6* Gemaal Verdoold	3,408,000	5.6	1.5
		† Krimpenerwaard			5.6
D.	Rijnland	7* Gouda	2,086,400	12.0	21.0

The performance indicator related to the freshwater availability reflects the shortage of freshwater. A perfect performance ($\mathcal{P}_w = 1$) is achieved when the water board can fulfil the freshwater demands at any time. Therefore, this performance indicator is a function of the freshwater shortage versus the demand, integrated over the period of interest:

$$\mathcal{P}_w = 1 - \frac{\int_T S dt}{\int_T D dt} \quad (6.7)$$

where T is the period of interest [s]; S the freshwater shortage (Eq. 6.5) [m³s⁻¹]; and D the freshwater demand [m³s⁻¹]. Note that \mathcal{P}_w is also bounded by zero due to which it cannot become negative: $\mathcal{P}_w \in [0, 1]$.

These two performance indicators can be weighed using a trade-off method (Fig. 6.3). We assessed this trade-off using multi-objective optimisation, which leads to the generation of Pareto-optimal solutions (e.g., Emmerich & Deutz, 2018). This results in a set of solutions that cannot be further improved upon (e.g., Deb, 2001); a so-called *a posteriori* method to inform decision-makers about the optimal alternatives without making a choice *a priori* (Miettinen, 1998). Note that this approach results in a collection of optimal solutions, not a single “optimal solution.” Here, “optimal” refers to the best trade-off between the chosen performance indicators, which is at best as good as the indicators themselves.

6.4 Results

6.4.1 Delayed throughput

The AIS data analysis revealed that 90.8% of the vessel voyages calling at the selected terminals are not affected by a shallower NWW of 11.5 m (Fig. 6.5).

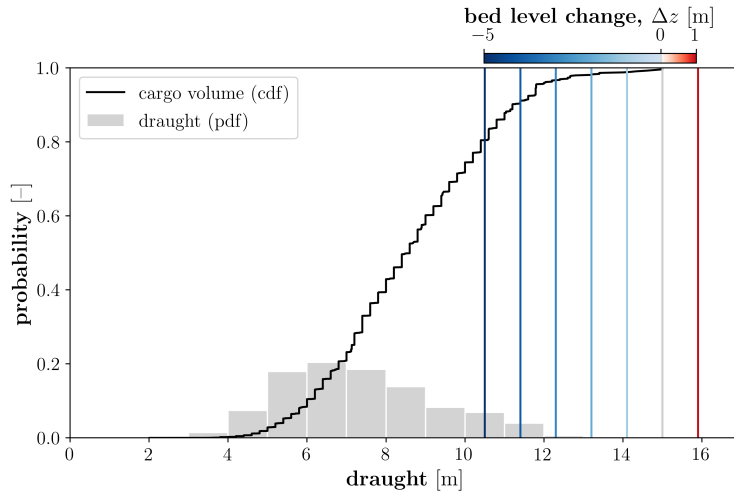


Figure 6.5: Vessel draught and cargo volume distributions based on AIS data. Vertical, coloured lines represent the maximum allowable draught for each bed level change as considered in this study. These are based on the Port of Rotterdam’s accessibility policy. Note that vessels with a draught greater than 12.0 m exist in the modelled fleet of call, with draughts up to 15.0 m. However, they undertake less than 1.0% of the total voyages and are therefore not clearly visible in the pdf.

6

However, since more cargo is transported by larger and deeper-draughted vessels, we found for this situation that 22.9% of the cargo will have to be transferred to the replacement coasters. The shallower the NWW, the more deeper-draughted vessels are impeded from navigating this channel, and the more trips with replacement vessels have to be made.

The nautical traffic model predicts that the inland part of the Port of Rotterdam is highly affected by a shallower NWW (Fig. 6.6): the average delivery time increases with a shallower NWW. This is mainly caused by the additional delay of transferring cargo to the replacement coasters, which increases with shallower MBLs. Consequently, the average ratio between the delay and delivery time of cargo increases. In addition, extra congestion arises as more vessels are required to transship the same amount of cargo. Delays due to tidal restrictions are also increasing, as with shallower depths more vessels are prone to tidal windows. However, this is only a marginal effect (Fig. 6.6).

Furthermore, we observed that a deeper NWW will not lead to a substantially better operating port for the current fleet of call. Although the delays due to tidal restrictions slightly decrease, the port remains subject to congestion of the berths. Hence, congestion is the dominating delaying factor in the port.

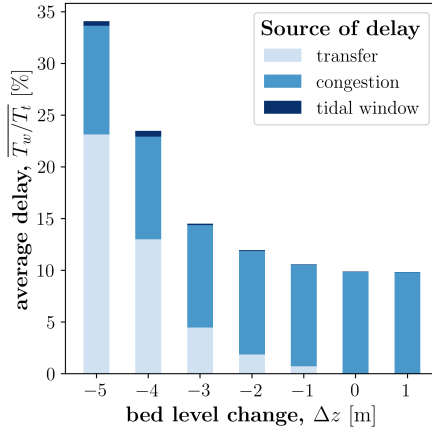


Figure 6.6: Contribution of the delay time to the total delivery time. Transfer delays are caused by transferring cargo between vessels; congestion results from unavailable berths; and delays due to tidal windows relate to the MBL level change.

6.4.2 Water shortages

The freshwater supply model predicts that freshwater availability generally improves with shallower bed levels (Fig. 6.7). The freshwater shortage decreases, as the water boards become more robust to a drop in the discharge of the NWW. This improves the starting position at the beginning of the drought and postpones and reduces the effects of the drought on the water intakes.

For the water boards in specific, the Delfland and Hollandse Delta water boards are the least susceptible to the drought conditions in their freshwater availability (Fig. 6.7b and c) despite being closest to the see (Fig. 6.2). The influence of reducing the MBL is, therefore, also least profound in these water boards. The other two water boards, however, show a greater dependence between freshwater shortages and the MBL (Fig. 6.7d and e).

This is related to the source of freshwater extraction: the Delfland and Hollandse Delta water boards mainly extract from the man-made freshwater lake in the southern RMD—the Haringvliet and the connected Brielse Meer—, which is more robust to droughts (Fig. 6.1). The other two water boards are more reliant on freshwater from the northern RMD, which is more strongly affected by droughts and changes in the water depth of the NWW.

Furthermore, further deepening the NWW—i.e., $\Delta z = +1.0$ m—barely affects the freshwater availability with respect to the reference case—i.e., $\Delta z = \pm 0.0$ m. It is only at the Schieland & Krimpernerwaard water board, there is a minor difference visible in the water shortages (Fig. 6.7e).

Note that the shortages in Figure 6.7 are expressed in volume per area, which causes the summation of shortages of all four water boards to be less than the sum of all water boards. In essence, the freshwater shortages in Figure 6.7 are expressed in rainfall deficits, which range between virtually zero (Fig. 6.7c and d)

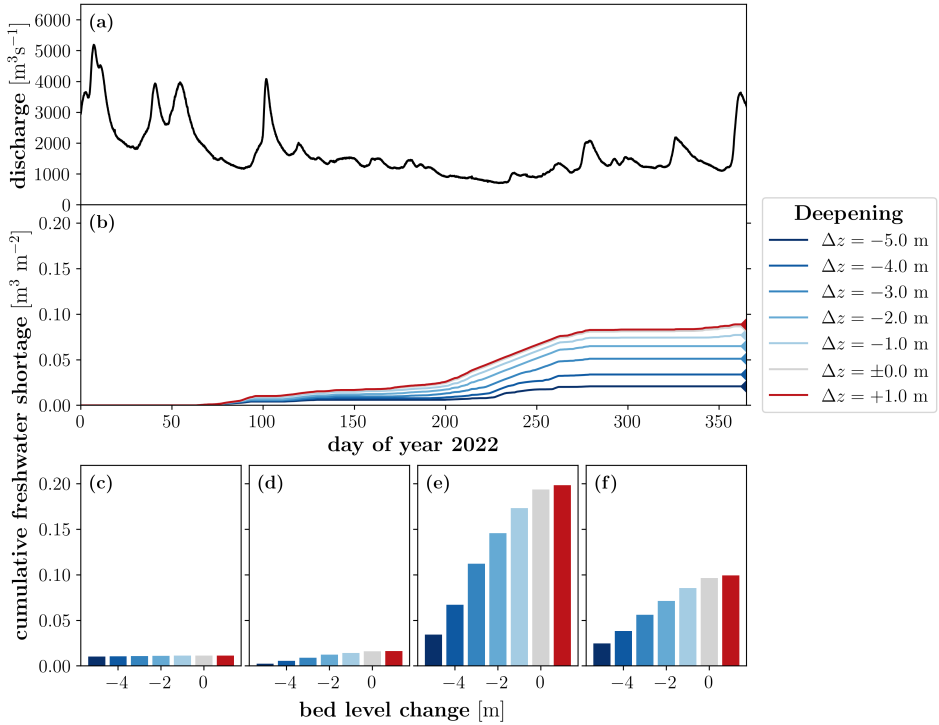


Figure 6.7: The influence of the MBL on the water shortages. (a) Discharge at Lobith; (b) temporal development of cumulative water shortages for all water boards; and cumulative water shortages per water board: (c) Delfland, (d) Hollandse Delta, (e) Schieland & Krimpernerwaard, and (f) Rijnland. Shortages are expressed as cumulative lack of freshwater (i.e., volume; time-integration of S , Eq. 6.5) per area of the water board.

to shy of 0.2 m (Fig. 6.7e) with the current MBL (16.2 m). Generally, the rainfall deficits—freshwater shortages—increase with increasing water depth.

6.4.3 Pareto-front

All water boards have a reduced freshwater availability performance with increasing MBL (Fig. 6.8), although the freshwater availability of the Delfland and Hollandse Delta water boards is barely impacted. This is in line with the limited shortages arising during the drought in these water boards (Fig. 6.7c and d). Thus with deeper waters—or increased MBL—comes a decreased freshwater performance, \mathcal{P}_w (Fig. 6.8). The exception being the deepening of the NWW compared to the reference case—i.e., there is a negligible difference between $\Delta z = \pm 0.0$ m and $\Delta z = +1.0$ m.

On the other hand, the port accessibility improves with a deeper NWW. The added value of deepening the NWW on the port performance is—in the current fleet composition—limited beyond the MBL of 16.2 m (Fig. 6.8). This is in line with

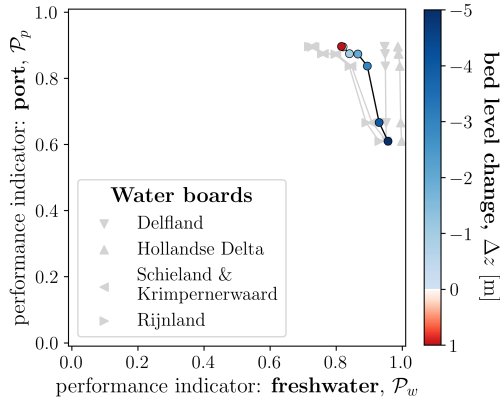


Figure 6.8: Pareto-front of performance indicators as a function of the water depth. The collective is coloured with the water depth, and individual water boards are presented in grey.

the expectations based on Figure 6.5, which show that less vessels are impacted by the MBL for increasing values of MBL.

6.5 Discussion

The MBL in the NWW has a profound influence on both performance indicators, although the sensitivity of the freshwater availability varies per water board (Fig. 6.8). The resulting Pareto-front is illustrative but also subject to the implemented assumptions in the models (Sec. 6.5.1). In addition to these assumptions, this section discusses two matters: (1) drought countermeasures other than shallowing (Sec. 6.5.2); and (2) value-based transformation of the Pareto-front (Sec. 6.5.3).

6.5.1 Model assumptions

As usual, the choice of models influences the results—in our case the shape of the Pareto-front. This study has implemented the hydrodynamic model that is used for port operations, where its main objective is the prediction of water levels and flow velocities. Nevertheless, the model has a good predictive power regarding the salinity (Fig. 6.4). However, inside smaller branches of the RMD its predictive power regarding salinity reduces. Therefore, more accurate hydrodynamic models might be useful to improve the predictive power in branches like the Hollandse IJssel, where multiple water intakes are situated (Fig. 6.2; e.g., Geraeds *et al.*, *in prep.* Gerritsma *et al.*, *in review*, describe detailed hydrodynamic models focused on salt dynamics in the RMD). Note, however, that the implementation of more detailed models comes at higher computational costs.

In the nautical traffic model, we were highly dependent on AIS data as input. Although generally of good quality, vessel laytimes and speeds were affected by frequently occurring location errors. These had to be detected and manually corrected—a procedure that likely affected the magnitude of the cargo transfer delays. The same holds for the assumption that the cargo throughput to the inland terminal is maintained by smaller replacement vessels, as well as the choice of replacement vessel type. Furthermore, OpenTNSim neglects tugs, pilots, background traffic, and terminal cargo flows (Bakker *et al.*, 2024), which affects the nautical traffic behaviour. Regarding the port performance indicator (Eq. 6.6), we found a significant dependency with the cargo volumes that were calculated from the vessel dimensions in the AIS data. As the vessel dimensions—especially the draught, which was manually corrected—in the AIS data are known to be susceptible to errors and uncertainties (Meyers *et al.*, 2022), the volume-based weighing of the waiting and transfer times, and hence the performance indicator itself, includes errors. Moreover, the required number of replacement vessels may be overestimated. Despite all these assumptions and possible errors, we believe that the state-of-the-art, nautical model performed as intended, and the resulting levels of port performance are trustworthy. However, further improvements to the quality of the AIS data, the nautical traffic model, and formulation of the port performance indicator are possible and preferable.

6

The freshwater availability and its related performance indicator (Eq. 6.7) strongly rely on the hydrodynamic model predictions of water level and salinity. Furthermore, the use of a basic (fresh)water balance comes with its limits, such as the constant freshwater demand, a single salinity threshold, and exclusion of precipitation input. Despite these simplifications, the results are in accordance with experienced shortages (van der Wiel *et al.*, 2021).

In this study, we have defined performance indicators according to our best understanding of the problem. For example, we reasoned that port performance based on cargo delays—i.e., port efficiency—would best describe the interest of the port. This performance indicator is most relevant for the accessibility and operability of the port infrastructure, given the interactions with the nautical traffic and physical environment. However, other performance indicators could have been used depending on the stakeholder interest; e.g., performance indicators based on cargo throughput, nautical safety, or vessel emissions. The same applies to the freshwater shortage, which focuses more on the instantaneous effects of the drought and less on the cumulative effects. The presented trade-off method is however flexible to support other sets of performance indicators. Note that the performance indicators implemented remain metrics and, thereby, are inherently incomplete. However, we purposefully used non-monetary metrics to describe the interests of the stakeholders as closely as possible.

At last, we investigated the trade-off for the severely dry year 2022 only, as we believe this year is most relevant for freshwater availability. A different (wet) period or simulation duration could have led to different results and may require differently formulated performance indicators.

6.5.2 Drought countermeasures

The simulated year of 2022 contained a severe drought resulting in an “extremely rare low flow” in the Rhine, especially during August (Toreti *et al.*, 2022; Wegman *et al.*, *in review*). Although we observe that shallower bed levels can significantly improve the resiliency of freshwater availability, a MBL of 11.2 m would not even be sufficient to protect all water boards in the RMD from water shortages during such a severe drought ($\Delta z = -5.0$ m in Fig. 6.7). Thus additional measures to secure drinking water safety are required, even when the NWW would be relatively shallow (i.e., MBL = 11.5 m). In other words, although important, shallowing alone cannot ensure freshwater availability in a densely populated delta like the RMD.

Currently, there is already a crisis plan with an alternative water supply system in place in the Netherlands to cope with extreme drought conditions by relocating freshwater between water boards—a plan that was also employed during the drought in 2022 (van der Heijden *et al.*, 2024). As stated in Section 6.2, we have not implemented this relocation plan, as it is a crisis plan that comes with serious costs (HydroLogic, 2018).

Instead of—or in addition to—such a crisis plan, more robust and permanent measures could be taken. Regarding the freshwater availability, there are four components that can alleviate the pressure during droughts: (1) increase the freshwater storage capacity (V_c); (2) increase the maximum extraction rate (E_{\max}); (3) reduce the freshwater demand (D); and/or (4) move water intakes away from salt sensitive regions. Note that these components should not be considered in isolation, but can be combined to establish a resilient freshwater management system.

The last component is also what makes the Delfland and Hollandse Delta water boards relatively insensitive to the MBL of the NWW: these water boards extract the majority of their freshwater from the southern RMD—namely the man-made, freshwater lake Haringvliet. Current plans to reconnect the Haringvliet with the North Sea by (partially) opening the Haringvliet sluices (Brevé *et al.*, 2019; de la Haye *et al.*, 2022) can lead to increased salinisation (Kranenburg *et al.*, 2023) and should therefore be carefully assessed (Hendrickx *et al.*, *in prep.* Ch. 7).

6.5.3 Performance valuation

The Pareto-front in Figure 6.8 clearly shows the trade-off between the port and freshwater performances arising from modifying the MBL. On average—i.e., all water boards collectively—the port performance is affected more by the depth of the NWW than the freshwater performance, shown by the angle of the Pareto-front and the range of the values covered.

Given a Pareto-front, the mathematically optimal solution can be achieved by maximising the square area below the Pareto-front (e.g., Emmerich & Deutz, 2018); this square is bound by the origin and the Pareto-front, i.e., $(\mathcal{P}_w, \mathcal{P}_p)$. However, the Pareto-front as presented in Figure 6.8 does not include the valuation of the solution space. Such a valuation is subjective and part of the decision- and policy-making process. The valuation of each individual performance indicator

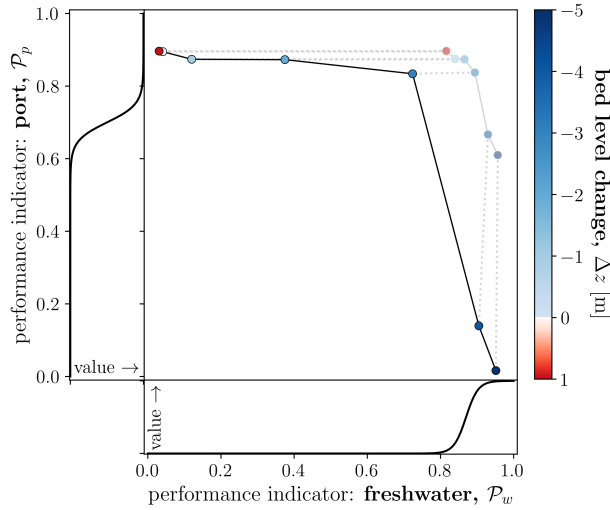


Figure 6.9: Valued Pareto-front based on arbitrary valuation functions. The unvalued Pareto-front is faded and presents the same data as in Figure 6.8. The valued Pareto-front follows from the transformation of this unvalued front with the valuation functions on the left and bottom of the figure using Equation (6.8).

6

is generally nonlinear, and can put limits on the allowable performance values. To maintain the intuitive visualisation of the Pareto-front, the valuation can be included by means of valuation functions:

$$\mathcal{V}_i(\mathbf{x}) = v_i(\mathcal{P}_i) \cdot \mathcal{P}_i(\mathbf{x}) \quad (6.8)$$

where \mathcal{V}_i is the valued performance indicator i [-]; v_i the valuation function of performance indicator i [-]; \mathcal{P}_i the (unvalued) performance indicator i [-]; and \mathbf{x} the design parameter(s).

The transformation of the Pareto-front as shown in Figure 6.8 due to arbitrary valuation functions is presented in Figure 6.9. Note that these valuation functions are arbitrarily defined and intended as examples of how they transform the Pareto-front. A minimum performance can be enforced by setting a very low valuation for performances below this minimum; e.g., in Figure 6.9, the port performance is required to be $\mathcal{P}_p \geq 0.6$ (approximately).

Although the valuation functions in Figure 6.9 are both smooth, tipping points that are relevant for stakeholders can be reflected by discontinuities. As the definition of such a valuation function is subjective, political, and subject to the zeitgeist, we have only included example valuation functions in Figure 6.9 and refer to, e.g., Greco *et al.* (2016) and Keeney and Raiffa (1993) for methods to define such functions, which are intended to reflect the stakeholder interests. Note that the function can depend on the period of interest and simulation time.

Figures 6.8 and 6.9 illustrate how insightful and intuitive the use of Pareto-fronts are in decision- and policy-making; they clearly show the trade-offs asso-

ciated with the decisions and policies at stake. These features make such visualisations also useful in communicating the decision- and policy-making process with the public, who are generally not experts in the field but highly affected by the decisions and policies being made. This is particularly useful in digital twins (Wannasin *et al.*, 2024), integrated assessment models (Pourteimouri *et al.*, 2024), and serious games (den Haan *et al.*, 2020, 2024).

Although we have limited ourselves to two performance indicators and one design parameter in this study, the presented approach—i.e., the use of design parameters, performance indicators and a Pareto-front—can easily be upscaled to multiple dimensions (e.g., Emmerich & Deutz, 2018). Note that with increasing dimensionality, visualising the trade-offs might become harder due to the human visual limit of three dimensions. Moreover, the construction of the complex multidimensional Pareto-front requires lots of Pareto-points, and hence lots of model simulations. Therefore, an effective sampling method—e.g., an adaptive sampling approach—could be used to limit the number of (expensive) model simulations (Gramacy & Lee, 2009; Hendrickx *et al.*, 2023a). Additionally, computationally efficient hydrodynamic and stakeholder models can be employed, which may come at the cost of precision and resolution. For example in this research, the idealised and simplified saltwater intrusion model of Biemond *et al.* (*in review*) could become useful in a fast prediction of the freshwater availability performance.

At last, we would like to highlight the general applicability and usefulness of the trade-off method approach in other case studies. An example is the decision on partially opening of the Haringvliet sluices in which freshwater availability and ecology have to be weighed (Sec. 6.5.2; Hendrickx *et al.*, *in prep.* Ch. 7). Other examples may contain the future design and management of the highly-urbanised and strongly pressured RMD and other world-wide deltas. Especially here, we foresee that the presented system-scale and objective approach would be a highly effective tool for decision- and policy-makers in obtaining the most effective solutions given the most urgent of challenges.

6.6 Conclusion

In this study, we have assembled a systematic method to quantify trade-offs of multiple dissimilar, conflicting stakeholder interests through Pareto-optimisation. We applied this method to explore the socio-economic implications of MBL change in the NWW, considering the severely dry year 2022. For this, we carefully selected objective, non-monetary performance indicators representing two major stakeholders in the area: (1) the Port of Rotterdam, and (2) the collection of governmental organisations extracting freshwater from the delta, i.e., the water boards. These indicators could be calculated based on two separate stakeholder models, namely a nautical traffic model and freshwater supply model. The models were fed with output of a hydrodynamic model of the RMD and other operational data, such as AIS data and main freshwater intake locations. Thus by varying the MBL of the NWW, we obtained the performances of the stakeholders. This resulted in

a Pareto-front that shows that shallower bed levels deteriorate port performance, while improving freshwater availability (Fig. 6.8).

We have shown that the obtained Pareto-fronts provide valuable insights in the trade-offs of interventions in a multidisciplinary setting. Although this study has limited its multidisciplinary assessment to two stakeholders, this approach can easily be extended to multiple dimensions—i.e., stakeholders. The Pareto-front is a visually intuitive way of showcasing the benefits and costs of various scenarios for different stakeholders. With the use of valuation functions, the Pareto-front can be transformed to represent performance values, maintaining the intuitive visual representation of Pareto-fronts (Fig. 6.9). These characteristics make Pareto-fronts useful tools for decision- and policy-makers as well as for communicating with the public.

Acknowledgements. We would like to thank Lamber Hulsen (Port of Rotterdam) for his contributions to the early stages of this research.

Author contributions. F.B., G.H., S.A., M.v.K. designed the research; F.B., G.H., L.K., S.I. performed the research; F.B., G.H. analysed the data; F.B., G.H. wrote the manuscript; and F.B., G.H., L.K., S.I., S.A., M.v.K. reviewed the manuscript.

Data availability. Data is available upon reasonable request to the corresponding author.

Software availability. Port logistics were modelled using OpenTNSim (Bakker & van Koningsveld, 2023).

7

TRADE-OFFS

Socio-ecology

7.1 Introduction

At the interface between freshwater river systems and the saline ocean waters, estuaries are valuable regions, both socio-economically and ecologically. Estuaries provide a multitude of natural and ecosystem services (Barbier *et al.*, 2011; Worm *et al.*, 2006), such as low-dynamic regions within an estuary that are often used as nurseries (Breine *et al.*, 2011; Tulp *et al.*, 2008). Due to the multitude of gradients present in estuaries—e.g., salinity—, they experience a high biodiversity (Mestdagh *et al.*, 2020; Tangelder *et al.*, 2017; Ysebaert *et al.*, 2003) despite the minimum in number of species thriving in brackish waters (Cloern *et al.*, 2017; Remane, 1934; Whitfield *et al.*, 2012).

This chapter is based on:

Hendrickx, G.G., Fivash, G.S., Gerritsma, A., Geraeds, M.E.G., and Pearson, S.G. (*in prep.*). Socio-ecological evaluation of estuary-scale interventions: Case study of reopening the Haringvliet, the Netherlands. To be submitted to *Ecological Engineering*.

In addition, coastal and estuarine regions are densely populated by humans, and these populations are expected to densify in the future (Maul & Duedall, 2019; Neumann *et al.*, 2015). In these regions, the natural dynamics largely dictate the provision of crucial functions; examples include (1) freshwater availability, which is susceptible to salt contamination due to the near-by saline seawater (e.g., Bakker *et al.*, *in review*; Costa *et al.*, 2023; Jones *et al.*, 2023); and (2) safety against flooding by natural sheltering and wave damping (e.g., Fairchild *et al.*, 2021; Temmerman *et al.*, 2013).

In an attempt to control the provision of these crucial functions, human interventions have had major impacts on estuarine systems (e.g., van Wesenbeeck *et al.*, 2014; Yang *et al.*, 2010). These interventions range from dredging activities to maintain naval transportation routes (de Vriend *et al.*, 2011; van Dijk *et al.*, 2021) to completely damming off estuaries for flood safety and/or freshwater availability (Figuroa *et al.*, 2022; Orton *et al.*, 2023; Tönis *et al.*, 2002). Human interventions are the product of weighing a multitude of—often conflicting—objectives, such as freshwater availability versus port accessibility (Bakker *et al.*, *in review*, Ch. 6).

However, the ecological consequences of such interventions are rarely considered in a similar manner (e.g., Bice *et al.*, 2023; van Wesenbeeck *et al.*, 2014), weighing the costs and benefits against each other. This is in part due to the conflicting interests within the ecological system itself (Bice *et al.*, 2023): The displacement of one habitat generally results in the creation of another. Therefore, weighing various ecological states inherently requires a subjective value judgement. Nevertheless, large-scale interventions—such as (partially) closing off an estuary—have tremendous implications for the ecological system (Smaal & Nienhuis, 1992; Yang *et al.*, 2010), and the ecosystem services provided by the area of interest.

One such closed-off estuary is the Haringvliet, located in the south-west of the Netherlands (Fig. 7.1). Since 1970, the Haringvliet is a semi-closed, freshwater system due to the construction of the Haringvliet sluices, which are part of the Delta Works. Prior to construction, the Haringvliet was an estuary in which the tidal range and salinity reached 50 kilometres landward (Bol & Kraak, 1998; Tönis *et al.*, 2002). Closing off the Haringvliet estuary with sluices that are opened only to release excess river discharge has improved flood safety as well as freshwater availability. However, this has been at the expense of removing a rare brackish, estuarine ecosystem (Tangelder *et al.*, 2017). In addition, the Haringvliet sluices also removed the connectivity between the North Sea and the Rhine-Meuse river system, limiting fish migration between the river system and the sea (Beeldman *et al.*, 2018; Hop & Vriese, 2011).

Recently, experiments with partially opening the gates during flood have been initiated to restore fish migration in this area with the so-called “Kierbesluit” (*trans.*: “Ajar policy”; Brevé *et al.*, 2019; de la Haye *et al.*, 2022). To ensure freshwater availability, a line was drawn between Middelharnis and Spui beyond which no saline influence was allowed, as all water intakes in the Haringvliet are east of this “Middelharnis-Spui line” (Fig. 7.1). As the bathymetry of the Haringvliet still resembles that of an active estuary with deep pits, opening the Haringvliet sluices—albeit slightly—can threaten the availability of freshwater in the region by

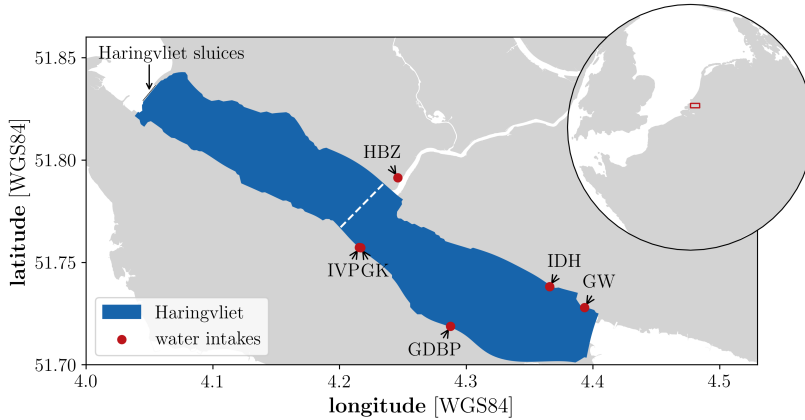


Figure 7.1: Haringvliet in the south west of the Netherlands, including the Haringvliet sluices and water intake locations (Tab. 7.3 for abbreviations). The white, dashed line indicates the “Middelharnis-Spui line”.

up-stirring of saline water that accumulates in these deep pits (Kranenburg *et al.*, 2023).

The case of the Haringvliet is a prime example of a trade-off between ecological impacts and natural resource availability: how to find a balance between these opposing goals? In past decades, much emphasis has been placed on the quantification and valuation of ecosystem services (e.g., Barbier *et al.*, 2011; Granek *et al.*, 2010; Heimhuber *et al.*, 2024; Worm *et al.*, 2006). However, the valuation of ecosystem services requires know-how about the ecosystems and how they will develop (Liquete *et al.*, 2013), which is by no means trivial. Furthermore, assessments using ecosystem services strongly focus on economic gains (Barbier *et al.*, 2011; Liquete *et al.*, 2013), such as the fishing industry (Heimhuber *et al.*, 2024). This leads to other values of ecosystem services to be underrepresented, such as ecologically valuable habitats.

Hence, the aim of this chapter is to provide a method to compare socio-ecological objectives in an estuarine system in which ecological objectives are fully accounted for, aiding decision- and policy-makers. In this way, we address the research question of how the ecological “stakeholder” could be incorporated in decision- and policy-making. As a case study, we use the Haringvliet in which current policy-making is concerned with such a socio-ecological trade-off. Note that making the ecological impacts of interventions insightful for decision- and policy-makers constitutes for a large part of the aim of this chapter.

7.2 Method

In this study, we used the Haringvliet as a case study in which the gates of the Haringvliet sluices were opened at different heights. At the basis, we used a hy-

hydrodynamic model of the Rhine-Meuse Delta, which is presented in Section 7.2.1. The implications of opening the gates were assessed by means of (1) ecological diversity (Sec. 7.2.2), and (2) freshwater availability (Sec. 7.2.3).

7.2.1 Hydrodynamic model

This study executed model simulations using the hydrodynamic modelling software Delft3D Flexible Mesh (Kernkamp *et al.*, 2011). This software is used to solve the Reynolds-averaged Navier-Stokes equations, assuming hydrostatic pressure and implementing the k - ε turbulence closure model.

The “RMD model” is a hydrodynamic model of the Rhine-Meuse Delta (Geraeds *et al.*, *in prep.* Gerritsma *et al.*, *in review*), which includes the Haringvliet. The model domain extends 35 km offshore of the Dutch coastline, where the grid resolution is $600 \times 1,200$ m, and refines towards the coastline to become 170×290 m. The river branches laterally span at least eight grid cells (20 m each), and depending on the river branch have a length of 60–100 m. In the Haringvliet, the cell size is approximately 135×75 m, and the Haringvliet sluices are included as operable structures.

We implemented a combined Z , σ -layering for the vertical discretisation: the top layers were defined as σ -layers that follow the temporal fluctuations of the water level, and the bottom layers maintain a constant cell thickness—so-called Z -layers—to better represent salt dynamics (Stelling & van Kester, 1994). There are nine σ -layers atop the Z -layers, which have a constant thickness of $\Delta z = 0.75$ m down to $z = -15$ m below which the thickness of the Z -layers grows by a factor of 1.15. A more detailed description of the RMD model can be found in Gerritsma *et al.* (*in review*).

The RMD model is executed for the year 2019, which has been calibrated and validated by Geraeds *et al.* (*in prep.*). In the reference simulation, the opening and closing of the Haringvliet sluices were based on water levels at both sides of the structure and represent the implementation of the “Kierbesluit.” For the other simulations, we applied a fixed level of the gates, i.e., a fixed flow area between the North Sea and the Haringvliet. All gates are completely closed when reaching $z = -5.50$ m NAP, and are 58.5 m wide—except for the outermost gates, which are 57.5 m wide—totalling to an opening width of $W_g = 992.5$ m. In addition to completely closing and opening of the Haringvliet sluices, we have also included intermediate opening of the gates; the height of the gates is notated as z_g , which is taken with respect to the bottom of the gates—i.e., $z_g = 0.00$ m for $z = -5.50$ m NAP. In all simulations, we have implemented a constant height of the gates, except for the reference case representing the “Kierbesluit,” which implements a time-varying height—i.e., $z_g = z_g(t)$. An overview of the simulations is presented in Table 7.1.

7.2.2 Ecological metric

In order to evaluate the ecological implications of opening/closing the Haringvliet sluices, we used EMMA (Ecotope-Map Maker based on Abiotics; Brunink & Hen-

Table 7.1: Overview of simulations. z_g is the height of the gates with respect to the bottom (i.e., $z = -5.50$ m NAP); and A_g is the flow area through the sluices, i.e., $A_g = z_g W_g$ with $W_g = 992.5$ m. The simulation “reference” represents the time-dependent opening regime as applied in 2019, which includes the “Kierbesluit” adaptation; and “open” represents the situation as if the gates have been removed from the Haringvliet sluices entirely.

Description	Opening/gate height	Flow area
	z_g [m]	A_g [m ²]
reference (“Kierbesluit”)	$z_g(t)$	$A_g(t)$
closed	0.00	0
partial	0.50	496
	1.50	1489
	2.10	2084
	2.75	2729
open	∞	∞

drickx, 2024). EMMA determines which ecotope is most likely to occupy an area based on the prevailing abiotic characteristics (based on Bouma *et al.*, 2005; Páree, 2021); these include three hydrodynamic variables that can readily be extracted from most hydrodynamic models: (1) water depth; (2) flow velocity; and (3) salinity. EMMA translates these three hydrodynamic variables to ecotope codes (Tab. 7.2), where we only consider soft substratum and limit the level of detail until which EMMA performs well (performance of 73.5% for listed classes in Tab. 7.2; Brunink & Hendrickx, 2024).

For this study, we implemented a small change to EMMA compared to Brunink and Hendrickx (2024) regarding the freshwater ecotopes: Areas with the yearly average of the tidal maximum salinity levels below 0.27 psu were labelled as *freshwater* ecotopes, regardless of the variability in the tidal maximum salinity levels. This threshold follows from the drinking water criteria in the Netherlands (Sec. 7.2.3). This small adaptation corrects the sensitivity to negligible fluctuations in salinity when the mean salinity is near zero.

The ecotope maps generated with EMMA were assessed in two manners: (1) the diversity of ecotopes; and (2) the change in ecotope area. In the first assessment, we used a simplified diversity metric—the Shannon index (Shannon, 1948)—to quantify the ecological richness of various model scenarios. The latter provided a more holistic view of the ecological impact, reflecting on three ecological aspects: (1) which ecotopes are present in the Haringvliet; (2) how much (relative) area do these ecotopes cover; and (3) how would the distribution of ecotopes transition between alternatives.

The Shannon index is originally a quantification of information (Shannon, 1948) and has often been used as a metric to quantify the biodiversity of an ecosystem (e.g., Kubicek *et al.*, 2019; Medeiros *et al.*, 2012; Smith *et al.*, 2023). Here, we used the index to quantify the diversity of the ecotopes, i.e., ecotope diversity (based on Shannon, 1948):

$$H' = - \sum_i^N p_i \ln p_i \quad (7.1)$$

Table 7.2: Meaning of ecotope-codes as used in EMMA. The ecotope-code is built-up as **ab.cd** with **a** the salinity label, **b** the substratum label, **c** the depth label, and **d** the hydrodynamics label. μ_s and σ_s are the annual mean and standard deviation of the depth-averaged, tidal salinity maxima [psu]; z_b is the bed level [m]; MLWS is mean-low-water-spring [m]; MHWN is mean-high-water-neap [m]; and μ_u is the annual mean of the tidal flow velocity maxima [ms^{-1}].

Class	Label	Meaning	Definition	
a	salinity	Z	marine	$\mu_s > 18 \text{ psu}^a$
		B	brackish	$5.4 \leq \mu_s \leq 18 \text{ psu}^a$
		F	freshwater	$\mu_s < 5.4 \text{ psu}^a$
		V	variable	$\mu_s < 4\sigma_s$
b	substratum	1	hard substratum ^b	
		2	soft substratum	
c	depth	1	sub-littoral	$z_b < \text{MLWS}$
		2	littoral	$\text{MLWS} \leq z_b \leq \text{MHWN}$
		3	supra-littoral	$z_b > \text{MHWN}$
d	hydrodynamics	1	high-energy	$\mu_u > 0.7 \text{ ms}^{-1}$
		2	low-energy	$\mu_u \leq 0.7 \text{ ms}^{-1}$
		3	stagnant	$\mu_u = 0.0 \text{ ms}^{-1}$

- a These thresholds are overruled when the variable classification applies (i.e., $\mu_s < 4\sigma_s$), except for $\mu_s \leq 0.27 \text{ psu}$ being freshwater (see text).
b The hard substratum is included here for completeness, as this study only considers the soft substratum.

where N is the number of ecotopes [-]; and p_i the area fraction of ecotope i [-], such that $\sum_i^N p_i = 1$.

From Equation (7.1), we can derive the evenness-index (Pielou, 1966), which we used as ecological performance indicator:

$$\mathcal{P}_e = \frac{H'}{\ln N} \in [0, 1] \quad (7.2)$$

Note that at the level of detail considered, there are 36 possible ecotopes (i.e., $N = 36$), which follows from the number of combinations possible with the labels in Table 7.2 with only soft substratum (i.e., **b** = 2).

The diversity in the form of the Shannon index (Eq. 7.1) was used as the basis of a single-value metric due to its close relation to ecosystem services (Hooper *et al.*, 2005; Loreau *et al.*, 2001; Worm *et al.*, 2006), which are frequently used in assessing nature-based solutions (e.g., Barbier *et al.*, 2011; Granek *et al.*, 2010; Heimhuber *et al.*, 2024). Furthermore, diversity is linked to ecological functioning, ecosystem resilience, and adaptability to changing environmental conditions (e.g., Elmqvist *et al.*, 2003; Limberger *et al.*, 2023; Loreau *et al.*, 2001; Yachi & Loreau, 1999). Diversity at the landscape-level—i.e., ecotope diversity—especially contributes to the resilience of an ecosystem (Folke *et al.*, 2002; Loreau *et al.*, 2003; Vasiliev, 2022). Hence, ecotope diversity enhances ecosystem resilience. Note, however, that such a single-value metric may facilitate “metric fixation” (Muller, 2021): the undesired single-minded focus on a metric without consideration of the complexity left-out.

Therefore, the ecotope maps were also presented as a barcode, showing the areal distribution of ecotopes in the area of interest, i.e., the p_i -values of a given system-state (e.g., Fig. 7.5). This ecotope barcode representation is similar to Timmerman *et al.* (2021), except that our barcode represents the whole area of interest instead of a single transect.

7.2.3 Socio-economic metric

The socio-economic metric was related to the freshwater availability in a similar fashion as in Bakker *et al.* (*in review*, Ch. 6): The operations of the water intakes reflect the interests of the inhabitants, agricultural sector, and industry. The water intakes withdraw freshwater based on free-flow, i.e., the water level outside must exceed a threshold water level for the water to flow into the intake by gravity. In the Netherlands, the salinity of the water is not allowed to exceed the critical threshold of $s_c = 150 \text{ mg Cl}^- \text{ l}^{-1}$ (or 0.27 psu). Thus, water extraction only occurs if the following two criteria are met:

$$\eta(t) > \eta_c \quad (7.3a)$$

$$s(t) < s_c \quad (7.3b)$$

where η is the water level [m]; s the salinity [psu]; and the subscript c reflects the critical threshold.

Due to fluctuations in supply and demand of freshwater, freshwater storage volumes are present in the water board's water systems, and so were incorporated in this study. Such storage functioned as the control volume in the freshwater mass balance:

$$\frac{dV}{dt} = E(\eta, s) - D(t) \quad (7.4)$$

where V is the freshwater storage volume [m^3]; E the extraction rate (Eq. 7.5) [m^3s^{-1}]; and D the freshwater demand [m^3s^{-1}].

The supply of freshwater followed a binary signal, based on whether the extraction criteria were met (i.e., Eqs. 7.3a and 7.3b):

$$E = \begin{cases} E_{\max} & \text{if Eqs. 7.3a and 7.3b} \\ 0 & \text{else} \end{cases} \quad (7.5)$$

where E_{\max} is the maximum extraction rate of a water intake [m^3s^{-1}].

The freshwater storage in Equation (7.4) cannot become negative, and is capped by a storage capacity:

$$0 \leq V \leq V_c \quad (7.6)$$

where V_c is the freshwater storage capacity [m^3].

From this mass balance, we defined water shortage as the demand that cannot be met. This means that the demand exceeds the extraction rate ($D > E$), while

Table 7.3: Water intake specifications in the Haringvliet. V_c : freshwater storage capacity; D : freshwater demand; E_{\max} : maximum extraction rate. Data provided by the water board Hollandse Delta.

Intake station	V_c [m ³]	D [m ³ s ⁻¹]	E_{\max} [m ³ s ⁻¹]
GK: Gemaal Koert	37,000	0.70	1.39
GDBP: Gemaal de Bommelse Polders	60,000	1.33	2.65
IVP: Inlaat van Pallandt	300,000	4.50	8.96
HBZ: Hevel Beningerwaard Zuidland	75,000	1.21	2.41
IDH: Inlaat den Hitsert	15,000	0.36	0.72
GW: Gemaal Westersepolder	12,000	0.10	0.20

the freshwater storage cannot cover the deficit ($V < D - E$):

$$S = \begin{cases} D - E - \max \left\{ -\frac{dV}{dt}; 0 \right\} & \text{if } V < D - E \\ 0 & \text{else} \end{cases} \quad (7.7)$$

Thus the freshwater shortage is defined as the freshwater demand that cannot be met, neither by the extraction rate, nor by the freshwater reserves. The max-term in Equation (7.7) represents the contribution of whatever is left in the storage to limit the shortage.

These shortages form the basis of the freshwater performance indicator:

$$\mathcal{P}_w = 1 - \frac{\int_T S \, dt}{\int_T D \, dt} \in [0, 1] \quad (7.8)$$

where T is the period of interest [s]; S the freshwater shortage [m³s⁻¹]; and D the freshwater demand [m³s⁻¹]. Note that $P_w \in [0, 1]$ follows from the freshwater shortage being bounded by null and the demand, i.e., $0 \leq S \leq D$. In essence, Equation (7.8) quantifies how much of the freshwater demand has been met over the period of interest, T .

The Haringvliet and its water intakes are managed under the jurisdiction of the Hollandse Delta water board, which covers 100,000s of people—including part of Rotterdam—, substantial agricultural land, and the majority of the Port of Rotterdam. There are six water intakes withdrawing from the Haringvliet and its surroundings, which are listed in Table 7.3, and their locations are shown in Figure 7.1.

7.3 Results

The impact of opening the Haringvliet sluices on the freshwater availability is non-existent for $z_g \leq 0.50$ m (Fig. 7.2)—including the reference case, $z_g = z_g(t)$. It is for $z_g \geq 1.50$ m that the capacity of the existing water intakes cannot keep up with the demand year-round, although the impact is very limited for $z_g = 1.50$ m, which only shows the occurrence of freshwater shortages at the end of the summer.

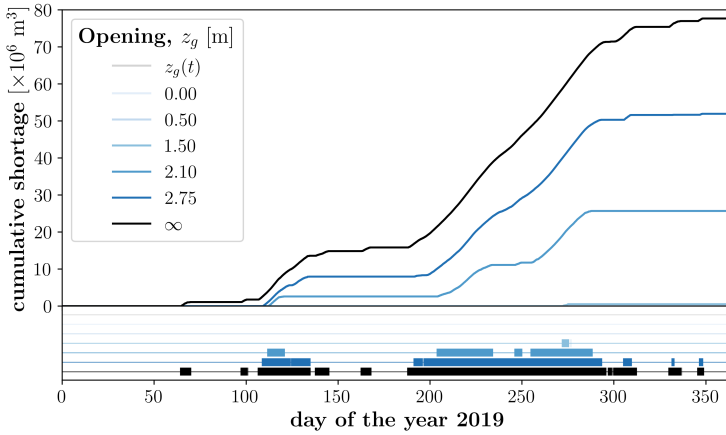


Figure 7.2: Freshwater shortages due to opening the Haringvliet sluices. The bars on the bottom display the moments of freshwater shortage, i.e., $S > 0$ (Eq. 7.7).

For $z_g \geq 1.50$ m, freshwater shortage increases with increasing the opening (Fig. 7.2). This relation is strongest between $z_g = 1.50$ m and $z_g = 2.75$ m, and becomes less for $z_g > 2.75$ m. Thus, there are phases in increased cumulative shortage due to the opening of the gates.

The minor dip in freshwater availability for $z_g = 1.50$ m arises from near-perfect performance of the western intakes (Fig. 7.3d), which are located near the “Middelharnis-Spui line.” Figure 7.3 shows that the “Middelharnis-Spui line” is a good indicator of performance loss of the western water intakes, illustrated by the loss of performance as soon as the 0.27-psu isohaline crosses this line. Further opening the gates results in threatening the freshwater availability, eventually also affecting water intakes farther upstream (i.e., GDBP; Fig. 7.1). The two eastern most water intakes are located outside the zone of impact (i.e., IDH and GW; Fig. 7.1), even when the gates are completely opened (Fig. 7.3g).

The increasing influence of salinity is also clearly reflected in the ecotope maps (Fig. 7.4): from a completely freshwater-based ecotope map for a closed Haringvliet ($z_g = 0.00$ m) to an almost completely variable-salinity ecotope map for an open Haringvliet ($z_g = \infty$). However, brackish ecotopes are barely returning to the Haringvliet, despite the salinity reaching levels above the freshwater-brackish threshold of $s_* = 5.4$ psu near the mouth (Fig. 7.3). This is caused by the variability in salinity that dominates these otherwise brackish regions, which causes the downstream region of the Haringvliet to be mainly classified as variable-salinity (Vx.xx). Note that also large patches of the otherwise freshwater regions are classified as such due to the high variability in salinity.

In addition to the change from freshwater to variable-salinity ecotopes, the hydrodynamic energy in the Haringvliet also increases with increasing opening of the gates as well as increased littoral zones. The increased hydrodynamic activity is concentrated in the channels remnant of the estuary before the closure. Thus,

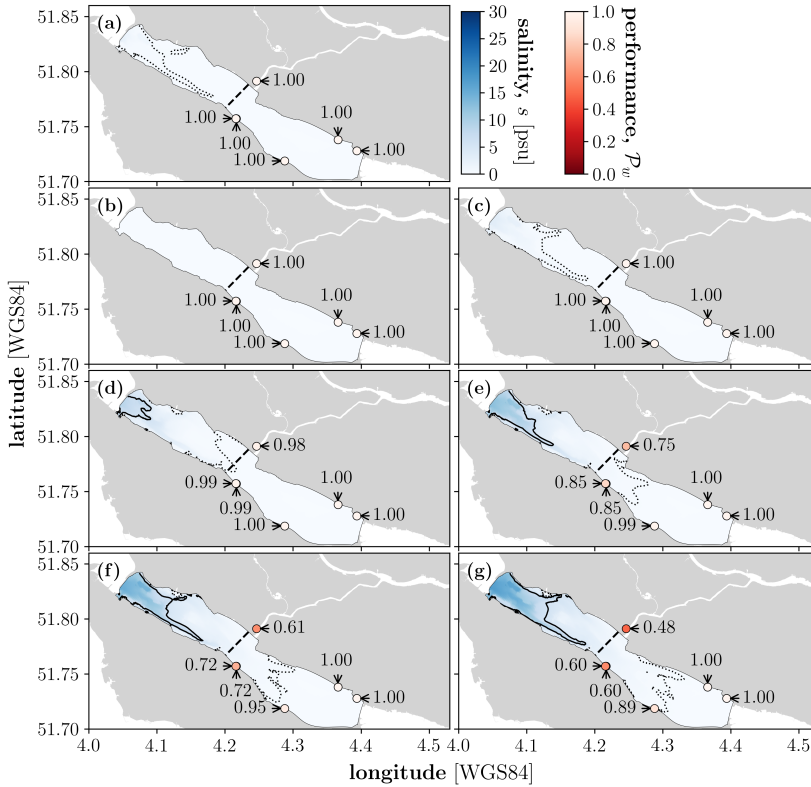


Figure 7.3: Annual mean of depth-averaged, tidal salinity maxima and up-time of water intakes. (a) $z_g = z_g(t)$ (reference), (b) $z_g = 0.00$ m (closed), (c) $z_g = 0.50$ m, (d) $z_g = 1.50$ m, (e) $z_g = 2.10$ m, (f) $z_g = 2.75$ m, and (g) $z_g = \infty$ (open). The drinking water salinity threshold of $s_c = 0.27$ psu is marked by the black, dotted contour line; and the freshwater-brackish threshold of $s^* = 5.4$ psu is marked by the black, solid contour line. The black, dashed line indicates the “Middelhamnis-Spui line.”

opening the Haringvliet sluices reintroduces the tidal dynamics into the system—or at least partially.

These changes in ecotope area between the various model simulations are clarified in Figure 7.5 by means of a Sankey diagram, which contains the system-states as ecotope barcodes: stacked colours whose height represent the relative area occupied by the ecotope with respect to the total area of the area of interest—i.e., the Haringvliet. Such a Sankey diagram shows where ecotopes transition to due to changing conditions, and thus what ecotopes they replace and are replaced by.

As a result of opening the Haringvliet sluices, the Haringvliet transitions from a low-dynamic, freshwater ecosystem to a more diverse system with a highly variable salinity and hydrodynamically active area near the mouth complementary to a low-dynamic, freshwater compartment near the back (Figs. 7.4 and 7.5). The level of opening determines the contribution of the variable salinity ecotopes (Fig. 7.5),

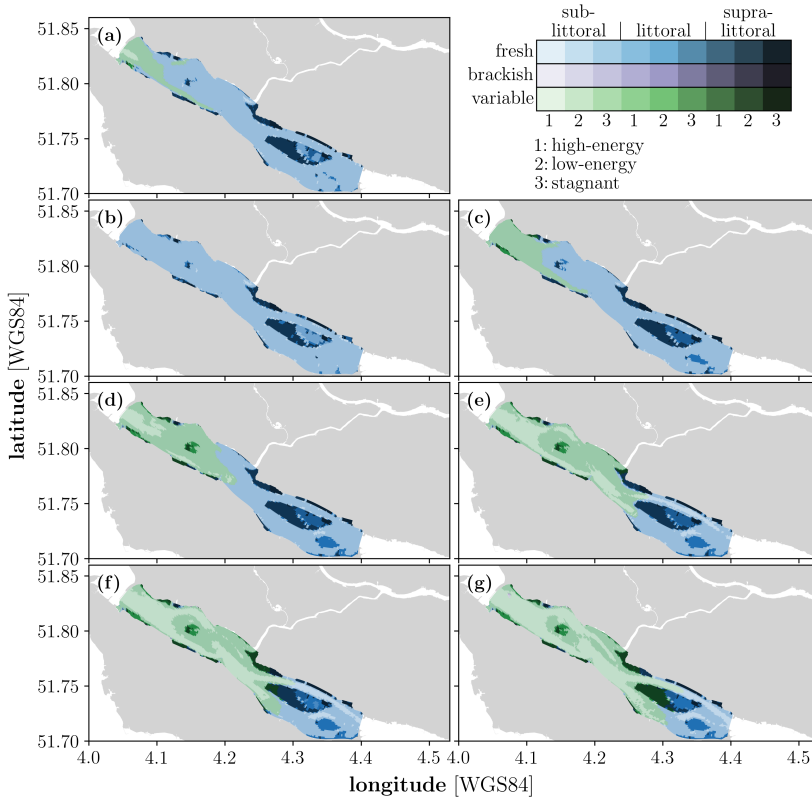


Figure 7.4: Ecotope-maps of the Haringvliet. (a) $z_g = z_g(t)$ (reference), (b) $z_g = 0.00$ m (closed), (c) $z_g = 0.50$ m, (d) $z_g = 1.50$ m, (e) $z_g = 2.10$ m, (f) $z_g = 2.75$ m, and (g) $z_g = \infty$ (open). Note that brackish ecotopes appear near the mouth of the Haringvliet with (partially) opened gates, but their contribution is very minimal, i.e., hard to see in the figure.

and how far these penetrate landward (Fig. 7.4). Nevertheless, even when the gates are completely opened, a substantial area remains suitable for freshwater ecotopes. Where for $z_g \leq 0.50$ m—including $z_g(t)$ —the Haringvliet is dominated by freshwater, low-energy environments (F2.12), variable salinity, high-energy environments (V2.11) become dominant for $z_g \geq 2.75$ m with substantial contributions of other ecotopes—the sub-littoral dominance remains for all levels of opening. This transition is an expected trend arising from further opening the gates: a transition from freshwater to variable salinity in combination with a transition from low to high energy hydrodynamics.

Opening the Haringvliet sluices clearly affects the freshwater availability negatively, and the ecological diversity positively. This trade-off is presented in Figure 7.6 as a Pareto-front: the two performance indicators are plotted against each other to illustrate what the effects are on both perspectives.

In line with the results presented in Figure 7.2, Figure 7.6 shows that the

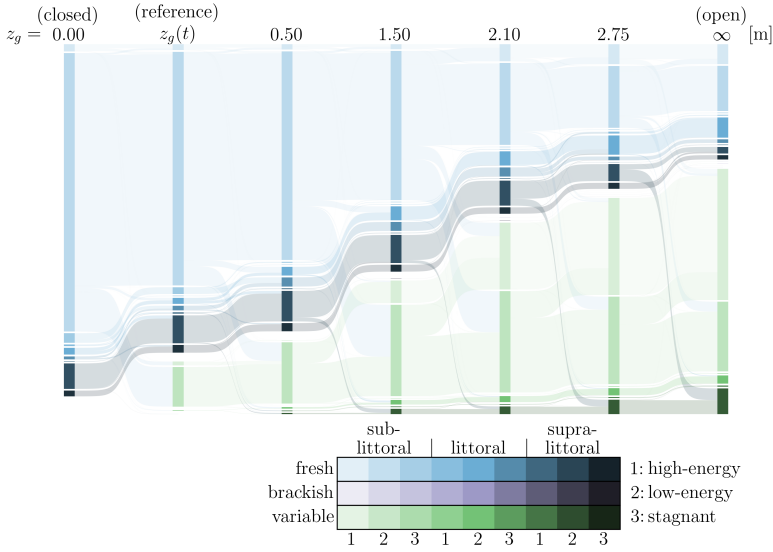


Figure 7.5: Sankey diagram of the ecotopes in the Haringvliet. Every ecotope barcode (stacked bar) represents the system’s ecological state by means of the relative areal contribution of every ecotope in the Haringvliet. The ecotope barcodes are connected by how the ecotopes transition between model simulations, i.e., ecological states.

7

freshwater availability remains unaffected up to $z_g = 0.50$ m—and is only barely impacted at $z_g = 1.50$ m. Meanwhile, the ecological performance increases, illustrated by the (almost) vertical line in Figure 7.6. Noteworthy is the enhanced ecological diversity in the Haringvliet as a result of the “Kierbesluit”—i.e., $z_g = z_g(t)$ —without compromising on the freshwater availability (compared to a closed Haringvliet, i.e., $z_g = 0.00$ m). It is not until the western-most water intakes get affected by the increasing salinity in the Haringvliet that the socio-economic performance indicator starts to drop: from a (near) perfect performance for $z_g \leq 1.50$ m to $\mathcal{P}_w = 0.70$ for a completely open connection—i.e., $z_g = \infty$.

Interestingly, there is a limit to the added value of the ecological diversity for further opening the gates. At the upper end of the opening heights, the ecotope diversity reduces with increasing opening, reaching an “optimum” at $z_g = 2.75$ m with $\mathcal{P}_e = 0.53$ (Fig. 7.6). This response follows from the definition of the area of interest: when freshwater ecotopes dominate the Haringvliet, increased opening reduces this dominance causing a more even ecotope distribution. However, when the variable-salinity ecotopes are dominant, further opening the sluices enhances this dominance due to which the evenness index—i.e., the ecological performance indicator (Eq. 7.2)—reduces. This change in dominant salinity class is also clearly visible in Figures 7.4 and 7.5. Note that this dip would not be visible if the area of interest would have been extended farther upstream.

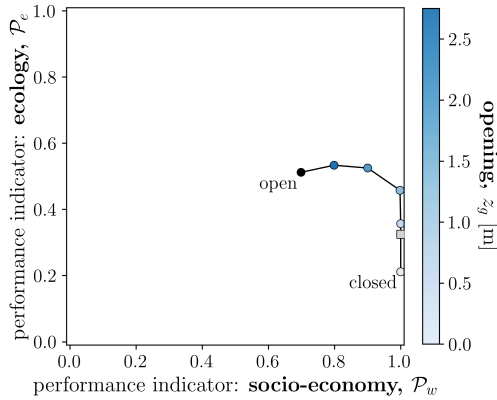


Figure 7.6: Pareto-front of socio-ecological performance indicators. The reference case is marked with a grey square; and the completely opened gates are coloured black.

7.4 Discussion

The Haringvliet sluices and their opening regime have a significant effect on the ecotope diversity as well as the freshwater availability. However, opening the gates only slightly—i.e., $z_g \leq 0.50$ m—improves the diversity without compromising on the freshwater availability (Fig. 7.6). Thus aside from re-establishing the connectivity between the Haringvliet and the North Sea for fish migration (Baas *et al.*, 2020; Bice *et al.*, 2023), the “Kierbesluit” also supports the development of a more diverse set of ecotopes in the Haringvliet (Fig. 7.4a and b).

Note, however, that the rare brackish, estuarine ecosystem present in the Haringvliet before its closure (Tangelder *et al.*, 2017) barely returns—if at all—, even with the gates completely opened (Fig. 7.4g). Although salinity levels are sufficiently high near the Haringvliet sluices to support a brackish ecosystem (Fig. 7.3e–g), the variability in salinity is such that this area is classified as variable-salinity (i.e., Vx.xx). This is related to the dominance and variability in freshwater input from the rivers. As a result, regions in the Haringvliet can become completely fresh and exceed well beyond the marine salinity threshold of 18 psu within a single year.

Variable conditions have been found to promote biodiversity, according to the intermediate disturbance hypothesis (e.g., Chesson, 1994; Connell, 1978; Dial & Roughgarden, 1998). In brief, this hypothesis states that at intermediate levels of disturbance, the ecosystem cannot be dominated by a specific (set of) species due to the changing conditions, resulting in an increased biodiversity (e.g., Hall *et al.*, 2012; Letten *et al.*, 2018). However, it is debatable whether this hypothesis holds for salinity fluctuations, especially for the salinity variability found in this study (Van Diggelen & Montagna, 2016): salinity levels of $s = 0$ psu and $s > 18$ psu within one year.

For the determination of the ecotopes, we simulated the year 2019, which was

a representative year regarding river discharges and storm surges (Geraeds *et al.*, *in prep.* taken over the last 120 years). Such long-term representative conditions are preferred for the use of EMMA (Bouma *et al.*, 2005; Brunink & Hendrickx, 2024). However, the functioning of the freshwater intakes is most stressed during droughts and storms, when there is limited freshwater inflow into the Haringvliet to mitigate salt intrusion. Therefore, the impact of (partially) opening the gates is expected to be more detrimental during droughts and storms than the results shown in this study (Fig. 7.2), likely hampering the freshwater performance—i.e., moving the front in Figure 7.6 leftward.

During such dry and stormy periods, a crisis policy of closing the gates temporarily to secure the freshwater availability could be adopted. Note, however, that a closed Haringvliet is not completely safe from saline influences, as saline water can still enter via the Spui—the northern branch connected to the North Sea (Fig. 7.1)—, causing saline contamination (Gerritsma *et al.*, *in review*). An additional measure could include a larger capacity of the eastern water intakes, i.e., increase their maximum extraction capacity and/or their storage capacity. Such an enlarged capacity of the eastern water intakes would also allow for opening the gates to $z_g \geq 1.50$ m during “normal” conditions.

In addition to the increased saline influence in the Haringvliet due to opening the sluices, this opening also reintroduces the tidal fluctuations in the system. The (partial) removal of the tidal breathing in an estuary is a common side-effect of large-scale interventions such as storm surge barriers (e.g., Nienhuis & Smaal, 1994; Ralston, 2022). However, the ecological benefits and water quality improvements achieved by reintroducing tidal dynamics are often stressed by nature restoration projects (e.g., Abbott *et al.*, 2020; Glamore *et al.*, 2021; Heimhuber *et al.*, 2024). The intertidal areas arising from tidal dynamics are ecologically valuable, providing several crucial ecosystem services (e.g., Barbier *et al.*, 2011; Costanza *et al.*, 1997), and have been found to reduce methane emissions of wetlands (Kroeger *et al.*, 2017; Rosentreter *et al.*, 2021).

For (partial) reintroduction of the tidal dynamics in the Haringvliet, the gates need to be opened to $z_g \geq 1.50$ m, which would more than double the littoral zone compared to a closed system (from 3.4% to 9.8% of the area; Fig. 7.7), while the supra-littoral zone remains similar (around 9–12%). Note that even when the Haringvliet sluices are completely closed, there is still some intertidal area (Fig. 7.7b)—i.e., tidal dynamics—due to its connectivity to the North Sea via the many branches of the Rhine-Meuse Delta. The “Kierbesluit” opening regime does little to enhance the littoral zone in the Haringvliet, while a permanent opening of $z_g = 0.50$ m—which is comparable to the time-averaged opening of the “Kierbesluit”—would almost double the littoral zone.

The aforementioned ecological value of intertidal areas can also be used as a goal with the implemented assessment method: The ecotope barcodes (i.e., Fig. 7.5) allow us to focus on specific, desired ecotopes that are considered (very) valuable and ecologically desirable. An example of such a focused assessment is presented in Figure 7.8 in which we highlight the presence of intertidal areas (i.e., xx.2x). The presence of this valuable collection of ecotopes clearly increases with increasing

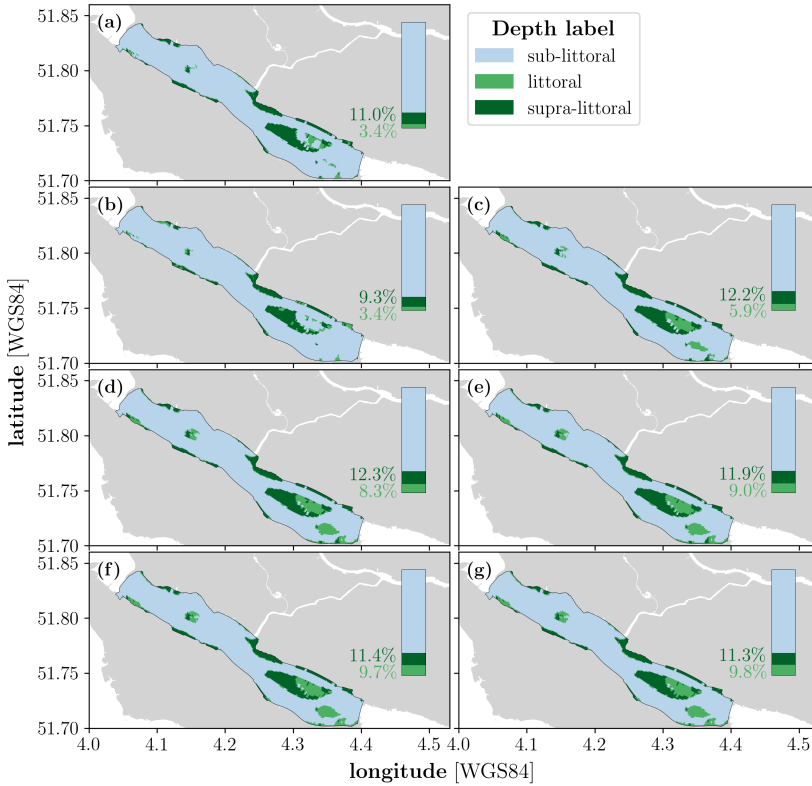


Figure 7.7: Littoral zoning in the Haringvliet. (a) $z_g = z_g(t)$ (reference), (b) $z_g = 0.00$ m (closed), (c) $z_g = 0.50$ m, (d) $z_g = 1.50$ m, (e) $z_g = 2.10$ m, (f) $z_g = 2.75$ m, and (g) $z_g = \infty$ (open). The bar-charts in the upper-right corners present the areal percentage of the intertidal area in the Haringvliet. Intertidal areas represent the littoral zone, which ranges between mean-low-water-spring (MLWS) and mean-high-water-neap (MHWN) according to EMMA (Bouma *et al.*, 2005; Brunink & Hendrickx, 2024).

opening of the Haringvliet sluices (Fig. 7.8), with the steepest increase for $z_g \leq 1.50$ m.

Although inherently incomplete, the performance indicators as defined in this study are illustrative of the socio-ecological trade-offs associated with the opening regime of the Haringvliet sluices. The resulting Pareto-front as presented in Figure 7.6 is an intuitive visualisation of the trade-offs between—in our case—socio-ecological interests. The overall performance of the collection of performance indicators can be determined by the square area under the curve (e.g., Emmerich & Deutz, 2018), i.e., the square consisting of the origin and $(\mathcal{P}_w, \mathcal{P}_e)$. Therefore, the Pareto-front is a useful tool for decision- and policy-makers, and aids in communicating the trade-offs between different measures to the general public.

Note that the performance indicators as presented in Figure 7.6 purposefully exclude any valuation, which is a subjective and political matter affected by the

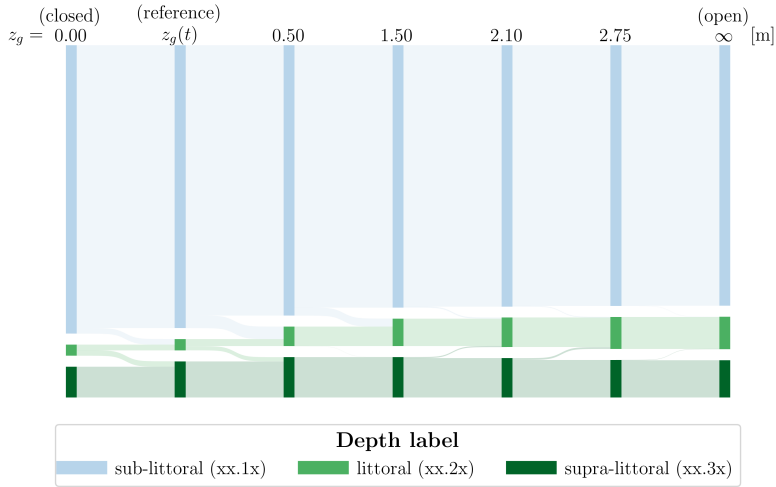


Figure 7.8: Sankey-diagram focused on littoral zoning. Every ecotope barcode represents the relative areal contribution to the Haringvliet.

zeitgeist. However, this is a key-step in decision- and policy-making, and can be achieved by the definition of valuation functions (Greco *et al.*, 2016; Keeney & Raiffa, 1993, for approaches to define such valuation functions). These valuation functions can be embedded in the intuitive visualisation of Pareto-fronts, maintaining their benefits in decision- and policy-making as well as communication to the public (Bakker *et al.*, *in review*, for the embedding of valuation functions).

The use of Pareto-fronts requires the quantification of performance indicators, which is where the contribution of EMMA to explore the potential ecological impact of different interventions is crucial. In addition to the subsequently derived diversity- and evenness-indices (Eqs. 7.1 and 7.2), the ecotope barcodes allow us to focus on specific, desired ecotopes. Goals could be set to ensure a minimum area for a specific ecotope—or set of ecotopes—that is considered of great ecological value, e.g., intertidal areas (Fig. 7.8). This method allows ecological interests to be set on equal footing with other stakeholders' interests, and a quantification of the ecological costs and benefits of large-scale, estuarine interventions.

7.5 Conclusion

In this study, we have implemented a hydrodynamic model to explore the effects of reopening the Haringvliet sluices on a socio-ecological trade-off: freshwater availability versus ecological diversity. The presented socio-ecological evaluation has shown that the ecological potential of the Haringvliet could substantially increase by opening the Haringvliet sluices—at least partially. The impact on the freshwater availability is expected to be limited up to an opening of $z_g = 1.50$ m. However, we did so for a representative year regarding river discharges and storm

surges—required for the ecological assessment—, while freshwater availability is more seriously threatened during drought and storm conditions.

The use of representative (non-monetary) performance indicators for the considered stakeholders allowed us to demonstrate the trade-offs in a clear fashion: the Pareto-front resulting from these performance indicators is an intuitive visualisation of the costs and benefits between stakeholders. In particular, the use of EMMA allowed us to explore and quantify the ecological implications of estuary-scale interventions, such as (partially) opening the Haringvliet sluices. We have thereby presented an approach in which ecological interests can be set on equal footing with other stakeholders' interests allowing for a similar incorporation of ecological implications in decision- and policy-making.

Acknowledgements. We are indebted to Peter M.J. Herman for his contributions to the early stages of the research design, which greatly added value to the study and subsequent manuscript. We would also like to thank Thijs Ijpelaar and Jermo de Miranda (Hoogheemraadschaap Hollandse Delta) for providing information about the water intakes included in this study. This work used the Dutch national e-infrastructure with the support of the SURF Cooperative using grant no. EINF-7152.

Author contributions. G.H., G.F., S.P. designed the research; A.G., M.G. developed the hydrodynamic model and provided model boundary conditions for the year 2019; G.H. performed the research; G.H. analysed the data; G.H. wrote the manuscript; and G.H., G.F., A.G., M.G., S.P. reviewed the manuscript.

Data availability. Data is available upon reasonable request to the corresponding author.

Software availability. This study builds upon the open-access tool EMMA (Ecotope-Map Maker based on Abiotics; Hendrickx & Brunink, 2023), which is a Python-based processing tool translating hydrodynamic model output data to ecotope maps.

IV | REFLECTION

The aim of the *reflection*-phase is to critically deliberate the role of nature-based solutions in an uncertain future, with a special focus on this thesis' topic: *nature-based solutions to mitigate salt intrusion*. Thus, the objective is to *reflect on the role of nature-based solutions with future uncertainties*.

First, the role of nature-based solutions is considered at a more general level in Chapter 8 with a special focus on unknown uncertainties inherent to the future. Subsequently, Chapter 9 reflects on this thesis and the implications it may have on future estuarine salt intrusion mitigation.



SYNTHESIS

8.1 Introduction

In recent years, the consequences of rapid changes in the climate and the challenges that they present for engineers have become apparent in extreme events (e.g., Pörtner *et al.*, 2023; Wetz & Yoskowitz, 2013). Examples include the recent drought in northwestern Europe due to extremely low river discharges (Toreti *et al.*, 2022); the devastating frequency of ocean heat waves causing mass coral bleaching events (Hughes *et al.*, 2018); and exceptionally large forest fires during the summer of 2019/2020 in Australia, aptly nicknamed the *Black Summer* (Collins *et al.*, 2021). Further climate change is expected to increase the gap between “normal” and “extreme” conditions (e.g., Gründemann *et al.*, 2022; Knutson *et al.*, 2010). These

This chapter is based on:

Hendrickx, G.G., Pearson, S.G., Antolínez, J.A.A., and Aarninkhof, S.G.J. (*in review*). DARE to proactively react to unknown uncertainties in the Anthropocene. Submitted to *Earth's Future*.

extreme events require (hydraulic) engineers to prepare for the unknown: New, unseen extremes will be—and are being—added to the records.

However, we live in a world in which optimal (engineering) designs are made while relying on future projections either by extrapolation of the present, or anticipating plausible future scenarios. Therefore, such unknown, extreme events are challenging to confront using current (hydraulic) engineering design and management practices. Questioning the extrapolation of present-day climate has inspired a wealth of research on creating plausible future scenarios of the climate system (e.g., Dingley *et al.*, 2023) and decision-making under deep uncertainty (e.g., Haasnoot *et al.*, 2024; Kwakkel *et al.*, 2016; Marchau *et al.*, 2019). Deep uncertainty represents the inability to know (1) which conceptual model to use, (2) which probabilities represent the uncertainty, and/or (3) which valuation functions to use, i.e., how to value the outcomes (Lempert *et al.*, 2003). Rather than trying to quantify deep uncertainty (e.g., Abadie *et al.*, 2017; Herman *et al.*, 2020; McInerney *et al.*, 2012; Reis & Shortridge, 2020), we propose to focus on designing systems such that the uncertain “input” has less influence on the “output”—i.e., the performance.

The main challenge for today’s engineers is in part related to the difficulty that arises when inferring the small probabilities associated with these extreme events (e.g., Abadie *et al.*, 2017; Klijn *et al.*, 2004): smaller probabilities require larger sample sizes and come with higher relative errors in their probabilities (Taleb, 2007). In practice, there is still widespread use among hydraulic engineers today of return periods to make design decisions and future protections (e.g., Hu *et al.*, 2024; Onchi-Ramos *et al.*, 2024; Wing *et al.*, 2024). However, this assumption is violated by the non-stationarity of a changing climate (e.g., Milly *et al.*, 2008), creating a need for more robust approaches.

Meanwhile, natural systems have been able to cope with changing climates without being designed to meet specific goals. Instead, these natural systems survive by containing diverse sets of species that thrive under different conditions (e.g., Elmqvist *et al.*, 2003; Folke *et al.*, 2002; Loreau *et al.*, 2001). As these conditions are constantly changing, species—and the natural systems they inhabit—adapt to these changes (e.g., Borsje *et al.*, 2011; Todd, 2008). At the same time, natural systems are robust to short-term fluctuations in the environmental conditions (e.g., Equihua *et al.*, 2020; Holling, 1973; Logan *et al.*, 2014). Even to such an extent that “pre-stressing” reduces the damage of a subsequent stress event (Ainsworth *et al.*, 2016; Berry & Gasch, 2008), which can be considered an “antifragile” component of natural systems (Taleb & Douady, 2013, more on the meaning of “antifragile” in Sec. 8.2.3). This approach of nature provides a plausible blueprint that could be emulated to help engineers face the challenges ahead.

In this chapter, we argue that we should implement nature’s own approach to dealing with uncertainties in engineering practice. In this light, we propose a conceptual framework that examines how we can reduce our dependency on knowing what the future holds by focusing on the output space. This concept is subsequently translated to practice in which we focus on physical aspects of hydraulic engineering. Over the past decades, this field has transitioned from

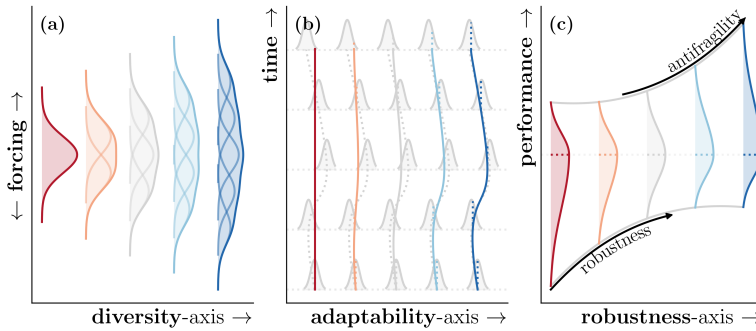


Figure 8.1: The three engineering dimensions and their corresponding axes in DARE: (a) forcing-dimension to *diversity*-axis; (b) time-dimension to *adaptability*-axis; and (c) performance-dimension to *robustness*-axis. The distributions in (a) and (b) both display performance-distributions, and in (c) they represent probability of performance with the dashed horizontal line being the expected performance. In all, the colours highlight the change along the DARE-axes.

“fighting against nature” to “building with nature” (de Vriend *et al.*, 2015; van Slobbe *et al.*, 2013) or “engineering with nature” (Bridges *et al.*, 2018). Here, we propose the next step in this transition: “building like nature.”

We first discuss how we, engineers, could learn from natural systems in dealing with unknown uncertainties in Section 8.2. In Section 8.3, we translate the introduced concept to practice, i.e., how to “build like nature” when faced with engineering challenges. We conclude this chapter with a brief reflection on what this design approach implies for engineering practices in Section 8.4.

8.2 DARE

Given certain forcing conditions and a time horizon, engineers are challenged to maximise performance of a system. In other words, there are three dimensions to the engineering challenge: (1) forcing, (2) time, and (3) performance. In an idealised world, all these three dimensions are fully understood and known. However, we do not live in such a world and every dimension contains (unknown) uncertainties. In addressing these uncertainties, we “build like nature” by following the principles of biomimetics (mimicking the natural system for engineering purposes; i.a., Bar-Cohen, 2006; Fayemi *et al.*, 2017; Hwang *et al.*, 2015). In doing so, we propose to project the aforementioned engineering dimensions on the following three axes in the solution space (Fig. 8.1): (1) diversity, (2) adaptability, and (3) robustness—hence, diverse, adaptive, and robust engineering (DARE). These axes are complementary but not exclusive, i.e., their implications are interconnected.

Here, we explain how these axes represent nature’s own approach, and how they translate to engineering challenges.

8.2.1 Diversity

In ecosystems, it has become clear that diversity facilitates resilience (e.g., Elmqvist *et al.*, 2003; Folke *et al.*, 2004; Limberger *et al.*, 2023; Loreau *et al.*, 2001; Vasiliev, 2022). In this respect, both diversity in system response and functionality are considered important for ecosystem resilience (Elmqvist *et al.*, 2003; Limberger *et al.*, 2023), which is essential for ecosystem survival in an uncertain environment (Elmqvist *et al.*, 2003; Folke *et al.*, 2002; Holling, 1973). Response diversity reflects the provision of the same ecosystem function by different species (Elmqvist *et al.*, 2003). This is a form of redundancy that allows for an ecosystem function to persist over a wide(r) range of forcing conditions; e.g., diversity in plankton species with different tolerances to pH maintained a high biomass of plankton during acidic conditions (Frost *et al.*, 1995).

Thus, the *diversity*-axis reflects the requirement for diversity in the engineering solution space. A diverse set of solutions to an engineering task results in a resilient approach—also in face of unknown uncertainties—by employing redundancy in the set(s) of solutions (e.g., Folke *et al.*, 2002; Loreau *et al.*, 2001). This axis is visualised in Figure 8.1a by the narrow, singular distribution (left) versus the wide, collective distribution (right).

8.2.2 Adaptability

The resilience of an ecosystem—hence the provision of its functions—depends on its ability to adapt to environmental changes and disturbances (Carpenter *et al.*, 2001; Folke *et al.*, 2004). This adaptability can be within species—e.g., different thermal tolerances of the same coral species due to different historical temperature exposure (Howells *et al.*, 2013)—as well as between species—e.g., changes in plant composition in the Himalaya due to a warming climate (Telwala *et al.*, 2013).

Also in engineering, the ability of adapting to changing conditions is essential in face of (unknown) uncertainties, which includes both self-accommodating solutions (e.g., Borsje *et al.*, 2011) and adaptive strategies (e.g., Haasnoot *et al.*, 2013). Adaptive measures can be considered upfront in combination with monitoring programs (e.g., Haasnoot *et al.*, 2013; Kwakkel *et al.*, 2015; Zandvoort *et al.*, 2018). The *adaptability*-axis implies an adaptive approach in which there is ample room to change course when new information arises (e.g., new knowledge or data) and/or when forcing conditions change on both the long- and short-term.

Long-term changes in forcing conditions are generally well-covered by self-accommodating solutions and/or adaptive strategies. In the short-term, such changes can be considered disturbances or extreme events. In such cases, solutions might work during exceptional, extreme conditions, but can cause undesired side-effects during “normal” conditions (e.g., estuarine storm surge barriers; Orton *et al.*, 2023; Ralston, 2022)—or vice versa (e.g., floodplains of rivers; Klijn *et al.*, 2004; Opperman *et al.*, 2009). An adaptive approach on such an event-timescale constitutes to the *adaptability*-axis. This is visualised in Figure 8.1b by a rigid, straight line approach (left) versus a flexible, curved line approach

(right). Note that the time-axis both reflects long-term changes—e.g., due to climate change—and short-term changes, such as extreme storm events.

8.2.3 Robustness

Natural systems are able to absorb—or dampen—environmental changes without dramatically altering their functions (e.g., Holling, 1973). Due to its living components, an ecosystem can recover from extreme events that damaged the ecosystem as long as the frequency and intensity of such events does not surpass the recovering potential of the ecosystem (e.g., Borsje *et al.*, 2011; Hooper *et al.*, 2005; Johnston *et al.*, 2019). Note that this recovery potential is strongly linked to the biodiversity of the ecosystem (e.g., Worm *et al.*, 2006). Thus the robustness of ecosystems is visible in limited fluctuations of its functions despite larger fluctuations in environmental conditions—up to a certain limit.

Therefore, we propose to aim for robustness in engineering designs instead of designs perfectly suited to a specific prediction of climate forcing, which is unattainable (Dessai *et al.*, 2009). Here, robustness is defined as reducing the variability in the output space given a certain condition or state (sometimes also referred to as “stability” and “resilience”; Herrera *et al.*, 2016; Holling, 1973; Taleb & Douady, 2013). In other words, the (unknown) uncertainties in future climate forcing (input) are only partially translated to the functioning—or performance—of the engineering design (output). Note that the aim of achieving robust solutions should focus on insensitivity to undesired outcomes (i.e., risks); sensitivity to desired outcomes (i.e., opportunities) is only beneficial (i.e., an antifragile system; Taleb & Douady, 2013). However, there is generally an upper limit to the performance (i.e., limited opportunities), due to which non-fragile (i.e., robust) systems are the highest attainable outcome.

Thus, the *robustness*-axis reflects the design of solutions that are insensitive towards undesired states (i.e., risks). Figure 8.1c visualises the robustness by reducing the variability of the lower-performance (left), and visualises antifragility by increasing the variability of the upper-performance (right).

8.3 Examples

In this section, we present two examples of DARE from the field of hydraulic engineering: (1) coastal flooding (Sec. 8.3.1), and (2) estuarine salt intrusion (Sec. 8.3.2). In the examples, we first introduce the challenge considered after which we reflect on how DARE could aid (hydraulic) engineers with that challenge.

8.3.1 Coastal flooding

Coastlines across the world are densely populated, with 40% of the world population living within 100 km from the coastline (Maul & Duedall, 2019) and this number is rising (Jongman *et al.*, 2012; Swain *et al.*, 2020). However, coastal regions are also highly susceptible to flooding (Neumann *et al.*, 2015; Paprotny

et al., 2018). Such flooding events have high social and economic costs (Hinkel *et al.*, 2014; Nicholls *et al.*, 2011), and thus are considered undesirable.

Coastal flooding is generally driven by extreme events such as storms and tropical cyclones (Almar *et al.*, 2021; Bevacqua *et al.*, 2020). Furthermore, climate change is driving changes in the frequency and intensity of such events (Emanuel, 2005; Knutson *et al.*, 2010; Lowe & Gregory, 2005), and thus in coastal flooding (Vitousek *et al.*, 2017). Next to the environmental uncertainties, modelling of (coastal) flooding is despite the many efforts still a challenging exercise (Bates *et al.*, 2005; Jafarzaghegan *et al.*, 2023; Leijnse *et al.*, 2021), which adds to the complexity and thereby also to the uncertainty of coastal flooding.

The many uncertainties related to coastal flooding fuel the already present challenges when designing coastal flood protection measures. DARE can provide help with this engineering challenge, which is described below per axis of DARE and visualised for tropical reef-lined coasts in Figure 8.2:

Diversity There are a multitude of ways to protect the coastline from flooding that are located at different sections of the cross-shore profile: (1) at the coastline itself, dikes and dunes provide a barrier to protect the hinterland from high waters and wave impact (Mulder *et al.*, 2011); and (2) in the nearshore zone, vegetated foreshores—e.g., mangroves and marshes—, living breakwaters as well as wide beaches dampen the wave energy before it reaches the dune or dike (Temmerman *et al.*, 2023; Toimil *et al.*, 2023). All these components can be combined to create a diverse set of flood mitigation measures. In Figure 8.2a-c, the components of a fringing reef on the wave runup are presented. This showcases that a (coral) reef by itself provides the option for a diverse solution set. The reef width, forereef slope, and reef friction all impact the wave runup. For example, a long reef flat and a high reef friction reduces the wave runup.

8

Adaptability Allowing for dynamics of the flood protection measures facilitates their adaptation to changing environmental conditions. In case of dunes, they partially erode during extreme conditions but this sediment is returned during calm conditions (Dodet *et al.*, 2019; Houser *et al.*, 2015; Suarez *et al.*, 2012). Dunes can even grow with sea level rise as long as there is sufficient sediment available (van IJendoorn *et al.*, 2021). Similarly, vegetated foreshores consist of natural ecosystems, which make them inherently adaptive to, e.g., sea level rise and environmental changes (Best *et al.*, 2018; Gijón Mancheño *et al.*, 2024; Reed *et al.*, 2018). This also holds for living breakwaters such as coral reefs, which can also grow with sea level rise (Perry *et al.*, 2018; van Woesik *et al.*, 2015) and acclimatise to changing environmental conditions (e.g., Gibbin *et al.*, 2018; Howells *et al.*, 2013; Hughes *et al.*, 2003; Logan *et al.*, 2014). The susceptibility of corals to a thermal stress event is shown in Figure 8.2d, where native corals show much less bleaching compared to transplanted corals adapted to a different thermal environment (Howells *et al.*, 2013).

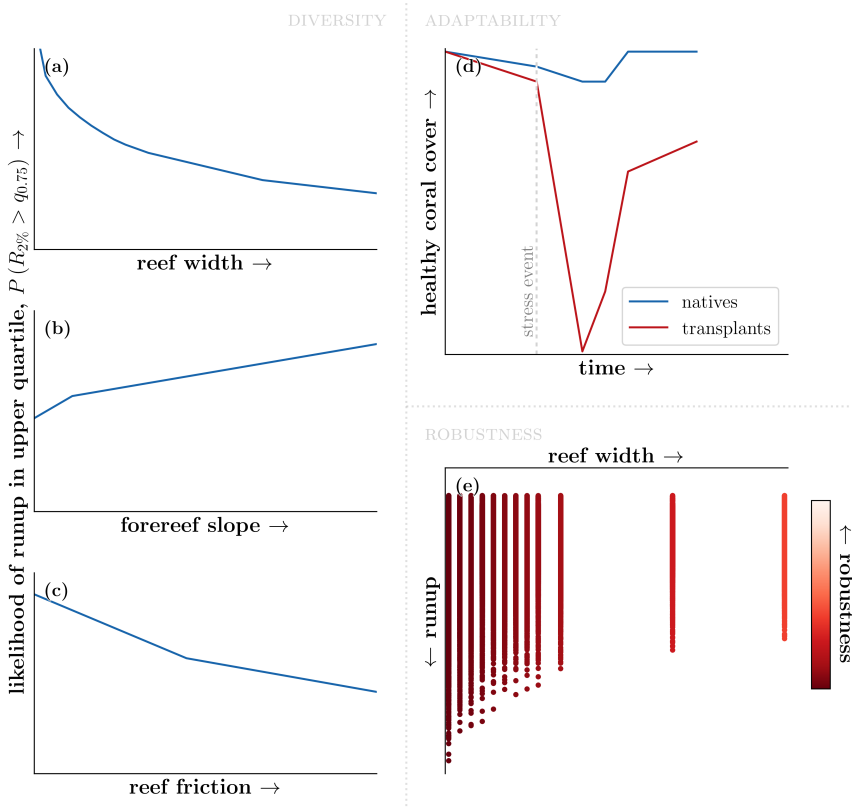


Figure 8.2: Conceptual implementation of the three axes of DARE on coastal flooding: (a-c) *diversity*-axis, likelihood of large wave runup (upper 25%-quantile); (d) *adaptability*-axis, coral susceptibility to a (thermal) stress event due to thermal acclimation; (e) *robustness*-axis, wave runup at the beach as function of the coral reef width. (Data sources used: Howells *et al.*, 2013; Pearson *et al.*, 2017a, see App. D for a description on the data processing for this figure.)

Robustness Robustness can be incorporated along the sections of the cross-shore profile, resulting in an overall robust coastline. Foredune blow-outs—i.e., gaps in the dunefront—contribute to the robustness of the beach-dune system (Laporte-Fauret *et al.*, 2022) by enhancing the interaction between beach and dune (Schwarz *et al.*, 2018), which increases the back-dune resilience in face of sea level rise (Arens *et al.*, 2013; Pye & Blott, 2017; Rangel-Buitrago *et al.*, 2023). Both (vegetated) foreshores and (living) breakwaters are robust measures in that they dampen the wave energy before it reaches the coastline: e.g., the vegetation density provides increased drag, resulting in wave damping (Mendez & Losada, 2004; Vuik *et al.*, 2016); and the width of coral reefs has a limiting effect on the wave height (Baldock *et al.*, 2020)

and runup (Pearson *et al.*, 2017b). Figure 8.2e shows that for increasing coral reef width, the wave runup becomes smaller and also shows less variability.

Reflecting on how DARE could be used to mitigate coastal flooding, different types of coastlines show different sets of solutions to consider. The sandy coastline with its crucial beach-dune system compromises large parts of the world's coastlines (Luijendijk *et al.*, 2018). The beach-dune system provides flood protection in various ways such as submerged sandbars, the beach, and dune(s) (Hanley *et al.*, 2014). Diversity can be built-in to the beach-dune system by combining different maintenance approaches, e.g., sand nourishments (Hanson *et al.*, 2002; Hoonhout & de Vries, 2017), vegetation (Feagin *et al.*, 2015, 2023; van Wiechen *et al.*, 2023), and allowing space for dune dynamics (Robin *et al.*, 2023; Ruessink *et al.*, 2018). Such dune dynamics as well as vegetation provides adaptive capacity via dune growth (van IJzendoorn *et al.*, 2021). Allowing for foredune blow-outs contribute to the robustness of the beach-dune system (Laporte-Fauret *et al.*, 2022) despite forming gaps in the front-line of a primary sea-defence: The added value of an increased resilience of the back-dune to sea level rise (Arens *et al.*, 2013; Pye & Blott, 2017; Rangel-Buitrago *et al.*, 2023) makes dunes with blow-outs more robust to changes in hydrodynamic forcing.

Another important contributor to coastal safety around the equator is a coral reef (Storlazzi *et al.*, 2019), which also provides substantial contributions to the local economy (Spalding *et al.*, 2017). Coral reefs have been found to work nicely in unison with two other ecosystems to protect against flooding, namely seagrasses and mangroves (Guannel *et al.*, 2016). As Figure 8.2a-c shows, there are various ways coral reefs can reduce wave runup—hence reduce flood risk. Furthermore, coral reefs can recover after storm damage (Fig. 8.2d; Mulla *et al.*, 2024) and grow with sea level rise (Perry *et al.*, 2018; van Woesik *et al.*, 2015). The robustness of coral reefs—and other living foreshores alike—shows in their suppressing effect on the wave height and runup, which becomes more prominent with, e.g., the width of the reef (Fig. 8.2e; Baldock *et al.*, 2020; Ferrario *et al.*, 2014; Pearson *et al.*, 2017b).

8.3.2 Estuarine salt intrusion

Estuaries form the interface between the rivers and the sea, which makes them economically attractive areas for human settlement. However, the supply of freshwater by the rivers to these settlements is under constant threat of saline contamination because they are close to the sea (Costall *et al.*, 2018; Nicholls & Cazenave, 2010; Wada *et al.*, 2011). As substantial estuarine salt intrusion results in contamination of freshwater, salt intrusion is considered socio-economically undesirable.

Estuarine salt intrusion is the result of an intricate interplay of several environmental forces (most notably the tide and river discharge; e.g., Geyer & MacCready, 2014), where the estuarine geomorphology sets the playground for these competing forces (Hendrickx *et al.*, 2023c; Veerapaga *et al.*, 2020). These environmental forces are shaped by uncertainties; e.g., the frequency and intensity of storms and droughts are expected to change due to climate change (Knutson *et al.*, 2010; Lee

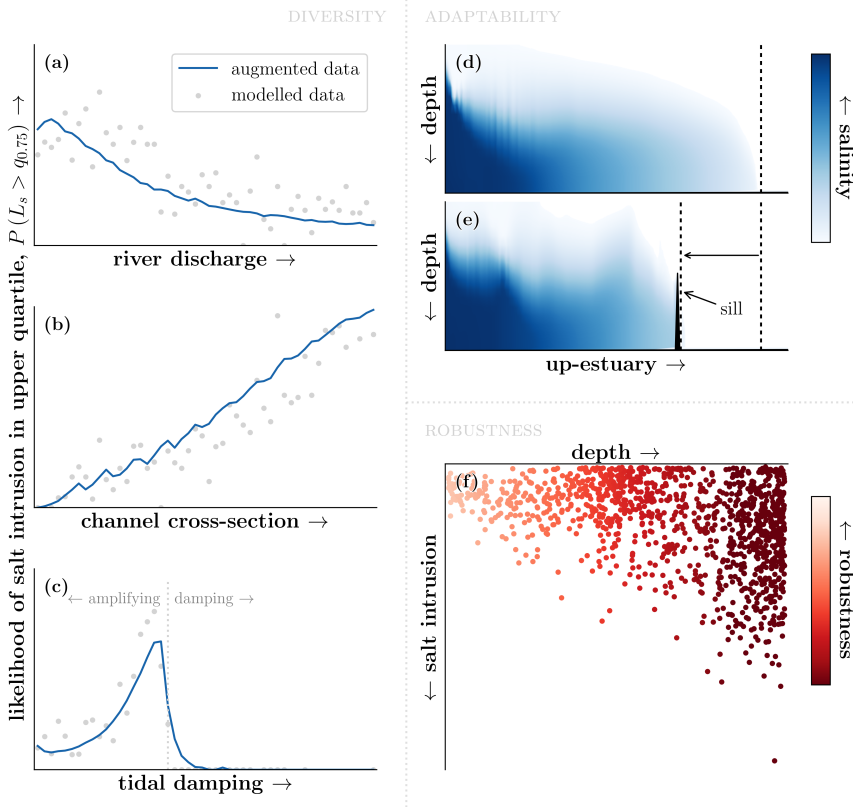


Figure 8.3: Conceptual implementation of the three axes of DARE on estuarine salt intrusion: (a–c) *diversity-axis*, likelihood of large salt intrusion length (upper 25%-quantile); (d,e) *adaptability-axis*, salt intrusion reduction due to placement of a temporary sill; (f) *robustness-axis*, salt intrusion variability as function of the water depth. (Data sources used: Hendrickx, 2022, 2023a; Hendrickx *et al.*, 2024a, see App. D for a description on the data processing for this figure.)

et al., 2024; Lowe & Gregory, 2005), which both have a significant influence on salt intrusion (Wegman *et al.*, *in review*; Yang & Zhang, 2024). In addition to these climatic uncertainties, (numerical) modelling of estuarine salt intrusion remains challenging (e.g., Fringer *et al.*, 2019), adding additional levels of uncertainty.

These sources of uncertainties—and other sources unmentioned and/or unknown—complicate the design of salt intrusion mitigation measures. Below we present how DARE can aid this engineering challenge considering the individual axes of DARE supported by data presented in Figure 8.3:

Diversity Figure 8.3a–c shows the likelihoods for substantial salt intrusion as function of three estuarine characteristics: river discharge, cross-sectional area, and tidal damping/amplification (Hendrickx *et al.*, 2023c). A low likelihood of salt intrusion can be achieved via different routes; aiming for a

multitude of them reduces the reliability on the efficacy of a single approach. Reflecting on Figure 8.3a–c, this means combining a large river discharge, small cross-section, and a damping or amplifying tidal signal. For example, maintaining a relatively small cross-section during high river discharges also ensures limited salt intrusion while experiencing droughts—i.e., during low discharge events.

Adaptability Figure 8.3d and e illustrate the effect of a sill in halting the salt wedge to propagate landward, i.e., reducing the salt intrusion. Here, a sill refers to a submerged dam made out of local sediments. Such a sill can be implemented as a temporary solution during (extremely) disadvantageous conditions—such as a drought (Fagerburg & Alexander, 1994; Johnson *et al.*, 1987)—, as it may cause a hindrance during “normal” conditions (Hendrickx *et al.*, 2024b). The implementation of a temporary sill during a drought is a perfect example of an adaptive contingency approach: In times of need, there is a plan of action ready to react to extreme conditions.

Robustness Figure 8.3f presents the salt intrusion as function of the water depth, where for lower depths the variability in the salt intrusion reduces due to which the estuary becomes more robust to environmental changes (Hendrickx *et al.*, 2023c). In other words, the salt intrusion is depth-limited. Note that in the case of estuarine salt intrusion, there is inherently a limit to the “performance” of zero salt intrusion. Therefore, it is impossible to attain an antifragile system (as proposed in Sec. 8.2.3).

As illustration of how DARE could translate to practice, let us consider a human-controlled delta such as the Ebro Delta (Spain; e.g., Alcaraz *et al.*, 2011; Ibáñez *et al.*, 2012), the Pearl River Delta (China; e.g., Yan *et al.*, 2016; Zhang *et al.*, 2012), or the Rhine-Meuse Delta (the Netherlands; e.g., Cox *et al.*, 2022; Ysebaert *et al.*, 2016). In such a system, the river discharge is somewhat controlled, enabling water managers to steer away from low discharge levels when possible (i.e., towards the right-hand side in Fig. 8.3a). However, droughts can make this goal unattainable, necessitating a diverse set of measures; e.g., enforcing a minimum channel depth. Setting a minimum channel depth adds a robust mitigation measure to the solution set (Fig. 8.3f). As there are generally limits to how shallow an estuary can be due to port accessibility demands, an adaptive measure can be included to construct a temporary sill during extreme conditions (Fig. 8.3d and e). The solution set can be further expanded by including other (robust) measures, such as placing water intakes farther away from the estuary mouth, and/or increase withdrawal/storage capacities of water intakes (Bakker *et al.*, *in review*; Hendrickx *et al.*, *in prep.* Chs. 6 and 7).

8.4 Implications

What does DARE mean for engineers in practice? Designing for extreme events—which are generally the leading design conditions—by means of a return period

is not future-proof. The concept of the “return period” is not only challenging to communicate, but it invalidly assumes climatic stationarity (Gründemann *et al.*, 2022; Knutson *et al.*, 2010; Milly *et al.*, 2008). In response, more complex, non-stationary statistical analyses to deal with an uncertain and changing climate have been developed (e.g., Méndez *et al.*, 2006; Radfar *et al.*, 2023; Ragno *et al.*, 2019). Instead of this focus on the input space, we propose that engineers shift in focus towards the output space: What are the desired regions in the output space—or solution space—and how can we achieve those? Following nature’s own approach and build like nature, we advocate DARE: diverse, adaptive, and robust engineering.

Acknowledgements. We would like to thank Peter Hendrickx for his editing suggestions on the early version of this work.

Author contributions. G.H., S.P., J.A., S.A. conceptualised the study; G.H. performed the study; G.H. made the visualisations; G.H., S.P. wrote the manuscript; and G.H., S.P., J.A., S.A. reviewed the manuscript.

Data availability. The datasets used in this study are publicly available: (1) the BEWARE-dataset (Bayesian Estimator for Wave Attack in Reef Environments; Pearson *et al.*, 2017a); (2) the dataset used in Mulla *et al.* (2024); (3) the NEESI-dataset (Numerical Experiments of Estuarine Salt Intrusion dataset; Hendrickx, 2023a); and (4) the dataset used in Hendrickx *et al.* (2024b).

Software availability. The implemented neural network is open-access and named ANNESI (Artificial Neural Network for Estuarine Salt Intrusion; Hendrickx, 2022).



CONCLUDING REMARKS

Nature-based solutions to mitigate salt intrusion.

It is a concise title entailing a multitude of fascinating aspects of active fields of research. It combines the multidisciplinary, system-oriented development of nature-based solutions with the highly non-linear character of salt intrusion in estuaries. Implicitly, the title calls for new assessment tools due to its multidisciplinary nature, and begs a critical reflection on nature-based solutions more generally.

Chapter 1 posed a few possible questions that may have arisen after reading the title. These—and many other—questions have been addressed in this dissertation. This chapter summarises the search undertaken for nature-based solutions to mitigate salt intrusion, and provides suggestions on how to continue on this topic.

9.1 Conclusions

The research objective of this dissertation implicitly asked: *Are there viable nature-based solutions to mitigate salt intrusion?* The short answer is “yes.” Where in the parameter space to search for these nature-based solutions has been explored

in Chapter 3. Therefore, Chapter 3 forms the backbone of this dissertation as well as any subsequent studies on the same topic.

The method as described in Chapter 2 enabled the execution of this extensive sensitivity analysis; the adaptive sampling approach aims to use the information available in the output space to inform the region of interest in the input space.

Three (nature-based) solutions have been addressed in detail: (1) placement of a temporary sill (Ch. 4); (2) reclamation or (re)introduction of intertidal areas (Ch. 5); and (3) reducing the water depth (Ch. 6). The latter is subsequently scrutinised to a multidisciplinary assessment, as part of the *evaluation*-phase (Pt. III). In addition to this socio-economic assessment, Chapter 7 includes the ecological perspective by which all three pillars of the *Building with Nature*-approach have been addressed.

At last, this dissertation contains a critical reflection on the concept of nature-based solutions, providing suggestions for a future-proof view on hydraulic engineering (Ch. 8).

9.1.1 Exploration

Explore the potential impact of estuary-scale modifications on salt intrusion.

As estuarine salt intrusion requires three-dimensional models, exploration is a computationally expensive exercise. Therefore, a novel sampling method has been introduced in Chapter 2; the use of statistical and machine learning techniques enabled us to cut computational costs by a factor of 1,250. The hybrid downscaling employed in this method puts enlightening sensitivity analyses within computational reach.

With the methodology as described in Chapter 2, the response of the estuarine salt intrusion to estuary-scale interventions is explored in Chapter 3. The extensive sensitivity analysis enabled a systematic cross-comparison of estuary-scale interventions. This resulted in a comprehensive overview of potential nature-based solutions. In Chapter 3, a ranking of estuary-scale modifications is presented based on the sensitivity of the salt intrusion to these modifications (Tab. 3.2, p. 57).

Most effective mitigation measures include the reduction of the conveyance cross-section and the increase in river discharge. Both the cross-sectional area and the river discharge determine the river flow velocity, which is the main driving force pushing the saline water out of the estuary. Therefore, it is reasonable that measures causing an increase in river flow have a profound effect on the estuarine salt intrusion, which can both be achieved via an increased river discharge and a reduced cross-sectional area—i.e., reduced depth and/or width.

Next are the modifications that impact the tidal signal; the tidal oscillatory movement introduces mixing in the estuary breaking up the stratification that promotes the estuarine circulation. Such modifications include changing the balance between bottom friction and width-convergence, as well as remodelling the intertidal area. Note, however, that tidal mixing reduces salt intrusion in a stratified estuary but may enhance salt intrusion in a well-mixed system (Ch. 5).

Other estuary-scale modifications included in the sensitivity analysis turn out to have at best a limited effect on the salt intrusion; these include varying the lateral depth in the channel or meandering of the estuary.

Due to the non-linear nature of estuarine salt intrusion, different measures are suitable under different circumstances. For example, Figure 3.8 (p. 50) shows the opposing effects of tidal damping on the salt intrusion: increasing the tidal damping in a tide-amplifying system enhances the salt intrusion, while in a damped system it reduces the salt intrusion. Thus, to determine which estuary-scale interventions are most promising under which conditions in mitigating estuarine salt intrusion, the extensive sensitivity analysis presented in Chapter 3 can be used as a starting point after which in-depth studies are required to further distil the efficacy of the measure in a given setting.

9.1.2 Conceptualisation

Conceptualise various nature-based solutions to mitigate salt intrusion.

Contrary to the general focus of most nature-based solutions, vegetation does not play a significant role in mitigating salt intrusion. This is reflected by the negligible effect of bottom friction on the intertidal flats on the salt intrusion (Ch. 3). Instead, system-oriented and estuary-scale modifications are key in the design and implementation of mitigation measures.

The findings of Chapter 3 prioritise which estuary-scale modifications are most promising in influencing the salt intrusion (Fig. 3.4 and Tab. 3.2, pp. 43 and 57). In general, there are two approaches to modifying the estuarine salt intrusion: (1) modify the forcing conditions; and/or (2) modify the estuarine geomorphology. Modification of the forcing conditions would generally be very effective; e.g., there is a very strong correlation between the river discharge and the salt intrusion length. However, this requires substantial infrastructural interventions often beyond the scope of feasibility—be it economically, physically, or environmentally—as well as sufficient upstream freshwater supply, which is generally the cause of (temporal) water shortages. Therefore, modifications to the morphology of the estuary constitutes a generally more feasible approach; e.g., modifying the cross-sectional area of the estuary has substantial effects on the salt intrusion.

The mitigation of estuarine salt intrusion can be achieved via two types of modification: (1) advection-based, whereby the landward advection of saline water is reduced; and (2) mixing-based, whereby the stratification-mixing balance is altered to limit salt intrusion. These two types are not exclusive, as any modification has implications in both.

Chapter 4 introduced a (temporary) sill to mitigate salt intrusion—a sill being a submerged dam. This mitigation measure aims to halt the advection of saline water in the lower part of the water column by means of an obstruction. In essence, the aim of the sill is to halt the saline bottom layer to move landward due to estuarine circulation. For strongly stratified systems with a minor tidal component, the salt wedge is clearly halted by the sill (Fig. 4.3, p. 69). However, the sill becomes less effective in mitigating salt intrusion for increasing tidal influence.

Chapter 5 showcases how the (re)introduction of intertidal areas modifies the salt intrusion. This estuary-scale modification alters the salt intrusion by affecting the balance between stratification and mixing. This balance is expressed by the Simpson number (Eq. 5.9, p. 89), which determines whether intertidal areas enhance or reduce the salt intrusion. Thus, the effect of increasing (or reducing) the mixing in an estuary is dictated by the current stratification-mixing balance in the estuary—i.e., the Simpson number.

The modification of the water depth—as discussed in Chapter 6—mainly addresses the squeezing of the cross-sectional area due to which the river flow increases (for the same discharge). In other words, the seaward advection of salinity increases with decreasing depth. However, modifying the water depth also changes the stratification-mixing balance: the balance moves in favour of the mixing. From a physical perspective, the strong correlation between the water depth and salt intrusion has long been known (see Ch. 3 for an overview). However, from a multidisciplinary perspective, reducing the water depth to mitigate salt intrusion worsens port accessibility; hence, there is an economic incentive to deepen estuaries. Because the estuarine water depth is generally an economic decision, Chapter 6 is encapsulated in the *evaluation*-phase (i.e., Pt. III).

9.1.3 Evaluation

Evaluate nature-based solutions in a multidisciplinary context.

The evaluation of nature-based solutions requires a multidisciplinary approach. This multidisciplinary nature results in multi-unitary comparisons, which complicate matters by comparing apples to oranges. However, systematically determining the consequences of interventions for multiple stakeholders allows the definition of trade-off curves (Chs. 6 and 7). Such trade-off curves do not aim to decide what the best solution is; the goal of such a curve is to visualise the benefits and drawbacks of interventions for all included stakeholders. The multi-unitary comparison would often be simplified by expressing all quantities in monetary units. This would, however, require (many) additional assumptions—which are potentially politically laden—and remove the nature of the trade-offs at play.

Chapter 6 addressed the trade-off between port logistics and accessibility versus freshwater availability during a severe drought—namely the summer of 2022 in the Netherlands. The case study presented in Chapter 6 included the Port of Rotterdam and four water boards in the Rhine-Meuse Delta. In this study, we focused on the maintained bed level of the estuary because of its opposing effects on the chosen stakeholders: Increased water depth is beneficial for port logistics, as larger, more efficient vessels can enter; however, this comes at the cost of increased salt intrusion, which hampers freshwater availability. These stakeholders have been reflected by two performance indicators based on (1) vessel waiting time for the port performance; and (2) freshwater shortages for the water intake performance. Analysis of these indicators by means of a Pareto-front puts the most recent deepening of the New Waterway into question, as the benefits for port accessibility are limited while the freshwater availability is further threatened.

In Chapter 7, another trade-off has been addressed, namely between ecological diversity and freshwater availability. Here, we focused on the closed-off Haringvliet in the Rhine-Meuse Delta, from which the Hollandse Delta water board extracts its freshwater. Since the (partial) closure of the Haringvliet as part of the Delta Works, this former estuary has become a freshwater lake. However, the ecological costs of this closure are high, due to which (partially) reopening the Haringvliet sluices is currently considered—the so-called “Kierbesluit” (*trans.*: “Ajar policy”). Chapter 7 presents a methodology to quantify the ecological impact of various interventions based on hydrodynamic model simulations. This is achieved by generating ecotope maps using EMMA (Ecotope-Map Maker based on Abiotics), which are subsequently used to determine the ecotope-diversity and generate ecotope bar-codes of the area of interest. The freshwater availability has been assessed similarly as in Chapter 6, i.e., based on freshwater shortages.

Although Chapters 6 and 7 both present two-dimensional trade-offs, the assessments methods can be scaled-up to multi-dimensional trade-offs. Key is that the dimensions are expressed by representative performance indicators, which are generally based on non-monetary units.

9.1.4 Reflection

Reflect on the role of nature-based solutions with future uncertainties.

The reflection on the role of nature-based solutions in light of future uncertainties—a result of the rapidly changing climate and socio-economics in general—requires a rethinking of the concept “nature-based solutions.” As nature-based solutions intend to draw solutions from natural processes, Chapter 8 argues to get inspiration from how natural systems deal with changing climates. Instead of focusing on meeting predetermined goals, natural systems survive—and thrive—due to diversity in species accustomed to various conditions. Every one of these species adapts to changes in the environment in a (slightly) different manner. Simultaneously, natural systems are robust to changes in the environment occurring on short time scales, and can even benefit from regular non-destructive stresses.

Along the lines of biomimicry, Chapter 8 proposes an (engineering) design philosophy based on nature’s own approach in dealing with (unknown) uncertainties: diverse, adaptive, and robust engineering (DARE). With DARE, the three dimensions of engineering challenges are translated to three axes in the solution space to better address the uncertainties related to them: (1) the forcing dimension to the *diversity*-axis; (2) the time dimension to the *adaptability*-axis; and (3) the performance dimension to the *robustness*-axis. Essentially, DARE is shifting the focus from the input space to the output space: What regions in the output space—or solution space—are desirable, and how to get there?

9.2 Advancements

This dissertation has provided advancements in both fields of research that it brings together: (1) *Building with Nature*, and (2) estuarine salt dynamics. In addition, the merging of these fields of research in itself is also a scientific—as well as a practical—advancement.

9.2.1 From output to input

The first step in the *Building with Nature*-approach is to understand the system (e.g., de Vriend *et al.*, 2015; van Koningsveld & Mulder, 2004; van Slobbe *et al.*, 2013). Chapter 2 advocates for the use of sensitivity analyses to increase this system understanding, and provides an adaptive approach in doing so. A focus on the variability in the output is more relevant for understanding the system at hand. Such an exploration of the output space—instead of exploring the input space—provides valuable insights into the reach of possibilities.

The sensitivity of the output to the input is also key in developing nature-based solutions: the *robustness*-axis of DARE (diverse, adaptive, and robust engineering; Ch. 8) is a direct derivation of the variation in the output space (App. D).

9.2.2 Salt intrusion modifiers

Estuarine salt intrusion is the result of the non-linear interplay between forcing conditions, largely influenced by the playground set by the estuarine morphology. Certain estuary-scale parameters have long been known to be of substantial influence on the salt intrusion—e.g., the water depth (e.g., Hansen & Rattray Jr., 1965). Over the decades that followed, additional relevant parameters have been investigated—e.g., intertidal area (e.g., Geyer *et al.*, 2020; Lyu & Zhu, 2019; Zhou *et al.*, 2020a). However, a cross-comparison of all these different factors was missing.

Chapter 3 provides such a cross-comparison for the influence of estuary-scale parameters on salt intrusion. The extensive sensitivity analysis executed confirms the dominance of the water depth and river discharge on the salt intrusion length. Some other parameters are shown to be of limited—or no—influence on the salt intrusion, which enabled us to rank the measures based on their effectiveness in mitigating estuarine salt intrusion (Tab. 3.2, p. 57). Therefore, the findings presented in Chapter 3 should be considered as a starting point for further research (Sec. 9.5), steered by Table 3.2 (p. 57).

Further investigations of a selected set of nature-based solutions—as presented in Chapters 4 and 5 and Section 9.5—show the relevance of system understanding on the salt intrusion mitigation ability of implementations. Most importantly, the same measure might reduce or enhance the salt intrusion based on (1) its implementation—e.g., the distance between the sill and the estuarine mouth (Ch. 4)—, and (2) the estuary—e.g., intertidal areas promote salt intrusion in well-mixed estuaries but reduce the intrusion for partially mixed and salt wedge estuaries

(Ch. 5). Note that not all mitigation measures have such a dual response: reducing the water depth will only reduce the salt intrusion (Ch. 6).

9.2.3 Multidisciplinary assessment

Chapters 6 and 7 present multidisciplinary assessment methods. Both methods promote and propose non-monetary evaluation metrics, supporting sustainable future policy-trajectories (IPBES, 2022; Pörtner *et al.*, 2023). These assessments are based on performance indicators per stakeholder (in line with de Vries *et al.*, 2021; van Koningsveld & Mulder, 2004), where we applied a novel port logistics model (OpenTNSim; Bakker & van Koningsveld, 2023, in Ch. 6), and a newly developed ecotope potential model (EMMA; Brunink & Hendrickx, 2024, in Ch. 7). Both these models build on hydrodynamic model data, which has also been used to determine the freshwater shortages in both Chapters 6 and 7. This enables the exploration of the multidisciplinary impacts of various interventions, as has been done in Chapters 6 and 7.

With the assessment methods presented in Chapters 6 and 7, all three components of the *Building with Nature*-approach can be included in decision- and policy-making: physics, ecology, and socio-economy (van Slobbe *et al.*, 2013). Especially a quantitative assessment method for ecological implications of interventions was missing, or fully focused on economic ecosystem services (e.g., Barbier *et al.*, 2011; Granek *et al.*, 2010; Heimhuber *et al.*, 2024; Liquete *et al.*, 2013; Worm *et al.*, 2006). However, the focus on the potential occurrence of ecotopes and subsequent translation to ecotope-diversity—i.e., diversity at the landscape level—functions as an indicator of the resilience of the (estuarine) ecosystem (e.g., Elmqvist *et al.*, 2003; Folke *et al.*, 2002; Limberger *et al.*, 2023; Loreau *et al.*, 2001; Loreau *et al.*, 2003; Vasiliev, 2022; Yachi & Loreau, 1999).

Thus, Chapters 6 and 7 propose—and provide proof of concept of—the use of non-monetary performance indicators for decision- and policy-making.

9.2.4 Building like nature

The *Building with Nature*-approach (e.g., de Vriend *et al.*, 2015) and similar design approaches (e.g., *Engineering with Nature*; Bridges *et al.*, 2018) aim to develop nature-based solutions. Although nature-based solutions have adopted many definitions (e.g., Hanson *et al.*, 2020; Seddon *et al.*, 2021), all include the inclusion of nature into engineering challenges and co-develop natural development (e.g., de Vriend *et al.*, 2015; Herrmann-Pillath *et al.*, 2022; Temmerman *et al.*, 2023). These developments have brought engineers from “fighting against nature” to “building with nature” (and alike; van Slobbe *et al.*, 2013).

In Chapter 8, the next step for (hydraulic) engineers is proposed: “building like nature.” Instead of focusing on better predictions—an idealistic approach (Dessai *et al.*, 2009)—we propose to focus on reducing our reliability on such predictions. Chapter 8 introduces the concept of DARE: diverse, adaptive, and robust engineering. DARE describes an engineering approach based on nature’s own approach in dealing with (unknown) uncertainties: (1) a diverse solution set

deals with the uncertainty in forcing conditions; (2) an adaptive approach tackles uncertainties along the temporal dimension; and (3) a robust solution limits the uncertainty of its performance.

9.3 Outcomes

This section provides an overview on how this dissertation influenced—or will influence—academic developments, practical applications, and societal challenges. This includes concrete translations from the research findings to follow-up studies and implementations as well as undertaken efforts to facilitate the uptake of these findings.

9.3.1 Implementations

The hybrid downscaling as described in Chapter 2 has proven effective in reducing computational costs. This has resulted in interest in the method (e.g., Wu & Wan, 2024) and how it can be applied on other topics. An example is the exploration of compound flooding in Charleston (SC, USA) in which this approach has been applied to gain insights into the non-linear interactions of the multivariate flooding drivers on flood damage (Terlinden-Ruhl *et al.*, *in review*).

The sensitivity analysis enabled by Chapter 2—i.e., Chapter 3—has been an inspiration for further research on the effects of various modifications of the estuary on the salt intrusion. Examples other than chapters in this dissertation include the effects of sand waves (Geerts *et al.*, *in review*), intertidal flats (Siemes *et al.*, *in review*), freshwater pulses (Huismans *et al.*, 2024), width-convergence (Martín-Llanes & López-Ruiz, 2024), and tidal damping (Zhong *et al.*, 2024). In addition, this extensive sensitivity analysis has informed *in-situ* studies as well, such as in Vietnam (Pham *et al.*, 2024), and Chile (Soto-Rivas *et al.*, 2024).

Furthermore, the sensitivity analysis provides a starting point for policy- and decision-makers tasked with assessing the implications of estuarine modifications. In combination with the evaluation of trade-offs as presented in Chapters 6 and 7 in which socio-economic and -ecological assessment tools are used (Bakker & van Koningsveld, 2023; Brunink & Hendrickx, 2024), the findings of this dissertation support policy- and decision-makers concerned with estuarine salt intrusion.

9.3.2 Open science

Everything that has been created as part of this research project has been made openly accessible, in line with the FAIR data principles (Wilkinson *et al.*, 2016). Considerable amounts of model simulations have been executed as part of this dissertation and all their input files have been shared via online repositories (Hendrickx, 2023a; Hendrickx & Pearson, 2024a; Hendrickx *et al.*, 2024a). The NEESI-dataset that supports Chapters 2, 3 and 8 also includes the core post-processed data (Hendrickx, 2023a). In addition, the trained neural network as used in Chapters 2, 3 and 8 is published as ANNESI (Hendrickx, 2022). To enhance

the accessibility of ANNESI, it has been coupled to a web-API: <https://annesi-web.netlify.app>.

The post-processing toolbox EMMA that has been developed by Brunink and Hendrickx (2024)—and which has been used in Chapter 7—is also freely accessible (Hendrickx & Brunink, 2023). We have put great effort in making EMMA as user-friendly as possible, and by making it open access, we invite others to contribute.

Also other developed modules are openly accessible, such as processing code for the salt flux decomposition as used in Chapters 4 and 5 (Hendrickx, 2023b). An overview of all developed modules as part of this dissertation have been collected on a dedicated GitHub-repository: <https://github.com/ghendrickx/SALTI Solutions>.

At last, all chapters in this dissertation that have also been published as papers—or are still in the review process—are freely and openly accessible (upon publication). This also holds for this dissertation itself.

9.4 Impact

As the previous sections have shown, the potential impact of this dissertation is twofold: (1) scientific, and (2) societal.

The potential scientific impact derives from the multiple scientific contributions that are collectively the main body of this dissertation—i.e., Chapters 2 to 8. In addition, parts of this dissertation have informed subsequent studies of which examples are presented in Section 9.3.1. Especially Chapter 3 has shown to be useful to the scientific community due to its cross-comparison of estuarine boundary conditions and morphological features and their impact on the salt intrusion length.

The potential societal impact mainly relates to Chapters 3 to 6, which present concrete salt intrusion mitigation measures. These suggested measures have informed Rijkswaterstaat—the governmental body responsible for the Dutch primary infrastructure—as well as others working on the topic of salt intrusion (e.g., Deltares). Further potential societal impact follows from contributions to ongoing debates regarding the Dutch vision on her relation with water. Chapter 6 questioned the general tendency to enhance water depths in port areas, and even considered doing the opposite—i.e., shallowing. Chapter 7 stepped in on the debate that inspired the “Kierbesluit” (*trans.*: “Ajar policy”) by providing a quantitative method for a socio-ecological assessment. At last, Chapter 8 provided a way forward for (hydraulic) engineers—and non-engineers alike—to think differently about (Knightian) uncertainty: less focus on predicting the unpredictable, and more focus on resilience towards “the unknown.”

9.5 Outlook

This dissertation includes the conceptualisation of three (nature-based) solutions to mitigate salt intrusion: (1) a (temporary) sill (Ch. 4); (2) enhancement of intertidal area (Ch. 5); and (3) reducing the water depth (Ch. 6). However, this

list is not exhaustive. For example, Chapter 3 concludes with a longer list of potential (nature-based) solutions (Tab. 3.2, p. 57). This section provides recommendations for potential nature-based solutions to mitigate salt intrusion, and proposes research questions reflecting these recommendations for future studies. These recommendations include opportunities not touched upon in detail earlier in this dissertation.

9.5.1 Discharge management

The strong correlation between the river discharge and the estuarine salt intrusion is apparent from Figure 3.4 (p. 43), and has also been analysed extensively in literature (e.g., Geyer & MacCready, 2014; Lee *et al.*, 2024; Monismith *et al.*, 2002; Ralston & Geyer, 2019; Savenije, 1993). This makes droughts also threatening for freshwater availability, as in addition to the reduced supply of freshwater, the available freshwater is simultaneously contaminated by intruding saline water.

However, the salt intrusion length does not respond similarly to an increase versus a decrease in river discharge (e.g., Biemond *et al.*, 2022; Chen, 2015; Gong & Shen, 2011; Hetland & Geyer, 2004; Kranenburg, 1986; MacCready, 1999; Monismith, 2017): The estuary responds faster to an increase in river discharge compared to a decrease. This asymmetric response forms the backbone of a potential salt intrusion mitigation measure that can be applied in intensely controlled systems, such as the Rhine-Meuse Delta (e.g., Cox *et al.*, 2021; Ysebaert *et al.*, 2016), the Pearl River Delta (e.g., Yan *et al.*, 2016; Zhang *et al.*, 2012), and the Ebro River (e.g., Alcaraz *et al.*, 2011; Ibáñez *et al.*, 2012). However, how this asymmetric response can be used to reduce salt intrusion remains an open question:

How can the river discharge signal be modified such that the salt intrusion is reduced with the same average river discharge?

Although Monismith (2017) concluded based on a simplified model that this asymmetric response cannot be exploited to reduce salt intrusion—it is even more likely to enhance salt intrusion—, exploratory model simulations with a 3D hydrodynamic model show a more nuanced story (App. E). Therefore, further developing our understanding on how salt intrusion responds to changes in river discharge might result in drought-management plans for discharge-controlled systems.

9.5.2 Tidal mixing energy

In Chapter 3, the tidal range on itself did not stand out as a key characteristic determining the estuarine salt intrusion length (Fig. 3.4, p. 43). However, when presented as the tidal damping—or amplification—as in Figure 3.8 (p. 50), the dual influence of the tide becomes apparent: both tidal damping and amplification reduce the salt intrusion length.

This dual influence of the tide has also been shown in estuaries around the world by means of different responses of the salt intrusion to the spring-neap fluctuations. In some estuaries, the salt intrusion reduces during spring tide—i.e., increased tidal

range—together with a reduced stratification. Examples of this response include Delaware Bay (NJ, USA; Geyer *et al.*, 2020), Hudson estuary (NY, USA; Lerczak *et al.*, 2009; Wang *et al.*, 2017), Johor Estuary (Malaysia; Hasan *et al.*, 2013), and Madoamen Estuary (China; Gong & Shen, 2011). In other estuaries, the salt intrusion increases during spring tide—i.e., showing the opposite response to changes in tidal range. Examples showing this response include Changjiang River (China; Xue *et al.*, 2009), and Maipo River (Chile; Soto-Rivas *et al.*, 2024).

A similar dual response in salt intrusion has been found as a result of modifying the intertidal area (Ch. 5). This similarity in response is motivated by the enhanced mixing induced by both an increased tidal range and enhanced intertidal area. Appendix F hypothesises that a regime shift based on the stratification-mixing balance is at play; as in Chapter 5, such a regime change is expected to be marked by the Simpson number (Eq. 5.9, p. 89).

As estuary-scale interventions are bound to modify the tidal signal, such modifications will have implications on the salt intrusion as well. For example, reducing the width-convergence due to port development in a tide-amplifying estuary is expected to enhance the salt intrusion (Fig. 3.8, p. 50). If this increased salt intrusion is indeed the result of reduced vertical mixing—as hypothesised in Appendix F—, countermeasures could focus on reintroducing the vertical mixing to limit the salt intrusion.

How does the stratification-mixing balance influence the effect of the tide on salt intrusion?

Note that the above question implicitly assumes that the stratification-mixing balance has a (significant) effect on how the tidal signal affects the salt intrusion.

9.5.3 Estuarine meandering

Although Chapter 3 shows no correlation between the meandering of the estuary and the salt intrusion (Fig. 3.10, p. 53), there are suggestions in literature that state the difference: e.g., Pein *et al.* (2018) presented a reduction in salt intrusion due to the introduction of local meanders, and Bo and Ralston (2022) also found a minimal reduction in salt intrusion by introducing sharp bends—no influence was found for smooth bends. However, the definition of the salt intrusion used by Pein *et al.* (2018) is unclear, and might have influenced their conclusions (Sec. 3.5.2.3, p. 52): it is not fully clear from Pein *et al.* (2018) whether they defined the salt intrusion length along the meandering thalweg of the estuary, or if they projected it on the axis perpendicular to the coastline. Nevertheless, Bo and Ralston (2022) showed a very small reduction in salt intrusion due to the introduction of (sharp) bends. However, the NEESI-dataset (i.e., Ch. 3) consists of mainly (very) smooth bends (not shown).

Thus the potential of meanders as salt intrusion mitigation measure remains an open-end; or stated differently, the potential increase in salt intrusion due to the removal of meanders, e.g., by straightening the estuary for navigability. The findings by Bo and Ralston (2022) and Pein *et al.* (2018) as well as Chapter 3

are not conclusive, but they open the door for further analyses on the effect of meanders on estuarine salt intrusion:

How can meanders in an estuary reduce the salt intrusion length?

Note that the above question implicitly asks whether meanders can (significantly) reduce the estuarine salt intrusion, which is by no means trivial (as previous studies have shown: Bo & Ralston, 2022; Pein *et al.*, 2018, as well as Ch. 3).

9.5.4 Tidal phase difference

Estuaries with side channels are prone to enhanced salt intrusion in the main channel due to a phenomenon called “tidal trapping” (e.g., Garcia *et al.*, 2022; MacVean & Stacey, 2011; Okubo, 1973; Schijf & Schönfléd, 1953). This mechanism is also related to the enhanced salt intrusion due to intertidal areas (Dronkers, 1978; Schijf & Schönfléd, 1953)—at least for well-mixed estuaries (Ch. 5).

Tidal phase differences occurring at the junction influence the salinity pattern in both the main and the side channels (e.g., Garcia *et al.*, 2022; Warner *et al.*, 2002; Wegman *et al.*, *in review*). This can even result in the side channel remaining fresh despite saline water passing by its mouth (Laan *et al.*, 2023; Wegman *et al.*, *in review*). Such behaviour is interesting in face of freshwater availability, and it has sparked a preliminary study (de Wilde, 2024); this study investigated the effects of the geometries of the main and side channels on the tidal phase difference.

Data has shown that the tidal phase difference between the main and side channels can keep the side channel (largely) fresh (Laan *et al.*, 2023; Wegman *et al.*, *in review*). However, the interplay of the main and side channels and how this influences the salinity patterns in both remains an open question:

How can the tidal phase difference between main and side channel minimise the salt intrusion in the side channel?

Sections 9.5.1 to 9.5.4 provide technical, physics-based suggestions on potential nature-based solutions to mitigate salt intrusion. However, as this dissertation has shown, the non-technical perspectives are just as relevant. The non-monetary assessments of Chapters 6 and 7 promote a different approach for decision- and policy-making, in which the relevant trade-offs present take centre stage. Subsequently, the DARE-concept presented in Chapter 8—which proposes a new paradigm of *building like nature*—is only the start of a debate on how engineers should approach societal needs. Therefore, this dissertation facilitates a more holistic discussion on the bigger picture of engineering and decision- and policy-making, pointing the way to more diverse, adaptive, and robust solutions for the challenges that lie ahead in an uncertain future.

EPILOGUE

This dissertation addressed nature-based solutions to mitigate salt intrusion. This is an increasingly relevant topic with growth of coastal communities due to economic opportunities in these regions (Maul & Duedall, 2019; Neumann *et al.*, 2015), where salt intrusion poses a significant threat to the freshwater availability of these coastal communities (Costall *et al.*, 2018; Wada *et al.*, 2011). In addition to the growing coastal communities, the climate is changing in unfavourable directions regarding freshwater availability: sea level rise as well as increased drought frequency and duration promote increased salt intrusion (e.g., Jones *et al.*, 2024; Lee *et al.*, 2024; Yang & Zhang, 2024). Mitigating salt intrusion can relieve part of the pressure on the freshwater reserves.

However, only focusing on mitigation of salt intrusion from a physical perspective is insufficient. There is only so much that can be done to mitigate salt intrusion before it collides with the interests of other stakeholders, as extensively covered in Chapters 6 and 7. Instead, a diverse set of approaches should be considered—in line with the *diversity*-axis of DARE (Ch. 8).

Note that this does not mean that salt intrusion mitigation cannot be useful in securing freshwater availability; there are, however, other complementary options available as well. Chapters 6 and 7 already implicitly or explicitly touched upon these options, which include—but are not limited to—(1) enlarging fresh-

water reserves from which can be drawn during times of need, such as a drought; (2) reducing freshwater demands (during a drought), e.g., by not cultivating salt-sensitive crops in (or near) coastal regions; and (3) moving water extraction points away from water bodies susceptible to salt contamination. These options—in combination with mitigation measures listed in this dissertation—provide a robust way forward regarding freshwater availability now and for generations to come.

However relevant and important, the aforementioned approaches to secure freshwater availability do not address the elephant in the room: The increasing strains on freshwater availability—i.e., increasing water stress—are the result of (anthropogenic) climate change (e.g., Jones *et al.*, 2024; Lee *et al.*, 2024)—next to the growing human population. Both these pressing developments are largely driven by economic growth.

This same economic growth is the main determinant on which decisions and policies are made, wherein more economic growth is regarded as a good thing—or even considered the sole goal. In doing so, decision- and policy-makers heavily rely on economic growth projections, which generally use Integrated Assessment Models (IAMs) such as the popular DICE (Dynamic Integrated model of Climate and the Economy; Nordhaus, 2018, for the latest version). In studies implementing DICE and similar models, the “optimal strategy” follows from economic optimisation alone—i.e., which strategy has the lowest monetary costs. Although earlier studies using DICE concluded an “optimal” global warming of 3–3.5°C by 2100 (Nordhaus, 1992), others have concluded recently that the well-below 2°C limit of the Paris Agreement “passes the cost-benefit test” (e.g., Glanemann *et al.*, 2020; Kotz *et al.*, 2024; Moore & Diaz, 2015; Yumashev *et al.*, 2019, of which some also use DICE).

On the other hand, economists using DICE and similar models have also concluded that (1) economic damages for 6°C global warming by 2100 would only be 1.4% of GDP (Dietz *et al.*, 2021); (2) the loss of the Atlantic Meridional Overturning Circulation (AMOC) would be economically beneficial (Anthoff *et al.*, 2016); (3) the disintegration of the Greenland ice sheet will have virtually no impact on The Economy (Nordhaus, 2019); and (4) the optimal strategy co-occurs with a high likelihood of disintegration of the West-Antarctic ice sheet (approx. 70%; Diaz & Keller, 2016).

Besides the questionable physical (and economic) soundness of such climate-economy assessments (e.g., Keen *et al.*, 2022; Pindyck, 2017), the wide spreading in the results and subsequent conclusions disfavours the use of such global, climate-economy IAMs (Keen, 2021). Essentially, these models are able to produce almost any result one desires (Pindyck, 2017) due to which they cannot be qualified as “useful” models (Box, 1976, 1979).

With the economic side of the story generally untested and unvalidated (Millner & McDermott, 2016), it would make sense to focus on the biophysical realm. This is not to say that all is known in climate—and other biophysical—models, but they have been tested and validated against real-world data and are grounded in the laws of physics. Thereby, climate models have proven their “usefulness.”

According to such climate models, every 0.1°C of global warming puts the Earth closer to its climate tipping points (Lenton *et al.*, 2019; Rockström *et al.*,

2023), which have the potential to put the Earth on a “Hothouse Earth” pathway with temperatures increasing irreversibly 4–5°C compared to pre-industrial levels (Steffen *et al.*, 2018). With economic growth considered the most important driver of climate change (e.g., Millner & McDermott, 2016) and threat to one of life’s most essential resources (i.e., [fresh]water; Alcamo *et al.*, 2007; Distefano & Kelly, 2017), economic growth as the “holy grail” for decision- and policy-makers is worth reconsidering.

This leaves the question whether it would be possible to inform decision- and policy-making using non-monetary instead of monetary units, and focus on the boundaries of the environmental system at hand? The approach advocated for in Chapters 6 to 8: Chapters 6 and 7 presented the trade-offs associated with estuary-scale interventions without the need of monetary units; and Chapter 8 advocates for *Building like Nature* (Sec. 9.2.4) in which the natural system and its physical boundaries form the basis.

Recent developments in spatial planning in the Netherlands show that such an approach is possible with the adopted policy “water en bodem sturend” (*trans.*: “guided by water and soil”; Baptist *et al.*, 2019; Ministry of Infrastructure and Water Management, 2022). This policy states that we should start from the environmental system at hand and determine its possibilities, instead of stating (unrealistic) desires that are subsequently enforced on an environmental system.

Thus, instead of making (important) decisions and policies solely on economic grounds, what if we set monetary units aside as decisive metrics for decision- and policy-making and focus on the possibilities within the boundaries of the environment instead? What if we stopped “optimising” in an environment that we cannot even model correctly? What if we DARE to proactively react to unknown uncertainties?

*When the money ain't the means
but the means is the money.
You start to compromise ideals
for dollars, morals, get bloody.*

Ren

REFERENCES

- Abadie, L. M., Galarraga, I., & de Murieta, E. S. (2017). Understanding risks in the light of uncertainty: low-probability, high-impact coastal events in cities. *Environmental Research Letters*, *12*(1), 014017. <https://doi.org/10.1088/1748-9326/aa5254>
- Abbott, B. N., Wallace, J., Nicholas, D. M., Karim, F., & Waltham, N. J. (2020). Bund removal to re-establish tidal flow, remove aquatic weeds and restore coastal wetland services—North Queensland, Australia. *PLOS ONE*, *15*(1), e0217531. <https://doi.org/10.1371/journal.pone.0217531>
- Adger, W. N., Hughes, T. P., Folke, C., Carpenter, S. R., & Rockström, J. (2005). Socio-ecological resilience to coastal disasters. *Science*, *309*(5737), 1036–1039. <https://doi.org/10.1126/science.1112122>
- Ainsworth, T. D., Heron, S. F., Ortiz, J. C., Mumby, P. J., Grech, A., Ogawa, D., Eakin, C. M., & Leggat, W. (2016). Climate change disables coral bleaching protection on the Great Barrier Reef. *Science*, *352*(6283), 338–342. <https://doi.org/10.1126/science.aac7125>
- Alcamo, J., Flörke, M., & Märker, M. (2007). Future long-term changes in global water resources driven by socio-economic and climatic changes. *Hydrological Sciences Journal*, *52*(2), 247–275. <https://doi.org/10.1623/hysj.52.2.247>
- Alcaraz, C., Caiola, N., & Ibáñez, C. (2011). Bioaccumulation of pollutants in the zebra mussel from hazardous industrial waste and evaluation of spatial distribution using GAMS. *Science of The Total Environment*, *409*(5), 898–904. <https://doi.org/10.1016/j.scitotenv.2010.11.015>
- Almar, R., Ranasinghe, R., Bergsma, E. W. J., Diaz, H., Melet, A., Papa, F., Vousdoukas, M., Athanasiou, P., Dada, O., Almeida, L. P., & Kestenare, E. (2021). A global analysis of extreme coastal water levels with implications for potential coastal overtopping. *Nature Communications*, *12*(1), 3775. <https://doi.org/10.1038/s41467-021-24008-9>

- Almaz, O. A., & Altiok, T. (2012). Simulation modeling of the vessel traffic in Delaware River: Impact of deepening on port performance. *Simulation Modelling Practice and Theory*, 22, 146–165. <https://doi.org/10.1016/j.simpat.2011.12.004>
- Anderson, D., Ruggiero, P., Antolínez, J. A. A., Méndez, F. J., & Allan, J. (2018). A climate index optimized for longshore sediment transport reveals interannual and multidecadal littoral cell rotations. *Journal of Geophysical Research: Earth Surface*, 123(8), 1958–1981. <https://doi.org/10.1029/2018JF004689>
- Anthoff, D., Estrada, F., & Tol, R. S. J. (2016). Shutting down the thermohaline circulation. *American Economic Review*, 106(5), 602–606. <https://doi.org/10.1257/aer.p20161102>
- Antolínez, J. A. A., Méndez, F. J., Anderson, D., Ruggiero, P., & Kaminsky, G. M. (2019). Predicting climate-driven coastlines with a simple and efficient multiscale model. *Journal of Geophysical Research: Earth Surface*, 124(6), 1596–1624. <https://doi.org/10.1029/2018JF004790>
- Antolínez, J. A. A., Méndez, F. J., Camus, P., Vitousek, S., Gonzales, E. M., Ruggiero, P., & Barnard, P. (2016). A multiscale climate emulator for long-term morphodynamics (MUSCLE-morpho). *Journal of Geophysical Research: Oceans*, 121, 775–791. <https://doi.org/10.1002/2015JC011107>
- Antolínez, J. A. A., Murray, A. B., Méndez, F. J., Moore, L. J., Farley, G., & Wood, J. (2018). Downscaling changing coastlines in a changing climate: The hybrid approach. *Journal of Geophysical Research: Earth Surface*, 123(2), 229–251. <https://doi.org/10.1002/2017JF004367>
- Arens, S. M., Mulder, J. P. M., Slings, Q. L., Geelen, L. H. W. T., & Damsma, P. (2013). Dynamic dune management, integrating objectives of nature development and coastal safety: Examples from the Netherlands. *Geomorphology*, 199, 205–213. <https://doi.org/10.1016/j.geomorph.2012.10.034>
- Ashton, A., Murray, A. B., & Arnault, O. (2001). Formation of coastline features by large-scale instabilities induced by high-angle waves. *Nature*, 414(6861), 296–300. <https://doi.org/10.1038/35104541>
- Athanasiou, P., van Dongeren, A. R., Giardino, A., Vousdoukas, M., Antolínez, J. A. A., & Ranasinghe, R. (2021). A clustering approach for predicting dune morphodynamic response to storms using typological coastal profiles: A case study at the Dutch coast. *Frontiers in Marine Science*, 8(September), 1–20. <https://doi.org/10.3389/fmars.2021.747754>
- Athanasiou, P., van Dongeren, A. R., Giardino, A., Vousdoukas, M., Antolínez, J. A. A., & Ranasinghe, R. (2022). Estimating dune erosion at the regional scale using a meta-model based on neural networks. *Natural Hazards and Earth System Sciences*, 22(12), 3897–3915. <https://doi.org/10.5194/nhess-22-3897-2022>
- Baas, V., Clabbers, N., Moens, J., Schuurke, E., Spierings, J., Termaat, E., & Wolma, A. (2020). *Opening of the Haringvliet: A stream of possibilities* (tech. rep.). Wageningen University, Wageningen, the Netherlands.
- Bakker, F. P., & van Koningsveld, M. (2023, September). Optimizing bed levels in ports based on port accessibility. In D. Cox (Ed.), *Coastal engineering proceedings* (papers.62). <https://doi.org/10.9753/icce.v37.papers.62>
- Bakker, F. P., Hendrickx, G. G., Keyzer, L. M., Iglesias, S. R., Aarninkhof, S. G. J., & van Koningsveld, M. (in review). Trading off dissimilar stakeholder interests: Changing the bed level of the main shipping channel of the rhine-meuse delta while considering freshwater availability. *Environmental Challenges*.
- Bakker, F. P., van der Werff, S., Baart, F., Kirichek, A., de Jong, S., & van Koningsveld, M. (2024). Port accessibility depends on cascading interactions between fleets, policies, infrastructure, and hydrodynamics. *Journal of Marine Science and Engineering*, 12(6), 1006. <https://doi.org/10.3390/jmse12061006>
- Bakker, T. M., Antolínez, J. A. A., Leijnse, T. W. B., Pearson, S. G., & Giardino, A. (2022). Estimating tropical cyclone-induced wind, waves, and surge: A general methodology based on representative tracks. *Coastal Engineering*, 176, 104154. <https://doi.org/10.1016/j.coastaleng.2022.104154>
- Baldock, T. E., Shabani, B., Callaghan, D. P., Hu, Z., & Mumby, P. J. (2020). Two-dimensional modelling of wave dynamics and wave forces on fringing coral reefs. *Coastal Engineering*, 155, 103594. <https://doi.org/10.1016/j.coastaleng.2019.103594>
- Banas, N. S., Hickey, B. M., MacCready, P., & Newton, J. A. (2004). Dynamics of Willapa Bay, Washington: A highly unsteady, partially mixed estuary. *Journal of Physical Oceanography*, 34(11), 2413–2427. <https://doi.org/10.1175/JPO2637.1>
- Baptist, M., van Hattum, T., Reinhard, S., van Buuren, M., de Rooij, B., Hu, X., van

- Rooij, S., Polman, N., van den Burg, S., Piet, G., Ysebaert, T., Walles, B., Veraart, J., Wamelink, W., Bregman, B., Bos, B., & Selnes, T. (2019). *A nature-based future for the Netherlands in 2120* (tech. rep.). Wageningen University & Research. Wageningen, the Netherlands. <https://doi.org/10.18174/512277>
- Barbier, E. B., Hacker, S. D., Kennedy, C., Koch, E. W., Stier, A. C., & Silliman, B. R. (2011). The value of estuarine and coastal ecosystem services. *Ecological Monographs*, *81*(2), 169–193. <https://doi.org/10.1890/10-1510.1>
- Bar-Cohen, Y. (2006). Biomimetics—using nature to inspire human innovation. *Bioinspiration & Biomimetics*, *1*(1), P1–P12. <https://doi.org/10.1088/1748-3182/1/1/P01>
- Bates, P. D., Dawson, R. J., Hall, J. W., Horritt, M. S., Nicholls, R. J., Wicks, J., & Ali Mohamed Hassan, M. A. (2005). Simplified two-dimensional numerical modelling of coastal flooding and example applications. *Coastal Engineering*, *52*(9), 793–810. <https://doi.org/10.1016/j.coastaleng.2005.06.001>
- Beeldman, P., Workel, K., & de Rooy, M. (2018). Re-opening the Rhine River for fish. In K. Brink, P. Gough, J. Royte, P. P. Schollem, & H. Wannings (Eds.), *From sea to source 2.0: Protection and restoration of fish migration in rivers worldwide* (pp. 234–241). World Fish Migration Foundation.
- Berry, D. B., & Gasch, A. P. (2008). Stress-activated genomic expression changes serve a preparative role for impending stress in yeast (J. S. Weissman, Ed.). *Molecular Biology of the Cell*, *19*(11), 4580–4587. <https://doi.org/10.1091/mbc.e07-07-0680>
- Best, J. (2019). Anthropogenic stresses on the world's big rivers. *Nature Geoscience*, *12*(1), 7–21. <https://doi.org/10.1038/s41561-018-0262-x>
- Best, U. S. N., Van der Wegen, M., Dijkstra, J., Willemsen, P. W. J. M., Borsje, B. W., & Roelvink, D. J. A. (2018). Do salt marshes survive sea level rise? Modelling wave action, morphodynamics and vegetation dynamics. *Environmental Modelling & Software*, *109*, 152–166. <https://doi.org/10.1016/j.envsoft.2018.08.004>
- Bevacqua, E., Vousdoukas, M. I., Zappa, G., Hodges, K., Shepherd, T. G., Maraun, D., Mentaschi, L., & Feyen, L. (2020). More meteorological events that drive compound coastal flooding are projected under climate change. *Communications Earth & Environment*, *1*(1), 47. <https://doi.org/10.1038/s43247-020-00044-z>
- Bice, C. M., Huisman, J., Kimball, M. E., Mallen-Cooper, M., Zampatti, B. P., & Gillanders, B. M. (2023). Tidal barriers and fish – Impacts and remediation in the face of increasing demand for freshwater and climate change. *Estuarine, Coastal and Shelf Science*, *289*, 108376. <https://doi.org/10.1016/j.ecss.2023.108376>
- Biamond, B., de Swart, H. E., Dijkstra, H. A., & Díez-Minguito, M. (2022). Estuarine salinity response to freshwater pulses. *Journal of Geophysical Research: Oceans*, *127*(11), 1–18. <https://doi.org/10.1029/2022JC018669>
- Biamond, B., Kranenburg, W., Huisman, Y., de Swart, H. E., & Dijkstra, H. A. (in review). Dynamics of salt intrusion in complex estuarine networks: An idealised model applied to the rhine-meuse delta. *EGU sphere, preprint*. <https://doi.org/10.5194/egusphere-2024-2322>
- Bo, T., & Ralston, D. K. (2022). Frontogenesis, mixing, and stratification in estuarine channels with curvature. *Journal of Physical Oceanography*, *52*(7), 1333–1350. <https://doi.org/10.1175/JPO-D-21-0298.1>
- Bol, R., & Kraak, A. (1998). Water- en zoutbeweging. In J. van Hees & H. Peters (Eds.), *Mer beheer haringvlietsluizen: Over de grens van zoet en zout* (Rijkswater, p. 211).
- Borsje, B. W., van Wesenbeeck, B. K., Dekker, F., Paalvast, P., Bouma, T. J., van Katwijk, M. M., & de Vries, M. B. (2011). How ecological engineering can serve in coastal protection. *Ecological Engineering*, *37*(2), 113–122. <https://doi.org/10.1016/j.ecoleng.2010.11.027>
- Bosboom, J., & Stive, M. J. F. (2021). *Coastal Dynamics*. TU Delft Open. <https://doi.org/10.5074/T.2021.001>
- Bouma, H., de Jong, D. J., Twisk, F., & Wolfstein, K. (2005). *A Dutch Ecotope System for Coastal Waters (ZES.1)* (tech. rep.). Rijkswaterstaat, Rijksinstituut voor Kust en Zee. Middelburg, the Netherlands.
- Box, G. E. P. (1976). Science and statistics. *Journal of the American Statistical Association*, *71*(356), 791–799. <https://doi.org/10.1080/01621459.1976.10480949>
- Box, G. E. P. (1979). Robustness in the strategy of scientific model building. In R. L. Launer & G. N. Wilkinson (Eds.), *Robustness in statistics* (pp. 201–236). Elsevier. <https://doi.org/10.1016/b978-0-12-438150-6.50018-2>

- Breine, J., Maes, J., Ollevier, F., & Stevens, M. (2011). Fish assemblages across a salinity gradient in the Zeeschelde estuary (Belgium). *Belgian Journal of Zoology*, *141*(2), 21–44.
- Brevé, N. W. P., Vis, H., & Breukelaar, A. W. (2019). Escape from the North Sea: the possibilities for pikeperch (*Sander lucioperca* L. 1758) to re-enter the Rhine and Meuse estuary via the Haringvlietdam, as revealed by telemetry. *Journal of Coastal Conservation*, *23*(1), 239–252. <https://doi.org/10.1007/s11852-018-0654-5>
- Bridges, T., Bourne, E. M., King, J., Kuzmitski, H., Moynihan, E., & Suedel, B. (2018, July). *Engineering With Nature: An Atlas*. U.S. Army Engineer Research & Development Center. <https://doi.org/10.21079/11681/27929>
- Brink, K., Gough, P., Royte, J., Schollema, P. P., & Wanningen, H. (2018). *From Sea to Source 2.0: Protection and restoration of fish migration in rivers worldwide*. World Fish Migration Foundation.
- Brunink, S., & Hendrickx, G. G. (2024). Predicting ecotopes from hydrodynamic model data: Towards an ecological assessment of nature-based solutions. *Nature-Based Solutions*, *6*, 100145. <https://doi.org/10.1016/j.nbsj.2024.100145>
- Bruun, P. (1954). *Coast Erosion and the Development of Beach Profiles* (tech. rep.). US Army Corps of Engineers. Vicksburg, MS, USA.
- Buitink, J., Tsiokanos, A., Geertsema, T., ten Velden, C., Bouaziz, L., & Sperna Weiland, F. (2023). *Implications of the KNMI'23 climate scenarios for the discharge of the Rhine and Meuse* (tech. rep.). Deltares. Delft, the Netherlands.
- Burchard, H., & Hetland, R. D. (2010). Quantifying the contributions of tidal straining and gravitational circulation to residual circulation in periodically stratified tidal estuaries. *Journal of Physical Oceanography*, *40*(6), 1243–1262. <https://doi.org/10.1175/2010JPO4270.1>
- Burchard, H., Hetland, R. D., Schulz, E., & Schuttelaars, H. M. (2011). Drivers of residual estuarine circulation in tidally energetic estuaries: Straight and irrotational channels with parabolic cross section. *Journal of Physical Oceanography*, *41*(3), 548–570. <https://doi.org/10.1175/2010JPO4453.1>
- Burchard, H., & Hofmeister, R. (2008). A dynamic equation for the potential energy anomaly for analysing mixing and stratification in estuaries and coastal seas. *Estuarine, Coastal and Shelf Science*, *77*(4), 679–687. <https://doi.org/10.1016/j.ecss.2007.10.025>
- Camus, P., Mendez, F. J., Medina, R., & Cofiño, A. S. (2011). Analysis of clustering and selection algorithms for the study of multivariate wave climate. *Coastal Engineering*, *58*(6), 453–462. <https://doi.org/10.1016/j.coastaleng.2011.02.003>
- Carpenter, S., Walker, B., Anderies, J. M., & Abel, N. (2001). From metaphor to measurement: Resilience of what to what? *Ecosystems*, *4*(8), 765–781. <https://doi.org/10.1007/s10021-001-0045-9>
- Chant, R. J., Sommerfield, C. K., & Talke, S. A. (2018). Impact of channel deepening on tidal and gravitational circulation in a highly engineered estuarine basin. *Estuaries and Coasts*, *41*(6), 1587–1600. <https://doi.org/10.1007/s12237-018-0379-6>
- Chatwin, P. C. (1976). Some remarks on the maintenance of the salinity distribution in estuaries. *Estuarine and Coastal Marine Science*, *4*(5), 555–566. [https://doi.org/10.1016/0302-3524\(76\)90030-X](https://doi.org/10.1016/0302-3524(76)90030-X)
- Chen, C., Beardsley, R. C., Cowles, G. W., Qi, J., Lai, Z., Gao, G., Stuebe, D., Liu, H., Xu, Q., Xue, P., Ge, J., Hu, S., Ji, R., Tian, R., Huang, H., Wu, L., Lin, H., Sun, Y., & Zhao, L. (2013). *An Unstructured Grid, Finite-Volume Community Ocean Model FVCOM User Manual* (tech. rep.). University of Massachusetts-Dartmouth. New Bedford, MA, USA.
- Chen, Q., Zhu, J., Lyu, H., Pan, S., & Chen, S. (2019). Impacts of topography change on saltwater intrusion over the past decade in the Changjiang Estuary. *Estuarine, Coastal and Shelf Science*, *231*, 106469. <https://doi.org/10.1016/j.ecss.2019.106469>
- Chen, Q., Li, Q., Lin, Y., Zhang, J., Xia, J., Ni, J., Cooke, S. J., Best, J., He, S., Feng, T., Chen, Y., Tonina, D., Benjankar, R., Birk, S., Fleischmann, A. S., Yan, H., & Tang, L. (2023). River damming impacts on fish habitat and associated conservation measures. *Reviews of Geophysics*, *61*(4), e2023RG000819. <https://doi.org/10.1029/2023RG000819>
- Chen, S.-N. (2015). Asymmetric estuarine responses to changes in river forcing: A consequence of nonlinear salt flux. *Journal of Physical Oceanography*, *45*(11), 2836–2847. <https://doi.org/10.1175/JPO-D-15-0085.1>
- Chen, W., Hendrickx, G. G., Bakker, F. P., Bootsma, J., van der Sande, W. M., Saccon, E., Siemes, P. C., Rutger W. A. Roos,

- & Hulscher, S. J. M. H. (*in prep.*). The effectiveness of nature-based solutions in mitigating salt intrusion in estuaries: A review. *Science of the Total Environment*.
- Cheng, P., de Swart, H. E., & Valle-Levinson, A. (2013). Role of asymmetric tidal mixing in the subtidal dynamics of narrow estuaries. *Journal of Geophysical Research: Oceans*, *118*(5), 2623–2639. <https://doi.org/10.1002/jgrc.20189>
- Cheng, P., Valle-Levinson, A., & de Swart, H. E. (2010). Residual currents induced by asymmetric tidal mixing in weakly stratified narrow estuaries. *Journal of Physical Oceanography*, *40*(9), 2135–2147. <https://doi.org/10.1175/2010JPO4314.1>
- Cheng, P., Wang, A., & Jia, J. (2017). Analytical study of lateral-circulation-induced exchange flow in tidally dominated well-mixed estuaries. *Continental Shelf Research*, *140*, 1–10. <https://doi.org/10.1016/j.csr.2017.03.013>
- Chesson, P. (1994). Multispecies competition in variable environments. *Theoretical Population Biology*, *45*(3), 227–276. <https://doi.org/10.1006/tpbi.1994.1013>
- Cloern, J. E., Jassby, A. D., Schraga, T. S., Nejad, E., & Martin, C. (2017). Ecosystem variability along the estuarine salinity gradient: Examples from long-term study of San Francisco Bay. *Limnology and Oceanography*, *62*(S1), S272–S291. <https://doi.org/10.1002/lno.10537>
- Cohn, D. A. (1996). Neural network exploration using optimal experiment design. *Neural Networks*, *9*(6), 1071–1083. [https://doi.org/10.1016/0893-6080\(95\)00137-9](https://doi.org/10.1016/0893-6080(95)00137-9)
- Collins, L., Bradstock, R. A., Clarke, H., Clarke, M. F., Nolan, R. H., & Penman, T. D. (2021). The 2019/2020 mega-fires exposed Australian ecosystems to an unprecedented extent of high-severity fire. *Environmental Research Letters*, *16*(4), 044029. <https://doi.org/10.1088/1748-9326/abeb9e>
- Connell, J. H. (1978). Diversity in tropical rain forests and coral reefs. *Science*, *199*(4335), 1302–1310. <https://doi.org/10.1126/science.199.4335.1302>
- Costa, Y., Martins, I., de Carvalho, G. C., & Barros, F. (2023). Trends of sea-level rise effects on estuaries and estimates of future saline intrusion. *Ocean and Coastal Management*, *236*, 106490. <https://doi.org/10.1016/j.ocecoaman.2023.106490>
- Costall, A., Harris, B., & Pigois, J. P. (2018). Electrical resistivity imaging and the saline water interface in high-quality coastal aquifers. *Surveys in Geophysics*, *39*(4), 753–816. <https://doi.org/10.1007/s10712-018-9468-0>
- Costanza, R., D'Arge, R., de Groot, R., Farber, S., Grasso, M., Hannon, B., Limburg, K., Naeem, S., O'Neill, R. V., Paruelo, J., Raskin, R. G., Sutton, P., & van den Belt, M. (1997). The value of the world's ecosystem services and natural capital. *Nature*, *387*(6630), 253–260. <https://doi.org/10.1038/387253a0>
- Cox, J. R., Huismans, Y., Knaake, S. M., Leuven, J. R. F. W., Vellinga, N. E., van der Vegt, M., Hoitink, A. J. F., & Kleinhans, M. G. (2021). Anthropogenic effects on the contemporary sediment budget of the lower Rhine-Meuse Delta channel network. *Earth's Future*, *9*(7), 1–22. <https://doi.org/10.1029/2020EF001869>
- Cox, J. R., Leuven, J. R. F. W., Pierik, H. J., van Egmond, M., & Kleinhans, M. G. (2022). Sediment deficit and morphological change of the Rhine-Meuse river mouth attributed to multi-millennial anthropogenic impacts. *Continental Shelf Research*, *244*, 104766. <https://doi.org/10.1016/j.csr.2022.104766>
- Dada, O. A., Li, G., Qiao, L., Ding, D., Ma, Y., & Xu, J. (2016). Seasonal shoreline behaviours along the arcuate Niger Delta coast: Complex interaction between fluvial and marine processes. *Continental Shelf Research*, *122*, 51–67. <https://doi.org/10.1016/j.csr.2016.03.002>
- de la Haye, M. A. A., Reeze, B., van der Jagt, H. A., & Verweij, G. L. (2022). *Vervolgrapportage ecologische toestand Harin guliet en Voordelta 'Lerend implementeren kierbesluit' 2020* (tech. rep.). Bureau Waardenburg. Culemborg, the Netherlands.
- De Leo, A., Tambroni, N., & Stocchino, A. (2022). Dispersion processes in weakly dissipative tidal channels. *Journal of Geophysical Research: Oceans*, *127*(10), e2021JC018315. <https://doi.org/10.1029/2021JC018315>
- Deb, K. (2001). *Multi-Objective Optimization using Evolutionary Algorithms*. Wiley. <https://www.wiley.com/en-us/Multi+Objective+Optimization+using+Evolutionary+Algorithms-p-9780471873396>
- Deltares. (2022). Delft3D Flexible Mesh, User Manual.
- den Haan, R.-J., Biemond, B., & Baart, F. (2024). Using an idealized network model as the physical module for a salt intrusion serious game. In I. Niesten, N. Tahsin, D. van Grootheest, H. Barneveld, K. Waldschläger, & T. Hoitink (Eds.), *Ncr days 2024* (pp. 58–

- 59). Netherlands Centre for River Studies. <https://research.tudelft.nl/en/publications/using-an-idealized-network-model-as-the-physical-module-for-a-sal>
- den Haan, R.-J., van der Voort, M. C., Baart, F., Berends, K. D., van den Berg, M. C., Straatsma, M. W., Geenen, A. J. P., & Hulscher, S. J. M. H. (2020). The Virtual River Game: Gaming using models to collaboratively explore river management complexity. *Environmental Modelling & Software*, *134*, 104855. <https://doi.org/10.1016/j.envsoft.2020.104855>
- de Nijs, M. A. J., Pietrzak, J. D., & Winterwerp, J. C. (2011). Advection of the salt wedge and evolution of the internal flow structure in the Rotterdam Waterway. *Journal of Physical Oceanography*, *41*(1), 3–27. <https://doi.org/10.1175/2010JPO4228.1>
- de Nijs, M. A. J., Winterwerp, J. C., & Pietrzak, J. D. (2009). On harbour siltation in the fresh-salt water mixing region. *Continental Shelf Research*, *29*(1), 175–193. <https://doi.org/10.1016/j.csr.2008.01.019>
- Dessai, S., Hulme, M., Lempert, R., & Pielke, R. (2009). Do we need better predictions to adapt to a changing climate? *Eos, Transactions American Geophysical Union*, *90*(13), 111–112. <https://doi.org/10.1029/2009EO130003>
- de Vet, P. L. M., van Prooijen, B. C., & Wang, Z. B. (2017). The differences in morphological development between the intertidal flats of the Eastern and Western Scheldt. *Geomorphology*, *281*, 31–42. <https://doi.org/10.1016/j.geomorph.2016.12.031>
- de Vriend, H. J., Capobianco, M., Chesher, T., de Swart, H. E., Latteux, B., & Stive, M. J. F. (1993). Approaches to long-term modelling of coastal morphology: A review. *Coastal Engineering*, *21*(1-3), 225–269. [https://doi.org/10.1016/0378-3839\(93\)90051-9](https://doi.org/10.1016/0378-3839(93)90051-9)
- de Vriend, H. J., van Koningsveld, M., Aarninkhof, S. G. J., de Vries, M. B., & Baptist, M. J. (2015). Sustainable hydraulic engineering through Building with Nature. *Journal of Hydro-Environment Research*, *9*(2), 159–171. <https://doi.org/10.1016/j.jher.2014.06.004>
- de Vriend, H. J., Wang, Z. B., Ysebaert, T., Herman, P. M. J., & Ding, P. (2011). Ecomorphological problems in the Yangtze Estuary and the Western Scheldt. *Wetlands*, *31*(6), 1033–1042. <https://doi.org/10.1007/s13157-011-0239-7>
- de Vries, I. (2014). *Toetsing robuustheid Brielse Meer voor zoetwatervoorziening* (tech. rep.). Deltares, Delft, the Netherlands.
- de Vries, M., van Koningsveld, M., Aarninkhof, S., & de Vriend, H. (2021). A systematic design approach for objectifying Building with Nature solutions. *Research in Urbanism Series*, *7*, 29–49. <https://doi.org/10.47982/rius.7.124>
- de Wilde, J. (2024). *Tidal phase differences in multi-branch systems and their effect on salt intrusion* [Master's thesis, Delft University of Technology].
- Dial, R., & Roughgarden, J. (1998). Theory of marine communities: The intermediate disturbance hypothesis. *Ecology*, *79*(4), 1412–1424. [https://doi.org/10.1890/0012-9658\(1998\)079\[1412:TOMCTI\]2.0.CO;2](https://doi.org/10.1890/0012-9658(1998)079[1412:TOMCTI]2.0.CO;2)
- Diaz, D., & Keller, K. (2016). A potential disintegration of the West Antarctic Ice Sheet: Implications for economic analyses of climate policy. *American Economic Review*, *106*(5), 607–611. <https://doi.org/10.1257/aer.p20161103>
- Dietz, S., Rising, J., Stoerk, T., & Wagner, G. (2021). Economic impacts of tipping points in the climate system. *Proceedings of the National Academy of Sciences*, *118*(34), e2103081118. <https://doi.org/10.1073/pnas.2103081118>
- Dijkstra, Y. M., & Schuttelaars, H. M. (2021). A unifying approach to subtidal salt intrusion modeling in tidal estuaries. *Journal of Physical Oceanography*, *51*(1), 147–167. <https://doi.org/10.1175/JPO-D-20-0006.1>
- Dingley, B., O'Rourke, E., Turner, B., CMIP Panel Members, WGCMI Infrastructure Panel Members, & CMIP7 Task Team Members. (2023). *CMIP Annual Report 2022-2023* (tech. rep.). World Climate Research Programme (WCRP). <https://doi.org/10.5281/zenodo.8101810>
- Distefano, T., & Kelly, S. (2017). Are we in deep water? Water scarcity and its limits to economic growth. *Ecological Economics*, *142*, 130–147. <https://doi.org/10.1016/j.ecolecon.2017.06.019>
- Dodet, G., Castelle, B., Masselink, G., Scott, T., Davidson, M., Floc'h, F., Jackson, D., & Suarez, S. (2019). Beach recovery from extreme storm activity during the 2013–14 winter along the Atlantic coast of Europe. *Earth Surface Processes and Landforms*, *44*(1), 393–401. <https://doi.org/10.1002/esp.4500>
- Dronkers, J. (1978). Longitudinal dispersion in shallow well-mixed estuaries. *Coastal Engi-*

- neering 1978, 2761–2777. <https://doi.org/10.1061/9780872621909.171>
- Dronkers, J., & van de Kreeke, J. (1986). Experimental determination of salt intrusion mechanisms in the Volkerak estuary. *Netherlands Journal of Sea Research*, 20(1), 1–19. [https://doi.org/10.1016/0077-7579\(86\)90056-6](https://doi.org/10.1016/0077-7579(86)90056-6)
- Dronkers, J. (2017). Convergence of estuarine channels. *Continental Shelf Research*, 144, 120–133. <https://doi.org/10.1016/j.csr.2017.06.012>
- Dykstra, S. L., Talke, S. A., Yankovsky, A. E., Torres, R., & Viparelli, E. (2024). Reflection of storm surge and tides in convergent estuaries with dams, the case of Charleston, USA. *Journal of Geophysical Research: Oceans*, 129(9), e2023JC020498. <https://doi.org/10.1029/2023JC020498>
- Elmqvist, T., Folke, C., Nyström, M., Peterson, G., Bengtsson, J., Walker, B., & Norberg, J. (2003). Response diversity, ecosystem change, and resilience. *Frontiers in Ecology and the Environment*, 1(9), 488–494. [https://doi.org/10.1890/1540-9295\(2003\)001\[0488:RDECAR\]2.0.CO;2](https://doi.org/10.1890/1540-9295(2003)001[0488:RDECAR]2.0.CO;2)
- Emanuel, K. A. (2005). Increasing destructiveness of tropical cyclones over the past 30 years. *Nature*, 436(7051), 686–688. <https://doi.org/10.1038/nature03906>
- Emmerich, M. T. M., & Deutz, A. H. (2018). A tutorial on multiobjective optimization: Fundamentals and evolutionary methods. *Natural Computing*, 17(3), 585–609. <https://doi.org/10.1007/s11047-018-9685-y>
- Equihua, M., Aldama, M. E., Gershenson, C., López-Corona, O., Munguía, M., Pérez-Maqueo, O., & Ramírez-Carrillo, E. (2020). Ecosystem antifragility: Beyond integrity and resilience. *PeerJ*, 8, 1–35. <https://doi.org/10.7717/peerj.8533>
- Fagerburg, T. L., & Alexander, M. P. (1994). *Underwater Sill Construction for Mitigating Salt Wedge Migration on the Lower Mississippi River* (tech. rep.). Hydraulic Laboratory, US Army Engineer Waterways Experiment Station, Vicksburg, MS, USA.
- Fairchild, T. P., Bennett, W. G., Smith, G., Day, B., Skov, M. W., Möller, I., Beaumont, N., Karunaratna, H., & Griffin, J. N. (2021). Coastal wetlands mitigate storm flooding and associated costs in estuaries. *Environmental Research Letters*, 16(7), 074034. <https://doi.org/10.1088/1748-9326/ac0c45>
- Fayemi, P. E., Wanieck, K., Zollfrank, C., Maranzana, N., & Aoussat, A. (2017). Biomimetics: Process, tools and practice. *Bioinspiration & Biomimetics*, 12(1), 011002. <https://doi.org/10.1088/1748-3190/12/1/011002>
- Feagin, R. A., Figlus, J., Zinnert, J. C., Sigrén, J., Martínez, M. L., Silva, R., Smith, W. K., Cox, D., Young, D. R., & Carter, G. (2015). Going with the flow or against the grain? The promise of vegetation for protecting beaches, dunes, and barrier islands from erosion. *Frontiers in Ecology and the Environment*, 13(4), 203–210. <https://doi.org/10.1890/140218>
- Feagin, R. A., Innocenti, R. A., Bond, H., Wengrove, M., Huff, T. P., Lomonaco, P., Tsai, B., Puleo, J., Pontiki, M., Figlus, J., Chavez, V., & Silva, R. (2023). Does vegetation accelerate coastal dune erosion during extreme events? *Science Advances*, 9(24). <https://doi.org/10.1126/sciadv.adg7135>
- Ferrario, F., Beck, M. W., Storlazzi, C. D., Micheli, F., Shepard, C. C., & Airoldi, L. (2014). The effectiveness of coral reefs for coastal hazard risk reduction and adaptation. *Nature Communications*, 5(1), 3794. <https://doi.org/10.1038/ncomms4794>
- Figuerola, S. M., Lee, G.-h., Chang, J., & Jung, N. W. (2022). Impact of estuarine dams on the estuarine parameter space and sediment flux decomposition: Idealized numerical modeling study. *Journal of Geophysical Research: Oceans*, 127, e2021JC017829. <https://doi.org/10.1029/2021JC017829>
- Fischer, H. B., List, E. J., Koh, R. C. Y., Imberger, J., & Brooks, N. H. (1979). *Mixing in Inland and Coastal Waters*. Academic Press. <https://doi.org/https://doi.org/10.1016/C2009-0-22051-4>
- Fischer, H. (1972). Mass transport mechanisms in partially stratified estuaries. *Journal of Fluid Mechanics*, 53(4), 671–687. <https://doi.org/10.1017/S0022112072000412>
- Folke, C., Carpenter, S., Elmqvist, T., Gunderson, L., Holling, C. S., & Walker, B. (2002). Resilience and sustainable development: Building adaptive capacity in a world of transformations. *AMBIO: A Journal of the Human Environment*, 31(5), 437–440. <https://doi.org/10.1579/0044-7447-31.5.437>
- Folke, C., Carpenter, S., Walker, B., Scheffer, M., Elmqvist, T., Gunderson, L., & Holling, C. S. (2004). Regime shifts, resilience, and biodiversity in ecosystem management. *Annual Review of Ecology, Evolution, and Systematics*, 35(1), 557–581. <https://doi.org/10.1146/annurev.ecolsys.35.021103.105711>

- Friedrichs, C. T., & Aubrey, D. G. (1988). Non-linear tidal distortion in shallow well-mixed estuaries: a synthesis. *Estuarine, Coastal and Shelf Science*, 27(5), 521–545. [https://doi.org/10.1016/0272-7714\(88\)90082-0](https://doi.org/10.1016/0272-7714(88)90082-0)
- Friedrichs, C. T., & Aubrey, D. G. (1994). Tidal propagation in strongly convergent channels. *Journal of Geophysical Research*, 99(C2), 3321–3336. <https://doi.org/10.1029/93JC03219>
- Friedrichs, C. T., & Madsen, O. S. (1992). Non-linear diffusion of the tidal signal in frictionally dominated embayments. *Journal of Geophysical Research*, 97(C4), 5637. <https://doi.org/10.1029/92jc00354>
- Fringer, O. B., Dawson, C. N., He, R., Ralston, D. K., & Zhang, Y. J. (2019). The future of coastal and estuarine modeling: Findings from a workshop. *Ocean Modelling*, 143(August), 101458. <https://doi.org/10.1016/j.ocemod.2019.101458>
- Frost, T. M., Carpenter, S. R., Ives, A. R., & Kratz, T. K. (1995). Species Compensation and Complementarity in Ecosystem Function. In C. G. Jones & J. H. Lawton (Eds.), *Linking species & ecosystems* (pp. 224–239). Springer US. <https://doi.org/10.1007/978-1-4615-1773-3{\-}22>
- Galván, C., Puente, A., & Juanes, J. A. (2021). Nested socio-ecological maps as a spatial planning instrument for estuary conservation and ecosystem-based management. *Frontiers in Marine Science*, 8, 730762. <https://doi.org/10.3389/fmars.2021.730762>
- Garcia, A. M. P., & Geyer, W. R. (2023). Tidal dispersion in short estuaries. *Journal of Geophysical Research: Oceans*, 128, e2022JC018883. <https://doi.org/10.1029/2022JC018883>
- Garcia, A. M. P., Geyer, W. R., & Randall, N. (2022). Exchange flows in tributary creeks enhance dispersion by tidal trapping. *Estuaries and Coasts*, 45(2), 363–381. <https://doi.org/10.1007/s12237-021-00969-4>
- Geerts, S. J., van der Sande, W. M., Geurts, B. J., Roos, P. C., M., T. T., & Hulscher, S. J. M. H. (in review). Estuarine sand dunes as a nature-based solution against salt intrusion. *Journal of Geophysical Research: Oceans*.
- Geraeds, M. E. G., Pietrzak, J. D., Gerritsma, A., Verlaan, M., & Katsman, C. A. (in prep.). The wind-driven response of salt intrusion in a salt wedge estuary. *Journal of Physical Oceanography*.
- Gerritsma, A., Verlaan, M., Geraeds, M. E. G., Huismans, Y., & Pietrzak, J. D. (in review). The effects of a storm surge event on salt intrusion: Insights from the rhine-meuse delta. *Journal of Geophysical Research: Oceans*.
- Geyer, W. R. (1997). Influence of wind on dynamics and flushing of shallow estuaries. *Estuarine, Coastal and Shelf Science*, 44(6), 713–722. <https://doi.org/10.1006/ecss.1996.0140>
- Geyer, W. R., & MacCready, P. (2014). The estuarine circulation. *Annual Review of Fluid Mechanics*, 46(1), 175–197. <https://doi.org/10.1146/annurev-fluid-010313-141302>
- Geyer, W. R., Ralston, D. K., & Chen, J.-L. (2020). Mechanisms of exchange flow in an estuary with a narrow, deep channel and wide, shallow shoals. *Journal of Geophysical Research: Oceans*, 125(12), e2020JC016092. <https://doi.org/10.1029/2020JC016092>
- Gibbin, E. M., Krueger, T., Putnam, H. M., Barott, K. L., Bodin, J., Gates, R. D., & Meibom, A. (2018). Short-term thermal acclimation modifies the metabolic condition of the coral holobiont. *Frontiers in Marine Science*, 5, 10. <https://doi.org/10.3389/fmars.2018.00010>
- Gijón Mancheño, A., Vuik, V., van Wesenbeeck, B. K., Jonkman, S. N., van Hespén, R., Moll, J. R., Kazi, S., Urrutia, I., & van Ledden, M. (2024). Integrating mangrove growth and failure in coastal flood protection designs. *Scientific Reports*, 14(1), 7951. <https://doi.org/10.1038/s41598-024-58705-4>
- Glamore, W., Rayner, D., Ruprecht, J., Sadat-Noori, M., & Khojasteh, D. (2021). Ecohydrology as a driver for tidal restoration: Observations from a Ramsar wetland in eastern Australia (J. M. Dias, Ed.). *PLOS ONE*, 16(8), e0254701. <https://doi.org/10.1371/journal.pone.0254701>
- Glanemann, N., Willner, S. N., & Levermann, A. (2020). Paris Climate Agreement passes the cost-benefit test. *Nature Communications*, 11(1), 110. <https://doi.org/10.1038/s41467-019-13961-1>
- Gong, W., Lin, Z., Chen, Y., Chen, Z., & Zhang, H. (2018). Effect of winds and waves on salt intrusion in the Pearl River estuary. *Ocean Science*, 14(1), 139–159. <https://doi.org/10.5194/os-14-139-2018>
- Gong, W., & Shen, J. (2011). The response of salt intrusion to changes in river discharge and tidal mixing during the dry season in the Modaomen Estuary, China. *Continental Shelf Research*, 31(7–8), 769–788. <https://doi.org/10.1016/j.csr.2011.01.011>
- Gramacy, R. B., & Lee, H. K. H. (2009). Adaptive design and analysis of supercomputer ex-

- periments. *Technometrics*, 51(2), 130–145. <https://doi.org/10.1198/TECH.2009.0015>
- Granek, E. F., Polasky, S., Kappel, C. V., Reed, D. J., Stoms, D. M., Koch, E. W., Kennedy, C. J., Cramer, L. A., Hacker, S. D., Barbier, E. B., Aswani, S., Ruckelshaus, M., Perillo, G. M. E., Silliman, B. R., Muthiga, N., Bael, D., & Wolanski, E. (2010). Ecosystem services as a common language for coastal ecosystem-based management. *Conservation Biology*, 24(1), 207–216. <https://doi.org/10.1111/j.1523-1739.2009.01355.x>
- Greco, S., Figueira, J. R., & Ehrgott, M. (Eds.). (2016). *Multiple Criteria Decision Analysis: State of the Art Surveys* (2nd ed.). Springer.
- Gründemann, G. J., van de Giesen, N., Brunner, L., & van der Ent, R. (2022). Rarest rainfall events will see the greatest relative increase in magnitude under future climate change. *Communications Earth & Environment*, 3(1), 235. <https://doi.org/10.1038/s43247-022-00558-8>
- Guannel, G., Arkema, K., Ruggiero, P., & Verutes, G. (2016). The power of three: Coral reefs, seagrasses and mangroves protect coastal regions and increase their resilience (C. N. Bianchi, Ed.). *PLoS ONE*, 11(7), e0158094. <https://doi.org/10.1371/journal.pone.0158094>
- Guha, A., & Lawrence, G. A. (2013). Estuary classification revisited. *Journal of Physical Oceanography*, 43(8), 1566–1571. <https://doi.org/10.1175/JPO-D-12-0129.1>
- Haasnoot, M., van Deursen, W. P. A., Guillaume, J. H. A., Kwakkel, J. H., van Beek, E., & Middelkoop, H. (2014). Fit for purpose? Building and evaluating a fast, integrated model for exploring water policy pathways. *Environmental Modelling and Software*, 60, 99–120. <https://doi.org/10.1016/j.envsoft.2014.05.020>
- Haasnoot, M., Di Fant, V., Kwakkel, J., & Lawrence, J. (2024). Lessons from a decade of adaptive pathways studies for climate adaptation. *Global Environmental Change*, 88, 102907. <https://doi.org/10.1016/j.gloenvcha.2024.102907>
- Haasnoot, M., Kwakkel, J. H., Walker, W. E., & ter Maat, J. (2013). Dynamic adaptive policy pathways: A method for crafting robust decisions for a deeply uncertain world. *Global Environmental Change*, 23(2), 485–498. <https://doi.org/10.1016/j.gloenvcha.2012.12.006>
- Hall, A. R., Miller, A. D., Leggett, H. C., Roxburgh, S. H., Buckling, A., & Shea, K. (2012). Diversity-disturbance relationships: Frequency and intensity interact. *Biology Letters*, 8(5), 768–771. <https://doi.org/10.1098/rsbl.2012.0282>
- Haney, R. L. (1991). On the pressure gradient force over steep topography in sigma coordinate ocean models. *Journal of Physical Oceanography*, 21(4), 610–619. [https://doi.org/10.1175/1520-0485\(1991\)021<0610:OTPGFO>2.0.CO;2](https://doi.org/10.1175/1520-0485(1991)021<0610:OTPGFO>2.0.CO;2)
- Hanley, M. E., Hoggart, S. P. G., Simmonds, D. J., Bichot, A., Colangelo, M. A., Bozzeda, F., Heurtefeux, H., Ondiviola, B., Ostrowski, R., Recio, M., Trude, R., Zawadzka-Kahlau, E., & Thompson, R. C. (2014). Shifting sands? Coastal protection by sand banks, beaches and dunes. *Coastal Engineering*, 87, 136–146. <https://doi.org/10.1016/j.coastaleng.2013.10.020>
- Hansen, D. V., & Rattray Jr., M. (1965). Gravitational circulation in straits and estuaries. *Journal of Marine Research*, 23, 104–122.
- Hansen, D. V., & Rattray Jr., M. (1966). New dimensions in estuary classification. *Limnology and Oceanography*, 11(3), 319–326. <https://doi.org/10.4319/lo.1966.11.3.0319>
- Hanson, H., Brampton, A., Capobianco, M., Dette, H. H., Hamm, L., Laustrup, C., Lechuga, A., & Spanhoff, R. (2002). Beach nourishment projects, practices, and objectives—a European overview. *Coastal Engineering*, 47(2), 81–111. [https://doi.org/10.1016/S0378-3839\(02\)00122-9](https://doi.org/10.1016/S0378-3839(02)00122-9)
- Hanson, H. I., Wickenberg, B., & Alkan Olsson, J. (2020). Working on the boundaries—How do science use and interpret the nature-based solution concept? *Land Use Policy*, 90, 104302. <https://doi.org/10.1016/j.landusepol.2019.104302>
- Harley, C. D. G., Hughes, A. R., Hultgren, K. M., Miner, B. G., Sorte, C. J. B., Thornber, C. S., Rodriguez, L. F., Tomanek, L., & Williams, S. L. (2006). The impacts of climate change in coastal marine systems. *Ecology Letters*, 9(2), 228–241. <https://doi.org/10.1111/j.1461-0248.2005.00871.x>
- Hasan, G. M. J., van Maren, D. S., & Fatt, C. H. (2013). Numerical study on mixing and stratification in the ebb-dominant Johor estuary. *Journal of Coastal Research*, 29(1), 201–215. <https://doi.org/10.2112/JCOASTRES-D-12-00053.1>
- He, C., Yin, Z.-Y., Stocchino, A., & Wai, O. W. H. (2023). Generation of macrovortices in estuarine compound channels. *Frontiers in Marine Science*, 10, 1082506. <https://doi.org/10.3389/fmars.2023.1082506>

- Heimhuber, V., Raoult, V., Glamore, W. C., Taylor, M. D., & Gaston, T. F. (2024). Restoring blue carbon ecosystems unlocks fisheries' potential. *Restoration Ecology*, 32(1), e14052. <https://doi.org/10.1111/rec.14052>
- Hendrickx, G. G. (2022). ANNESI: An open-source artificial neural network for estuarine salt intrusion. <https://doi.org/10.4121/19307693>
- Hendrickx, G. G. (2023a). NEESI: Numerical Experiments of Estuarine Salt Intrusion dataset. <https://doi.org/10.4121/22272247>
- Hendrickx, G. G. (2023b). NumPy-based Salt Flux Decomposition. <https://doi.org/10.4121/bccbe767-667b-40ba-a4d1-d8fcad900772>
- Hendrickx, G. G., Antolínez, J. A. A., & Herman, P. M. J. (2023a). Predicting the response of complex systems for coastal management. *Coastal Engineering*, 182, 104289. <https://doi.org/10.1016/j.coastaleng.2023.104289>
- Hendrickx, G. G., Antolínez, J. A. A., Herman, P. M. J., & Aarninkhof, S. G. J. (2023b, September). Estuarine sensitivity to nature-based salt intrusion mitigation measures. In D. Cox (Ed.), *Coastal engineering proceedings* (management.146). <https://doi.org/10.9753/icce.v37.management.146>
- Hendrickx, G. G., & Brunink, S. (2023). EMMA: Ecotope-Map Maker based on Abiotics. <https://doi.org/10.4121/0100fc5a-a99c-4002-9864-3faade3899e3.v1>
- Hendrickx, G. G., Fivash, G. S., Pearson, S. G., Gerritsma, A., Geraeds, M. E. G., & Aarninkhof, S. G. J. (in prep.). Socio-ecological evaluation of estuary-scale interventions. *Ecological Engineering*.
- Hendrickx, G. G., Herman, P. M. J., Dijkstra, J. T., Storlazzi, C. D., & Toth, L. T. (2021). Online-coupling of widely-ranged timescales to model coral reef development. *Environmental Modelling and Software*, 143, 105103. <https://doi.org/10.1016/j.envsoft.2021.105103>
- Hendrickx, G. G., Kranenburg, W. M., Antolínez, J. A. A., Huismans, Y., Aarninkhof, S. G. J., & Herman, P. M. J. (2023c). Sensitivity of salt intrusion to estuary-scale changes: A systematic modelling study towards nature-based mitigation measures. *Estuarine, Coastal and Shelf Science*, 295, 108564. <https://doi.org/10.1016/j.ecss.2023.108564>
- Hendrickx, G. G., Manuel, L. A., Pearson, S. G., Aarninkhof, S. G. J., & Meselhe, E. A. (2024a). Dataset underlying the study “An earthen sill as a measure to mitigate salt intrusion in estuaries”. <https://doi.org/10.4121/10d493df-8efb-442b-8c3d-04e92bcf4c4e>
- Hendrickx, G. G., Manuel, L. A., Pearson, S. G., Aarninkhof, S. G. J., & Meselhe, E. A. (2024b). An earthen sill as a measure to mitigate salt intrusion in estuaries. *Estuaries and Coasts*, 47(5), 1199–1208. <https://doi.org/10.1007/s12237-024-01359-2>
- Hendrickx, G. G., Meselhe, E. A., Herman, P. M. J., & Aarninkhof, S. G. J. (2023d, April). A sill as nature-based solution to mitigate salt intrusion. In P. Wang, E. Floyer, & J. D. Rosati (Eds.), *Coastal sediments 2023* (pp. 2003–2007). World Scientific. https://doi.org/10.1142/9789811275135_{-}_0184
- Hendrickx, G. G., & Pearson, S. G. (2024a). Dataset underlying the study “On the effects of intertidal area on estuarine salt intrusion”. <https://doi.org/10.4121/c357f1c7-dea8-4971-b5a1-c54c42e4172a>
- Hendrickx, G. G., & Pearson, S. G. (2024b). On the effects of intertidal area on estuarine salt intrusion. *Journal of Geophysical Research: Oceans*, 129(9), e2023JC020750. <https://doi.org/10.1029/2023JC020750>
- Hendrickx, G. G., Pearson, S. G., Antolínez, J. A. A., & Aarninkhof, S. G. J. (in review). DARE to proactively react to unknown uncertainties in the Anthropocene. *Earth's Future*.
- Herman, J. D., Quinn, J. D., Steinschneider, S., Giuliani, M., & Fletcher, S. (2020). Climate Adaptation as a control problem: Review and perspectives on dynamic water resources planning under uncertainty. *Water Resources Research*, 56(2), e24389. <https://doi.org/10.1029/2019WR025502>
- Herrera, M., Abraham, E., & Stoianov, I. (2016). A graph-theoretic framework for assessing the resilience of sectorised water distribution networks. *Water Resources Management*, 30(5), 1685–1699. <https://doi.org/10.1007/s11269-016-1245-6>
- Herrmann-Pillath, C., Hiedanpää, J., & Soini, K. (2022). The co-evolutionary approach to nature-based solutions: A conceptual framework. *Nature-Based Solutions*, 2, 100011. <https://doi.org/10.1016/j.nbsj.2022.100011>
- Hesen, P. (2021). *Projectbeslissing KWA+: Maatregelenpakket B2* (tech. rep.). Hoogheemraadschap De Stichtse Rijnlanden en Hoogheemraadschap van Rijnland.
- Hetland, R. D., & Geyer, W. R. (2004). An idealized study of the structure of long, par-

- tially mixed estuaries. *Journal of Physical Oceanography*, 34(12), 2677–2691. <https://doi.org/10.1175/JPO2646.1>
- Hey, R. D., & Thorne, C. R. (1986). Stable channels with mobile gravel beds. *Journal of Hydraulic Engineering*, 112(8), 671–689. [https://doi.org/10.1061/\(asce\)0733-9429\(1986\)112:8\(671\)](https://doi.org/10.1061/(asce)0733-9429(1986)112:8(671))
- Hinkel, J., Lincke, D., Vafeidis, A. T., Perrette, M., Nicholls, R. J., Tol, R. S. J., Marzeion, B., Fettweis, X., Ionescu, C., & Levermann, A. (2014). Coastal flood damage and adaptation costs under 21st century sea-level rise. *Proceedings of the National Academy of Sciences*, 111(9), 3292–3297. <https://doi.org/10.1073/pnas.1222469111>
- Holling, C. S. (1973). Resilience and stability of ecological systems. *Annual Review of Ecology and Systematics*, 4(1), 1–23. <https://doi.org/10.1146/annurev.es.04.110173.000245>
- Hong, B., & Shen, J. (2012). Responses of estuarine salinity and transport processes to potential future sea-level rise in the Chesapeake Bay. *Estuarine, Coastal and Shelf Science*, 104–105, 33–45. <https://doi.org/10.1016/j.ecss.2012.03.014>
- Hoonhout, B., & de Vries, S. (2017). Aeolian sediment supply at a mega nourishment. *Coastal Engineering*, 123, 11–20. <https://doi.org/10.1016/j.coastaleng.2017.03.001>
- Hooper, D. U., Chapin, F. S., Ewel, J. J., Hector, A., Inchausti, P., Lavorel, S., Lawton, J. H., Lodge, D. M., Loreau, M., Naeem, S., Schmid, B., Setälä, H., Symstad, A. J., Vandermeer, J., & Wardle, D. A. (2005). Effects of biodiversity on ecosystem functioning: A consensus of current knowledge. *Ecological Monographs*, 75(1), 3–35. <https://doi.org/10.1890/04-0922>
- Hop, J., & Vriese, F. T. (2011). *Vismigratie Rijn-Maasstroombgebied* (tech. rep.). ATKB. Rotterdam, the Netherlands.
- Houser, C., Wernette, P., Rentschlar, E., Jones, H., Hammond, B., & Trimble, S. (2015). Post-storm beach and dune recovery: Implications for barrier island resilience. *Geomorphology*, 234, 54–63. <https://doi.org/10.1016/j.geomorph.2014.12.044>
- Howells, E. J., Berkelmans, R., van Oppen, M. J. H., Willis, B. L., & Bay, L. K. (2013). Historical thermal regimes define limits to coral acclimatization. *Ecology*, 94(5), 1078–1088. <https://doi.org/10.1890/12-1257.1>
- Hu, X., Fang, G., & Ge, Y. (2024). Joint probability analysis and mapping of typhoon-induced wind, wave, and surge hazards along southeast China. *Ocean Engineering*, 311, 118844. <https://doi.org/10.1016/j.oceaneng.2024.118844>
- Hughes, T. P., Baird, A. H., Bellwood, D. R., Card, M., Connolly, S. R., Folke, C., Grosberg, R., Hoegh-Guldberg, O., Jackson, J. B. C., Kleypas, J. A., Lough, J. M., Marshall, P. A., Nyström, M., Palumbi, S. R., Pandolfi, J. M., Rosen, B., & Roughgarden, J. (2003). Climate change, human impacts, and the resilience of coral reefs. *Science*, 301(5635), 929–933. <https://doi.org/10.1126/science.1085046>
- Hughes, T. P., Anderson, K. D., Connolly, S. R., Heron, S. F., Kerry, J. T., Lough, J. M., Baird, A. H., Baum, J. K., Berumen, M. L., Bridge, T. C., Claar, D. C., Eakin, C. M., Gilmour, J. P., Graham, N. A. J., Harrison, H., Hobbs, J.-P. A., Hoey, A. S., Hoogenboom, M., Lowe, R. J., ... Wilson, S. K. (2018). Spatial and temporal patterns of mass bleaching of corals in the Anthropocene. *Science*, 359(6371), 80–83. <https://doi.org/10.1126/science.aan8048>
- Huisman, Y., Leummens, L., Rodrigo, S. M. T., Laan, S. C., Kranenburg, W. M., van der Wijk, R., & van Veen, N. P. (2024). The effectiveness of fresh-water pulses to mitigate salt intrusion into the Lek River. In K. Nawarat, N. Panno, T. Duong, J. Reynolds, M. van der Wegen, D. Roelvink, & N. McKenna (Eds.), *Nck days* (pp. 64–65). https://www.nck-web.org/content/documents/Book_of_Abstracts_2024-compressed.pdf#page=64%20https://www.nck-web.org/boa-2024/835-the-effectiveness-of-fresh-water-pulses-to-mitigate-salt-intrusion-into-the-lek-river
- Hunt, J. N. (1964). Tidal oscillations in estuaries. *Geophysical Journal of the Royal Astronomical Society*, 8(4), 440–455. <https://doi.org/10.1111/j.1365-246X.1964.tb03863.x>
- Hwang, J., Jeong, Y., Park, J. M., Lee, K. H., Hong, J. W., & Choi, J. (2015). Biomimetics: Forecasting the future of science, engineering, and medicine. *International Journal of Nanomedicine*, 10, 5701–5713. <https://doi.org/10.2147/IJN.S83642>
- HydroLogic. (2015). *Verzilting door verdieping Nieuwe Waterweg en Botlek* (tech. rep. No. december). HydroLogic. Amersfoort, the Netherlands.
- HydroLogic. (2018). *Vervolgonderzoek kosten en effecten permanente oostelijke zoetwateraanvoer voor West-Nederland* (tech. rep.). HydroLogic. Amersfoort, the Netherlands.

- HydroLogic. (2019a). *Optimalisatie Wateraanvoer West-Nederland* (tech. rep.). HydroLogic. Amersfoort, the Netherlands.
- HydroLogic. (2019b). *Rijn-Maasmonding: Slim Watermanagement Redeneerlijn Wattertekort* (tech. rep.). HydroLogic. Amersfoort, the Netherlands.
- Ibáñez, C., Alcaraz, C., Caiola, N., Rovira, A., Trobajo, R., Alonso, M., Duran, C., Jiménez, P. J., Munné, A., & Prat, N. (2012). Regime shift from phytoplankton to macrophyte dominance in a large river: Top-down versus bottom-up effects. *Science of The Total Environment*, 416, 314–322. <https://doi.org/10.1016/j.scitotenv.2011.11.059>
- IPBES. (2022). *Methodological Assessment Report on the Diverse Values and Valuation of Nature of the Intergovernmental Science-Policy Platform on Biodiversity and Ecosystem Services* (P. Balvanera, U. Pascual, M. Christie, B. Baptiste, & D. González-Jiménez, Eds.; tech. rep.). IPBES. Bonn, Germany. <https://doi.org/10.5281/zenodo.6522522>
- Itzkin, M., Moore, L. J., Ruggiero, P., Hovenga, P. A., & Hacker, S. D. (2022). Combining process-based and data-driven approaches to forecast beach and dune change. *Environmental Modelling and Software*, 153, 105404. <https://doi.org/10.1016/j.envsoft.2022.105404>
- Jafarzadegan, K., Moradkhani, H., Pappenberger, F., Moftakhari, H., Bates, P., Abbaszadeh, P., Marsooli, R., Ferreira, C., Cloke, H. L., Ogden, F., & Duan, Q. (2023). Recent advances and new frontiers in riverine and coastal flood modeling. *Reviews of Geophysics*, 61(2), e2022RG000788. <https://doi.org/10.1029/2022RG000788>
- Jay, D. A., & Musiak, J. D. (1994). Particle trapping in estuarine tidal flows. *Journal of Geophysical Research: Oceans*, 99(C10), 20445–20461. <https://doi.org/10.1029/94JC00971>
- Jebara, T. (2004). *Machine Learning: Discriminative and Generative* (1st). Springer Science+Business Media New York. <https://doi.org/10.1007/978-1-4419-9011-2>
- Johnson, B. H., Boyd, M. B., & Keulegan, G. H. (1987). *A Mathematical Study of the Impact on Salinity Intrusion of Deepening the Lower Mississippi River Navigation Channel* (tech. rep.). Hydraulic Laboratory, US Army Engineer Waterways Experiment Station. Vicksburg, MS, USA.
- Johnston, M. A., Hickerson, E. L., Nuttall, M. F., Blakeway, R. D., Sterne, T. K., Eckert, R. J., & Schmahl, G. P. (2019). Coral bleaching and recovery from 2016 to 2017 at East and West Flower Garden Banks, Gulf of Mexico. *Coral Reefs*, 38, 787–799. <https://doi.org/10.1007/s00338-019-01788-7>
- Jones, E. R., Bierkens, M. F. P., & van Vliet, M. T. H. (2024). Current and future global water scarcity intensifies when accounting for surface water quality. *Nature Climate Change*, 1–7. <https://doi.org/10.1038/s41558-024-02007-0>
- Jones, E. R., Bierkens, M. F. P., Wanders, N., Sutanudjaja, E. H., van Beek, L. P. H., & van Vliet, M. T. H. (2023). DynQual v1.0: a high-resolution global surface water quality model. *Geoscientific Model Development*, 16(15), 4481–4500. <https://doi.org/10.5194/gmd-16-4481-2023>
- Jongbloed, H., Schuttelaars, H. M., Dijkstra, Y. M., Donkers, P. B., & Hoitink, A. J. F. (2022). Influence of wind on subtidal salt intrusion and stratification in well-mixed and partially stratified estuaries. *Journal of Physical Oceanography*, 52(12), 3139–3158. <https://doi.org/10.1175/JPO-D-21-0291.1>
- Jongman, B., Ward, P. J., & Aerts, J. C. (2012). Global exposure to river and coastal flooding: Long term trends and changes. *Global Environmental Change*, 22(4), 823–835. <https://doi.org/10.1016/j.gloenvcha.2012.07.004>
- Katsman, C. A., Sterl, A., Beersma, J. J., van den Brink, H. W., Church, J. A., Hazeleger, W., Kopp, R. E., Kroon, D., Kwadijk, J., Lammensen, R., Lowe, J., Oppenheimer, M., Plag, H. P., Ridley, J., von Storch, H., Vaughan, D. G., Vellinga, P., Vermeersen, L. L. A., van de Wal, R. S. W., & Weisse, R. (2011). Exploring high-end scenarios for local sea level rise to develop flood protection strategies for a low-lying delta—the Netherlands as an example. *Climatic Change*, 109(3-4), 617–645. <https://doi.org/10.1007/s10584-011-0037-5>
- Keen, S. (2021). The appallingly bad neoclassical economics of climate change. *Globalizations*, 18(7), 1149–1177. <https://doi.org/10.1080/14747731.2020.1807856>
- Keen, S., Lenton, T. M., Garrett, T. J., Rae, J. W. B., Hanley, B. P., & Grasselli, M. (2022). Estimates of economic and environmental damages from tipping points cannot be reconciled with the scientific literature. *Proceedings of the National Academy of Sciences*, 119(21). <https://doi.org/10.1073/pnas.2117308119>

- Keeney, R. L., & Raiffa, H. (1993, July). *Decisions with Multiple Objectives*. Cambridge University Press. <https://doi.org/10.1017/cbo9781139174084>
- Kennard, R. W., & Stone, L. A. (1969). Computer aided design of experiments. *Technometrics*, 11(1), 137–148. <https://doi.org/10.1080/00401706.1969.10490666>
- Kernkamp, H. W. J., Van Dam, A., Stelling, G. S., & de Goede, E. D. (2011). Efficient scheme for the shallow water equations on unstructured grids with application to the Continental Shelf. *Ocean Dynamics*, 61(8), 1175–1188. <https://doi.org/10.1007/s10236-011-0423-6>
- Kjerfve, B. (1978). Bathymetry as an indicator of net circulation in well mixed estuaries. *Limnology and Oceanography*, 23(4), 816–821. <https://doi.org/10.4319/lo.1978.23.4.0816>
- Klijn, F., van Buuren, M., & van Rooij, S. A. M. (2004). Flood-risk management strategies for an uncertain future: Living with Rhine River floods in the Netherlands? *AMBIO: A Journal of the Human Environment*, 33(3), 141–147. <https://doi.org/10.1579/0044-7447-33.3.141>
- Klijn, F., van Velzen, E., ter Maat, J., & Hunink, J. (2012). *Zoetwatervoorziening in Nederland: Aangescherpte landelijke knelpuntenanalyse 21e eeuw* (tech. rep.). Deltares, Delft, the Netherlands.
- Knutson, T. R., McBride, J. L., Chan, J., Emanuel, K. A., Holland, G., Landsea, C., Held, I., Kossin, J. P., Srivastava, K., & Sugi, M. (2010). Tropical cyclones and climate change. *Nature Geoscience*, 3, 157–163. <https://doi.org/10.1038/ngeo779>
- Kohonen, T. (1982). Self-organized formation of topologically correct feature maps. *Biological Cybernetics*, 43(1), 59–69. <https://doi.org/10.1007/BF00337288>
- Kotz, M., Levermann, A., & Wenz, L. (2024). The economic commitment of climate change. *Nature*, 628(8008), 551–557. <https://doi.org/10.1038/s41586-024-07219-0>
- Kragtwijk, N. G., Zitman, T. J., Stive, M. J. F., & Wang, Z. B. (2004). Morphological response of tidal basins to human interventions. *Coastal Engineering*, 51(3), 207–221. <https://doi.org/10.1016/j.coastaleng.2003.12.008>
- Kranenburg, C. (1986). A time scale for long-term salt intrusion in well-mixed estuaries. *Journal of Physical Oceanography*, 16(7), 1329–1331. [https://doi.org/10.1175/1520-0485\(1986\)016<1329:ATSFLT>2.0.CO;2](https://doi.org/10.1175/1520-0485(1986)016<1329:ATSFLT>2.0.CO;2)
- Kranenburg, W., van der Kaaij, T., Tiessen, M., Friocourt, Y., & Blaas, M. (2022). Salt intrusion in the Rhine Meuse Delta: Estuarine circulation, tidal dispersion or surge effect. *Proceedings of the 39th IAHR World Congress*, (June), 5601–5608. <https://doi.org/10.3850/IAHR-39WC2521711920221058>
- Kranenburg, W. M., Tiessen, M. C. H., Blaas, M., & Van Veen, N. P. (2023). Circulation, stratification and salt dispersion in a former estuary after reintroducing seawater inflow. *Estuarine, Coastal and Shelf Science*, 282, 108221. <https://doi.org/10.1016/j.ecss.2023.108221>
- Kranenburg, W. M., van der Kaaij, T., & Nolte, A. J. (2015). *Evaluatie van het OSR-model voor zoutindringing in de Rijn-Maasmonding (II)* (tech. rep.). Deltares, Delft, the Netherlands. <https://publications.deltares.nl/1220070-000b.pdf>
- Kroeger, K. D., Crooks, S., Moseman-Valtierra, S., & Tang, J. (2017). Restoring tides to reduce methane emissions in impounded wetlands: A new and potent Blue Carbon climate change intervention. *Scientific Reports*, 7(1), 11914. <https://doi.org/10.1038/s41598-017-12138-4>
- Kubicek, A., Breckling, B., Hoegh-Guldberg, O., & Reuter, H. (2019). Climate change drives trait-shifts in coral reef communities. *Scientific Reports*, 9(1), 3721. <https://doi.org/10.1038/s41598-019-38962-4>
- Kuijper, K., & van Rijn, L. C. (2011). Analytical and numerical analysis of tides and salinities in estuaries; Part II: Salinity distributions in prismatic and convergent tidal channels. *Ocean Dynamics*, 61(11), 1743–1765. <https://doi.org/10.1007/s10236-011-0454-z>
- Kumar, S., Lawrence, D. M., Dirmeyer, P. A., & Sheffield, J. (2013). Less reliable water availability in the 21st century climate projections. *Earth's Future*, 2(3), 152–160. <https://doi.org/10.1002/2013EF000159>
- Kwakkel, J. H., Haasnoot, M., & Walker, W. E. (2015). Developing dynamic adaptive policy pathways: A computer-assisted approach for developing adaptive strategies for a deeply uncertain world. *Climatic Change*, 132(3), 373–386. <https://doi.org/10.1007/s10584-014-1210-4>
- Kwakkel, J. H., Haasnoot, M., & Walker, W. E. (2016). Comparing robust decision-making and dynamic adaptive policy pathways for model-based decision support under

- deep uncertainty. *Environmental Modelling & Software*, 86, 168–183. <https://doi.org/10.1016/j.envsoft.2016.09.017>
- Laan, S., Huismans, Y., Rodrigo, S., Leumens, L., & Kranenburg, W. (2023). *Effect bodemligging op verzilting Nieuwe Waterweg, Nieuwe Maas en Lek ten behoeve van de Basisrieverbodemligging (BRL)* (tech. rep.). Deltares, Delft, the Netherlands. <https://publications.deltares.nl/11208075.010.0001.pdf>
- Landuyt, D., Broekx, S., D'hondt, R., Engelen, G., Aertsens, J., & Goethals, P. L. M. (2013). A review of Bayesian belief networks in ecosystem service modelling. *Environmental Modelling and Software*, 46, 1–11. <https://doi.org/10.1016/j.envsoft.2013.03.011>
- Laporte-Fauret, Q., Castelle, B., Marieu, V., Nicolae-Lerma, A., & Rosebery, D. (2022). Foredune blowout formation and subsequent evolution along a chronically eroding high-energy coast. *Geomorphology*, 414(August), 108398. <https://doi.org/10.1016/j.geomorph.2022.108398>
- Latteux, B. (1995). Techniques for long-term morphological simulation under tidal action. *Marine Geology*, 126(1-4), 129–141. [https://doi.org/10.1016/0025-3227\(95\)00069-B](https://doi.org/10.1016/0025-3227(95)00069-B)
- Lee, J., Biemond, B., de Swart, H., & Dijkstra, H. A. (2024). Increasing risks of extreme salt intrusion events across European estuaries in a warming climate. *Communications Earth & Environment*, 5(1), 60. <https://doi.org/10.1038/s43247-024-01225-w>
- Leijnse, T., van Ormondt, M., Nederhoff, K., & van Dongeren, A. (2021). Modeling compound flooding in coastal systems using a computationally efficient reduced-physics solver: Including fluvial, pluvial, tidal, wind- and wave-driven processes. *Coastal Engineering*, 163(December 2019), 103796. <https://doi.org/10.1016/j.coastaleng.2020.103796>
- Lempert, R., Popper, S., & Banks, S. (2003, April). *Shaping the Next One Hundred Years: New Methods for Quantitative, Long-Term Policy Analysis*. RAND Corporation. <https://doi.org/10.7249/MR1626>
- Lenton, T. M., Rockström, J., Gaffney, O., Rahmstorf, S., Richardson, K., Steffen, W., & Schellnhuber, H. J. (2019). Climate tipping points — too risky to bet against. *Nature*, 575(7784), 592–595. <https://doi.org/10.1038/d41586-019-03595-0>
- Lerczak, J. A., & Geyer, W. R. (2004). Modeling the lateral circulation in straight, stratified estuaries. *Journal of Physical Oceanography*, 34(6), 1410–1428. [https://doi.org/10.1175/1520-0485\(2004\)034\(1410:MTLCLIS\)2.0.CO;2](https://doi.org/10.1175/1520-0485(2004)034(1410:MTLCLIS)2.0.CO;2)
- Lerczak, J. A., Geyer, W. R., & Chant, R. J. (2006). Mechanisms driving the time-dependent salt flux in a partially stratified estuary. *Journal of Physical Oceanography*, 36(12), 2296–2311. <https://doi.org/10.1175/JPO2959.1>
- Lerczak, J. A., Geyer, W. R., & Ralston, D. K. (2009). The temporal response of the length of a partially stratified estuary to changes in river flow and tidal amplitude. *Journal of Physical Oceanography*, 39(4), 915–933. <https://doi.org/10.1175/2008JPO3933.1>
- Letten, A. D., Dhami, M. K., Ke, P.-J., & Fukami, T. (2018). Species coexistence through simultaneous fluctuation-dependent mechanisms. *Proceedings of the National Academy of Sciences*, 115(26), 6745–6750. <https://doi.org/10.1073/pnas.1801846115>
- Leuven, J. R. F. W., Pierik, H. J., van der Vegt, M., Bouma, T. J., & Kleinhans, M. G. (2019). Sea-level-rise-induced threats depend on the size of tide-influenced estuaries worldwide. *Nature Climate Change*, 9(12), 986–992. <https://doi.org/10.1038/s41558-019-0608-4>
- Leuven, J. R. F. W., van Maanen, B., Lexmond, B. R., van der Hoek, B. V., Spruijt, M. J., & Kleinhans, M. G. (2018a). Dimensions of fluvial-tidal meanders: Are they disproportionately large? *Geology*, 46(10), 923–926. <https://doi.org/10.1130/G45144.1>
- Leuven, J. R. F. W., Verhoeve, S. L., van Dijk, W. M., Selaković, S., & Kleinhans, M. G. (2018b). Empirical assessment tool for bathymetry, flow velocity and salinity in estuaries based on tidal amplitude and remotely-sensed imagery. *Remote Sensing*, 10(12). <https://doi.org/10.3390/rs10121915>
- Limberger, R., Daugaard, U., Gupta, A., Krug, R. M., Lemmen, K. D., van Moorsel, S. J., Suleiman, M., Zuppinger-Dingley, D., & Petchev, O. L. (2023). Functional diversity can facilitate the collapse of an undesirable ecosystem state. *Ecology Letters*, 26(6), 883–895. <https://doi.org/10.1111/ele.14217>
- Liquete, C., Piroddi, C., Drakou, E. G., Gurney, L., Katsanevakis, S., Charef, A., & Egoh, B. (2013). Current status and future prospects for the assessment of marine and coastal ecosystem services: A systematic review (S. J. Bograd, Ed.). *PLoS ONE*, 8(7), e67737. <https://doi.org/10.1371/journal.pone.0067737>

- Little, S., Lewis, J. P., & Pietkiewicz, H. (2022). Defining estuarine squeeze: The loss of upper estuarine transitional zones against in-channel barriers through saline intrusion. *Estuarine, Coastal and Shelf Science*, *278*, 108107. <https://doi.org/10.1016/j.ecss.2022.108107>
- Logan, C. A., Dunne, J. P., Eakin, C. M., & Donner, S. D. (2014). Incorporating adaptive responses into future projections of coral bleaching. *Global Change Biology*, *20*(1), 125–139. <https://doi.org/10.1111/gcb.12390>
- Loreau, M., Naeem, S., Inchausti, P., Bengtsson, J., Grime, J. P., Hector, A., Hooper, D. U., Huston, M. A., Raffaelli, D., Schmid, B., Tilman, D., & Wardle, D. A. (2001). Biodiversity and ecosystem functioning: Current knowledge and future challenges. *Science*, *294*(5543), 804–808. <https://doi.org/10.1126/science.1064088>
- Loreau, M., Mouquet, N., & Gonzalez, A. (2003). Biodiversity as spatial insurance in heterogeneous landscapes. *Proceedings of the National Academy of Sciences of the United States of America*, *100*(22), 12765–12770. <https://doi.org/10.1073/pnas.2235465100>
- Lowe, J., & Gregory, J. (2005). The effects of climate change on storm surges around the United Kingdom. *Philosophical Transactions of the Royal Society A: Mathematical, Physical and Engineering Sciences*, *363*(1831), 1313–1328. <https://doi.org/10.1098/rsta.2005.1570>
- Luijendijk, A., Hagenaaars, G., Ranasinghe, R., Baart, F., Donchyts, G., & Aarninkhof, S. (2018). The state of the world's beaches. *Scientific Reports*, *8*(1), 6641. <https://doi.org/10.1038/s41598-018-24630-6>
- Luijendijk, A. P., de Schipper, M. A., & Ranasinghe, R. (2019). Morphodynamic acceleration techniques for multi-timescale predictions of complex sandy interventions. *Journal of Marine Science and Engineering*, *7*(3), 78. <https://doi.org/10.3390/jmse7030078>
- Lyu, H., & Zhu, J. (2019). Impacts of tidal flat reclamation on saltwater intrusion and freshwater resources in the Changjiang estuary. *Journal of Coastal Research*, *35*(2), 314–321. <https://doi.org/10.2112/JCOASTRES-D-18-00077.1>
- MacCready, P. (1999). Estuarine adjustment to changes in river flow and tidal mixing. *Journal of Physical Oceanography*, *29*(4), 708–726. [https://doi.org/10.1175/1520-0485\(1999\)029<0708:EATCIR>2.0.CO;2](https://doi.org/10.1175/1520-0485(1999)029<0708:EATCIR>2.0.CO;2)
- MacCready, P. (2007). Estuarine adjustment. *Journal of Physical Oceanography*, *37*(8), 2133–2145. <https://doi.org/10.1175/JPO3082.1>
- MacCready, P., & Geyer, W. R. (2010). Advances in estuarine physics. *Annual Review of Marine Science*, *2*(1), 35–58. <https://doi.org/10.1146/annurev-marine-120308-081015>
- MacKay, D. J. C. (1992). Information-based objective functions for active data selection. *Neural Computation*, *4*(4), 590–604. <https://doi.org/10.1162/neco.1992.4.4.590>
- MacVean, L. J., & Stacey, M. T. (2011). Estuarine dispersion from tidal trapping: A new analytical framework. *Estuaries and Coasts*, *34*(1), 45–59. <https://doi.org/10.1007/s12237-010-9298-x>
- Mansur, M., Hopkins, J., & Chen, Q. (2023). Estuarine response to storm surge and sea-level rise associated with channel deepening: a flood vulnerability assessment of southwest Louisiana, USA. *Natural Hazards*, *116*(3), 3879–3897. <https://doi.org/10.1007/s11069-023-05841-1>
- Marchau, V. A. W. J., Walker, W. E., Bloemen, P. J. T. M., & Popper, S. W. (Eds.). (2019). *Decision Making under Deep Uncertainty: From Theory to Practice*. Springer International Publishing. <https://doi.org/10.1007/978-3-030-05252-2>
- Martín-Llanes, G., & López-Ruiz, A. (2024). The role of estuarine convergence on the salinity distribution and the estuary response to short river discharge pulses. *Estuarine, Coastal and Shelf Science*, *306*, 108893. <https://doi.org/10.1016/j.ecss.2024.108893>
- Maul, G. A., & Duedall, I. W. (2019). Demography of Coastal Populations. In C. W. Finkl & C. Makowski (Eds.), *Encyclopedia of coastal science* (pp. 692–700). Springer International Publishing. https://doi.org/10.1007/978-3-319-93806-6_{\}}115
- McInerney, D., Lempert, R., & Keller, K. (2012). What are robust strategies in the face of uncertain climate threshold responses? *Climatic Change*, *112*(3-4), 547–568. <https://doi.org/10.1007/s10584-011-0377-1>
- McKay, M. D., Beckman, R. J., & Conover, W. J. (1979). A comparison of three methods for selecting values of input variables in the analysis of output from a computer code. *Technometrics*, *21*(2), 239–245. <https://doi.org/10.1080/00401706.2000.10485979>

- Medeiros, J. P., Chaves, M. L., Silva, G., Azeda, C., Costa, J. L., Marques, J. C., Costa, M. J., & Chainho, P. (2012). Benthic condition in low salinity areas of the Mira estuary (Portugal): Lessons learnt from freshwater and marine assessment tools. *Ecological Indicators*, *19*, 79–88. <https://doi.org/10.1016/j.ecolind.2011.09.008>
- Mekonnen, M. M., & Hoekstra, A. Y. (2016). Sustainability: Four billion people facing severe water scarcity. *Science Advances*, *2*(2). <https://doi.org/10.1126/sciadv.1500323>
- Mendez, F. J., & Losada, I. J. (2004). An empirical model to estimate the propagation of random breaking and nonbreaking waves over vegetation fields. *Coastal Engineering*, *51*(2), 103–118. <https://doi.org/10.1016/j.coastaleng.2003.11.003>
- Méndez, F. J., Menéndez, M., Luceño, A., & Losada, I. J. (2006). Estimation of the long-term variability of extreme significant wave height using a time-dependent Peak Over Threshold (POT) model. *Journal of Geophysical Research: Oceans*, *111*(C7), C07024. <https://doi.org/10.1029/2005JC003344>
- Mestdagh, S., Fang, X., Soetaert, K., Ysebaert, T., Moens, T., & Van Colen, C. (2020). Seasonal variability in ecosystem functioning across estuarine gradients: The role of sediment communities and ecosystem processes. *Marine Environmental Research*, *162*, 105096. <https://doi.org/10.1016/j.marenvres.2020.105096>
- Meyers, S. D., Yilmaz, Y., & Luther, M. E. (2022). Some methods for addressing errors in static AIS data records. *Ocean Engineering*, *264*, 112367. <https://doi.org/10.1016/j.oceaneng.2022.112367>
- Miettinen, K. (1998). A Posteriori Methods. In *Nonlinear multiobjective optimization* (pp. 77–113). Springer, Boston, MA. https://doi.org/10.1007/978-1-4615-5563-6_{-}4
- Miller, P. W., & Hiatt, M. (2024). Hydrometeorological drivers of the 2023 Louisiana water crisis. *Geophysical Research Letters*, *51*(10), e2024GL108545. <https://doi.org/10.1029/2024GL108545>
- Millner, A., & McDermott, T. K. J. (2016). Model confirmation in climate economics. *Proceedings of the National Academy of Sciences*, *113*(31), 8675–8680. <https://doi.org/10.1073/pnas.1604121113>
- Milly, P. C. D., Betancourt, J., Falkenmark, M., Hirsch, R. M., Kundzewicz, Z. W., Lettenmaier, D. P., & Stouffer, R. J. (2008). Stationarity is dead: Whither water management? *Science*, *319*(5863), 573–574. <https://doi.org/10.1126/science.1151915>
- Ministry of Infrastructure and Water Management. (2022, November 25). *Water en bodem sturend* [IENW/BSK-2022/283041].
- Monismith, S. G. (2017). An integral model of unsteady salinity intrusion in estuaries. *Journal of Hydraulic Research*, *55*(3), 392–408. <https://doi.org/10.1080/00221686.2016.1274682>
- Monismith, S. G., Kimmerer, W., Burau, J. R., & Stacey, M. T. (2002). Structure and flow-induced variability of the subtidal salinity field in northern San Francisco Bay. *Journal of Physical Oceanography*, *32*(11), 3003–3019. [https://doi.org/10.1175/1520-0485\(2002\)032\(3003:SAFIVO\)2.0.CO;2](https://doi.org/10.1175/1520-0485(2002)032(3003:SAFIVO)2.0.CO;2)
- Moore, F. C., & Diaz, D. B. (2015). Temperature impacts on economic growth warrant stringent mitigation policy. *Nature Climate Change*, *5*(2), 127–131. <https://doi.org/10.1038/nclimate2481>
- Morris, R. K. A. (2013). Geomorphological analogues for large estuarine engineering projects: A case study of barrages, causeways and tidal energy projects. *Ocean & Coastal Management*, *79*, 52–61. <https://doi.org/10.1016/j.ocecoaman.2012.05.010>
- Mulder, J. P., Hommes, S., & Horstman, E. M. (2011). Implementation of coastal erosion management in the Netherlands. *Ocean and Coastal Management*, *54*(12), 888–897. <https://doi.org/10.1016/j.ocecoaman.2011.06.009>
- Mulla, A. J., Denis, V., Lin, C.-H., Fong, C.-L., Shiu, J.-H., & Nozawa, Y. (2024). Natural coral recovery despite negative population growth. *Ecology*, *105*(9), e4368. <https://doi.org/10.1002/ecy.4368>
- Muller, J. Z. (2021). The perils of metric fixation. *Medical teacher*, *43*(6), 622–624. <https://doi.org/10.1080/0142159X.2020.1840745>
- Neumann, B., Vafeidis, A. T., Zimmermann, J., & Nicholls, R. J. (2015). Future coastal population growth and exposure to sea-level rise and coastal flooding - A global assessment. *PLOS ONE*, *10*(3), e0118571. <https://doi.org/10.1371/journal.pone.0118571>
- Nguyen, V. T., & Le, V. A. (2023). Fluid mud properties and nautical depth estimation: A case study in navigation channel of Duyen Hai Port, Vietnam. *Ocean Engineering*, *284*, 115163. <https://doi.org/10.1016/j.oceaneng.2023.115163>
- Nicholls, R. J., & Cazenave, A. (2010). Sea-level rise and its impact on coastal zones. *Science*,

- 328(5985), 1517–1520. <https://doi.org/10.1126/science.1185782>
- Nicholls, R. J., Marinova, N., Lowe, J. A., Brown, S., Vellinga, P., de Gusmão, D., Hinkel, J., & Tol, R. S. J. (2011). Sea-level rise and its possible impacts given a ‘beyond 4 oC world’ in the twenty-first century. *Philosophical Transactions of the Royal Society A: Mathematical, Physical and Engineering Sciences*, 369(1934), 161–181. <https://doi.org/10.1098/rsta.2010.0291>
- Nidzietko, N. J., & Ralston, D. K. (2012). Tidal asymmetry and velocity skew over tidal flats and shallow channels within a macrotidal river delta. *Journal of Geophysical Research: Oceans*, 117(3), C03001. <https://doi.org/10.1029/2011JC007384>
- Nienhuis, P. H., & Smaal, A. C. (1994). The Oosterschelde estuary, a case-study of a changing ecosystem: An introduction. *Hydrobiologia*, 282–283(1), 1–14. <https://doi.org/10.1007/BF00024616>
- Nnafie, A., de Swart, H. E., De Maerschalck, B., Van Oyen, T., van der Vegt, M., & van der Wegen, M. (2019). Closure of secondary basins causes channel deepening in estuaries with moderate to high friction. *Geophysical Research Letters*, 46(22), 13209–13216. <https://doi.org/10.1029/2019GL084444>
- Nordhaus, W. D. (1992). An optimal transition path for controlling greenhouse gases. *Science*, 258(5086), 1315–1319. <https://doi.org/10.1126/science.258.5086.1315>
- Nordhaus, W. D. (2018). Projections and uncertainties about climate change in an era of minimal climate policies. *American Economic Journal: Economic Policy*, 10(3), 333–360. <https://doi.org/10.1257/pol.20170046>
- Nordhaus, W. D. (2019). Economics of the disintegration of the Greenland ice sheet. *Proceedings of the National Academy of Sciences*, 116(25), 12261–12269. <https://doi.org/10.1073/pnas.1814990116>
- Nunes, R. A., & Simpson, J. H. (1985). Axial convergence in a well-mixed estuary. *Estuarine, Coastal and Shelf Science*, 20(5), 637–649. [https://doi.org/10.1016/0272-7714\(85\)90112-X](https://doi.org/10.1016/0272-7714(85)90112-X)
- Okubo, A. (1973). Effect of shoreline irregularities on streamwise dispersion in estuaries and other embayments. *Netherlands Journal of Sea Research*, 6(1-2), 213–224. [https://doi.org/10.1016/0077-7579\(73\)90014-8](https://doi.org/10.1016/0077-7579(73)90014-8)
- Olabarrieta, M., Geyer, W. R., Coco, G., Friedrichs, C. T., & Cao, Z. (2018). Effects of density-driven flows on the long-term morphodynamic evolution of funnel-shaped estuaries. *Journal of Geophysical Research: Earth Surface*, 123(11), 2901–2924. <https://doi.org/10.1029/2017JF004527>
- Onchi-Ramos, K., Rodríguez-Cuevas, C., Couder-Castañeda, C., & Padilla-Pérez, D.-A. (2024). Flood risk assessment of the Garita River in the urban zone of San Luis Potosí City, by hydrodynamic modeling. *Scientific Reports*, 14(1), 15891. <https://doi.org/10.1038/s41598-024-66743-1>
- Opperman, J. J., Galloway, G. E., Fargione, J., Mount, J. F., Richter, B. D., & Secchi, S. (2009). Sustainable floodplains through large-scale reconnection to rivers. *Science*, 326(5959), 1487–1488. <https://doi.org/10.1126/science.1178256>
- Orton, P., Ralston, D., van Prooijen, B., Secor, D., Ganju, N., Chen, Z., Fernald, S., Brooks, B., & Marcell, K. (2023). Increased utilization of storm surge barriers: A research agenda on estuary impacts. *Earth's Future*, 11, e2022EF002991. <https://doi.org/10.1029/2022EF002991>
- Ourloglou, O., Stefanidis, K., & Dimitriou, E. (2020). Assessing nature-based and classical engineering solutions for flood-risk reduction in urban streams. *Journal of Ecological Engineering*, 21(2), 46–56. <https://doi.org/10.12911/22998993/116349>
- Paprotny, D., Sebastian, A., Morales-Nápoles, O., & Jonkman, S. N. (2018). Trends in flood losses in Europe over the past 150 years. *Nature Communications*, 9(1), 1985. <https://doi.org/10.1038/s41467-018-04253-1>
- Paree, E. (2021). *Toelichting op de zoute ecotopenkaart Westerschelde 2020: Biologische monitoring zoute rijkswateren* (tech. rep.). Rijkswaterstaat. Rotterdam, the Netherlands. <https://puc.overheid.nl/rijkswaterstaat/doc/PUC.642216.31/1/>
- Pearson, S. G., Storlazzi, C. D., van Dongeren, A. R., Tissier, M. F. S., & Reniers, A. J. H. M. (2017a). BEWARE database: A Bayesian-based system to assess wave-driven flooding hazards on coral reef-lined coasts. <https://doi.org/10.5066/F7T43S20>
- Pearson, S. G., Storlazzi, C. D., van Dongeren, A. R., Tissier, M. F. S., & Reniers, A. J. H. M. (2017b). A Bayesian-based system to assess wave-driven flooding hazards on coral reef-lined coasts. *Journal of Geophysical Research: Oceans*, 122(12), 10099–10117. <https://doi.org/10.1002/2017JC013204>
- Pein, J., Valle-Levinson, A., & Stanev, E. V. (2018). Secondary circulation asymmetry in

- a meandering, partially stratified estuary. *Journal of Geophysical Research: Oceans*, 123(3), 1670–1683. <https://doi.org/10.1002/2016JC012623>
- Perk, L., van Rijn, L. C., Koudstaal, K., & Fordeyn, J. (2019). A rational method for the design of sand dike/dune systems at sheltered sites; Wadden Sea coast of Texel, The Netherlands. *Journal of Marine Science and Engineering*, 7(9), 324. <https://doi.org/10.3390/jmse7090324>
- Perry, C. T., Alvarez-Filip, L., Graham, N. A. J., Mumby, P. J., Wilson, S. K., Kench, P. S., Manzello, D. P., Morgan, K. M., Slangen, A. B. A., Thomson, D. P., Januchowski-Hartley, F., Smithers, S. G., Steneck, R. S., Carlton, R., Edinger, E. N., Enochs, I. C., Estrada-Saldívar, N., Hayward, M. D. E., Kolodziej, G., ... MacDonald, C. (2018). Loss of coral reef growth capacity to track future increases in sea level. *Nature*, 558(7710), 396–400. <https://doi.org/10.1038/s41586-018-0194-z>
- Pham, T. V., Thi Do, T. A., Tran, H. D., & Thi Do, A. N. (2024). Assessing groundwater potential for mitigating salinity issues in agricultural areas of southern Dong Nai province, Vietnam. *Groundwater for Sustainable Development*, 25, 101177. <https://doi.org/10.1016/j.gsd.2024.101177>
- Pielou, E. C. (1966). The measurement of diversity in different types of biological collections. *Journal of Theoretical Biology*, 13(100), 131–144. [https://doi.org/10.1016/0022-5193\(66\)90013-0](https://doi.org/10.1016/0022-5193(66)90013-0)
- Pindyck, R. S. (2017). The use and misuse of models for climate policy. *Review of Environmental Economics and Policy*, 11(1), 100–114. <https://doi.org/10.1093/reep/rew012>
- Pont, D., Day, J. W., Hensel, P., Franquet, E., Torre, F., Rioual, P., Ibáñez, C., & Coulet, E. (2002). Response scenarios for the deltaic plain of the Rhône in the face of an acceleration in the rate of sea-level rise with special attention to Salicornia-type environments. *Estuaries*, 25(3), 337–358. <https://doi.org/10.1007/BF02695978>
- Port of Rotterdam. (2024). *Throughput Port of Rotterdam* (tech. rep.). Port of Rotterdam, Rotterdam, the Netherlands.
- Pörtner, H.-O., Scholes, R. J., Arneith, A., Barnes, D. K. A., Burrows, M. T., Diamond, S. E., Duarte, C. M., Kiessling, W., Leadley, P., Managi, S., McElwee, P., Midgley, G., Ngo, H. T., Obura, D., Pascual, U., Sankaran, M., Shin, Y. J., & Val, A. L. (2023). Overcoming the coupled climate and biodiversity crises and their societal impacts. *Science*, 380(6642). <https://doi.org/10.1126/science.abl4881>
- Pourteimouri, P., den Haan, R.-J., Kwadijk, J., & van der Voort, M. (2024). Developing an integrated assessment model for salt intrusion mitigation measures in delta systems. In I. Niesten, N. Tahsin, D. van Grootheest, H. Barneveld, K. Waldschläger, & T. Hoitink (Eds.), *Ncr days* (pp. 113–114). Netherlands Centre for River Studies.
- Prandle, D., & Rahman, M. M. (1980). Tidal response in estuaries. *Journal of Physical Oceanography*, 10, 1552–1573. [https://doi.org/10.1175/1520-0485\(1980\)010<1552:TRIE>2.0.CO;2](https://doi.org/10.1175/1520-0485(1980)010<1552:TRIE>2.0.CO;2)
- Pye, K., & Blott, S. J. (2017). Evolution of a sediment-starved, over-stabilised dunefield: Kenfig Burrows, South Wales, UK. *Journal of Coastal Conservation*, 21(5), 685–717. <https://doi.org/10.1007/s11852-017-0506-8>
- Radfar, S., Galiatsatou, P., & Wahl, T. (2023). Application of nonstationary extreme value analysis in the coastal environment – A systematic literature review. *Weather and Climate Extremes*, 41, 100575. <https://doi.org/10.1016/j.wace.2023.100575>
- Ragno, E., AghaKouchak, A., Cheng, L., & Sadegh, M. (2019). A generalized framework for process-informed nonstationary extreme value analysis. *Advances in Water Resources*, 130, 270–282. <https://doi.org/10.1016/j.advwatres.2019.06.007>
- Ralston, D. K. (2022). Impacts of storm surge barriers on drag, mixing, and exchange flow in a partially mixed estuary. *Journal of Geophysical Research: Oceans*, 127(4), 1–21. <https://doi.org/10.1029/2021JC018246>
- Ralston, D. K., & Geyer, W. R. (2019). Response to channel deepening of the salinity intrusion, estuarine circulation, and stratification in an urbanized estuary. *Journal of Geophysical Research: Oceans*, 124(7), 4784–4802. <https://doi.org/10.1029/2019JC015006>
- Ralston, D. K., Geyer, W. R., & Lerczak, J. A. (2008). Subtidal salinity and velocity in the Hudson River estuary: Observations and modeling. *Journal of Physical Oceanography*, 38(4), 753–770. <https://doi.org/10.1175/2007JPO3808.1>
- Ralston, D. K., Geyer, W. R., & Lerczak, J. A. (2010a). Structure, variability, and salt flux in a strongly forced salt wedge estuary. *Journal of Geophysical Research: Oceans*,

- 115(C6), C06005. <https://doi.org/10.1029/2009JC005806>
- Ralston, D. K., Geyer, W. R., Lerczak, J. A., & Scully, M. E. (2010b). Turbulent mixing in a strongly forced salt wedge estuary. *Journal of Geophysical Research: Oceans*, 115(12), C12024. <https://doi.org/10.1029/2009JC006061>
- Rangel-Buitrago, N., Gracia C, A., & Neal, W. J. (2023). Dune ecosystems along the central Caribbean coast of Colombia: Evolution, human influences, and conservation challenges. *Ocean & Coastal Management*, 243(June), 106767. <https://doi.org/10.1016/j.ocecoaman.2023.106767>
- Reed, D., van Wesenbeeck, B., Herman, P. M. J., & Meselhe, E. (2018). Tidal flat-wetland systems as flood defenses: Understanding biogeomorphic controls. *Estuarine, Coastal and Shelf Science*, 213, 269–282. <https://doi.org/10.1016/j.ecss.2018.08.017>
- Reis, J., & Shortridge, J. (2020). Impact of uncertainty parameter distribution on robust decision making outcomes for climate change adaptation under deep uncertainty. *Risk Analysis*, 40(3), 494–511. <https://doi.org/10.1111/risa.13405>
- Remane, A. (1934). Die Brackwasserfauna. *Verhandlungen Der Deutschen Zoologischen Gesellschaft*, 36, 34–74. <https://www.vliz.be/imisdocs/publications/ocrd/214770.pdf>
- Rijkswaterstaat. (2019). *Water Management in the Netherlands* (tech. rep.). Rijkswaterstaat.
- Rijkswaterstaat. (2023). *Watermanagementcentrum Nederland: Jaaroverzicht 2022* (tech. rep.). Watermanagementcentrum Nederland. Lelystad, the Netherlands.
- Robin, N., Billy, J., Nicolae Lerma, A., Castelle, B., Hesp, P. A., Rosebery, D., Fauny, C., Deparis, J., Marieu, V., Bouchet, C., & Miot da Silva, G. (2023). Natural remobilization and historical evolution of a modern coastal transgressive dunefield. *Earth Surface Processes and Landforms*, 48(5), 1064–1083. <https://doi.org/10.1002/esp.5535>
- Rockström, J., Gupta, J., Qin, D., Lade, S. J., Abrams, J. F., Andersen, L. S., Armstrong McKay, D. I., Bai, X., Bala, G., Bunn, S. E., Ciobanu, D., DeClerck, F., Ebi, K., Gifford, L., Gordon, C., Hasan, S., Kanie, N., Lenton, T. M., Loriani, S., . . . Zhang, X. (2023). Safe and just Earth system boundaries. *Nature*, 619(7968), 102–111. <https://doi.org/10.1038/s41586-023-06083-8>
- Rolls, R. J. (2011). The role of life-history and location of barriers to migration in the spatial distribution and conservation of fish assemblages in a coastal river system. *Biological Conservation*, 144(1), 339–349. <https://doi.org/10.1016/j.biocon.2010.09.011>
- Rosentreter, J. A., Borges, A. V., Deemer, B. R., Holgerson, M. A., Liu, S., Song, C., Melack, J., Raymond, P. A., Duarte, C. M., Allen, G. H., Olefeldt, D., Poulter, B., Battin, T. I., & Eyre, B. D. (2021). Half of global methane emissions come from highly variable aquatic ecosystem sources. *Nature Geoscience*, 14(4), 225–230. <https://doi.org/10.1038/s41561-021-00715-2>
- Rueda, A., Cagigal, L., Pearson, S. G., Antolínez, J. A. A., Storlazzi, C. D., van Dongeren, A. R., Camus, P., & Méndez, F. J. (2019). HyCReWW: A Hybrid Coral Reef Wave and Water level metamodel. *Computers and Geosciences*, 127, 85–90. <https://doi.org/10.1016/j.cageo.2019.03.004>
- Ruessink, B. G. (2006). A Bayesian estimation of parameter-induced uncertainty in a nearshore alongshore current model. *Journal of Hydroinformatics*, 8(1), 37–49. <https://doi.org/10.2166/jh.2006.009>
- Ruessink, B. G., Arens, S. M., Kuipers, M., & Donker, J. J. A. (2018). Coastal dune dynamics in response to excavated foredune notches. *Aeolian Research*, 31, 3–17. <https://doi.org/10.1016/j.aeolia.2017.07.002>
- Saccon, E., Hendrickx, G. G., Hulscher, S. J. M. H., Bouma, J., Tjeerd, & van de Koppel, J. (in review). Wetland topography drives salinity resilience in freshwater tidal ecosystems. *Ecological Engineering*.
- Saccon, E., Hendrickx, G. G., Hulscher, S. J. M. H., Bouma, T. J., & van de Koppel, J. (2024). Dataset underlying the study “Wetland topography drives salinity resilience in freshwater tidal ecosystems”. <https://doi.org/10.4121/93d8d223-e2ab-486e-a85b-da14789532d4>
- Saltelli, A. (2002). Making best use of model evaluations to compute sensitivity indices. *Computer Physics Communications*, 145(2), 280–297. [https://doi.org/10.1016/S0010-4655\(02\)00280-1](https://doi.org/10.1016/S0010-4655(02)00280-1)
- Saltelli, A., Ratto, M., Tarantola, S., & Campolongo, F. (2006). Sensitivity analysis practices: Strategies for model-based inference. *Reliability Engineering and System Safety*, 91(10–11), 1109–1125. <https://doi.org/10.1016/j.res.2005.11.014>
- Saltelli, A., Tarantola, S., & Chan, K. P. S. (1999). A quantitative model-independent

- method for global sensitivity analysis of model output. *Technometrics*, 41(1), 39–56. <https://doi.org/10.1080/00401706.1999.10485594>
- Savenije, H. H. G. (1989). Salt intrusion model for high-water slack, low-water slack, and mean tide on spread sheet. *Journal of Hydrology*, 107(1-4), 9–18. [https://doi.org/10.1016/0022-1694\(89\)90046-2](https://doi.org/10.1016/0022-1694(89)90046-2)
- Savenije, H. H. G. (1993). Predictive model for salt intrusion in estuaries. *Journal of Hydrology*, 148(1-4), 203–218. [https://doi.org/10.1016/0022-1694\(93\)90260-G](https://doi.org/10.1016/0022-1694(93)90260-G)
- Savenije, H. H. G., Toffolon, M., Haas, J., & Veling, E. J. M. (2008). Analytical description of tidal dynamics in convergent estuaries. *Journal of Geophysical Research: Oceans*, 113(C10). <https://doi.org/10.1029/2007JC004408>
- Savenije, H. H. G., & Veling, E. J. M. (2005). Relation between tidal damping and wave celerity in estuaries. *Journal of Geophysical Research: Oceans*, 110(C4), 1–10. <https://doi.org/10.1029/2004JC002278>
- Scheres, B., & Schüttrumpf, H. (2019). Enhancing the ecological value of sea dikes. *Water (Switzerland)*, 11(8), 1617. <https://doi.org/10.3390/w11081617>
- Schiff, J. B., & Schönfeld, J. C. (1953). Theoretical considerations on the motion of salt and freshwater. *Minnesota International Hydraulics Convention*, 321–333.
- Schulz, E., Schuttelaars, H. M., Gräwe, U., & Burchard, H. (2015). Impact of the depth-to-width ratio of periodically stratified tidal channels on the estuarine circulation. *Journal of Physical Oceanography*, 45(8), 2048–2069. <https://doi.org/10.1175/JPO-D-14-0084.1>
- Schwarz, C., Brinkkemper, J., & Ruessink, G. (2018). Feedbacks between biotic and abiotic processes governing the development of foredune blowouts: A review. *Journal of Marine Science and Engineering*, 7(1), 2. <https://doi.org/10.3390/jmse7010002>
- Scott, F., Antolínez, J. A. A., McCall, R. T., Storlazzi, C. D., Reniers, A. J. H. M., & Pearson, S. G. (2020). Hydro-morphological characterization of coral reefs for wave runup prediction. *Frontiers in Marine Science*, 7, 361. <https://doi.org/10.3389/fmars.2020.00361>
- Seddon, N., Smith, A., Smith, P., Key, I., Chausson, A., Girardin, C., House, J., Srivastava, S., & Turner, B. (2021). Getting the message right on nature-based solutions to climate change. *Global Change Biology*, 27(8), 1518–1546. <https://doi.org/10.1111/gcb.15513>
- Seitz, R. D., Wennhage, H., Bergström, U., Lippcius, R. N., & Ysebaert, T. (2014). Ecological value of coastal habitats for commercially and ecologically important species. *ICES Journal of Marine Science*, 71(3), 648–665. <https://doi.org/10.1093/icesjms/fst152>
- Shannon, C. E. (1948). A mathematical theory of communication. *Bell System Technical Journal*, 27(4), 623–656. <https://doi.org/10.1002/j.1538-7305.1948.tb00917.x>
- Siemes, R. W. A., Duong, T. M., Borsje, B. W., & Hulscher, S. J. M. H. (in review). Estuarine salt intrusion during extreme events affected by human interventions and sea level rise: A 3d modelling study of a highly engineered estuary.
- Simpson, J. H., Brown, J., Matthews, J., & Allen, G. (1990). Tidal straining, density currents, and stirring in the control of estuarine stratification. *Estuaries*, 13(2), 125–132. <https://doi.org/10.2307/1351581>
- Slangen, A. B. A., Carson, M., Katsman, C. A., van de Wal, R. S. W., Köhl, A., Vermeersen, L. L. A., & Stammer, D. (2014). Projecting twenty-first century regional sea-level changes. *Climatic Change*, 124(1-2), 317–332. <https://doi.org/10.1007/s10584-014-1080-9>
- Smaal, A. C., & Nienhuis, P. H. (1992). The Eastern Scheldt (the Netherlands), from an estuary to a tidal bay: A review of responses at the ecosystem level. *Netherlands Journal of Sea Research*, 30(100), 161–173. [https://doi.org/10.1016/0077-7579\(92\)90055-J](https://doi.org/10.1016/0077-7579(92)90055-J)
- Small, C., & Nicholls, R. J. (2003). A global analysis of human settlement in coastal zones. *Journal of Coastal Research*, 19(3), 584–599. <https://about.jstor.org/terms>
- Smith, J. G., Free, C. M., Lopazanski, C., Brun, J., Anderson, C. R., Carr, M. H., Claudet, J., Dugan, J. E., Eurich, J. G., Francis, T. B., Hamilton, S. L., Mouillot, D., Raimondi, P. T., Starr, R. M., Ziegler, S. L., Nickols, K. J., & Caselle, J. E. (2023). A marine protected area network does not confer community structure resilience to a marine heatwave across coastal ecosystems. *Global Change Biology*, 29(19), 5634–5651. <https://doi.org/10.1111/gcb.16862>
- Sobol', I. M. (1993). Sensitivity estimates for nonlinear mathematical models. *Mathematical Modelling and Computational Experiments*, 1(4), 407–414.
- Sobol', I. M. (2001). Global sensitivity indices for nonlinear mathematical models and their

- Monte Carlo estimates. *Mathematics and Computers in Simulation*, 55(1-3), 271–280. [https://doi.org/10.1016/S0378-4754\(00\)00270-6](https://doi.org/10.1016/S0378-4754(00)00270-6)
- Soto-Rivas, K., Flores, R. P., Williams, M., & Escauriaza, C. (2024). Understanding salinity intrusion and residence times in a small-scale bar-built estuary under drought scenarios: The Maipo River estuary, Central Chile. *Journal of Marine Science and Engineering*, 12(7), 1162. <https://doi.org/10.3390/jmse12071162>
- Spalding, M., Burke, L., Wood, S. A., Ashpole, J., Hutchison, J., & zu Ermgassen, P. (2017). Mapping the global value and distribution of coral reef tourism. *Marine Policy*, 82, 104–113. <https://doi.org/10.1016/j.marpol.2017.05.014>
- Sperna Weiland, F., Hegnauer, M., Bouaziz, L., & Beersma, J. (2015). *Implications of the KNMI'14 climate scenarios for the discharge of the Rhine and Meuse* (tech. rep.). Deltares, Delft, the Netherlands.
- Stacey, M. T., Brennan, M. L., Burau, J. R., & Monismith, S. G. (2010). The tidally averaged momentum balance in a partially and periodically stratified estuary. *Journal of Physical Oceanography*, 40(11), 2418–2434. <https://doi.org/10.1175/2010JPO4389.1>
- Stacey, M. T., Fram, J. P., & Chow, F. K. (2008). Role of tidally periodic density stratification in the creation of estuarine subtidal circulation. *Journal of Geophysical Research: Oceans*, 113(C8). <https://doi.org/10.1029/2007JC004581>
- Stacey, M. T., & Ralston, D. K. (2005). The scaling and structure of the estuarine bottom boundary layer. *Journal of Physical Oceanography*, 35(1), 55–71. <https://doi.org/10.1175/JPO-2672.1>
- Steffen, W., Rockström, J., Richardson, K., Lenton, T. M., Folke, C., Liverman, D., Summerhayes, C. P., Barnosky, A. D., Cornell, S. E., Crucifix, M., Donges, J. F., Fetzer, I., Lade, S. J., Scheffer, M., Winkelmann, R., & Schellnhuber, H. J. (2018). Trajectories of the Earth system in the Anthropocene. *Proceedings of the National Academy of Sciences*, 115(33), 8252–8259. <https://doi.org/10.1073/pnas.1810141115>
- Stelling, G. S., & van Kester, J. A. T. M. (1994). On the approximation of horizontal gradients in sigma co-ordinates for bathymetry with steep bottom slopes. *International Journal for Numerical Methods in Fluids*, 18(10), 915–935. <https://doi.org/10.1002/flid.1650181003>
- Stocchino, A., Besio, G., Angiolani, S., & Brocchini, M. (2011). Lagrangian mixing in straight compound channels. *Journal of Fluid Mechanics*, 675, 168–198. <https://doi.org/10.1017/S0022112011000127>
- Stockdon, H. F., Holman, R. A., Howd, P. A., & Sallenger, A. H. (2006). Empirical parameterization of setup, swash, and runup. *Coastal Engineering*, 53(7), 573–588. <https://doi.org/10.1016/j.coastaleng.2005.12.005>
- Storlazzi, C. D., Reguero, B. G., Cole, A. D., Lowe, E., Shope, J. B., Gibbs, A. E., Nickel, B. A., McCall, R. T., van Dongeren, A. R., & Beck, M. W. (2019). *Rigorously Valuing the Role of U.S. Coral Reefs in Coastal Hazard Risk Reduction* (tech. rep.). U.S. Geological Survey, Reston, VA, USA. <https://doi.org/10.3133/ofr20191027>
- Suanez, S., Cariolet, J. M., Cancouët, R., Ardhuin, F., & Delacourt, C. (2012). Dune recovery after storm erosion on a high-energy beach: Vougot Beach, Brittany (France). *Geomorphology*, 139–140, 16–33. <https://doi.org/10.1016/j.geomorph.2011.10.014>
- Swain, D. L., Wing, O. E. J., Bates, P. D., Done, J. M., Johnson, K. A., & Cameron, D. R. (2020). Increased flood exposure due to climate change and population growth in the United States. *Earth's Future*, 8(11), e2020EF001778. <https://doi.org/10.1029/2020EF001778>
- Taleb, N. N., & Douady, R. (2013). Mathematical definition, mapping, and detection of (anti)fragility. *Quantitative Finance*, 13(11), 1677–1689. <https://doi.org/10.1080/14697688.2013.800219>
- Taleb, N. N. (2007). Black Swans and the domains of statistics. *The American Statistician*, 61(3), 198–200. <https://doi.org/10.1198/000313007X219996>
- Tangelder, M., Winter, E., & Ysebaert, T. (2017). *Ecologie van zoet-zout overgangen in deltagebieden: Literatuurstudie en beoordeling van een scenario in het Volkerak-Zoommeer* (tech. rep.). Wageningen University & Research, Wageningen, the Netherlands. <https://doi.org/10.18174/436428>
- Telwala, Y., Brook, B. W., Manish, K., & Pandit, M. K. (2013). Climate-induced elevational range shifts and increase in plant species richness in a Himalayan biodiversity epicentre (K. P. Van Niel, Ed.). *PLoS ONE*, 8(2), e57103. <https://doi.org/10.1371/journal.pone.0057103>
- Temmerman, S., Horstman, E. M., Krauss, K. W., Mullarney, J. C., Pelckmans, I., & Schoutens, K. (2023). Marshes and man-

- groves as nature-based coastal storm buffers. *Annual Review of Marine Science*, 15, 95–118. <https://doi.org/10.1146/annurev-marine-040422-092951>
- Temmerman, S., Meire, P., Bouma, T. J., Herman, P. M. J., Ysebaert, T., & de Vriend, H. J. (2013). Ecosystem-based coastal defence in the face of global change. *Nature*, 504(7478), 79–83. <https://doi.org/10.1038/nature12859>
- Terlinden-Ruhl, L. J. R., Couasnon, A., Eilander, D., Hendrickx, G. G., Mares-Nasarre, P. M. N., & Antolínez, J. A. A. (in review). Exploring uncertainty to reduce the computational cost of compound flood risk assessments: A case study of charleston county. *Natural Hazards and Earth System Sciences*.
- Timmerman, A., Haasnoot, M., Middelkoop, H., Bouma, T., & McEvoy, S. (2021). Ecological consequences of sea level rise and flood protection strategies in shallow coastal systems: A quick-scan barcoding approach. *Ocean & Coastal Management*, 210, 105674. <https://doi.org/10.1016/j.ocecoaman.2021.105674>
- Todd, P. A. (2008). Morphological plasticity in scleractinian corals. *Biological Reviews*, 83(3), 315–337. <https://doi.org/10.1111/j.1469-185X.2008.00045.x>
- Toimil, A., Losada, I. J., Álvarez-Cuesta, M., & Le Cozannet, G. (2023). Demonstrating the value of beaches for adaptation to future coastal flood risk. *Nature Communications*, 14(1), 3474. <https://doi.org/10.1038/s41467-023-39168-z>
- Tónis, I. E., Stam, J. M. T., & van de Graaf, J. (2002). Morphological changes of the Haringvliet estuary after closure in 1970. *Coastal Engineering*, 44(3), 191–203. [https://doi.org/10.1016/S0378-3839\(01\)00026-6](https://doi.org/10.1016/S0378-3839(01)00026-6)
- Toreti, A., Bavera, D., Acosta Navarro, J., Cammalleri, C., de Jager, A., Di Ciollo, C., Hrast Essenfelder, A., Maetens, W., Masante, D., Magni, D., Mazzeschi, M., & Spinoni, J. (2022). *Drought in Europe August 2022* (tech. rep.). Publications Office of the European Union. Luxembourg. <https://doi.org/10.2760/264241>
- Toreti, A., Belward, A., Perez-Dominguez, I., Naumann, G., Luterbacher, J., Cronie, O., Seguini, L., Manfron, G., Lopez-Lozano, R., Baruth, B., van den Berg, M., Dentener, F., Ceglar, A., Chatzopoulos, T., & Zampieri, M. (2019). The exceptional 2018 European water seesaw calls for action on adaptation. *Earth's Future*, 7(6), 652–663. <https://doi.org/10.1029/2019EF001170>
- Tulp, I., Bolle, L. J., & Rijnsdorp, A. D. (2008). Signals from the shallows: In search of common patterns in long-term trends in Dutch estuarine and coastal fish. *Journal of Sea Research*, 60(1–2), 54–73. <https://doi.org/10.1016/j.seares.2008.04.004>
- Unie van Waterschappen. (2022). WAVES. <https://live-waves.databank.nl/>
- Valle-Levinson, A. (2008). Density-driven exchange flow in terms of the Kelvin and Ekman numbers. *Journal of Geophysical Research: Oceans*, 113(C4). <https://doi.org/10.1029/2007JC004144>
- van den Brink, M., Huismans, Y., Blaas, M., & Zwolsman, G. (2019). Climate change induced salinization of drinking water inlets along a tidal branch of the Rhine River: Impact assessment and an adaptive strategy for water resources management. *Climate*, 7(4), 49. <https://doi.org/10.3390/cli7040049>
- van der Heijden, S., Koomen, A., & Menke, M. (2024). *Mogelijke varianten Klimaatbestendige Zoetwatervoorziening Hoofdwatersysteem* (tech. rep.). Arcadis. Amersfoort, the Netherlands.
- van der Wal, D., Lambert, G. I., Ysebaert, T., Plancke, Y. M. G., & Herman, P. M. J. (2017). Hydrodynamic conditioning of diversity and functional traits in subtidal estuarine macrozoobenthic communities. *Estuarine, Coastal and Shelf Science*, 197, 80–92. <https://doi.org/10.1016/j.ecss.2017.08.012>
- van der Wiel, K., Lenderink, G., & de Vries, H. (2021). Physical storylines of future European drought events like 2018 based on ensemble climate modelling. *Weather and Climate Extremes*, 33, 100350. <https://doi.org/10.1016/j.wace.2021.100350>
- van der Wijk, R. (2016). *Afvoerverdeling en beschikbare metingen Rijnmaasmonding* (tech. rep.). Deltares. Delft, the Netherlands. <https://publications.deltares.nl/1230077-001-0008.pdf>
- van der Wijk, R. (2020). *Draaiboek Serious Game Rijn-Maasmonding* (tech. rep.). Deltares. Delft, the Netherlands.
- Van Diggelen, A. D., & Montagna, P. A. (2016). Is salinity variability a benthic disturbance in estuaries? *Estuaries and Coasts*, 39(4), 967–980. <https://doi.org/10.1007/s12237-015-0058-9>
- van Alphen, J., Haasnoot, M., & Diermanse, F. (2022). Uncertain accelerated sea-level rise, potential consequences, and adaptive strate-

- gies in the Netherlands. *Water*, 14(10), 1527. <https://doi.org/10.3390/w14101527>
- van Berchum, E. C., Mobley, W., Jonkman, S. N., Timmermans, J. S., Kwakkel, J. H., & Brody, S. D. (2019). Evaluation of flood risk reduction strategies through combinations of interventions. *Journal of Flood Risk Management*, 12, e12506. <https://doi.org/10.1111/jfr3.12506>
- van Dijk, W. M., Cox, J. R., Leuven, J. R. F. W., Cleveringa, J., Taal, M., Hiatt, M. R., Sonke, W., Verbeek, K., Speckmann, B., & Kleinhans, M. G. (2021). The vulnerability of tidal flats and multi-channel estuaries to dredging and disposal. *Anthropocene Coasts*, 4(1), 36–60. <https://doi.org/10.1139/anc-2020-0006>
- van IJzendoorn, C. O., de Vries, S., Hallin, C., & Hesp, P. A. (2021). Sea level rise outpaced by vertical dune toe translation on prograding coasts. *Scientific Reports*, 11(1), 12792. <https://doi.org/10.1038/s41598-021-92150-x>
- van Koningsveld, M., & Mulder, J. P. M. (2004). Sustainable coastal policy developments in the Netherlands. A systematic approach revealed. *Journal of Coastal Research*, 20(2), 375–385. [https://doi.org/10.2112/1551-5036\(2004\)020\[0375:SCPDIT\]2.0.CO;2](https://doi.org/10.2112/1551-5036(2004)020[0375:SCPDIT]2.0.CO;2)
- van Koningsveld, M., Verheij, H. J., Taneja, P., & de Vriend, H. (Eds.). (2023, February). *Ports and Waterways – Navigating the changing world*. TU Delft Open. <https://doi.org/10.5074/T.2021.004>
- van Prooijen, B. C., Battjes, J. A., & Uijtewaald, W. S. J. (2005). Momentum exchange in straight uniform compound channel flow. *Journal of Hydraulic Engineering*, 131(3), 175–183. [https://doi.org/10.1061/\(asce\)0733-9429\(2005\)131:3\(175\)](https://doi.org/10.1061/(asce)0733-9429(2005)131:3(175))
- van Rijn, L. C. (2011). Analytical and numerical analysis of tides and salinities in estuaries; Part I: Tidal wave propagation in convergent estuaries. *Ocean Dynamics*, 61(11), 1719–1741. <https://doi.org/10.1007/s10236-011-0453-0>
- van Slobbe, E., de Vriend, H. J., Aarninkhof, S., Lulofs, K., de Vries, M., & Dircke, P. (2013). Building with Nature: In search of resilient storm surge protection strategies. *Natural Hazards*, 65(1), 947–966. <https://doi.org/10.1007/s11069-012-0342-y>
- van Wesenbeeck, B. K., Mulder, J. P. M., Marchand, M., Reed, D. J., de Vries, M. B., de Vriend, H. J., & Herman, P. M. J. (2014). Damming deltas: A practice of the past? Towards nature-based flood defenses. *Estuarine, Coastal and Shelf Science*, 140, 1–6. <https://doi.org/10.1016/j.ecss.2013.12.031>
- van Wesenbeeck, B. K., Wolters, G., Antolínez, J. A. A., Kalløe, S. A., Hoffland, B., de Boer, W. P., Çete, C., & Bouma, T. J. (2022). Wave attenuation through forests under extreme conditions. *Scientific Reports*, 12(1), 1–8. <https://doi.org/10.1038/s41598-022-05753-3>
- van Wiechen, P. P. J., de Vries, S., Reniers, A. J. H. M., & Aarninkhof, S. G. J. (2023). Dune erosion during storm surges: A review of the observations, physics and modelling of the collision regime. *Coastal Engineering*, 186, 104383. <https://doi.org/10.1016/j.coastaleng.2023.104383>
- van Woesik, R., Golbuu, Y., & Roff, G. (2015). Keep up or drown: Adjustment of western Pacific coral reefs to sea-level rise in the 21st century. *Royal Society Open Science*, 2(7). <https://doi.org/10.1098/rsos.150181>
- van Zaanen, I., Ottink, R., & Sibma, M. (2022). *Droogtezeizoen 2022* (tech. rep.). Infram. Maarn, the Netherlands.
- Vasiliev, D. (2022). The role of biodiversity in ecosystem resilience. *IOP Conference Series: Earth and Environmental Science*, 1072, 012012. <https://doi.org/10.1088/1755-1315/1072/1/012012>
- Veerapaga, N., Shintani, T., Azhikodan, G., & Yokoyama, K. (2020). Study on salinity intrusion and mixing types in a conceptual estuary using 3-D hydrodynamic simulation: Effects of length, width, depth, and bathymetry. In K. Nguyen, S. Guillou, P. Gourbesville, & J. Thiébot (Eds.), *Estuaries and coastal zones in times of global change* (pp. 13–30). Springer Singapore. https://doi.org/10.1007/978-981-15-2081-5_{-}2
- Veldkamp, T. I. E., Wada, Y., de Moel, H., Kumm, M., Eisner, S., Aerts, J. C. J. H., & Ward, P. J. (2015). Changing mechanism of global water scarcity events: Impacts of socioeconomic changes and inter-annual hydro-climatic variability. *Global Environmental Change*, 32, 18–29. <https://doi.org/10.1016/j.gloenvcha.2015.02.011>
- Villemonte, J. R. (1947). Submerged-weir discharge studies. *Engineering News Record*, 139, 866–869.
- Vinke, F., Turpijn, B., van Gelder, P., & van Koningsveld, M. (2024). Inland shipping response to discharge extremes – A 10 years case study of the Rhine. *Climate Risk Management*, 43, 100578. <https://doi.org/10.1016/j.crm.2023.100578>

- Vinke, F., van Koningsveld, M., van Dorsser, C., Baart, F., van Gelder, P., & Vellinga, T. (2022). Cascading effects of sustained low water on inland shipping. *Climate Risk Management*, 35, 100400. <https://doi.org/10.1016/j.crm.2022.100400>
- Vitousek, S., Barnard, P. L., Fletcher, C. H., Frazer, N., Erikson, L., & Storlazzi, C. D. (2017). Doubling of coastal flooding frequency within decades due to sea-level rise. *Scientific Reports*, 7(1), 1399. <https://doi.org/10.1038/s41598-017-01362-7>
- Vörösmarty, C. J., Green, P., Salisbury, J., & Lammers, R. B. (2000). Global water resources: Vulnerability from climate change and population growth. *Science*, 289(5477), 284–288. <https://doi.org/10.1126/science.289.5477.284>
- Vuik, V., Jonkman, S. N., Borsje, B. W., & Suzuki, T. (2016). Nature-based flood protection: The efficiency of vegetated foreshores for reducing wave loads on coastal dikes. *Coastal Engineering*, 116, 42–56. <https://doi.org/10.1016/j.coastaleng.2016.06.001>
- Wada, Y., van Beek, L. P. H., van Kempen, C. M., Reckman, J. W. T. M., Vasak, S., & Bierkens, M. F. P. (2010). Global depletion of groundwater resources. *Geophysical Research Letters*, 37(20). <https://doi.org/10.1029/2010GL044571>
- Wada, Y., van Beek, L. P. H., Viviroli, D., Dürr, H. H., Weingartner, R., & Bierkens, M. F. P. (2011). Global monthly water stress: 2. Water demand and severity of water stress. *Water Resources Research*, 47(7). <https://doi.org/10.1029/2010WR009792>
- Walstra, D. J. R., Hoekstra, R., Tonnon, P. K., & Ruessink, B. G. (2013). Input reduction for long-term morphodynamic simulations in wave-dominated coastal settings. *Coastal Engineering*, 77, 57–70. <https://doi.org/10.1016/j.coastaleng.2013.02.001>
- Walther, G. R., Post, E., Convey, P., Menzel, A., Parmesan, C., Beebee, T. J. C., Fromentin, J. M., Hoegh-Guldberg, O., & Bairlein, F. (2002). Ecological responses to recent climate change. *Nature*, 416(6879), 389–395. <https://doi.org/10.1038/416389a>
- Wang, F., Huang, G. H., Fan, Y., & Li, Y. P. (2020). Robust subsampling ANOVA methods for sensitivity analysis of water resource and environmental models. *Water Resources Management*, 34(10), 3199–3217. <https://doi.org/10.1007/s11269-020-02608-2>
- Wang, T., Geyer, W. R., & MacCreedy, P. (2017). Total exchange flow, entrainment, and diffusive salt flux in estuaries. *Journal of Physical Oceanography*, 47(5), 1205–1220. <https://doi.org/10.1175/JPO-D-16-0258.1>
- Wang, Z. B., Jeuken, C., & de Vriend, H. J. (1999). *Tidal asymmetry and residual sediment transport in estuaries: A literature study and application to the Western Scheldt* (tech. rep.). WL — Delft Hydraulics. Delft, the Netherlands. <http://repository.tudelft.nl/assets/uuid:08911ef5-5ee8-4a8b-9432-5a5a5dfaa142/z2749dr.pdf>
- Wannasin, C., Biemond, B., Wullems, B., Blokhuijsen, T., Tiessen, M., Baart, F., & Kwadijk, J. (2024). Virtual Delta: A digital twin for real-time forecasting and management of saltwater intrusion in the Rhine-Meuse delta. *EGU General Assembly*, 12982. <https://doi.org/10.5194/EGUSPHERE-EGU24-12982>
- Warner, J. C., Geyer, W. R., & Lerczak, J. A. (2005). Numerical modeling of an estuary: A comprehensive skill assessment. *Journal of Geophysical Research: Oceans*, 110(5), 1–13. <https://doi.org/10.1029/2004JC002691>
- Warner, J. C., Schoellhamer, D., Burau, J. R., & Schladow, G. (2002). Effects of tidal current phase at the junction of two straits. *Continental Shelf Research*, 22(11–13), 1629–1642. [https://doi.org/10.1016/S0278-4343\(02\)00026-2](https://doi.org/10.1016/S0278-4343(02)00026-2)
- Wegman, T. M., Pietrzak, J. D., Horner-Devine, A. R., Dijkstra, H. A., & Ralston, D. K. (in review). Forcing mechanisms of salt intrusion in a low-lying river delta during a prolonged drought. *Journal of Geophysical Research: Oceans*.
- Wei, X., Kumar, M., & Schuttelaars, H. M. (2017). Three-dimensional salt dynamics in well-mixed estuaries: Influence of estuarine convergence, Coriolis, and bathymetry. *Journal of Physical Oceanography*, 47(7), 1843–1871. <https://doi.org/10.1175/JPO-D-16-0247.1>
- Wetz, M. S., & Yoskowitz, D. W. (2013). An ‘extreme’ future for estuaries? Effects of extreme climatic events on estuarine water quality and ecology. *Marine Pollution Bulletin*, 69(1–2), 7–18. <https://doi.org/10.1016/j.marpolbul.2013.01.020>
- Whitfield, A. K., Elliott, M., Basset, A., Blaber, S. J. M., & West, R. J. (2012). Paradigms in estuarine ecology - A review of the Remane diagram with a suggested revised model for estuaries. *Estuarine, Coastal and Shelf Science*, 97, 78–90. <https://doi.org/10.1016/j.ecss.2011.11.026>

- Wilkinson, M. D., Dumontier, M., Aalbersberg, I. J., Appleton, G., Axton, M., Baak, A., Blomberg, N., Boiten, J.-W., da Silva Santos, L. B., Bourne, P. E., Bouwman, J., Brookes, A. J., Clark, T., Crosas, M., Dillo, I., Dumon, O., Edmunds, S., Evelo, C. T., Finkers, R., . . . Mons, B. (2016). The FAIR guiding principles for scientific data management and stewardship. *Scientific Data*, 3(1), 160018. <https://doi.org/10.1038/sdata.2016.18>
- Wing, O. E. J., Bates, P. D., Quinn, N. D., Savage, J. T. S., Uhe, P. F., Cooper, A., Collings, T. P., Addor, N., Lord, N. S., Hatchard, S., Hoch, J. M., Bates, J., Probyn, I., Himsworth, S., Rodríguez González, J., Brine, M. P., Wilkinson, H., Sampson, C. C., Smith, A. M., . . . Haigh, I. D. (2024). A 30 m global flood inundation model for any climate scenario. *Water Resources Research*, 60(8). <https://doi.org/10.1029/2023WR036460>
- Worm, B., Barbier, E. B., Beaumont, N., Duffy, J. E., Folke, C., Halpern, B. S., Jackson, J. B. C., Lotze, H. K., Micheli, F., Palumbi, S. R., Sala, E., Selkoe, K. A., Stachowicz, J. J., & Watson, R. (2006). Impacts of biodiversity loss on ocean ecosystem services. *Science*, 314(5800), 787–790. <https://doi.org/10.1126/science.1132294>
- Wu, W., & Wan, L. (2024). Coastal ecological and environmental management under multiple anthropogenic pressures: A review of theory and evaluation methods. In X. H. Wang & L. Qiao (Eds.), *Current trends in estuarine and coastal dynamics: Observations and modelling* (pp. 385–415). Elsevier. <https://doi.org/10.1016/C2022-0-03285-2>
- Xue, P., Chen, C., Ding, P., Beardsley, R. C., Lin, H., Ge, J., & Kong, Y. (2009). Saltwater intrusion into the Changjiang River: A model-guided mechanism study. *Journal of Geophysical Research: Oceans*, 114(2), C02006. <https://doi.org/10.1029/2008JC004831>
- Yachi, S., & Loreau, M. (1999). Biodiversity and ecosystem productivity in a fluctuating environment: The insurance hypothesis. *Proceedings of the National Academy of Sciences*, 96(4), 1463–1468. <https://doi.org/10.1073/pnas.96.4.1463>
- Yan, D., Werners, S. E., Huang, H. Q., & Ludwig, F. (2016). Identifying and assessing robust water allocation plans for deltas under climate change. *Water Resources Management*, 30(14), 5421–5435. <https://doi.org/10.1007/s11269-016-1498-0>
- Yang, J., & Zhang, W. (2024). Storm-induced saltwater intrusion responds divergently to sea level rise in a complicated estuary. *Environmental Research Letters*, 19(1), 014011. <https://doi.org/10.1088/1748-9326/ad0e32>
- Yang, Z., Sobocinski, K. L., Heatwole, D., Khangaonkar, T., Thom, R., & Fuller, R. (2010). Hydrodynamic and ecological assessment of nearshore restoration: A modeling study. *Ecological Modelling*, 221(7), 1043–1053. <https://doi.org/10.1016/j.ecolmodel.2009.07.011>
- Yang, Z., & Wang, T. (2015). Responses of estuarine circulation and salinity to the loss of intertidal flats: A modeling study. *Continental Shelf Research*, 111, 159–173. <https://doi.org/10.1016/j.csr.2015.08.011>
- Ysebaert, T., Herman, P. M. J., Meire, P., Craeymeersch, J., Verbeek, H., & Heip, C. H. R. (2003). Large-scale spatial patterns in estuaries: Estuarine macrobenthic communities in the Schelde estuary, NW Europe. *Estuarine, Coastal and Shelf Science*, 57(1–2), 335–355. [https://doi.org/10.1016/S0272-7714\(02\)00359-1](https://doi.org/10.1016/S0272-7714(02)00359-1)
- Ysebaert, T., van der Hoek, D.-J., Wortelboer, R., Wijsman, J. W. M., Tangelder, M., & Nolte, A. (2016). Management options for restoring estuarine dynamics and implications for ecosystems: A quantitative approach for the Southwest Delta in the Netherlands. *Ocean & Coastal Management*, 121, 33–48. <https://doi.org/10.1016/j.ocecoaman.2015.11.005>
- Yuan, R., & Zhu, J. (2015). The effects of dredging on tidal range and saltwater intrusion in the Pearl River estuary. *Journal of Coastal Research*, 316(6), 1357–1362. <https://doi.org/10.2112/JCOASTRES-D-14-00224.1>
- Yumashev, D., Hope, C., Schaefer, K., Riemann-Campe, K., Iglesias-Suarez, F., Jafarov, E., Burke, E. J., Young, P. J., Elshorbany, Y., & Whiteman, G. (2019). Climate policy implications of nonlinear decline of Arctic land permafrost and other cryosphere elements. *Nature Communications*, 10(1), 1900. <https://doi.org/10.1038/s41467-019-09863-x>
- Zandvoort, M., van der Vlist, M. J., & van den Brink, A. (2018). Handling uncertainty through adaptiveness in planning approaches: Comparing adaptive delta management and the water diplomacy framework. *Journal of Environmental Policy & Planning*, 20(2), 183–197. <https://doi.org/10.1080/1523908X.2017.1347035>

- Zhang, E., Savenije, H. H. G., Wu, H., Kong, Y., & Zhu, J. (2011). Analytical solution for salt intrusion in the Yangtze Estuary, China. *Estuarine, Coastal and Shelf Science*, *91*(4), 492–501. <https://doi.org/10.1016/j.ecss.2010.11.008>
- Zhang, M., Dai, Z., Bouma, T. J., Bricker, J., Townend, I., Wen, J., Zhao, T., & Cai, H. (2021). Tidal-flat reclamation aggravates potential risk from storm impacts. *Coastal Engineering*, *166*, 130868. <https://doi.org/10.1016/j.coastaleng.2021.103868>
- Zhang, Z., Cui, B., Fan, X., Zhang, K., Zhao, H., & Zhang, H. (2012). Wetland network design for mitigation of saltwater intrusion by replenishing freshwater in an estuary. *Clean - Soil, Air, Water*, *40*(10), 1036–1046. <https://doi.org/10.1002/clea.201100735>
- Zhao, T., Xiong, S., Tian, Y., Wu, Y., Li, B., & Chen, X. (2024). Compound dry and hot events over major river basins of the world from 1921 to 2020. *Weather and Climate Extremes*, *44*, 100679. <https://doi.org/10.1016/j.wace.2024.100679>
- Zhong, Z., Yu, M., Yu, W., Jia, L., & Mo, J. (2024). Impact of human-induced alterations in bathymetry and geometry on tidal and salt dynamics: Thresholds for morphological dimensions in a convergent estuary. *Journal of Hydrology*, *645*, 132143. <https://doi.org/10.1016/j.jhydrol.2024.132143>
- Zhou, J., Stacey, M. T., Holleman, R. C., Nuss, E., & Senn, D. B. (2020a). Numerical investigation of baroclinic channel-shoal interaction in partially stratified estuaries. *Journal of Geophysical Research: Oceans*, *125*(4), e2020JC016135. <https://doi.org/10.1029/2020JC016135>
- Zhou, Z., Chen, L., Tao, J., Gong, Z., Guo, L., van der Wegen, M., Townend, I., & Zhang, C. (2020b). The role of salinity in fluvio-deltaic morphodynamics: A long-term modelling study. *Earth Surface Processes and Landforms*, *45*(3), 590–604. <https://doi.org/10.1002/esp.4757>
- Zhu, J., Weisberg, R. H., Zheng, L., & Han, S. (2015). Influences of channel deepening and widening on the tidal and nontidal circulations of Tampa Bay. *Estuaries and Coasts*, *38*(1), 132–150. <https://doi.org/10.1007/s12237-014-9815-4>
- Zilio, M. I., London, S., Perillo, G. M. E., & Cintia Piccolo, M. (2013). The social cost of dredging: The Bahia Blanca Estuary case. *Ocean and Coastal Management*, *71*, 195–202. <https://doi.org/10.1016/j.ocecoaman.2012.09.008>

APPENDICES

A.	ANNESI	195
B.	Supplementary material: Chapters 2 and 3	197
C.	Supplementary material: Chapter 5	207
D.	Supplementary material: Chapter 8	211
E.	Nature-based solution: Discharge management	215
F.	Nature-based solution: Tidal mixing energy	225



Chapters 2 and 3 employ the use of a neural network. This neural network has been named ANNESI: *Artificial Neural Network for Estuarine Salt Intrusion* (Hendrickx, 2022). It has been trained on the dataset used for the sensitivity analysis, as described in Chapters 2 and 3, the NEESI dataset (*Numerical Experiments of Estuarine Salt Intrusion*; Hendrickx, 2023a). ANNESI is open-source, and has been incorporated as the backend model of a web-API: <https://annesi-web.netlify.app/>.

A.1 Architecture

The neural network is a multilayer perceptron, which is a feedforward artificial neural network where every node of a layer communicates with every node in an adjacent layer. The neural network used for this study contains three hidden layers with 50 nodes each between the input layer of thirteen nodes and the output layer with two nodes. The activation function used between all layers is the rectifying—or ReLU—function.

This appendix is based on the supplementary material of:

Hendrickx, G.G., Antolínez, J.A.A., and Herman, P.M.J. (2023). Predicting the response of complex systems for coastal management. *Coastal Engineering*, **182**:104289.

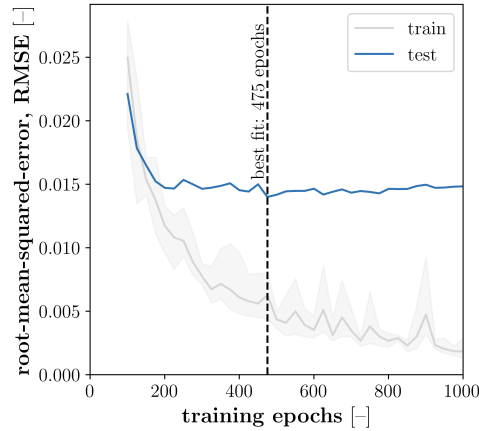


Figure A.1: Training progress of neural network. Until 475 epochs, the neural network is improving; after 475 epochs, the neural network is being over-fitted.

A.2 Training

The neural network is trained and validated by randomly splitting the dataset in two separate datasets: (1) a training dataset (80%), and (2) a testing (or validation) dataset (20%). The training dataset is used to train the neural network, and the testing dataset is used to test—or validate—the neural network. The neural network never “sees” the latter to prevent over-fitting of the network.

Because the training is resolved throughout with backpropagation, increasing the number of epochs—i.e., updating the many fitting coefficients—makes the neural network better predict the output: The root-mean-squared-error (RMSE) of both the training and the testing datasets decrease. However, there is a tipping point after which the RMSE of the testing dataset increases; this is the moment the neural network is being over-fit. This behaviour is visualised in Figure A.1.

B

SUPPLEMENTARY MATERIAL

Chapters 2 and 3

B.1 Parameter definitions

The thirteen input parameters are further clarified in Appendices B.1.1 and B.1.2, for respectively the forcing conditions and the geometric features.

This appendix is based on the supplementary material of:

Hendrickx, G.G., Antolínez, J.A.A., and Herman, P.M.J. (2023). Predicting the response of complex systems for coastal management. *Coastal Engineering*, **182**:104289.

Hendrickx, G.G., Kranenburg, W.M., Antolínez, J.A.A., Huismans, Y., Aarninkhof, S.G.J., and Herman, P.M.J. (2023). Sensitivity of salt intrusion to estuary-scale changes: A systematic modelling study towards nature-based mitigation measures *Estuarine, Coastal and Shelf Science*, **295**:108564.

B.1.1 Forcing

The tidal boundary condition is represented by the S_2 -tide—i.e., a wave period of 43,200 s is used, which equals 12 hours. This boundary condition is imposed at the uppermost offshore boundary, which is 30 km from the coast.

The storm surge level is imposed as a rise in water level, which increases for one half of the day after which it fades away again. Thus, following a triangular shape in time (based on Perk *et al.*, 2019).

The river discharge is imposed as a constant input of freshwater, i.e. not varying over time and a salinity of $s = 0$ psu.

B.1.2 Geometry

Some of the geometric features change in longitudinal direction due to the convergence of the estuary; these are the channel depth, channel width, and flat width. The channel depth and channel width at the upstream boundary are a function of the river discharge (modified from Hey & Thorne, 1986; Leuven *et al.*, 2018b):¹

$$d_c(x = L) = d_c(Q) = 0.33 \cdot (3.5Q)^{0.35} \quad (\text{B.1a})$$

$$W_c(x = L) = W_c(Q) = 3.67 \cdot (3.5Q)^{0.45} \quad (\text{B.1b})$$

where d_c is the channel depth [m]; Q the river discharge [m^3s^{-1}]; and W_c the channel width [m].

The channel depth linearly reduces from its definition at the mouth (Tabs. 2.1 and 3.1, pp. 18 and 37) towards this minimum depth as a function of the river discharge; while the channel width follows an exponential decay (Figs. 2.2 and 3.1, pp. 20 and 38):

$$d_c(x) = -\frac{d_c^0 - d_c(Q)}{L} \cdot x + d_c^0 \quad (\text{B.2a})$$

$$W_c(x) = W_c(Q) + (W_c^0 - W_c(Q)) \exp[-\gamma x] \quad (\text{B.2b})$$

where d_c is the channel depth [m]; L the length of the estuarine domain [m]; x the longitudinal coordinate [m]; W_c the channel width [m]; and γ the convergence [m^{-1}].

In all the above statements, the channel depth represents the lateral averaged channel depth. However, due to the bottom curvature, κ_c , the channel depth varies in lateral direction:

$$\tilde{d}_c(x, y) = d_c(x) + \kappa_c \left(\frac{1}{12} W_c(x)^2 - y^2 \right) \quad (\text{B.3})$$

where \tilde{d}_c is the lateral varying channel depth [m]; d_c the lateral averaged channel depth [m]; κ_c the bottom curvature [m^{-1}]; W_c the channel width; and x and y are the longitudinal and lateral coordinates, respectively [m].

B.2 Physical restrictions input space

To ensure the parameter combinations to be physically sound, some restrictions are enforced on the input space. These restrictions are listed below:

¹The expressions by Leuven *et al.* (2018b) are related to Q instead of $3.5Q$. This factor of 3.5 is added to translate from gravel beds to sand beds for which the Shields stability parameter has been used.

Channel depth The channel depth at the mouth of the estuary has to be larger than, or equal to, the channel depth at the upstream boundary. This results in a relation between the channel depth at the mouth and the river discharge (Eq. B.1a):

$$d_c(x=0) \geq d_c(x=L) = 0.33 \cdot (3.5Q)^{0.35} \quad (\text{B.4})$$

where d_c is the channel depth [m]; x the longitudinal axis, with $x=0$ the mouth and $x=L$ the upstream boundary; and Q the river discharge [m^3s^{-1}].

Channel width The channel width at the mouth of the estuary has to be larger than, or equal to, the channel width at the upstream boundary. This results in a relation between the channel width at the mouth and the river discharge (Eq. B.1b):

$$W_c(x=0) \geq W_c(x=L) = 3.67 \cdot (3.5Q)^{0.45} \quad (\text{B.5})$$

where W_c is the channel width [m]; x the longitudinal axis, with $x=0$ the mouth and $x=L$ the upstream boundary; and Q the river discharge [m^3s^{-1}].

Flat depth The flat depth is described as the product of the flat depth ratio, r_d , and the tidal range, a . The flat depth has to be smaller than the channel depth:

$$\frac{1}{2}r_d a = d_f < d_c \quad (\text{B.6})$$

where r_d is the flat depth ratio [-]; a the tidal range [m]; d_f the flat depth [m]; and d_c the channel depth [m].

Flat width The flat width is limited to the channel width; the flat width has to be smaller than, or equal to, the channel width:

$$W_f \leq W_c \quad (\text{B.7})$$

where W_f is the flat width [m]; and W_c the channel width [m].

Bottom curvature The bottom curvature is capped such that the boundaries of the channel—which are shallower due to the bottom curvature—do not rise above the flat depth. Because the channel depth is defined as the average water depth in the channel of the estuary, a slightly more strict maximum bottom curvature is imposed, related to the channel depth instead of the flat depth (and the channel width):

$$\kappa_c \leq \frac{3}{5} \frac{d_c}{W_c^2} \quad (\text{B.8})$$

where κ_c is the bottom curvature [m^{-1}]; d_c the channel depth [m]; and W_c the channel width [m]. Note that this restriction is valid as long as $d_f \leq \frac{1}{10}d_c$, with d_f being the flat depth ($d_f = \frac{1}{2}r_d a$) [m]. This holds for all value combinations possible.

Meander amplitude The meander amplitude is capped by the total width of the estuary, based on empirical findings by Leuven *et al.* (2018a):

$$A_m \leq 2.5(W_c + W_f)^{1.1} \quad (\text{B.9})$$

where A_m is the meander amplitude [m]; W_c the channel width [m]; and W_f the flat width [m].

Meander length The meander length is related to the meander amplitude and should be within a range based on this parameter—again based on empirical findings by Leuven *et al.* (2018a):

$$27.044A_m^{0.786} \leq L_m \leq 71.429A_m^{0.833} \quad (\text{B.10})$$

where A_m is the meander amplitude [m]; and L_m the meander length [m].

Flow velocity A first-order estimate of the flow velocity in the estuary is considered to verify if the parameter combinations do not result in unrealistically large velocities. Flow velocities above 2 ms^{-1} are considered unrealistic. The first-order estimates are based on the combination of river flow and tidal flow, where the latter is determined using the tidal prism (based on van Rijn, 2011):

$$P = \frac{1}{2}a \left(\frac{W_c^{\min}}{\delta} (1 - \exp[-\delta L]) + \frac{W_c - W_c^{\min}}{\gamma + \delta} (1 - \exp[-(\gamma + \delta)L]) \right) \quad (\text{B.11a})$$

with

$$W_c^{\min} = 3.67 \cdot (3.5Q)^{0.45} \quad (\text{B.11b})$$

$$\delta = -\frac{1}{2}\gamma + \mu \quad (\text{B.11c})$$

$$\mu = \frac{k}{\sqrt{2}} \sqrt{\xi + \sqrt{\xi^2 + (mT)^2}} \quad (\text{B.11d})$$

$$\xi = -1 + \left(\frac{\gamma}{2k} \right)^2 \quad (\text{B.11e})$$

$$k = \frac{1}{T\sqrt{gd_c}} \quad (\text{B.11f})$$

$$m = \frac{8}{3\pi} \frac{n_c u_t}{d_c} \quad (\text{B.11g})$$

$$u_t = \frac{a}{2\sqrt{2}} \sqrt{\frac{g}{d_c}} \quad (\text{B.11h})$$

where P is the tidal prism [m^3]; a the tidal range [m]; W_c^{\min} the minimum channel width [m]; δ the tidal damping coefficient [m^{-1}]; L the length of the estuary [m]; W_c the channel width [m]; γ the convergence [m^{-1}]; Q the river discharge [m^3s^{-1}]; μ the damping parameter [m^{-1}]; k the wave number [m^{-1}]; m the friction parameter [s^{-1}]; T the tidal wave period [s]; d_c the channel depth [m]; and u_t the estimation of the tidal flow velocity [ms^{-1}].

The representative flow velocity in the estuary is defined as:

$$u = \frac{Q}{W_c d_c} + \frac{2P}{TW_c d_c} \quad (\text{B.12})$$

where u is the representative flow velocity [ms^{-1}]; and all other symbols are provided above. This representative flow velocity is subjected to an upper bound:

$$u \leq 2.0 \text{ [ms}^{-1}\text{]} \quad (\text{B.13})$$

B.3 Input and output spaces

The restrictions on the input space—and thereby potential correlations between input parameters—are clearly visible in the matrix-plot presented in Figure B.1. This figure also includes the relations between the input and output data, including the mixing parameter, M , and the freshwater Froude number, Fr_f (Eqs. 2.1/3.1 and 2.2/3.2, pp. 18 and 35). The input parameters are presented in gray and the output variables in blue to create a visual distinction between the two.

B.4 Relative salt intrusion gradients

In Chapter 3, a total overview of the variability of the relative gradient to the river discharge (p_Q) is presented in Figure 5. Supplementary to this single figure, the similar figures for all the thirteen input parameters except the discharge are presented in Figure B.2 (pp. 203–206)—for the discharge, see Figure 3.5 (p. 46).

B

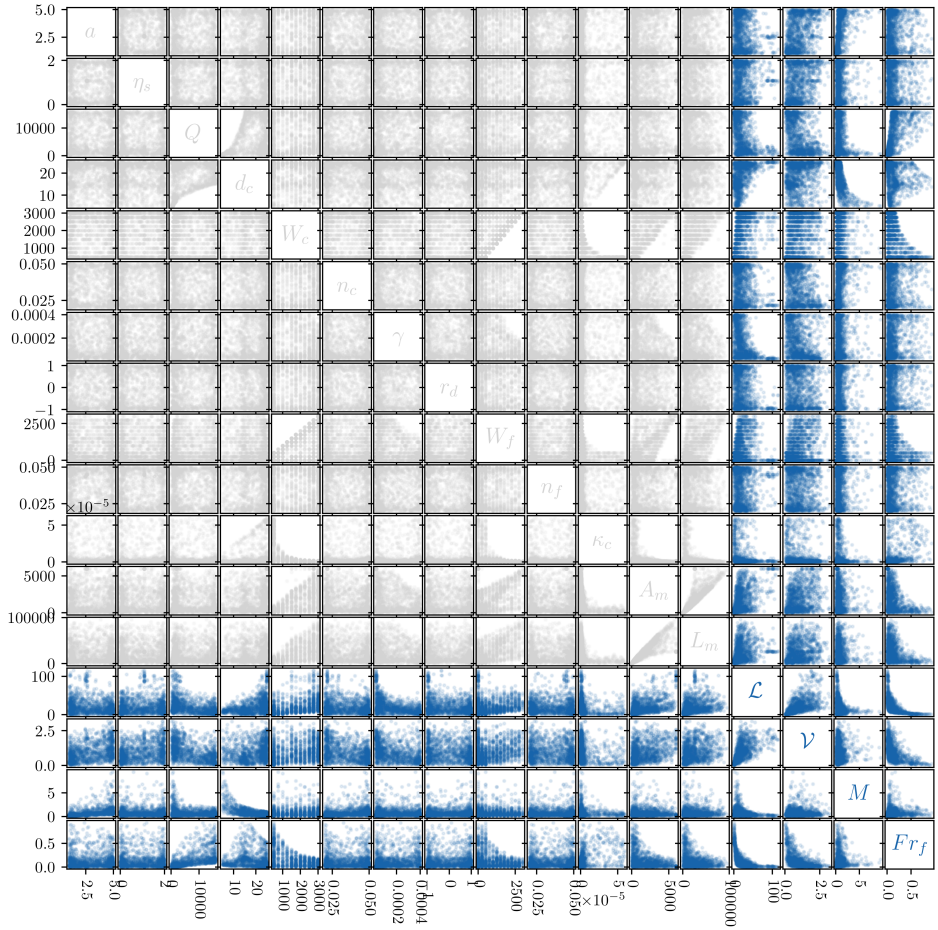


Figure B.1: Sampled input and output spaces, including the non-dimensional parameters making up the M, Fr_f -space as proposed by Geyer and MacCready (2014) (cf. Eqs. nput and output data, including the mixing parameter, M , and the freshwater Froude number, Fr_f (Eqs. 2.1/3.1 and 2.2/3.2)).

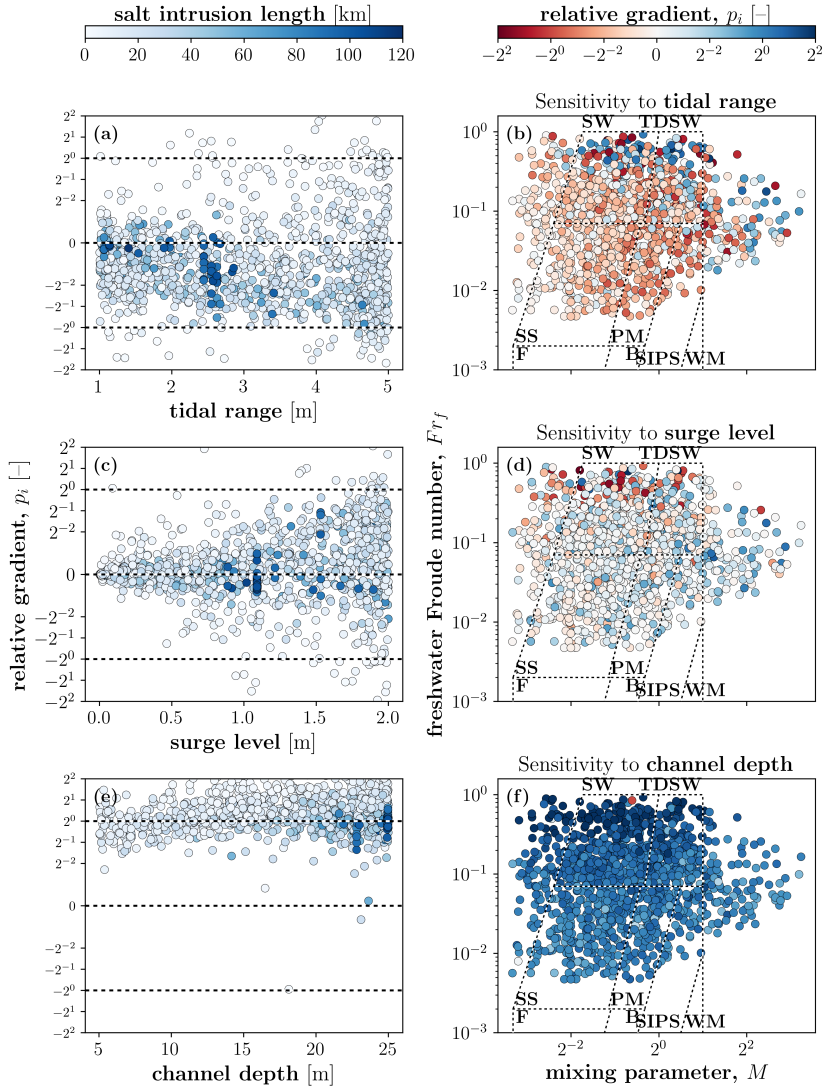


Figure B.2: The relative gradient in salt intrusion with respect to (a,b) tidal range, a ; (c,d) surge level, η_s ; (e,f) channel depth, d_c . Left column: p_i as function of variable; right column: p_i displayed on the M, Fr_f -space. SW: salt wedge; TDSW: time-dependent salt wedge; SS: strongly stratified; PM: partially mixed; F: fjord; B: bay; SIPS: strain-induced periodic straining; WM: well-mixed

B

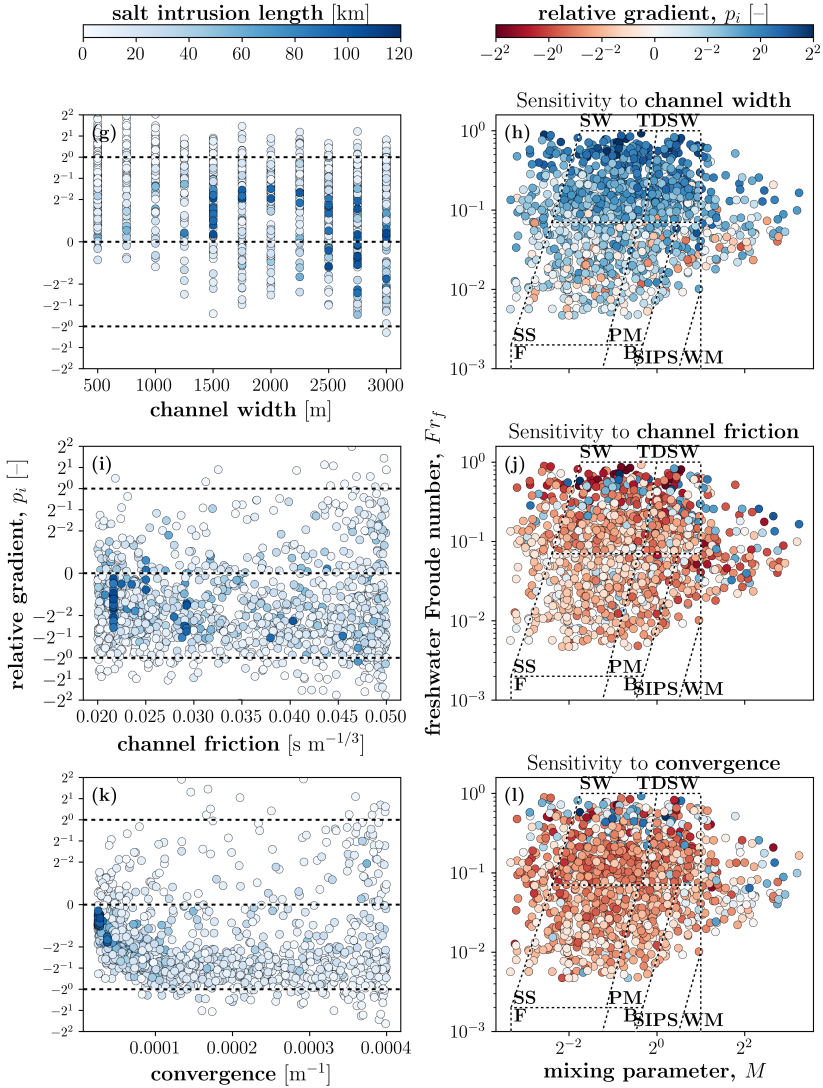


Figure B.2: (*cont.*) The relative gradient in salt intrusion with respect to (g,h) channel width, W_c ; (i,j) channel friction, n_c ; (k,l) convergence, γ . Left column: p_i as function of variable; right column: p_i displayed on the M, Fr_f -space. **SW**: salt wedge; **TDSW**: time-dependent salt wedge; **SS**: strongly stratified; **PM**: partially mixed; **F**: fjord; **B**: bay; **SIPS**: strain-induced periodic straining; **WM**: well-mixed

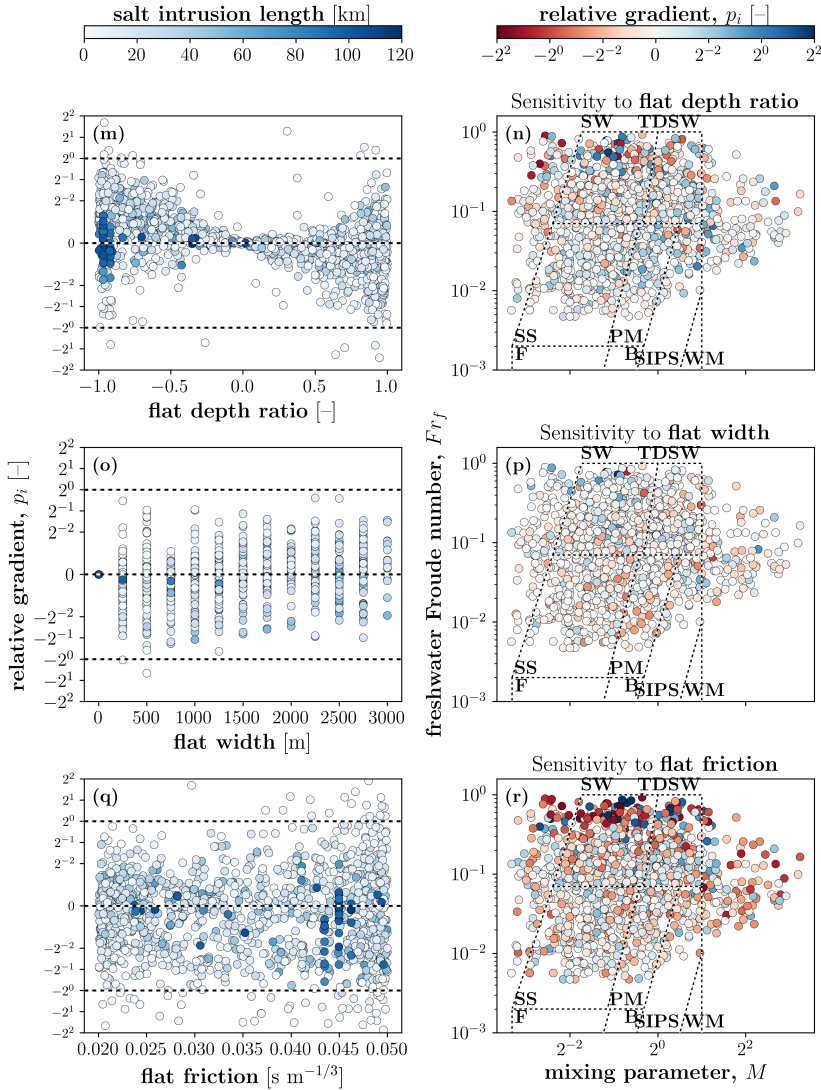


Figure B.2: (*cont.*) The relative gradient in salt intrusion with respect to (m,n) flat depth ratio, r_d ; (o,p) flat width, W_f ; (q,r) flat friction, n_f . Left column: p_i as function of variable; right column: p_i displayed on the M, Fr_f -space. SW: salt wedge; TDSW: time-dependent salt wedge; SS: strongly stratified; PM: partially mixed; F: fjord; B: bay; SIPS: strain-induced periodic straining; WM: well-mixed

B

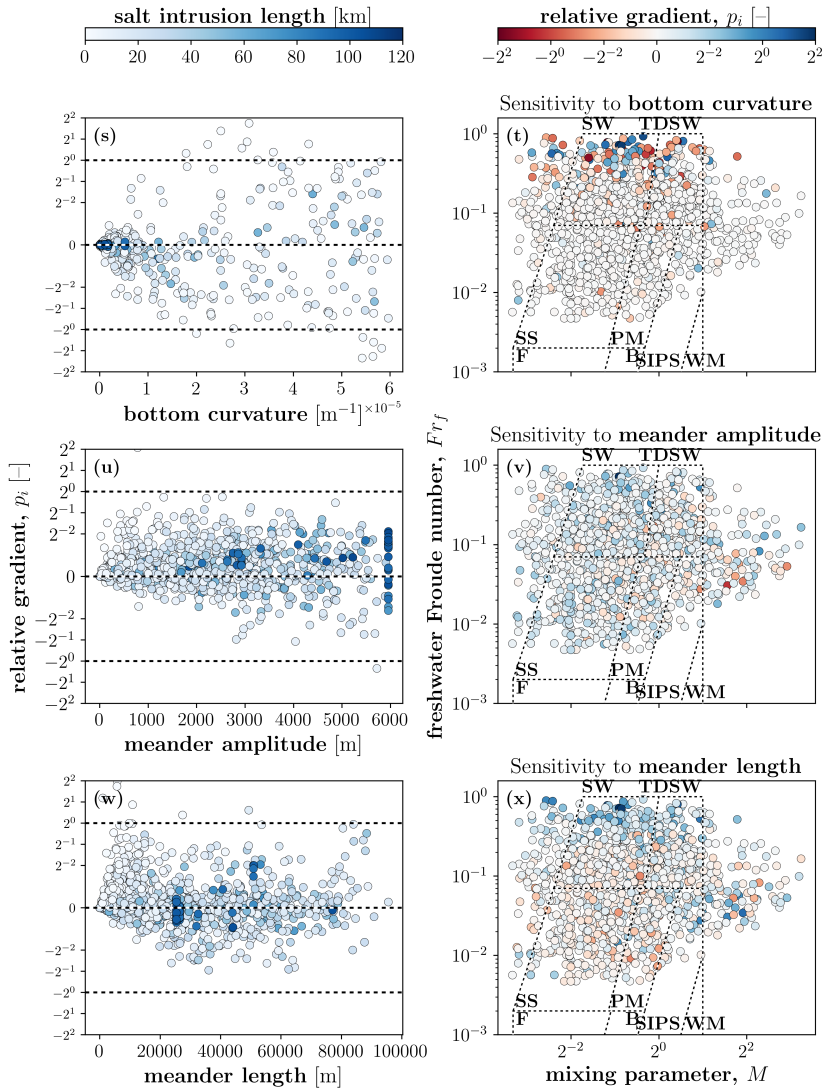
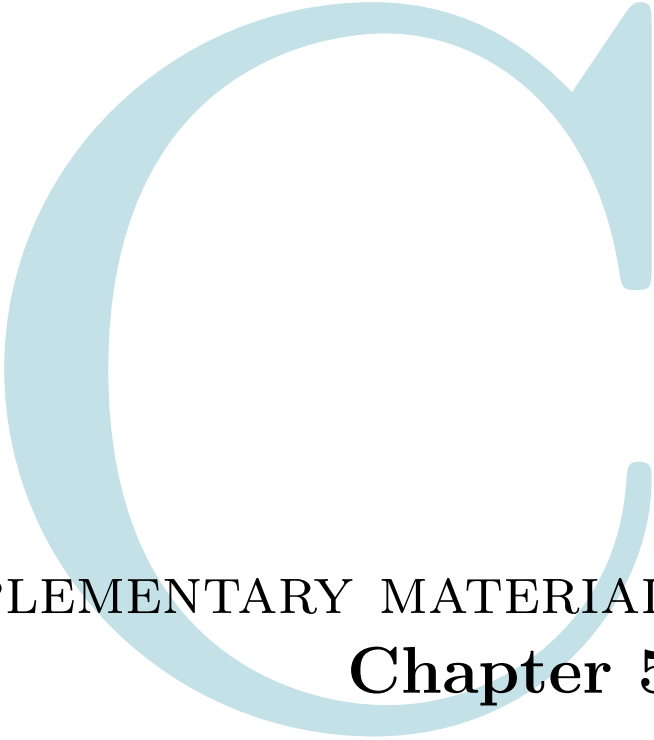


Figure B.2: (*cont.*) The relative gradient in salt intrusion with respect to (s,t) bottom curvature, κ_c ; (u,v) meander amplitude, A_m ; (w,x) meander length, L_m . Left column: p_i as function of variable; right column: p_i displayed on the M, Fr_f -space. SW: salt wedge; TDSW: time-dependent salt wedge; SS: strongly stratified; PM: partially mixed; F: fjord; B: bay; SIPS: strain-induced periodic straining; WM: well-mixed



SUPPLEMENTARY MATERIAL

Chapter 5

Two overviews of the full along-channel spatial distributions of all salt flux decompositions (Sec. 5.2.3, p. 81) performed are included in this supplementary material:

1. Salt flux decomposition collapsing the whole estuarine width—i.e., channel and intertidal area—on the x -axis: Figure C.1 (p. 209).
2. Salt flux decomposition collapsing the channel cross-section and intertidal area separately on the x -axis: Figure C.2 (p. 210).

Salt flux components are all normalised by the maximum (absolute) salt flux related to the net flow in a given estuary:

$$|F_1^{\max}| = \max |F_1| \quad (\text{C.1})$$

where $|F_1^{\max}|$ is the maximum seaward salt flux [$\text{psu m}^3\text{s}^{-1}$]; and F_1 the salt flux related to the net flow (Eq. 5.6a, p. 82) [$\text{psu m}^3\text{s}^{-1}$].

This appendix is based on the supplementary material of:

Hendrickx, G.G., and Pearson, S.G. (2024). On the effects of intertidal area on estuarine salt intrusion. *Journal of Geophysical Research: Oceans*, **29**(9):e2023JC020750.

The total salt flux is the sum of the four salt flux components, and is normalised similarly—i.e., $|F_1^{\max}|$ (Eq. C.1). The same holds for the salt flux components distinguishing between the channel and intertidal area (Fig. C.2). This normalisation—which enables cross-comparison—allows the separated salt flux components to reach values larger than one—or smaller than negative one. This is, e.g., the case for the salt flux related to the net flow for well-mixed estuaries (Fig. C.2c), as well as the total salt fluxes in the well-mixed estuaries (Fig. C.2o). This implies that there are opposing flux directions, which cancel out when aggregated over the width.

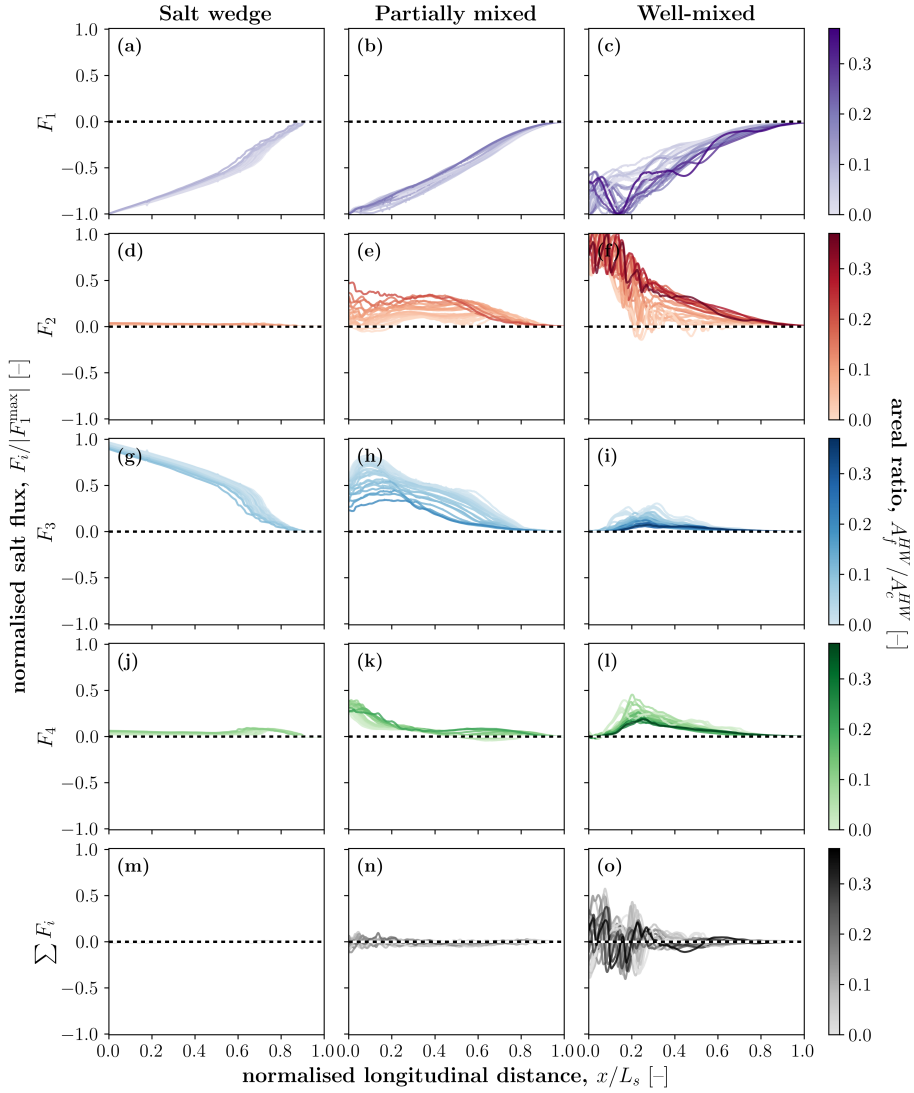


Figure C.1: Salt flux decomposition for three estuary classes: salt flux related to (a–c) the net flow (F_1), (d–f) the tidal oscillation (F_2), (g–i) the estuarine circulation (F_3), (j–l) the time-dependent shear (F_4), and (m–o) the sum of the salt flux components ($\sum F_i$). The estuary classes are (a,d,g,j,n) salt wedge, (b,e,h,k,n) partially mixed, and (c,f,i,l,o) well-mixed. Positive values reflect landward fluxes, and vice versa.

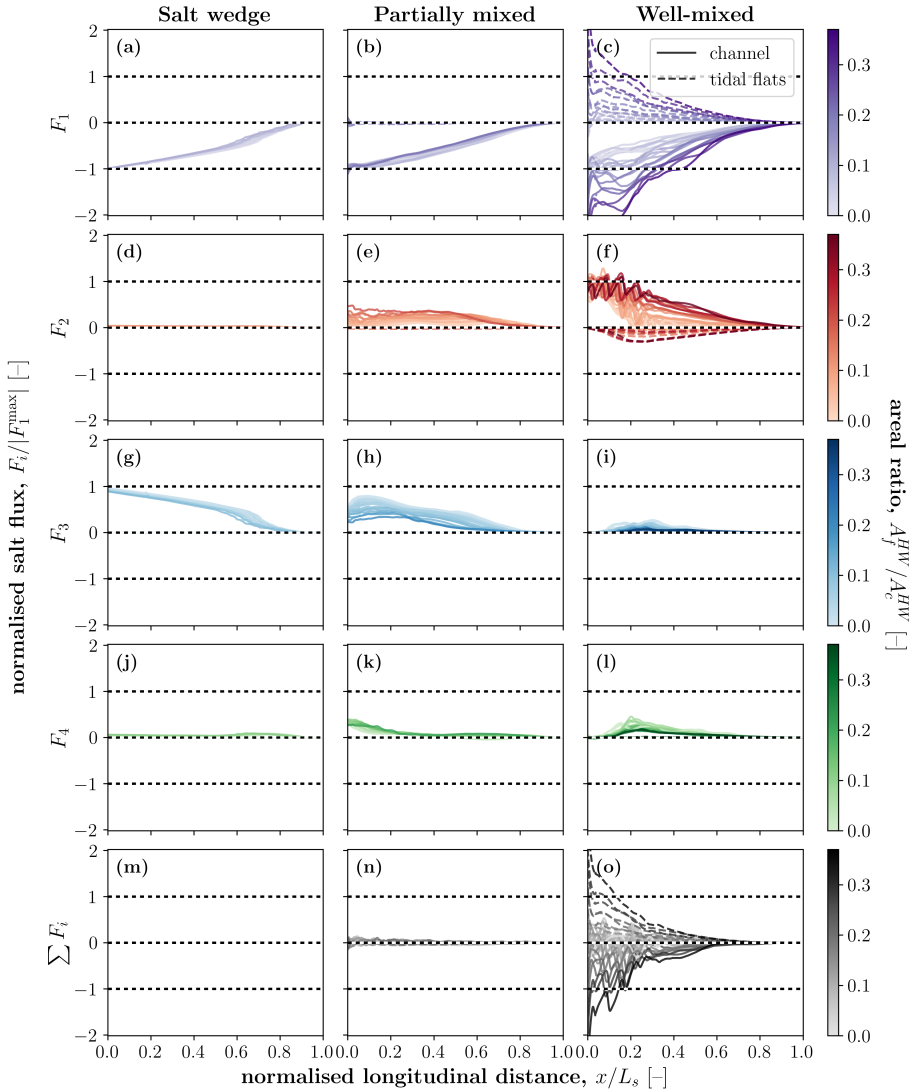


Figure C.2: Salt flux decomposition for three estuary classes distinguishing between channel and intertidal area: salt flux related to (a–c) the net flow (F_1), (d–f) the tidal oscillation (F_2), (g–i) the estuarine circulation (F_3), (j–l) the time-dependent shear (F_4), and (m–o) the sum of the salt flux components ($\sum F_i$). The estuary classes are (a,d,g,j,n) salt wedge, (b,e,h,k,n) partially mixed, and (c,f,i,l,o) well-mixed. Positive values reflect landward fluxes, and vice versa.

D

SUPPLEMENTARY MATERIAL

Chapter 8

The three axes of DARE—diversity, robustness, and adaptability—have been implemented on coastal flooding and estuarine salt intrusion mitigation measures. Here, the definitions and processing behind Figures 8.2 and 8.3 (pp. 143 and 145) are provided.

Diversity The *diversity*-axis in both figures (i.e., Figs. 8.2a-c and 8.3a-c) have been similarly processed. For Figure 8.2a-c, we used the BEWARE-dataset (Pearson *et al.*, 2017a); and for Figure 8.3a-c, we used the NEESI-dataset (Hendrickx, 2023a, labelled as “modelled data”,), which has been augmented with a neural network that has been trained using this dataset: ANNESI (labelled as “augmented data”; Hendrickx, 2022).

The BEWARE-dataset includes seven input variables, and four output variables that have been subdivided into frequency-components, such as infragravity contribution (for more details, see Pearson *et al.*, 2017b). In the displayed plots, we included (coral) reef characteristics that display a clear effect on the wave runup. All three displayed variables are drawn from the seven input variables.

This appendix is based on the supplementary material of:

Hendrickx, G.G., Pearson, S.G., Antolínez, J.A.A., and Aarninkhof, S.G.J. (*in review*). DARE to proactively react to unknown uncertainties in the Anthropocene. Submitted to *Earth's Future*.

The NEESI-dataset includes thirteen input parameters, and two output variables (for more details, see Hendrickx *et al.*, 2023a, 2023c, i.e., Chs. 2 and 3). In the displayed plots, we included the most relevant estuarine characteristics with respect to the salt intrusion (for a sensitivity analysis, see Hendrickx *et al.*, 2023c). The river discharge (Fig. 8.3a) is one of the thirteen input parameters; the channel cross-section (Fig. 8.3b) is the product of the channel depth and width; and the tidal damping follows from the description by van Rijn (2011), which is similarly determined in Hendrickx *et al.* (2023c):

$$\delta = \frac{1}{2} \left(\frac{f}{c_t} - \gamma \right) \quad (\text{D.1})$$

with

$$\begin{aligned} f &= \frac{8}{3\pi} \frac{gn_c^2 u_t}{d_c^{4/3}} \\ c_t &= \sqrt{gd_c} \\ u_t &= \frac{a}{2\sqrt{2}} \sqrt{\frac{g}{d_c}} \end{aligned}$$

where δ is the tidal damping coefficient [m^{-1}]; f a friction coefficient [s^{-1}]; c_t the frictionless tidal wave celerity [ms^{-1}]; γ the (width) convergence [m^{-1}]; g the gravitational acceleration [$g = 9.81 \text{ ms}^{-2}$]; n_c the channel friction, expressed as Manning's n [$\text{sm}^{-1/3}$]; u_t the tidal velocity [ms^{-1}]; d_c the channel depth [m]; and a the tidal range [m].

On the vertical axis, we display the likelihood of the wave runup (Fig. 8.2a-c) or salt intrusion length (Fig. 8.3a-c) to be in the upper 25%-quartile (i.e., $P(y > q_{0.75})$). This has been calculated by binning the x -variable ($n = 50$) and determining per bin what the likelihood—i.e., what percentage of the data—is within this upper 25%-quartile:

$$P_i(y_i > q_{0.75}) = \frac{N(y_i > q_{0.75})}{N(y_i)} \quad (\text{D.2})$$

where P_i is the likelihood/probability in bin i ; y_i are the values of salt intrusion in bin i ; and $q_{0.75}$ the values of the full set of y that are in the upper 25% of the data.

As factorial sampling has been used to define the input space of the BEWARE-dataset, the bins follow the included values per input variable.

Adaptability The *adaptability*-axis in Figure 8.2d presents data from Howells *et al.* (2013). The plot shows the effect of a thermal stress event on the healthy coral cover on a reef at Miall Island (southern Great Barrier Reef, Australia) from April 2008 to March 2009. The effect of thermal history—i.e., thermal acclimatisation—has been studied by transplanting corals from Magnetic Island (central GBR) to Miall island. The southern corals (“transplants”) are used to cooler temperatures and are more affected by a heat event than the central corals (“natives”), which are more accustomed to warmer waters and thus less susceptible to heat events. The difference does not originate from different coral species, as all studied colonies in Howells *et al.* (2013) are of the same coral species: *Acropora millepora*.

The *adaptability*-axis in Figure 8.3d and e includes data from Hendrickx *et al.* (2024b), which is open access (Hendrickx *et al.*, 2024a). The plots show the effect of placing a (temporary) sill in a micro-tidal system on the salt intrusion length. Figure 8.3d and e are visualisations of hydrodynamic model output.

Robustness The *robustness*-axis in both Figures (i.e., Fig. 8.2e and Fig. 8.3f) are similarly processed. For Figure 8.2e, we used the BEWARE-dataset (Pearson *et al.*, 2017a); and for Figure 8.3f, we used the NEESI-dataset (Hendrickx, 2023a). Figure 8.2e displays the (reef) width against the wave runup, and Figure 8.3f the (channel) depth against the salt intrusion length.

The robustness is determined by binning the width ($n = 12$) and depth ($n = 50$), and determining the standard deviation of the output variable per bin—i.e., the conditional standard deviation of y given x . Subsequently, the robustness increases with decreasing variation in the output (e.g., Taleb & Douady, 2013):

$$R(x_i) = -\sigma(y_i|x_i) \tag{D.3}$$

where R is the robustness; x_i the (representative) value of width/depth for bin i ; y_i the (representative) value of wave runup/salt intrusion length for bin i ; and σ the standard deviation.

FE

NATURE-BASED SOLUTION

Discharge management

E.1 Introduction

A multitude of studies have shown the strong (negative) correlation between the salt intrusion and river discharge (e.g., Hendrickx *et al.*, 2023c; Monismith *et al.*, 2002; Ralston & Geyer, 2019; Savenije, 1993): salt intrusion reduces with increasing discharge, and vice versa. With projections of reduced river discharge and an increased frequency of extreme droughts due to climate change (Lee *et al.*, 2024), salt intrusion is a major threat to freshwater availability in coastal regions (Costall *et al.*, 2018).

In addition to the strong correlation of salt intrusion to a constant discharge, salt intrusion reacts differently to an increase in river flow compared to a decreasing discharge (e.g., Biemond *et al.*, 2022; Chen, 2015; Gong & Shen, 2011; Hetland & Geyer, 2004; Kranenburg, 1986; MacCready, 1999; Monismith, 2017): The estuary responds quicker to an increase in river discharge compared to a decrease.

This asymmetric response of the salt intrusion to temporal changes in discharge might be a useful mechanism to “exploit” during a drought when river discharge is scarce—and so the supply of much-desired freshwater. Monismith (2017) investigated a similar opportunity with counterproductive results: the salt intrusion increased with variable river discharge compared to a constant river discharge. They reached these results using a simplified model in which the tide is represented by a dispersion coefficient.

The aim here is to investigate whether the discharge fluctuations can be used to

Table E.1: Input parameters including their values or ranges and corresponding units. The idealised geomorphology of the estuaries is inspired by the Westerschelde (the Netherlands), Pungue (Mozambique), and Hau (Vietnam).

Parameter	Symbol	Value	Unit
Tidal range	a	1.0 – 4.0	m
River discharge (ref.)	Q_0	200 – 3,000	m^3s^{-1}
Depth	d	10.0	m
Width	W	2,500	m
Bottom friction	n	0.023	$\text{m}^{-1/3}\text{s}$
Convergence	γ	5.6×10^{-5}	m^{-1}

preserve scarce freshwater reserves while maintaining a given salt intrusion length. In this exploratory study, the discharge fluctuations are synced with the tidal oscillation with differing phase differences.

E

E.2 Method

E.2.1 Input space

For this study, we used a similar input space as in Hendrickx and Pearson (2024b, Ch. 5), with the difference being a variable river discharge (Tab. E.1). We have included two types of discharge change: (1) a step-change in river discharge; and (2) a fluctuating river discharge with the same period as the tide. The step-change is either a 50% increase or decrease in river discharge; and the oscillating discharge has an amplitude of 50% around its mean value.

Thus, the time-dependent discharges can be expressed as follows:

$$Q_s(t) = \begin{cases} Q_0 & \text{for } t < t_s \\ (1 \pm r_Q) Q_0 & \text{for } t \geq t_s \end{cases} \quad (\text{E.1a})$$

$$Q_f(t) = Q_0 (1 + r_Q \sin[\omega t - \phi]) \quad (\text{E.1b})$$

where, Q_s is the step-changed river discharge [m^3s^{-1}]; Q_f the fluctuating river discharge [m^3s^{-1}]; Q_0 the reference river discharge [m^3s^{-1}]; r_Q the discharge ratio, in both cases, $r_Q = 1/2$ [-]; t is time [s]; t_s the timing of the step-change [s]; ω the tidal frequency [s^{-1}]; and ϕ the phase difference with the tidal signal [rad]:

$$\eta(t) = \frac{a}{2} \sin[\omega t] \quad (\text{E.2})$$

where η is the offshore boundary water level [m]; and a the tidal range [m].

Note, however, that the phase lags are imposed at the upstream boundary condition—i.e., the river discharge—located 200 km from the estuary mouth. This means that the effects of the changing discharge take time to reach the area of interest. The same holds for the tidal wave, which is imposed 30 km offshore from the estuary mouth. In both cases, the information of changing conditions—either discharge or water level—is transported at the speed of the wave celerity. Using the wave celerity's definition for shallow water flow ($c = \sqrt{gd}$) and the water depths of 10 and 30 m for the estuary

Table E.2: Boundary conditions per estuary class. The estuarine Richardson numbers are based on Equation (E.4).

Class	a [m]	Q_0 [m ³ s ⁻¹]	Ri_E [-]
Salt wedge	1.0	3,000	4.87
Partially mixed	2.0	500	0.101
Well-mixed	4.0	200	0.00507

and the shelf, respectively, the effective phase lag between the boundary conditions is approximately π radians. Thus, the effective phase lag equals:

$$\phi^* = \phi - \pi \quad (\text{E.3})$$

where ϕ is the imposed phase lag between the tidal and discharge signals [rad].

Furthermore, three estuary classes are considered based on the estuarine Richardson number (Fischer, 1972):

$$Ri_E = \frac{g\beta s_0 Q_0}{W u_t^3} \quad (\text{E.4})$$

where g is the gravitational acceleration [$g = 9.81 \text{ ms}^{-2}$]; β the haline contraction coefficient [$\beta = 7.6 \times 10^{-4} \text{ psu}^{-1}$]; s_0 the salinity (at the mouth) [$s_0 = 30 \text{ psu}$]; Q_0 the (reference) river discharge [m³s⁻¹]; W the width [m]; and u_t the tidal flow velocity [ms⁻¹], which is estimated as:

$$u_t \approx \frac{a}{2\sqrt{2}} \sqrt{\frac{g}{d}}$$

where a is the tidal range [m]; and d the depth [m]. This estimation of the tidal velocity equals the root-mean-squared velocity of a monochromatic (tidal) wave.

The estuarine Richardson number describes the level of stratification in an estuary from which three classes are derived: (1) $Ri_E > 0.8$, salt wedge; (2) $0.08 < Ri_E < 0.8$, partially mixed; and (3) $Ri_E < 0.08$, well-mixed. These criteria have been used in determining the sets of boundary conditions, as presented in Table E.2.

E.2.2 Hydrodynamic model

The input space as described in Appendix E.2.1 is simulated with the use of Delft3D Flexible Mesh, a process-based hydrodynamic modelling software (Kernkamp *et al.*, 2011). This modelling software numerically solves for the Reynolds-averaged Navier-Stokes equations with the assumption of hydrostatic pressure and the implementation of the k - ϵ turbulence closure model.

Similar as in Hendrickx and Pearson (2024b) and Hendrickx *et al.* (2023a, 2023c, 2024b, Chs. 2 to 5), the model domain consists of two parts: (1) the shelf, and (2) the estuary. The shelf is a 30×30 km square domain with a grid resolution varying from $1,000 \times 1,000$ m at the offshore boundaries to 62.5×62.5 m at the estuary mouth. This transition in grid resolution is achieved by steps of a factor two: from $1,000 \times 1,000$ m to 500×500 m, etc. These different grid resolutions are glued together using triangular grid cells.

The estuary is schematised as a deformed rectangle of 200 km long and a converging width towards its upstream boundary: the estuary is 2,500 m wide at the mouth (Tab. E.1) and reaches 600 m at its upstream end. The grid resolutions are similar in

Table E.3: Response time-scales for step-change river discharge. T_r^\uparrow : response time-scale with increasing river discharge, i.e., reducing salt intrusion; T_r^\downarrow : response time-scale with reducing river discharge, i.e., increasing salt intrusion.

Estuary class	T_r^\uparrow [h]	T_r^\downarrow [h]
salt wedge	19.76	48.96
partially mixed	25.98	43.10
well-mixed	43.38	249.4

the estuary compared to the shelf, with 62.5×62.5 m grid cells at the mouth enlarging to $< 250 \times 1,000$ m upstream. The high resolution—i.e., 62.5×62.5 m—reaches 150 km upstream after which the grid transitions to a coarser resolution, again facilitated by triangular grid cells.

As this study focuses on salt dynamics, the hydrodynamic model simulations are executed in three dimensions. The vertical axis is discretised using Z, σ -layers: a combination of Z -layers topped with five σ -layers. The Z -layers are used for the majority of the water column as they are better suitable for computing pycnoclines (Stelling & van Kester, 1994). At $z = -4.0$ m, the interface between the two discretisation schemes is located. Depending on the tidal range (Tab. E.2) and the moment in the tidal cycle, the thickness of the σ -layers changes, with $\Delta\sigma \in [0.4, 1.2]$ m. The Z -layers maintain a constant thickness of $\Delta Z = 1.0$ m down to $z_{cst} = -10.0$ m after which they exponentially grow with a factor 1.10 each cell, which only occurs offshore.

E

E.3 Results

The results are presented in parts based on the type of discharge development: (1) step-change in Appendix E.3.1; and (2) oscillating in Appendix E.3.2.

E.3.1 Step-change

The step-change river discharge signal follows an exponential function of the following form:

$$L_s(t \geq t_s) = L_s^\infty + \Delta L_s \exp\left[-\frac{t - t_s}{T_r}\right] \quad (\text{E.5})$$

where L_s^∞ is the salt intrusion length of the new quasi-steady state [m]; ΔL_s the difference in salt intrusion length due to the change in river discharge [m]; and T_r the response time-scale [s].

The exponential fits to both the increasing and the decreasing salt intrusion length due to the step-change river discharge are displayed in Figure E.1 together with the tide-averaged salt intrusion length. In Figure E.1, the exponential transition to the new quasi-steady state of the salt intrusion length is apparent.

Figure E.1 also shows the longer response time of a decreasing river discharge, i.e., an increasing salt intrusion length. In addition, the three estuary classes show a distinct difference in response times with the well-mixed estuary being substantially slower to respond. All six response time-scales are listed in Table E.3.

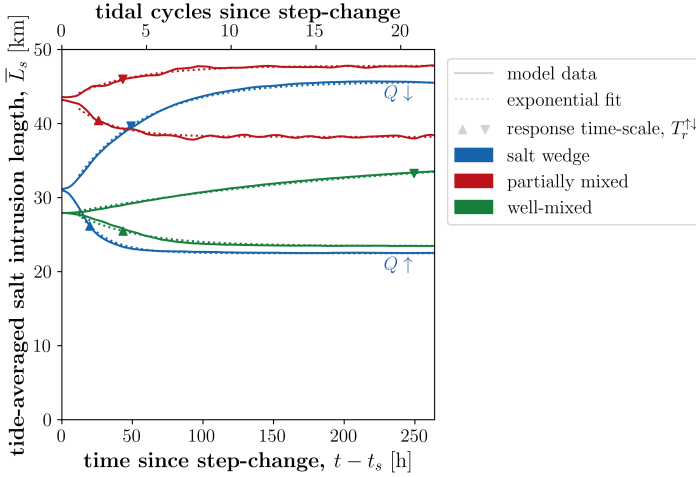


Figure E.1: Salt intrusion development in response to step-change in river discharge (Eq. E.1a). Exponential fits follow the expression given in Equation (E.5).

E

E.3.2 Oscillations

The river discharge oscillating with the tidal signal results in a limited effect on the tide-averaged salt intrusion (Fig. E.2). Generally, the oscillating discharge signal barely affects the salt intrusion length. While the well-mixed estuary is especially insensitive to the oscillating discharge, the salt wedge and partially mixed estuaries show some sensitivity: an increased salt intrusion for $\phi \in \{\frac{1}{2}\pi, \pi\}$ (i.e., discharge peak during low water or flood); and a decreased salt intrusion for $\phi \in \{0, \frac{3}{2}\pi\}$ (i.e., discharge peak during high water or ebb).

In addition to the tide-averaged minor effects, the phasing of the oscillations shifts slightly for the salt wedge estuary as well as the partially mixed (Fig. E.3a and b), but again the well-mixed estuary shows the same signal for the reference case as well as every phase lag (Fig. E.3c).

E.4 Discussion

Taking the effective phase lag into account (Eq. E.3), a very minor reduction in salt intrusion can be achieved when the peak river discharge is after the tidal flood—i.e., high water to ebb. This means that when the tidally oscillating salt intrusion length is at its farthest, the peak in river discharge pushes it out.

The salt intrusion length in Figure E.3 oscillates clearly with the tidal frequency. However, as both the tidal and the discharge signal share this frequency, it may be hard to discern which forcing condition drives the oscillation. To differentiate, we can use the formulation by Hetland and Geyer (2004) for the salt intrusion length under oscillating forcing:

$$L_s(t) = \bar{L}_s + \frac{\Delta L_s}{1 + (\omega T_r)^2} (\sin[\omega t] - \omega T_r \cos[\omega t]) \quad (\text{E.6})$$

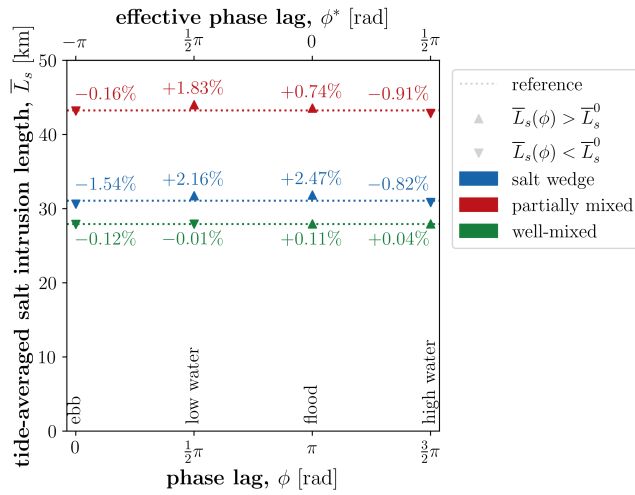


Figure E.2: Tide-averaged salt intrusion length for different phase lags. The reference is based on a constant river discharge (or $r_Q = 0$ in Eq. E.1b), denoted as L_s^0 ; and $\bar{L}_s(\phi)$ represents the oscillating discharge signal.

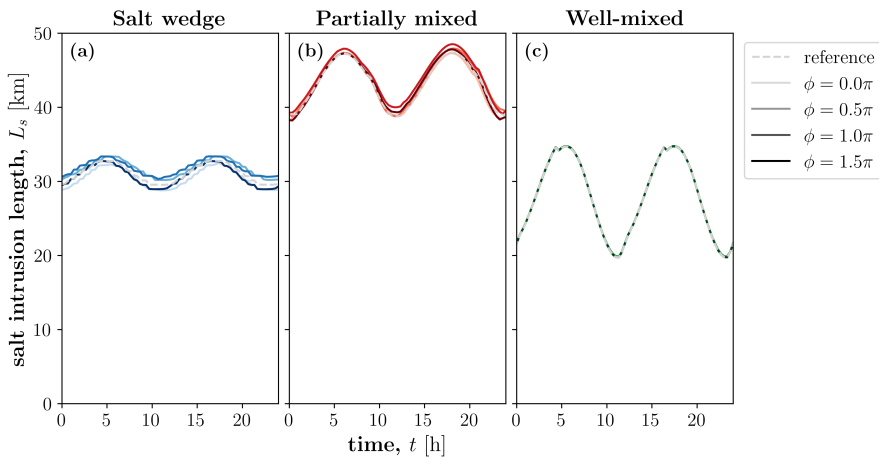


Figure E.3: Salt intrusion development in response to oscillating river discharge. The coloured, dashed lines represent the tidal oscillation of the salt intrusion length; and the grey, dashed lines represent the salt intrusion length with constant river discharge, i.e., the reference case.

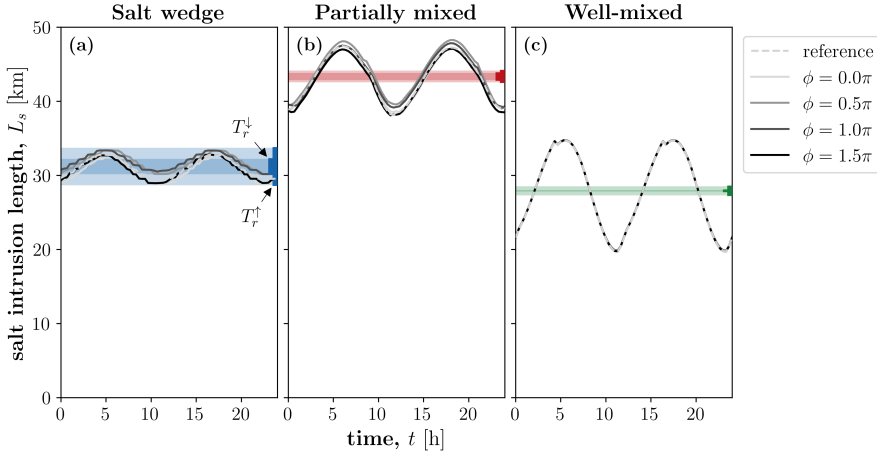


Figure E.4: Range of oscillating salt intrusion due to river discharge fluctuations. The ranges are based on the analytical solution given by Equation (E.6) using both response time-scales, increasing and decreasing.

Table E.4: Estuarine sensitivity to oscillating river discharge. T_r^\uparrow : response time-scale with increasing river discharge, i.e., reducing salt intrusion; T_r^\downarrow : response time-scale with reducing river discharge, i.e., increasing salt intrusion; ω forcing frequency, which in all cases equals the tidal forcing, $\omega = 1.45 \times 10^{-4} \text{ s}^{-1}$.

Estuary class	ωT_r^\uparrow [-]	ωT_r^\downarrow [-]
salt wedge	10.34	25.64
partially mixed	13.60	22.57
well-mixed	22.71	130.6

where \bar{L}_s is the tide-average salt intrusion length [m]; and ΔL_s the maximum difference in salt intrusion length of the tidal cycle [m].

Figure E.4 shows the same data as in Figure E.3 in grey-scale and presents the range of the salt intrusion over the oscillations following Equation (E.6). Per estuary class, both response time-scales are used in Equation (E.6) (Tab. E.3).

For the salt wedge estuary, the oscillating salt intrusion falls within the bandwidth of Equation (E.6) with the lower response time-scale, i.e., T_r^\uparrow (Fig. E.4a). However, for the other estuary classes, Equation (E.6) substantially under-predicts the fluctuations of the salt intrusion length (Fig. E.4b and c). This is on one hand interesting, as Equation (E.6) was developed for partially mixed estuaries (Hetland & Geyer, 2004). On the other hand, the discharge for the salt wedge estuary is substantially larger than for the other two estuaries (Tab. E.2), and so the 50% fluctuation results in larger absolute values. In addition, the tidal oscillation becomes more dominant with increasing tidal range, which is smallest for the salt wedge and largest for the well-mixed estuary (Tab. E.2).

Nevertheless, it remains questionable whether there is a substantial influence of the river discharge on the salt intrusion length. As Hetland and Geyer (2004) stated, the

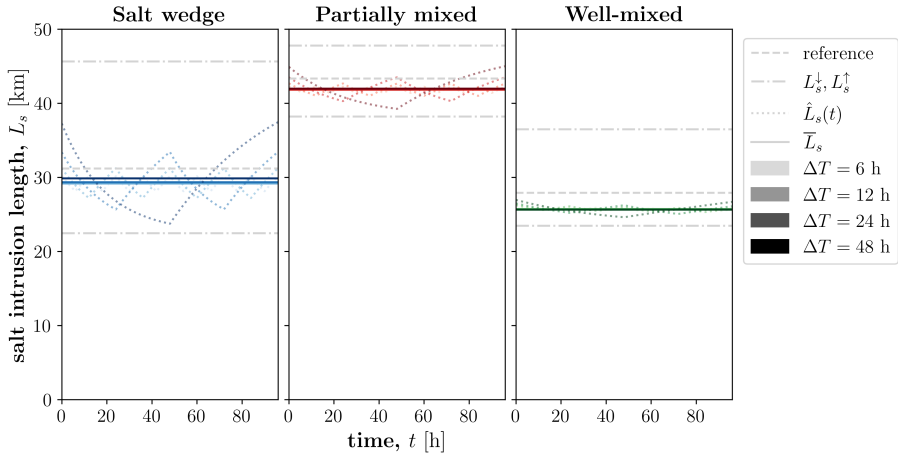


Figure E.5: Salt intrusion length estimates for a block-wave discharge signal. The salt intrusion length is estimated with Equation (E.7), and the block-wave discharge signal is described by Equation (E.8). The reference salt intrusion (dashed line) follows from a constant river discharge, Q_0 .

estuarine salt intrusion will respond very little for $\omega T_r \gg 1$; with the smallest value in this study being $\omega T_r > 10$ (Tab. E.4).

The results shown in Figures E.2 to E.4 are representative for a sinusoidal discharge signal (i.e., Eq. E.1b). However, Monismith (2017) investigated a block-wave signal. Although no hydrodynamic model runs with such a signal have been executed, we can explore its potential using the following numerical approximation:

$$\hat{L}_s(t) \rightarrow L_s^{n+1} = L_s^n + \left(L_s^{\downarrow} - L_s^n \right) \frac{\Delta t}{T_r^{\downarrow}} \quad (\text{E.7})$$

where L_s^{n+1} is the salt intrusion length at $t + \Delta t$ [m]; L_s^n the salt intrusion length at t [m]; L_s^{\downarrow} the equilibrium salt intrusion length for either an increased river discharge (L_s^{\uparrow}), or a decreased river discharge (L_s^{\downarrow}), i.e., equal to L_s^∞ in Equation (E.5) [m]; Δt the time step [s]; and T_r^{\downarrow} the response time-scale for either an increased river discharge (T_r^{\uparrow}), or a decreased river discharge (T_r^{\downarrow}), i.e., equal to T_r in Equation (E.5) [s]. The values for L_s^{\downarrow} and T_r^{\downarrow} are determined using Equation (E.5).

The block-wave discharge signal changes from increased to decreased river discharge at the interval ΔT —and vice versa:

$$Q_b(t) = \begin{cases} (1 + r_Q) Q_0 & \text{for } t/\Delta T \in [2m, 2m + 1) \\ (1 - r_Q) Q_0 & \text{for } t/\Delta T \in [2m + 1, 2m + 2) \end{cases} \quad m \in \mathcal{N} \quad (\text{E.8})$$

where Q_b is the block-wave river discharge [m^3s^{-1}]; r_Q the discharge ratio as in Equations (E.1a) and (E.1b) [$r_Q = 1/2$]; and ΔT the block-duration, or step-interval [s].

The results of Equation (E.7) to the block-wave discharge (Eq. E.8) are presented in Figure E.5. Note that for $Q_b = (1 + r_Q) Q_0$, Equation (E.7) uses L_s^{\uparrow} and T_r^{\uparrow} —and vice versa.

According to Equation (E.7), the salt intrusion length does reduce in case of a block-wave discharge signal—albeit minor (3–8%). These findings contradict Monismith

(2017)—who applied analytical approximations for the response time-scales—suggesting there remain questions unanswered regarding river discharge management as a means of salt intrusion mitigation.

E.5 Outlook

This study explored the effects of various river discharge signals on the temporal development of the salt intrusion length. Both a step-change and an oscillating signal have been simulated using a process-based hydrodynamic model; and a block-wave signal has been explored using a simple numerical scheme (Eq. E.7).

These findings agree with literature about the asymmetric response of salt intrusion to temporal changes in river discharge: the response time-scale is smaller for an increasing river discharge, and vice versa ($T_r^\uparrow < T_t^\downarrow$, Tab. E.3). Also the oscillating discharge signal shows minor effects on the salt intrusion length, which can be explained by the relatively short forcing time-scale compared to the response time-scale (Tab. E.4) due to which the salt intrusion will respond very little (Hetland & Geyer, 2004). However, the block-wave discharge signal as explored by Monismith (2017) shows different results compared to this study (Fig. E.5); Figure E.5 shows some potential to reduce the salt intrusion by releasing pulses of freshwater such that the temporal average discharge remains the same (i.e., $\bar{Q}_b = Q_0$ in Eq. E.8). Note that the results presented in Figure E.5 are based on a relatively simple estimation of the estuarine response to a block-wave signal (i.e., Eq. E.7).

All in all, using the asymmetric response of salt intrusion length to temporal changes in river discharges should not be excluded from the options to control salt intrusion during a drought. The effects might be minor (e.g., Fig. E.5), but they could be enough to relieve the water stress during a drought, depending on the location(s) of freshwater intakes.

This exploratory study leads to the following next steps in investigating the options of modifying the discharge signal to save freshwater during a drought while pushing back the salt intrusion; i.e., the recommendations for follow-up studies are as follows:

1. Explore a block-wave discharge signal in more detail.
2. Explore a wider range of estuarine settings.
3. Explore with different forcing time-scales.
4. Perform physical experiments, small-scale or large-scale.

F

NATURE-BASED SOLUTION

Tidal mixing energy

F.1 Introduction

The tide has a profound effect on the salt intrusion (e.g., Geyer & MacCready, 2014; Kuijper & van Rijn, 2011; Lerczak *et al.*, 2009). However, the relation between the tide and the salt intrusion is by no means straightforward. In Chapter 3, the tidal range on itself did not stand out as a key characteristic determining the estuarine salt intrusion length (Fig. 3.4, p. 43). However, when presented as the tidal damping—or amplification—as in Figure 3.8 (p. 50), the dual influence of the tidal range becomes apparent: both tidal damping and amplification reduce the salt intrusion length.

This dual influence of the tidal range has also been shown in estuaries around the world by means of different responses of the salt intrusion to the spring-neap cycle: (1) increased salt intrusion during spring tide (i.e., larger tidal range); or (2) increased salt intrusion during neap tide (i.e., smaller tidal range). Examples of the first include Delaware Bay (NJ, USA; Geyer *et al.*, 2020), Hudson Estuary (NY, USA; Lerczak *et al.*, 2009; Wang *et al.*, 2017), Johor Estuary (Malaysia; Hasan *et al.*, 2013), and Madoamen Estuary (China; Gong & Shen, 2011); examples of the latter include Changjian River (China; Xue *et al.*, 2009), and Maipo River (Chile; Soto-Rivas *et al.*, 2024).

That the tidal energy has a dual effect on the salt intrusion is also reflected in how the tidal energy is generally represented in analytical approaches: using horizontal and vertical diffusivity coefficients (K_h and K_v). These coefficients are subsequently approx-

imated as being proportional to the tidal flow velocity (i.e., $K_h \propto u_t$ and $K_v \propto u_t$; e.g., Banas *et al.*, 2004; Guha & Lawrence, 2013; MacCready, 1999, 2007; Ralston *et al.*, 2008; Schijf & Schönflöd, 1953). In well-mixed estuaries, the estimate of the salt intrusion length is linearly related to the horizontal diffusion coefficient (i.e., $L_s \propto K_h$; e.g., Chatwin, 1976; Dijkstra & Schuttelaars, 2021; MacCready, 1999; Savenije, 1989). While in partially mixed and salt wedge estuaries, the estimate of the salt intrusion length is inversely related to the vertical eddy viscosity coefficient (i.e., $L_s \propto K_v^{-1}$; e.g., Chatwin, 1976; Dijkstra & Schuttelaars, 2021; Monismith *et al.*, 2002; Schijf & Schönflöd, 1953). This suggests that the salt intrusion either increases with tidal energy ($L_s \propto K_h \propto u_t$), or decreases with tidal energy ($L_s \propto K_v^{-1} \propto u_t^{-1}$). When combined, the dependence of the salt intrusion length on the tidal flow velocity—i.e., the tidal energy—would cancel out: $L_s \propto K_h K_v^{-1} \propto u_t u_t^{-1}$. As there is a profound influence of the tidal velocity on the salt intrusion length, a regime shift is expected to be at play, where in one regime the salt intrusion *increases* with increasing tidal velocity and *decreases* in another regime.

F.2 Hypothesis

In Chapter 5, a similar dual response in salt intrusion has been found as a result of modifying the intertidal area. In the case of the intertidal area, this discrepancy in estuarine response is related to the stratification-mixing balance expressed by the Simpson number (e.g., Burchard *et al.*, 2011; Geyer & MacCready, 2014; Stacey *et al.*, 2010, repeated from Eq. 5.9, p. 89):

$$Si = -\frac{g\beta d_c^2}{c_f u_t^2} \frac{\partial s}{\partial x} \quad (\text{F.1})$$

with

$$c_f = \frac{gn_c^2}{d_c^{1/3}}$$

$$u_t = \frac{a}{2\sqrt{2}} \sqrt{\frac{g}{d_c}}$$

where, g is the gravitational acceleration [$g = 9.81 \text{ ms}^{-2}$]; β the haline contraction coefficient [$\beta = 7.6 \times 10^{-4} \text{ psu}^{-1}$]; d_c the channel depth [m]; c_f the dimensionless friction coefficient [-]; u_t the tidal flow velocity [ms^{-1}]; s the salinity [psu]; n_c the Manning's n coefficient (in the channel) [$\text{m}^{-1/3}\text{s}$]; and a the tidal range [m]. Note that the tidal flow velocity (u_t) is estimated as the root-mean-squared velocity of a monochromatic wave.

Reiterating the findings of Chapter 5: for permanently stratified estuaries ($Si > 0.2$), the intertidal area reduces the salt intrusion; otherwise ($Si < 0.2$), the intertidal area enhances the salt intrusion. This relates to the dominant landward salt flux, which in the case of permanently stratified estuaries is the estuarine circulation (and tidal oscillation otherwise).

The aforementioned regime shift is, therefore, expected to be related to the Simpson number as well. This would imply that the dual response shown in Figure 3.8 (p. 50) is correlated to the Simpson number. In Figure 3.8, the salt intrusion is presented as function of the tidal damping, which is defined following van Rijn (2011, repeated from Eq. 3.7, p. 49):

$$\delta = \frac{1}{2} \left(\frac{f}{c_t} - \gamma \right) \quad (\text{F.2})$$

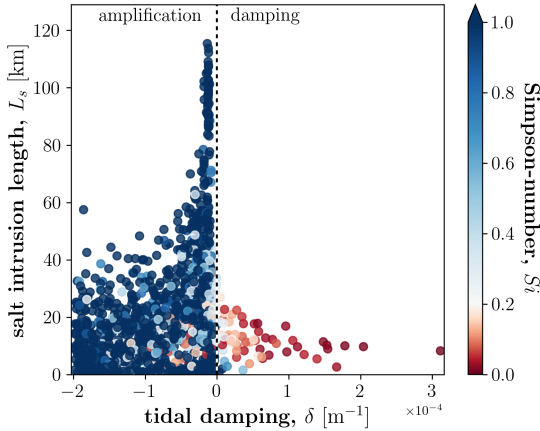


Figure F.1: Salt intrusion length as function of the tidal damping coloured by the Simpson number (δ and Si , Eqs. F.2 and F.1). Data from the NEESI-dataset (Hendrickx, 2023a). A negative damping coefficient reflects tidal amplification. Colour-coding based on Simpson number diverging from the critical Simpson number, $Si_c = 0.2$.

with

$$f = \frac{8}{3\pi} \frac{c_f u_t}{d_c}$$

$$c_t = \sqrt{gd_c}$$

where f is a friction parameter [s^{-1}]; c_t the frictionless tidal wave celerity [ms^{-1}]; and γ the convergence [m^{-1}]. Note that the damping coefficient is positive when the tidal range is damped, and negative when the tide is amplified; i.e., the tidal damping coefficient describes the tidal propagation by the following exponential decay function:

$$a(x) = a_0 \exp[-\delta x]$$

where a_0 is the tidal range at the mouth of the estuary [m].

Figure F.1 coloured the data presented in Figure 3.8 (p. 50) with the Simpson number (Si , Eq. F.1). The results presented in Figure F.1 suggest there to be a correlation: when the tidal range is amplified ($\delta < 0$), the Simpson number is generally above its critical value ($Si > 0.2$) representing the permanently stratified estuary; and for a dampened tide ($\delta > 0$), the Simpson number is generally below its critical value ($Si < 0.2$). Amplification of the tidal amplitude along the estuary—i.e., increasing the tidal energy—promotes tidal mixing, which reduces the stratification as well as the Simpson number. As the magnitude of the estuarine circulation scales with the Simpson number (Burchard & Hetland, 2010; Geyer & MacCready, 2014)—a scaling that becomes stronger for large Simpson numbers (i.e., $Si > 0.2$; Geyer & MacCready, 2014; Ralston *et al.*, 2008)—, increasing the tidal energy is expected to reduce the salt intrusion. However, the opposite is expected for non-permanently stratified estuaries (i.e., $Si < 0.2$), where an increased tidal energy would enhance the salt intrusion. Thus, damping of the tidal signal ($\delta > 0$) is expected to cause a reduction in salt intrusion. This line of reasoning is based on the discussion in Chapter 5 (i.e., Sec. 5.4).

F.3 Outlook

All in all, Figure F.1—as well as Figure 3.8 (p. 50)—show a clear nonlinear interaction between the tide and the salt intrusion length. In Dijkstra and Schuttelaars (2021), whether the salt intrusion length is dominated by the vertical mixing (i.e., $L_s \propto K_v^{-1}$) or the horizontal dispersion (i.e., $L_s \propto K_h$) is related to a regime shift marked by the importance of the gravitational circulation versus the dispersive transport. This is effectively the same as the regime shift based on the importance of the salt flux components related to the estuarine circulation and the tidal oscillation as found in Chapter 5, which was subsequently linked to the Simpson number. The regime shift in Dijkstra and Schuttelaars (2021) can also be linked to the Simpson number (squared)—i.e., the inverse of the tidal energy (squared).

The exploration presented in this appendix suggests that the regime shift associated with the dual response of the estuarine salt intrusion to the tide is determined by the stratification-mixing balance—here, expressed as the Simpson number (Eq. F.1). This leads to the following suggestion for a research question regarding follow-up investigations:

How does the stratification-mixing balance influence the effect of the tide on the salt intrusion?

Note that this question implicitly asks whether the stratification-mixing balance has a (significant) impact on how the tide affects the estuarine salt intrusion.

POSTFACE

“The goal of nature-based solutions to mitigate salt intrusion is fascinating, as such a goal cannot be achieved. To me, this project is a success when I am proven wrong.”

It is, indeed, a fascinating goal; a goal not many people have had considered prior. A goal that motivated a PhD project, which finalised with plenty of undiscovered pathways to explore.

Although this dissertation has shown the potential of nature-based solutions in mitigating salt intrusion, the initial disbelief in the achievability of this goal is not completely invalid: Nature-based solutions are generally coupled to the implementation of vegetation and/or sessile animals for the benefit of humans. Such an organism-focused approach would, indeed, be unsuccessful in mitigating salt intrusion. Nevertheless, the marriage between nature-based solutions and estuarine salt intrusion is not doomed to end up in a divorce. With this dissertation, the two have been put in the same room and the combination has been successfully tried. Whether we have become too narrow-minded about the concept of nature-based solutions, or the concept itself has become too narrowly scoped is a subjective matter—and possibly both true.

That is not to say that disproving the posed null-hypothesis was straightforward—not at all. We explored what drives estuarine salt intrusion, and conceptualised possible mitigation measures. We evaluated the multidisciplinary nature of estuaries, and reflected on what constitutes as nature-based solution. We dared to re-imagine how engineers could facilitate societal demands. All in pursue to develop nature-based solutions to mitigate salt intrusion.

Four years have passed since these words. All that time, they have stayed in the back of my mind. Whether it was the curiosity to explore this fascinating goal, or the drive to disprove its unachievability, I am not certain—probably a combination of the two. In either way, I believe this project has been a success.

Gijs Hendrickx

ACKNOWLEDGEMENTS

In my humble opinion, the acknowledgements are the hardest to write: I am doomed to forget people that are worth mentioning. Nevertheless, I have done my utmost best.

Let me start at the beginning of this PhD journey; I would like to thank my initial promoters Peter Herman and Stefan Aarninkhof. Thank you for your guidance and the trust you have put in me from the start. Within the same breath, I would also like to thank my copromoters Stuart Pearson and José Antolínez, who combinedly took over the role of Peter upon his retirement.

Peter, it remains unfortunate that you retired 1.5 years too early. Nevertheless, as a researcher *pur sang*, you fuelled my inner-researcher: questioning the “known” and having a curiosity beyond your formal training. Over the years, starting with my MSc thesis, I have watched and—hopefully—learned. Where you are an engineering ecologist, I approach from the other side—an ecological engineer. Let us meet in the middle.

Stefan, starting in the middle of the COVID-19 lockdown was not easy, but you guarded my sanity by assuring that I would not see the walls coming at me. It is interesting how you manage to always ask the annoying but important questions; always your mind on the bigger picture. Especially nearing the final stages, you kept your focus on the planning: how to finish in time. I really appreciate

this person-centric aspect of your supervision. Although, you almost lost this composure when we turned “philosophical” with Chapter 8.

Stuart, our first “meeting” regarding you replacing Peter as supervisor had an interesting setting: You wanted to make sure that you could provide what I was looking for in a supervisor. It was exactly that attitude I was looking for, and I think that our collaboration since has been fascinating, interesting, and fruitful. You may not have been an expert in the field of estuarine salt intrusion at the start of our journey but I think you have caught up remarkably fast—what took me two years felt like two months for you.

José, initially maybe not officially involved in my PhD, officiously you were. As soon as I reached out regarding a sampling challenge, you opened up a barrel of knowledge on various techniques unknown to me until then. Without you, the backbone of this dissertation (Chs. 2 and 3) would not have been—and who knows what this dissertation would have looked like? I think nothing like it. Although you also joined later as a copromotor, you took me under your (academic) wings from the start and put me in contact with your academic network, which almost felt like speed-dating for academics due to the many people you introduced me to.

Beside my supervisors, I would also like to thank all contributors to the chapters, and thereby to this dissertation: Ariana Torres-Knoop, Avelon Gerritsma, Ehab Meselhe, Floor Bakker, Gregory Fivash, Herman Kernkamp, Laura Manuel, Lennart Keyzer, Mark van Koningsveld, Marlein Geraeds, Sebastian Iglesias, Wouter Kranenburg, and Ymkje Huismans.

Ariana, our collaboration started off with us not really knowing how to achieve a dynamic pipeline for hundreds of model simulations. As an employee of SURF, you took up this task and helped us out greatly. You introduced me to the wonderful world of computer science via discussions and code-alongs. Without your contributions, our plans for a extensive sensitivity analysis would have remained plans—you helped translating them to practice. We are indebted to your assistance.

Herman, you have spent a tremendous amount of time talking me through the inner-workings of Delft3D Flexible Mesh. Your knowledge and enthusiasm have been inspiring; you even continued your online “lecture” from home when you had to prepare to go on holiday. Thank you very much for the time and effort you put in me to better understand the software.

Wouter and Ymkje, you guided me in my initial explorations on the topic of estuarine salt intrusion. As I was new to the topic and unfamiliar with the literature, this has given a boost to my start-up of the research.

Ehab, thank you very much for hosting me for three months at Tulane University. It has been a great experience to which you contributed greatly. You made sure I felt at home and took me along visits to the US Army Corps of Engineers, a boat trip on the Lower Mississippi River, a science symposium, among others.

Laura—or should I refer to you as dr. Manuel nowadays?—, thank you for helping me through the jungle of data-sources in the USA and showing me some nice tricks in getting all relevant data. In addition, I would also like to take the opportunity to thank everybody at the Tulane River and Coastal Centre: Ahmed

Khalifa, Ali Abdelrahim, Emma House, Kelin Hu, Md Nazmul Azim Beg, and Sherif Ahmed. I enjoyed my stay in NOLA thanks to you; the Mardi Gras parades, the field trip, the lunches, the symposium, and much more.

Floor, our collaboration has been obvious from the beginning. This does not mean it was less rewarding. I liked the way of working we maintained throughout this collaboration, which started off with co-supervising a MSc student, Sebastian. With slightly different approaches to doing research, I think we pushed each other in a favourable direction for which the collaborative paper stands as a proof (i.e., Ch. 6). A piece of work made possible by contributions of Lennart and Mark as well.

Gregory, you stepped in as my “personal ecologist” with Peter retiring. Your enthusiasm from the start was a great motivator for our collaborative study. You broaden my view into the wonderful world of ecology.

Avelon and Marlein, many thanks for sharing and trusting me with your precious model of the Rhine-Meuse Delta. Without your dedication and efforts in creating, calibrating, and validating this model, we would not have been able to do our socio-ecological evaluation (i.e., Ch. 7).

I would also like to thank the independent members of my committee: Caroline Katsman, Hans Burchard, Giovanni Coco, Karline Soetaert, and Zheng Bing Wang. Your time, effort, and interest in this dissertation is greatly valued. Also many thanks to the anonymous reviewers of our publications for their time, effort, and interest in our work. You made it quite hard from time to time and we occasionally may have disagreed, but your critical assessments of our work have greatly improved the end-products.

During these past four years, I have had the pleasure to collaborate with others as well on additional studies. Thank you Eleonora Saccon, Lucas Terlinden-Ruhl, Soesja Brunink, and Weiqiu Chen for joining forces and the great collaborations.

Eleonora, it has been great working with you, creating a nice bridge between engineering and ecology. Lucas, which started off as a MSc thesis has evolved in a nice publication—exceptional outcome for a MSc thesis but well-deserved. Soesja, our collaboration also started off as a MSc thesis that grew into a nice publication and some processing software. Weiqiu, despite moving to China for a professorship, you have been able to maintain leading a large review paper on a topic closely related to this dissertation. I have to thank you for including me in this great endeavour.

Maybe not cemented in writing, but it is only fair to acknowledge the diverse contributions of all participating in the SALTISolutions-project. Of course a thanks to Julie Pietrzak for leading the project without whom this and a multitude of other dissertations would not have been. Despite being physically far apart, I want to thank all involved in the project for sharing their knowledge, the interesting discussions, and fun times we had over the years: Cem, Shraavan, Tess, Marlein, Fateme, Inge, Daan, Henk, Bouke, Jiyong, Wessel, Eleonora, Rutger, Weiqiu, Jesse, Floor, Robert-Jan, Paran, Bas, Avelon, Mo, and many more.

A special thanks goes to Avelon, Floor, Henk, Marlein, and Tess for the (almost) weekly coffee-moments. These weekly meet-ups started off during COVID-19 partly as a measure to check-in on each other, partly to see a face instead of reading papers all day. The continuation of this “tradition” is greatly valued and it has helped me a lot throughout those four years. These weekly coffees felt a bit like sanity-checks and provided a safe setting where I could speak openly about anything. I want to thank you all for creating such a safe-haven.

Most of my days as PhD, I have spent in room 3.62; the office everybody wanted to be part of. This, of course, largely due to the great colleagues residing here. Bart, Jakob, Floris, Mario, Paul, Su, Vincent, you added a spark of party to doing a PhD with music-hour every Thursday to get into the mood for drinks at PSOR. The day-start with coffee, because the engine needs its fuel to run on. The discussions on the best IDE for Python, and valuable advice on figures, text, and even emails. Thank you all for supporting me throughout my PhD journey.

Of course the awesomeness of colleagues did not stop at the walls of our room; the many coffee breaks with the whole floor to re-caffeinate, vent frustrations, talk research, solve coding problems, and also just to get out of that chair. Plenty of reasons to cycle 34 kilometres everyday—or at least, when the weather allowed it.

Luckily, there was also a life outside academia. Family and friends have made that clear time and again. To my friends—Bestuur 124, Churlen, De Groep, MDP-271, and everybody who cannot be categorised in one of these groups—, thank you for pulling me out of my PhD-cocoon and be the perfect distraction. Your interest in my research is really appreciated, and the subsequent notion that there is so much more to do even more so.

Last but certainly not least, to my family; thank you very, very much for your support throughout this journey. Bas, voor de fascinerende gesprekken die zo nu en dan een filosofisch tintje kregen. Sam, voor de smaakvolle momenten waarbij je me motiveert om net weer een stapje gekker te doen in de keuken. Pa, het was fijn om een terugvalbasis te hebben en een proefkonijn voor mijn onderzoekswerk. Je interesse in mijn onderzoek en de publicaties die eruit zijn gekomen waren motiverend; het was een teken dat mijn werk ook relevant is buiten academia. Ma, voor al je zorgen om mij als persoon. Je zorgde ervoor dat ik mezelf niet verloor in mijn onderzoek—onderzoek doen is leuk, maar het moet niet ten koste gaan van de onderzoeker.

Thank you all for joining me along this great journey.

Gijs Hendrickx
Rotterdam, November 2024

ABOUT THE AUTHOR

Gijs Hendrickx was born on March 25, 1995, in Bergen op Zoom, the Netherlands. In 2013, he concluded his secondary education (gymnasium) at Gymnasium 't Juvenaat Heilig Hart in Bergen op Zoom.

Thereafter, he moved to Delft to pursue a BSc as well as a MSc in Civil Engineering at Delft University of Technology. During his BSc, he spent three months in Kumasi, Ghana, working on a greenhouse design and business plan together with two fellow students from TU Delft (but different BSc-studies).

The MSc was focused on hydraulic engineering, and more specifically coastal and river engineering; a harbinger for the interest in estuarine dynamics explored in this dissertation. As part of the MSc, he worked two months in Buenos Aires, Argentina, on the port development of Bahía Blanca in a multidisciplinary team of six MSc-students. Eventually, the MSc was concluded with a thesis at Deltares on biophysically modelling coral reefs. If it were not for COVID-19, he would have had the opportunity to present this work at the Dutch national conference for coastal research (NCK).

During this MSc thesis, his curiosity-driven appetite for research reached the surface, which subsequently resulted in starting his PhD in the Coastal Engineering section at Delft University of Technology in November 2020.



Photo by © Alex Hendrickx

Personalia

Gijs Gabriël Hendrickx

March 25, 1995; Bergen op Zoom, the Netherlands

LinkedIn: <https://www.linkedin.com/in/gijshendrickx/>

Education

2016–2020 MSc Civil Engineering, Delft University of Technology

2013–2016 BSc Civil Engineering, Delft University of Technology

2007–2013 VWO, Gymnasium 't Juvenaat Heilig Hart

Employment

2020–2024 PhD candidate, Delft University of Technology

2020–2020 Engineer, TWD

LIST OF PUBLICATIONS

Articles

First-authored articles

7. **Hendrickx, G.G.**, Pearson, S.G., Antolínez, J.A.A., and Aarninkhof, S.G.J. (*in review*). DARE to proactively react to unknown uncertainties in the Anthropocene. Submitted to *Earth's Future*. [Chapter 8]
6. **Hendrickx, G.G.**, Fivash, G.S., Gerritsma, A., Geraeds, M.E.G., and Pearson, S.G. (*in prep.*). Socio-ecological evaluation of estuary-scale interventions: Case study of reopening the Haringvliet, the Netherlands. To be submitted to *Ecological Engineering*. [Chapter 7]
5. **Hendrickx, G.G.**, and Pearson, S.G. (2024). On the effects of intertidal area on estuarine salt intrusion. *Journal of Geophysical Research: Oceans*, **29**(9):e2023JC020750. doi:[10.1029/2023JC020750](https://doi.org/10.1029/2023JC020750). [Chapter 5]
4. **Hendrickx, G.G.**, Manuel, L.A., Pearson, S.G., Aarninkhof, S.G.J., and Meselhe, E.A. (2024). An earthen sill as a measure to mitigate salt intrusion in estuaries. *Estuaries and Coasts*, **47**(5):1199–1208. doi:[10.1007/s12237-024-01359-2](https://doi.org/10.1007/s12237-024-01359-2). [Chapter 4]

3. **Hendrickx, G.G.**, Kranenburg, W.M., Antolínez, J.A.A., Huismans, Y., Aarninkhof, S.G.J., and Herman, P.M.J. (2023). Sensitivity of salt intrusion to estuary-scale changes: A systematic modelling study towards nature-based mitigation measures *Estuarine, Coastal and Shelf Science*, **295**:108564. doi:[10.1016/j.ecss.2023.108564](https://doi.org/10.1016/j.ecss.2023.108564). [Chapter 3]
2. **Hendrickx, G.G.**, Antolínez, J.A.A., and Herman, P.M.J. (2023). Predicting the response of complex systems for coastal management. *Coastal Engineering*, **182**:104289. doi:[10.1016/j.coastaleng.2023.104289](https://doi.org/10.1016/j.coastaleng.2023.104289). [Chapter 2]
1. **Hendrickx, G.G.**, Herman, P.M.J., Dijkstra, J.T., Storlazzi, C.D., and Toth, L.T. (2021). Online-coupling of widely-ranged timescales to model coral reef development. *Environmental Modelling & Software*, **143**:105103. doi:[10.1016/j.envsoft.2021.105103](https://doi.org/10.1016/j.envsoft.2021.105103).

Co-authored articles

5. Chen, W., **Hendrickx, G.G.**, Bakker, F.P., Bootsma, J., van der Sande, W.M., Saccon, E., Siemes, R.W.A., Roos, P.C., and Hulscher, S.J.M.H. (*in prep.*). The effectiveness of nature-based solutions in mitigating salt intrusion in estuaries: A review. To be submitted to *Science of the Total Environment*,
4. Terlinden-Ruhl, L., Couasnon, A., Eilander, D., **Hendrickx, G.G.**, Mares-Nasarre, P.M.N., and Antolínez, J.A.A. (*in review*). Exploring uncertainty to reduce the computational cost of compound flood risk assessments: A case study of Charleston County. Submitted to *Natural Hazards and Earth System Sciences*.
3. Saccon, E., **Hendrickx, G.G.**, Hulscher, S.J.M.H., Bouma, T.J., and van de Koppel, J. (*in review*). Wetland topography drives salinity resilience in freshwater tidal ecosystems. Submitted to *Ecological Engineering*.
2. Bakker, F.P., **Hendrickx, G.G.**, Keyzer, L.M., Iglesias, S.R., Aarninkhof, S.G.J., and van Koningsveld, M. (*in review*). Trading off dissimilar stakeholder interests: Changing the bed level of the main shipping channel of the Rhine-Meuse Delta while considering freshwater availability. Submitted to *Environmental Challenges*. [Chapter 6]
1. Brunink, S., and **Hendrickx, G.G.** (2024). Predicting ecotopes from hydrodynamic model data: Towards an ecological assessment of nature-based solutions. *Nature-Based Solutions*, **6**:100145. doi:[10.1016/j.nbsj.2024.100145](https://doi.org/10.1016/j.nbsj.2024.100145).

Datasets and software

8. Saccon, E., **Hendrickx, G.G.**, Hulscher, S.J.M.H., Bouma, T.J., and van de Koppel, J. (2024). *Dataset underlying the study* “Wetland topography

- drives salinity resilience in freshwater tidal ecosystems*". 4TU.ResearchData. doi:[10.4121/93d8d223-e2ab-486e-a85b-da14789532d4](https://doi.org/10.4121/93d8d223-e2ab-486e-a85b-da14789532d4).
7. **Hendrickx, G.G.**, and Pearson, S.G. (2024). *Dataset underlying the study "On the effects of intertidal area on estuarine salt intrusion"*. 4TU.ResearchData. Dataset. doi:[10.4121/c357f1c7-dea8-4971-b5a1-c54c42e4172a](https://doi.org/10.4121/c357f1c7-dea8-4971-b5a1-c54c42e4172a). [Chapter 5]
 6. **Hendrickx, G.G.**, Manuel, L.A., Pearson, S.G., Aarninkhof, S.G.J., and Meselhe, E.A. (2024). *Dataset underlying the study "An earthen sill as a measure to mitigate salt intrusion in estuaries"* 4TU.ResearchData. Dataset. doi:[10.4121/10d493df-8efb-442b-8c3d-04e92bcf4c4e](https://doi.org/10.4121/10d493df-8efb-442b-8c3d-04e92bcf4c4e). [Chapters 4 and 8]
 5. **Hendrickx, G.G.**, and Brunink, S. (2023). *EMMA: Ecotope-Map Maker based on Abiotics*. 4TU.ResearchData. Software. doi:[10.4121/0100fc5a-a99c-4002-9864-3faade3899e3](https://doi.org/10.4121/0100fc5a-a99c-4002-9864-3faade3899e3). [Chapter 7]
 4. **Hendrickx, G.G.** (2023). *Salt Flux Decomposition: NumPy-based salt flux decomposition*. 4TU.ResearchData. Software. doi:[10.4121/bccbe767-667b-40ba-a4d1-d8fcad900772](https://doi.org/10.4121/bccbe767-667b-40ba-a4d1-d8fcad900772). [Chapters 4 and 5]
 3. **Hendrickx, G.G.** (2023). *NEESI: Numerical Experiments of Estuarine Salt Intrusion*. 4TU.ResearchData. Dataset. doi:[10.4121/22272247](https://doi.org/10.4121/22272247). [Chapters 2, 3 and 8]
 2. **Hendrickx, G.G.** (2022). *ANNESI: An open-source Artificial Neural Network for Estuarine Salt Intrusion*. 4TU.ResearchData. Software. doi:[10.4121/19307693](https://doi.org/10.4121/19307693). [Chapters 2, 3 and 8]
 1. **Hendrickx, G.G.** (2022). *CoralModel: A Python-based model that resembles the biophysical interactions on a coral reef*. 4TU.ResearchData. Software. doi:[10.4121/19164869](https://doi.org/10.4121/19164869).

Conference proceedings

First-authored conference proceedings

3. **Hendrickx, G.G.**, Pearson, S.G., and Aarninkhof, S.G.J. (2024, September). *Engineering guidelines for nature-based solutions to mitigate salt intrusion* [oral presentation]. International Conference on Coastal Engineering 2024. Rome, Italy.
2. **Hendrickx, G.G.**, Meselhe, E.A., Herman, P.M.J., and Aarninkhof, S.G.J. (2023, April). *A sill as nature-based solution to mitigate salt intrusion* [poster presentation]. Coastal Sediments 2023. New Orleans, LA, United States of America. doi:[10.1142/9789811275135_0184](https://doi.org/10.1142/9789811275135_0184).

1. **Hendrickx, G.G.**, Antolínez, J.A.A., Herman, P.M.J., and Aarninkhof, S.G.J. (2022, December). *Estuarine sensitivity to nature-based salt intrusion mitigation measures* [oral presentation]. International Conference on Coastal Engineering 2022. Sydney, Australia. doi:[10.9753/icce.v37.management.146](https://doi.org/10.9753/icce.v37.management.146).

Other conference contributions

7. **Hendrickx, G.G.**, Manuel, L.A., Pearson, S.G., Aarninkhof, S.G.J., and Meselhe, E.A. (2024, March). *When and where to construct a sill to mitigate estuarine salt intrusion* [oral presentation]. NCK Days 2024. Amersfoort, the Netherlands.
6. de Wilde, J., Kranenburg, W.M., Huismans, Y., Pietrzak, J.D., **Hendrickx, G.G.** (2024, March). *Tidal phase differences in multi-branch systems and their effect on salinity intrusion* [oral presentation]. NCK Days 2024. Amersfoort, the Netherlands.
5. **Hendrickx, G.G.**, Meselhe, E.A., Aarninkhof, S.G.J., and Herman, P.M.J. (2023, April). *Designing a sill to mitigate salt intrusion* [oral presentation]. Lower Mississippi River Science Symposium 2023. New Orleans, LA, United States of America.
4. **Hendrickx, G.G.**, Aarninkhof, S.G.J., and Herman, P.M.J. (2022, March). *Estuarine sensitivity to salt intrusion mitigation measures* [oral presentation]. NCK Days 2022. Enschede, the Netherlands.
3. **Hendrickx, G.G.**, Antolínez, J.A.A., Aarninkhof, S.G.J., Huismans, Y., Kranenburg, W.M., and Herman, P.M.J. (2022, March). *Combining machine learning and process-based models to enhance the understanding of estuarine salt intrusion and development of estuary-scale nature-based solutions* [oral presentation]. Ocean Sciences Meeting 2022. Online (due to COVID-19).
2. **Hendrickx, G.G.**, Aarninkhof, S.G.J., and Herman, P.M.J. (2021, March). *Nature-based solutions to mitigate salt intrusion* [oral presentation]. NCK Days 2021. Online (due to COVID-19).
1. **Hendrickx, G.G.**, Dijkstra, J.T., Herman, P.M.J., Luijendijk, A.P., and Pietrzak, J.D. (2020, March). *Predicting the survival of coral reefs* [oral presentation]. NCK Days 2020. Cancelled (due to COVID-19).